NORTHWESTERN UNIVERSITY

Segmented Polyhydroxyurethane as Novel Non-Isocyanate Polyurethane Functional Materials

A DISSERTATION

SUBMITTED TO THE GRADUATE SCHOOL
IN PARTIAL FULFILLMENT OF THE REQUIREMENTS

For the degree
DOCTOR OF PHILOSOPHY
Field of Chemical Engineering

By
Goliath Beniah

EVANSTON, ILLINOIS
March 2017

ABSTRACT

Segmented Polyhydroxyurethane as Novel Non-Isocyanate Polyurethane Functional Materials

Goliath Beniah

Polyurethane (PU) is an important commodity polymer with a broad range of applications. Increasing regulations on isocyanates have prompted investigations into alternative routes to PU. Cyclic carbonate aminolysis leading to polyhydroxyurethane (PHU) is a promising alternative. This dissertation describes the first fundamental investigation of the synthesis and properties of segmented, nanophase-separated PHUs as thermoplastic elastomer. The hydroxyl groups and soft-segment choice are critical to the development of nanophase separation and elastomeric properties.

Nanophase separation in segmented PHUs made with polytetramethylene oxide (PTMO)-based soft segment is accompanied by broad interphases having a wide range of local composition due to some level of phase mixing from hard-segment hydroxyl groups to soft-segment ether oxygen. Consequently, PTMO-based PHUs exhibit potential as sound and vibration damping materials over broad temperature ranges, a function unattainable by conventional, neat thermoplastic PU (TPU) elastomer.

Nanophase separation can be significantly tuned via judicious choice of soft segment. PTMO-based soft segments yield nanophase-separated PHUs with broad interphase whereas polybutadiene-co-acrylonitrile (PBN)-based soft segments yield nanophase-separated PHUs with a much sharper domain interphase similar to that of conventional TPU. Using three carbonate hard-segment structures having motifs similar to commonly used diisocyanates, it is

demonstrated that both hard-segment and soft-segment structures often cooperatively influence the nanophase separation and properties of PHUs. The impact of chain extender structure on the properties of PHUs was investigated. Norbornane-based chain extender enables significant improvement in the properties of PHUs. The impact of amide-based diamine diamide (DDA) chain extender on the properties of PHUs was investigated. DDA chain extender enables significant improvement in nanophase separation and properties of PHU systems where significant phase mixing were previously observed.

Finally, the impact of hydroxyl group functionalization on the properties of PTMO-based PHU was investigated. Hydroxyl group functionalization leads to loss of nanophase separation due to disruption to interurethane hydrogen bonding indicating that interurethane hydrogen bonding is important to the formation of nanophase-separated PHU.

ACKNOWLEDGMENTS

First and foremost, I would like to express my sincerest gratitude to my adviser, Prof. John M. Torkelson. I would like to thank him for believing in me and allowing me to continue my PhD education in his group. I am extremely indebted toward his hard work and dedication in mentoring me in research and effective communication. I owe my personal development as an individual and as a researcher to him.

I would also like to thank past and present members of the Torkelson group: Anthony Tan, Tian Lan, Lawrence Chen, Krishnan Iyer, Emily Leitsch, Shadid Askar, Elizabeth Dhulst, Lanhe Zhang, Kailong Jin, Xi Chen, Tong Wei, Lingqiao Li. Special thanks to Emily Leitsch who has mentored me in the initial years of polyurethane (PU) research in the group and also to fellow PU team Kailong Jin and Liz Dhulst. Thanks to downstairs office members for making the office a fun place in the last few months of my PhD.

This PhD dissertation would not be possible without the productive collaboration I have enjoyed in the past three years. I would like to thank my collaborators at The Dow Chemical Company: Dr. William H. Heath, Dr. Junho Jeon, and Dr. Matthew D. Miller and at the Chemistry department at Northwestern University: Dr. Kun Liu, Dr. Brice E. Uno, Prof Karl A. Scheidt, David J. Fortman and Prof. William R. Dichtel.

I also would like to thank members of the shared facilities who have provided me with numerous help with my experiments: Mr. Mark Sinew for providing assistance with tensile testing, Jerry Carsello for assistance with small angle X-ray experiments, Jeffrey Sundwall from the instrument shop for assistance with tool fabrication. I also would like to thank Prof. L. C. Brinson for generous use of dynamic mechanical analysis instrument and Min Zhang for the help with scheduling.

I am also extremely indebted toward the generous care, support and prayers from the

saints in Evanston and The Church in Chicago. It was such a blessing to have had many meals in many Friday meetings with the Roberts and members of the Friday group meetings. Many thanks to Lawrence Chen, Marty & Debbie Robert, Bill and Carol Barker, Patrice, Qing Yu, Jane, Christine, Linhua and Stacey Hu. I am also thankful for the care of many brothers and sisters in Evanston: Manny Choy, Preston Wang, Charlie and Barb Azarello, Andy and Jina Yun, John and Thawivann Spalding, and many more on Christian on Campus that I cannot list.

And of course, last but not least, I would like to thank my parents, Ali Muda Salim and Evelina Tansri Ghazali for raising me up for the last 28 years and for encouraging and supporting me to pursue my passion and education. I really hope that after I graduate, I will be able to give them a better life which they have not been able to enjoy in Indonesia.

TABLE OF CONTENTS

Page

ABSTRACT 3

ACKNOWLEDGEMENTS 5

TABLE OF CONTENTS 7

LIST OF FIGURES 11

LIST OF TABLES 14

LIST OF SCHEMES 15

1. Introduction 16

2. Background 24

2.1 Introduction 24

2.2 Polyurethane 24

2.3 Health Issues and Regulations on Isocyanates 27

2.4 Transurethanization 28

2.5 Cyclic Carbonate Aminolysis 30

2.5.1 Synthesis of Linear PHUs 30

2.5.2 Synthesis of Crosslinked PHUs 36

2.5.3 Synthesis of Segmented PHUs 40

2.6 Thermoplastic Polyurethane Elastomers, Hydrogen Bonding & Nanophase Separation 41

2.7 Structure Property Relationships in Segmented PUs 44

2.7.1 Influence of Diisocyanate Hard-Segment Structure 44

2.7.2 Influence of Soft-Segment Structure 48

2.7.3 Influence of Chain Extender Structure 50

2.7.4 Studies on Diamine Diamide Chain Extender 51

3. Non-Isocyanate Thermoplastic Polyhydroxyurethane Elastomer via Cyclic Carbonate Aminolysis.....55

3.1 Introduction 55

3.2 Experimental 56

3.2.1 Materials 57

3.2.2 Synthesis 57

3.2.3 Characterization 65

3.3 Results and Discussion 68

3.4 Conclusions 84

Appendix A 85

4. Novel Thermoplastic Polyhydroxyurethane Elastomer as Effective Damping Materials over Broad Temperature Ranges 99

4.1 Introduction 99

4.2 Experimental 103

4.3 Results and Discussion 108

4.4 Conclusions 123

Appendix B.....125

5. Tuning Nanophase Separation Behavior in Segmented Polyhydroxyurethane via Judicious Choice of Soft Segment.....135

5.1 Introduction 135

5.2 Experimental 139

5.2.1 Materials 139

5.2.2 Synthesis of PHUs 139

5.2.3 Characterization of PHUs 141

5.3 Results and Discussion 143

5.3.1 Synthesis and Characterization of PHU Molecular Structure.....143
5.3.2 SAXS 144
5.3.3 DMA 146
5.3.4 DSC.....152
5.3.5 AFM.....155
5.3.6 FTIR.....156
5.3.7 Tensile Testing.....159
5.4 Conclusions 159
Appendix C.....161
6. Combined Effect of Carbonate and Soft-Segment Molecular Structure on the Nanophase Separation and Properties of Segmented Polyhydroxyurethane.....172
6.1 Introduction 172
6.2 Experimental 178
6.2.1 Materials 177
6.2.2 Synthesis of Bis-Carbonate Monomers 177
6.2.3 Synthesis of PHUs 178
6.2.4 Characterization 180
6.3 Results and Discussion.....182
6.3.1 Synthesis 182
6.3.2 Influence of Hard-Segment Structure in PTMO-based PHUs.....183
6.3.3 Influence of Hard-Segment Structure in PBN-based PHUs 190
6.4 Conclusions 201
Appendix D 202
7. Tuning the Properties of Segmented Polyhydroxyurethane via Chain Extender Structure
.....220

7.1 Introduction 220
7.2 Experimental 223
7.3 Results and Discussion 226
7.4 Conclusions 240
Appendix E 242
8. Non-Isocyanate Thermoplastic Polyhydroxyurethane Elastomers: Amide-Based Chain Extender Yields Enhanced Nanophase Separation and Properties in Polyhydroxyureethane 250
8.1 Introduction 250
8.2 Experimental 254
8.3 Results and Discussion 259
8.4 Conclusions 274
Appendix F 276
9. Functionalization of Hydroxyl Groups in Segmented Polyhydroxyurethane Eliminates Nanophase Separation 284
9.1 Introduction 284
9.2 Experimental 285
9.3 Results and Discussion 287
9.4 Conclusions 293
Appendix G 295
10. Conclusions and Recommendation 300
10.1 Conclusions 300
10.2 Recommendation for Future Study 306
References 309

LIST OF FIGURES

Figures	Title	Page
2.1	a) Reaction of isocyanate and alcohol to produce urethane linkage, b) structures of commonly used diisocyanates.	25
2.2	a) Transurethanization reaction between dicarbamate and diol generating urethane bond and alcohol byproduct, b) reaction of dihydroxylalkylcarbamate with diol generating urethane bond and ethylene glycol, c) reaction of dimethylcarbonate with diamine to generate dicarbamate monomer, d) ring opening of ethylene carbonate with diamine to obtain dihydroxyalkylcarbamate monomer, e) structure of bifunctional monomer with alcohol and carbamate groups, f) structure of BHCH molecule.	29
2.3	Reactions of five-, six-, seven-, and eight-membered-ring carbonates with diamine to obtain PHUs.	31
2.4	Chemical structures of carbonate monomers investigated in PHU synthesis.	34
2.5	Chemical structures of carbonate monomers used in the synthesis of crosslinked PHUs.	38
2.6	Chemical structures of amide-based diamine diamide chain extenders.	52
3.1	Mechanical behavior of the traditional segmented PU, PU-PEG/PDO/30. a) Segmented PU material previous to extension. b) Segmented PU material during extension. c) Segmented PU material after release of extensive force. d) Example tensile curve obtained for PU-PEG/PDO/30.	69
3.2	Thermal property characterization of analogous PEG-based PU (PU-PEG/PDO/30) and PHU (PHU-PEG1k/DP/30) materials. a) Representative DSC curve for PU-PEG/PDO/30. The soft-segment T_g is relatively narrow at about -20 °C while the hard-segment T_g is broad with a midpoint around 110 °C. b) Representative DSC curve for PHU-PEG1k/DP/30. This material exhibits a soft-segment T_g around -20 °C, a melting peak associated with the PEG-based soft segment, and no discernable hard-segment T_g. c) Representative DMA profiles for PU-PEG/PDO/30 and PHU-PEG1k/DP/30. The PU material exhibits a soft-segment T_g followed by a large rubbery plateau region, while the PHU material flows and slips from the testing grips shortly after passing through the soft-segment glass transition.	70
3.3	a) Room-temperature flow properties of PEG1k/XYL/40 PHU, b) room-temperature flow properties of PPG/XYL/40 PHU, c) representation of the expected hard-segment hydrogen bonding interaction between amide groups and carbonyl groups in traditional PU, d) representation of the hydrogen bonding interaction leading to phase mixing in PEG-based PHUs. (The urethane carbonyl appears non-bonded due to hydrogen bonding between adjacent hydroxyl groups and readily accessible soft segment ether oxygen.) e) ATR-FTIR spectra for PPG-, PEG-, and PTMO-based PHUs at 40% hard-segment content.	73
3.4	a) Representative tensile curves for segmented PU and PHUs which exhibit a	76

robust elastomeric response. (See Figure 3.5a for response between 0-300% elongation.) b) Hysteresis of reversible elastomeric recovery exhibited by the PTMO/CYC/40 PHU. Data were collected in the tensile geometry by stretching to 100% strain at 130 mm/min. Samples were returned to 0% strain, and 10 cycles were completed.

3.5 a) Representative tensile curves of materials which show yield points, b) representative tensile curves for segmented PU and PHUs which exhibit a robust elastomeric response between 0 to 300% elongation at break. 77

3.6 SAXS patterns for PTMO-based PHUs; peaks are indicative of nanophase separation. Interdomain spacings are indicated in the figure legend. 79

3.7 Representative DMA profile of the PTMO/CYC/40 PHU. Sample exhibits tan $\delta \geq 0.3$ over an 81 °C temperature range, which is desirable for acoustic and vibrational damping. 82

4.1 SAXS patterns of PHUs chain extended with (a) 1,3 cyclohexane bis(methyl amine), CYCDA-30 through CYCDA-60. 111

4.2 Representative stress-strain curves of PHUs chain extended with 1,3-cyclohexane bis(methyl amine) with hard-segment content of 30 to 60 wt%. Inset: Representative stress-strain curves of CYCDA samples at low elongation. 112

4.3 Temperature dependences of tensile storage modulus (*E*'), loss modulus (*E*"), and tan δ of (a) CYCDA-30, (b) HMDA-30, and (c) pXDA-30 PHUs. 116

4.4 Temperature dependences of tensile storage modulus (E'), loss modulus (E'), and tan δ of (a) analogous PU made with PTMO (M_n = 2000 g/mol), 2,4 TDI and 1,4-cyclohexane dimethanol and (b) analogous PU made with PTMO (M_n = 2000 g/mol), 2,4 TDI and 1,6-hexanediol at 30 wt% hard-segment content. 118

4.5 Temperature dependences of tan δ of (a) CYCDA-30 through CYCDA-60, (b) HMDA-30 through HMDA-60 and (c) pXDA-30 through pXDA-60. 121

5.1 Small-angle X-ray scattering patterns of PTMO-30, PBN18-30 and PBN10-30. 145

5.2 Temperature dependences of storage modulus (*E*'), loss modulus (*E*") and loss factor (tan δ) of PHUs synthesized with a) PTMO soft segment, PTMO-30, and b) polybutadiene-co-acrylontrile, 18 wt% acrylonitrile soft segment, PBN18-30. 148

5.3 Temperature dependences of storage modulus (*E*'), loss modulus (*E*") and loss factor (tan δ) of PHUs synthesized with polybutadiene-co-acrylonitrile soft segments at a) 30 wt% hard-segment content (PBN18-30 and PBN10-30) and b) 40 wt% hard-segment content (PBN18-40 and PBN10-40). 150

5.4 Thermal properties of PHUs as characterized by DSC. a) Representative heat flow curves of PHUs at a heating rate of 10 °C/min and, b) first derivative heat flow curves of PHUs. 153

5.5 FTIR spectra of the carbonyl regions representing free, non-hydrogen bonded urethane carbonyl (~1730 cm^{-1}) and hydrogen bonded urethane carbonyl (~1700 cm^{-1}). PBN-based PHUs show peaks centered at ~1670 and 1640 cm^{-1}, associated with free and hydrogen bonded amide carbonyl in the soft segment. 157

5.6 Representative stress-strain curves of PHUs characterized by uniaxial tensile 158

testing.
6.1 Small-angle X-ray scattering patterns of PTMO-based PHUs. 184
6.2 Temperature dependences of storage modulus (*E*'), loss modulus (*E*") and loss factor (tan δ) of a) PTMO-DVBDCC, b) PTMO-RBC, and c) PTMO-BPADC. Arrows indicate region in which tan δ ≥ 0.3. 185
6.3 Representative stress-strain curves of PTMO-based PHUs. 189
6.4 Small-angle X-ray scattering patterns of PBN-based PHUs. 191
6.5 Temperature dependences of storage modulus (*E*'), loss modulus (*E*") and loss factor (tan δ) of a) PBN-DVBDCC, b) PBN-RBC, and c) PBN-BPADC. 192
6.6 Representative stress-strain curves of PBN-based PHUs. 194
6.7 Hysteresis profile of (a) PBN-DVBDCC, (b) PBN-RBC, and (c) PBN-BPADC. Enlarged version of PBN-RBC profile can be found in Figure D16. 196
7.1 a) SAXS data of 50 wt% hard-segment content as a function of chain extender PHUs and b) SAXS data of NORB-based PHUs at several hard-segment contents. 228
7.2 Temperature dependence of storage modulus (*E*'), loss modulus (*E*"), and tan δ of a) DAB-50, b) IPDA-50, c) MBC-50, and d) NORB-50. 229
7.3 Representative stress-strain curves of 50 wt% hard-segment content PHUs as a function of chain extender. 233
7.4 Temperature dependence of a) storage modulus (*E*'), b) loss modulus (*E*"), and c) tan δ of PHUs chain extended with norbornane diamine at several hard-segment contents. 237
7.5 Representative stress-strain curves of PHUs chain extended with norbornane diamine at several hard-segment contents. 238
8.1 SAXS patterns of PEO-based PHUs. 261
8.2 Temperature dependences of tensile storage modulus (*E*'), loss modulus (*E*"), and tan δ of a) PEO1, b) PEO2, and c) PEO3. 263
8.3 FTIR spectra of PEO-based PHUs in the carbonyl regions. 265
8.4 SAXS patterns of PTMO-based PHUs. 267
8.5 Temperature dependences of tensile storage modulus (*E*'), loss modulus (*E*"), and tan δ of a) PTMO1, b) PTMO2, c) PTMO3, and d) PTMO4. 268
8.6 Representative stress-strain curves of PTMO-based PHUs 272
8.7 Hysteresis profile of a) PTMO3, and b) PTMO4. 273
9.1 Reaction scheme for the synthesis of segmented polyhydroxyurethane and subsequent functionalization of hydroxyl groups with benzoyl chloride. 288
9.2 Temperature dependences of storage modulus (*E*'), loss modulus (*E*") and loss tangent (tan δ) for a) segmented PHU before functionalization (PHU-O), and b) after functionalization (PHU-F). 290
9.3 SAXS results of segmented PHU before functionalization (PHU-O) and after functionalization (PHU-F). 291

LIST OF TABLES

No.	Title	Page
3.1	Segmented PHU material formulations.	72
3.2	Tensile and thermal properties of segmented PHUs and a comparison PU.	75
3.3	Apparent Molecular Weight Averages of PHUs.	81
4.1	Composition, thermal properties as determined from dynamic mechanical analysis, interdomain spacings determined from SAXS and temperature range with good damping performance of PTMO-based PHUs. HS: hard segment, CE: chain extender, SS: soft segment.	105
4.2	Mechanical properties of PTMO-based PHUs at various hard-segment contents produced with three different chain extenders.	114
5.1	Summary of interdomain spacing, thermal and mechanical properties of PTMO- and PBN-based PHUs.	147
6.1	Summary of properties of PHUs.	188
7.1	Summary of properties of 50 wt% hard-segment content PHUs as a function of chain extender structure.	234
7.2	Summary of properties of PHUs with norbornane diamine chain extender as a function of hard-segment content.	239
8.1	Summary of properties of PEO-based PHUs.	256
8.2	Summary of properties of PTMO-based PHUs.	257

LIST OF SCHEMES

No.	Title	Page
3.1	Reaction schemes for the synthesis of PU-PEG/PDO/30 and an analogous PEG-based PHU (PEG1k/DP/30).	60
3.2	Monomer structures and reaction scheme employed for the synthesis of segmented PHUs. The soft segments are (1) 1000 g/mol carbonate-terminated PEG, (2) 730 g/mol carbonate-terminated PPG, (3) 1700 g/mol amine-terminated PTMO, and (4) 1700 g/mol amine-terminated PEG. The hard segment exists as a mixture of 1,3- and 1,4- isomers of divinylbenzene dicyclocarbonate (DVBDCC). The amine chain extenders employed were *m*-xylylenediamine or 1,3-cyclohexanebis(methylamine). The PHU product is a simplified structure showing the two possible types of hydroxyurethane linkages created, primary and secondary; a mixture of these products is expected. Depending on the formulation, the R' group could represent the amine chain-extender backbone or the soft-segment backbone, and the R group could represent the hard-segment structure or the backbone of the soft segment.	62
4.1	Reaction scheme for the formation of segmented PHUs from DVBDCC, PTMO and chain extenders. The PHUs can either possess a 1° or 2° hydroxyl group; a mixture of these products is expected.	106
5.1	Reaction schemes for synthesis of PTMO-based and PBN-based PHUs.	140
6.1	Formation of bis-carbonate monomers.	175
6.2	Reaction scheme for the synthesis of segmented PHUs with different hard-segment carbonate and soft-segment structures.	179
7.1	Chemical structure of chain extenders used in this study.	224
8.1	Reaction scheme for the syntheses of PEO- and PTMO-based PHUs with diamine diamide (DDA) chain extender.	253

CHAPTER 1

Introduction

World-wide production of polyurethane (PU) was estimated to be 18 million tons in 2016. This accounts for approximately 5% of total global polymer production worldwide (Nohra 2013, Delebecq 2013, Engels 2013, Blattmann 2014). PU ranks sixth in terms of annual global polymer production. Due to its highly modular structure and diverse range of attainable material properties, PU has found utility in many applications including flexible foam, rigid foam, coatings, adhesives, sealants, elastomers etc. PU products are used in building and construction, automotive, footwear, packaging and other industries. PU is produced from a step-growth polymerization involving isocyanate and alcohol (Engels 2013). Isocyanate has been the subject of intense scrutiny and regulation in recent years from various regulatory bodies across the globe. The United States Environmental Protection Agency has released several action plans against commonly used diisocyanates: toluene diisocyanate and methylene diphenylene diisocyanate. In the European Union, chemical industries using isocyanates are also facing challenges to adapt to the new Registration, Evaluation, Authorization and Restriction of Chemicals (REACH) regulations enacted in 2009 (Official Journal of European Union 2009, US EPA 2011, US EPA 2015). These regulations have created an impetus for exploration of alternative chemistries for the synthesis of non-isocyanate PU (NIPU) or PU-like materials.

There are two major approaches to NIPU synthesis: transurethanization and cyclic carbonate aminolysis (Guan 2011, Blattmann 2014, Maisonneuve 2014). In transurethanization, a diurethane or dicarbamate monomer is first formed and then reacted with an alcohol at elevated temperature in a transurethane exchange reaction that releases low boiling point alcohol as byproduct. In cyclic carbonate aminolysis, five-, six-, seven-, or eight-membered-ring carbonates

is reacted with a primary amine resulting in a urethane bond with an additional primary and/or hydroxyl groups adjacent to the urethane linkage. This PU-like polymer is called polyhydroxyurethane (PHU).

Cyclic carbonate aminolysis is an important alternative to make PU-like material. This chemistry has been investigated extensively by many researchers since several decades ago. The majority of these investigations concern the synthesis of single-phase thermoplastics, crosslinked thermosets and reaction catalysis. There has been a significant number of studies that reported the reaction between small molecule difunctional carbonate with small molecule diamine, resulting in linear PHUs with single glass transition temperature (T_g) (Tomita 2001a, Tomita 2001b, Tomita 2001c, Tomita 2001d, Tomita 2001e, Lee 2015, Maisonneuve 2014, Mazurek-Budzyńska 2016, Bähr 2012a, Bähr 2012b, Benyahya 2011, Benyahya 2012, Van Velthoven 2015, Firdaus 2013, Yuen 2016). There are also many reports on reactions between multifunctional carbonates with multifunctional amines, which produce networked PHUs (Javni 2008, Javni 2013, Schmidt 2016, Poussard 2016, Fleischer 2013, Blattmann 2016a, Blattmann 2016b, Blattmann 2016c, Besse 2015, Besse 2013b, Matsukizono 2015, Matsukizono 2016a, Matsukizono 2016b). Due to its slow reaction kinetics, considerable efforts have been spent to increase its reaction rate through the use of catalyst and investigation of reaction parameters such as the effect of solvents, temperature and cyclic carbonate functionality (Ochiai 2005a, Lambeth 2015, Lombardo 2015, Blain 2014, Duval 2015). Ultimately, an important goal of exploring alternative chemistry is to create NIPU materials with properties competitive with those of PU. However, these past investigations on PHU, while important, fail to take note of an important fact that a significant fraction of commercial PU consists of linear, segmented PU copolymers. Segmented PUs are made of soft segment, with T_g well below room temperature and hard segment, with T_g well above room temperature. The incompatibility between hard and soft segments results in phase separation usually with nanoscale disperse domain size, i.e., nanophase

separation (Holden 2004, Engels 2013, Oertel 1994). At the commencement of research documented in this dissertation, there had been no investigation on segmented, nanophase-separated PHUs in the open literature. The primary aim of this dissertation research was to develop segmented nanophase separated PHUs and to study their properties. This research also aimed at understanding the role of hydroxyl groups in modifying nanophase separation, and to provide understanding on how to control and tune segmented PHU properties through structure-property-relationships.

The work performed in this dissertation is important from a basic scientific standpoint. Polyhydroxyurethanes possess additional hydroxyl groups adjacent to every urethane linkage; the impact of these hydroxyl groups on the nanophase separation and properties of segmented PHUs is virtually unknown. Nanophase separation in segmented PUs results from the thermodynamic incompatibility between the hard and soft segments as well as hydrogen bonding between the urethane linkages. The extent of and how to control nanophase separation in segmented PUs have been well understood from over five decades of investigations. Hydroxyl groups are hydrogen bond donors. The presence of these additional hydrogen bond donors can introduce additional complications to the nanophase separation and associated properties in segmented PHU.

From a technological point of view, the study of linear, segmented, nanophase-separated PHUs is important for various applications, e.g., as thermoplastic elastomer. Appropriately designed nanophase-separated PUs possess hard domains dispersed in a rubbery matrix; these dispersed, hard nanodomains act as physical crosslinking sites that provide resistance during tensile deformation. The hard domains soften at high temperature, enabling their thermoplastic processability. From our study, we found that the nanophase separation behavior conferred by phase mixing from intersegmental hydrogen bonding of hard-segment hydroxyl groups to soft segments can also lead to properties that are not attainable in conventional PUs, i.e., that is as

acoustic and vibration damping materials over broad temperature ranges. Furthermore, understanding of structure-property-relationships of segmented PHUs is needed to design NIPU materials with material properties competitive with isocyanate-based PU. To achieve this goal, strategies that allows for tunability of thermal and mechanical properties are explored.

This dissertation is formatted in such a way that each chapter can be read separately. For every chapter, an appropriate background is provided, followed by the experimental procedure, results and discussions, as well as conclusions. Background information necessary to understand the research performed in this dissertation is provided in Chapter 2, including an overview of PU chemistry, its applications, and regulations on isocyanates. This is followed by a review of past studies on the synthesis and characterization of NIPUs. Because of the strong emphasis on structure-property-relationships characterization in segmented PHUs in this dissertation, a review past structure-property-relationship studies of segmented PUs is also provided.

In Chapter 3, the novel synthesis and characterization of nanophase-separated PHUs in which the soft-segments form the major phase is described. This approach allows for the possibility of making materials related to thermoplastic PU elastomers (TPUs) but without the use of isocyanate-based chemistry used in PU synthesis. We demonstrate the critical role of the hydroxyl groups in PHUs in modifying the phase behavior of PHUs relative to TPUs. Because hydroxyl groups present in the hard segments of PHUs can undergo hydrogen bonding with oxygen atoms present in PHU soft segments, soft segment/hard segment combinations that lead to well nanophase-separated TPUs can result in single-phase PHUs, e.g., with polyethylene glycol (PEO)-based soft segments. By sterically hindering or diluting such hydrogen bonding interactions by use of polypropylene oxide (PPO)-based or polytetramethylene oxide (PTMO)-based soft segments, it is possible to achieve nanophase-separated PHUs. In the case of PTMO-based PHUs, the nanophase separation is accompanied by partial phase mixing, meaning that the nanophase-separated structures possess broad interphase regions with a wide range of local

compositions. As a result, PTMO-based PHUs exhibit exceptional, broad-temperature range acoustic and vibration damping characteristics, a function that is not observed with conventional TPUs.

Based on the interesting result obtained for PTMO-based PHUs in Chapter 3, Chapter 4 describes a much more detailed study of the synthesis and characterization of segmented, nanophase-separated, thermoplastic PHU elastomers using PTMO-based soft segment, as well as their application as damping materials. The nanophase-separated structures of these PHUs are accompanied with broad interphases possessing a wide range of local composition due to some level of phase mixing caused by hydrogen bonding of the hydroxyl groups in the hard segment to oxygen atoms in PTMO soft segment. Consequently, PTMO-based PHUs have broad glass transition ranges and have the potential to serve as broad-temperature-range acoustic and vibration damping materials. Using a well-known criterion for assessing good damping behavior via dynamic mechanical analysis ($\tan \delta \geq 0.30$), we show that these PHUs possess $\tan \delta \geq 0.30$ over exceptionally broad temperature ranges of at least 60 °C and beyond. We also show that these temperature ranges, including location and breadth, are tunable via simple variation of hard-segment content and chain-extender structure. We also demonstrate that this property of PTMO-based PHUs is not observed in conventional, PTMO-based thermoplastic PU elastomer (TPU) by itself. In fact, TPUs are often made into cross-linked, interpenetrating polymer networks with secondary polymeric components to achieve broad-temperature-range damping capability.

In Chapter 5, we demonstrate that nanophase separation behavior in segmented PHUs can be significantly tuned via judicious choice of soft segment. Use of a PTMO-based soft segment results in nanophase-separated PHUs with broad interphases. The switch to a polybutadiene-based soft segment results in nanophase-separated PHUs with a much sharper, narrower interphase, evidenced by sharp tan δ peaks near soft-segment and hard-segment glass transition

temperatures. Such response, akin to that observed in conventional, isocyanate-based TPU, is obtained because of the lack of hydrogen bonding acceptor in polybutadiene-based soft-segment which suppresses intersegmental hydrogen bonding. This study demonstrates that a simple change in the soft-segment composition can yield major tunability in nanophase separation behavior, thereby enabling access to properties produced by conventional TPU.

In Chapter 6, we study the impact of hard-segment structure on the nanophase separation and properties of segmented PHUs using three carbonate molecules having motifs similar to commonly used diisocyanates: divinylbenzene dicyclocarbonate (DVBDCC), bisphenol A dicarbonate (BPADC), and resorcinol bis-carbonate (RBC). These carbonates were formulated with two different soft segments: polytetramethylene oxide (PTMO)- and polybutadiene-co-acrylonitrile (PBN)-based soft segments. Characterization results reveal that hard-segment and soft-segment structures often cooperatively influence the resulting morphology and properties of segmented PHUs. Unlike segmented PUs, where any diisocyanate used in synthesis generally leads to well nanophase-separated materials, in PTMO-based formulations BPADC leads to fully phase-mixed PHU whereas DVBDCC and RBC lead to nanophase-separated PHUs with relatively broad interphase regions. Suppressing intersegmental hydrogen bonding with PBN-based soft segment leads to well nanophase-separated PHUs for all three hard-segment structures.

In Chapter 7, we investigated the influence of chain extender structure on the properties of segmented PHUs made with PTMO-based soft segment using four chain extender molecules. In PHUs with 50 wt% hard-segment content, values of flow temperature, tensile strength, and elongation at break can be tuned via chain extender structure from 57 to 105 °C, 1.6 to 22.4 MPa, and 70 to 500 %. These PHUs also exhibit tan $\delta \geq 0.30$ over broad temperature ranges, indicating their potential as effective damping materials. We also found that PHU with norbornane-based chain extender exhibits, to the best of our knowledge, the best thermal and

mechanical properties of segmented PHUs reported to date. Further optimization through variation of hard-segment content in norbornane-based PHUs affords broad tunability in tensile strength from 0.5 to 22.4 MPa with tan $\delta \geq 0.30$ spanning temperature range as large as 85 °C.

In Chapter 8, we explored the use of amide-based, diamine diamide chain extender in the synthesis of segmented PHUs made from PEO- and PTMO-based soft segments. Characterizations of these PHUs reveal that the use of amide-based DDA chain extender achieved unprecedented improvements in nanophase separation, thermal and mechanical properties over segmented PHUs without DDA chain extender. In PEO-based soft segment, previously known to yield only phase-mixed PHUs, use of DDA chain extender yields nanophase-separated PHUs above certain hard-segment content, as characterized by small-angle X-ray scattering. In PTMO-based soft segment, previously known to yield nanophase-separated PHUs with broad interphase, use of DDA chain extender produces nanophase-separated PHUs with sharp domain interphase, with wide, relatively temperature-independent rubbery plateau regions and much improved thermal properties with flow temperature as high as 200 °C. These PTMO-based PHUs exhibits tunable mechanical properties with Young's modulus ranging from 6.6 to 43.2 MPa, tensile strengths ranging from 2.4 to 6.7 MPa, and elongation at break of ~300 %. Cyclic tensile testing shows that these PHUs exhibit elastomeric recovery with attributes very similar to conventional, isocyanate-based thermoplastic PU elastomers.

In Chapter 9, we studied the impact of hydroxyl group functionalization on the properties of segmented PHU. Segmented PHU was synthesized with PTMO-based soft segment and the pendant hydroxyl groups were functionalized via an esterification reaction with benzoyl chloride; the properties of the PHUs were characterized before and after functionalization. Such functionalization leads to loss of nanophase-separated morphology. This behavior may be explained by the disruption of interurethane hydrogen bonding due to steric hindrance of bulky, benzoyl chloride side group. This study shows that interurethane hydrogen bonding is needed for

effective nanophase separation to occur in PTMO-based PHUs.

Chapter 10 summarizes the results of this dissertation and provides conclusions. Suggestions for potential future studies in the area of segmented PHUs are also provided.

CHAPTER 2

Background

2.1 Introduction

This chapter provides the background information necessary to understand the work performed in this thesis. It begins with an overview of polyurethane (PU) and its applications as well as challenges associated with increasing regulations on its precursor, isocyanate. This is followed by a review of two alternative approaches for synthesizing non-isocyanate PU: transurethanization and cyclic carbonate aminolysis. The synthesis of polyhydroxyurethane (PHU) via cyclic carbonate aminolysis has emerged to be one of the most promising chemistries to make PU-like materials. A short review of research efforts related to the synthesis of single-phase PHUs, crosslinked PHUs and segmented PHUs is also provided. This is followed by a brief review of past studies on structure-property-relationships on segmented, nanophase-separated PUs including the influence of diisocyanate hard-segment, soft-segment, and chain extender structures on nanophase separation and properties of segmented PUs.

2.2 Polyurethane

Polyurethane was first developed over seven decades ago by Dr. Otto Bayer in Germany (Bayer 1947). Due to the diversity of available starting materials, PUs can possess highly modular structure and very diverse range of polymer properties. In terms of global polymer production, PU ranks sixth with an estimated annual total production of about 18 million tons in 2016 (Delebecq 2013). PU is obtained from a step growth polymerization of polyisocyanates with polyalcohol (see Figure 2.1a) (Oertel 1994, Engels 2013). The most commonly used isocyanates are toluene diisocyanate (TDI), comprising of isomers 2,4-TDI and 2,6-TDI and

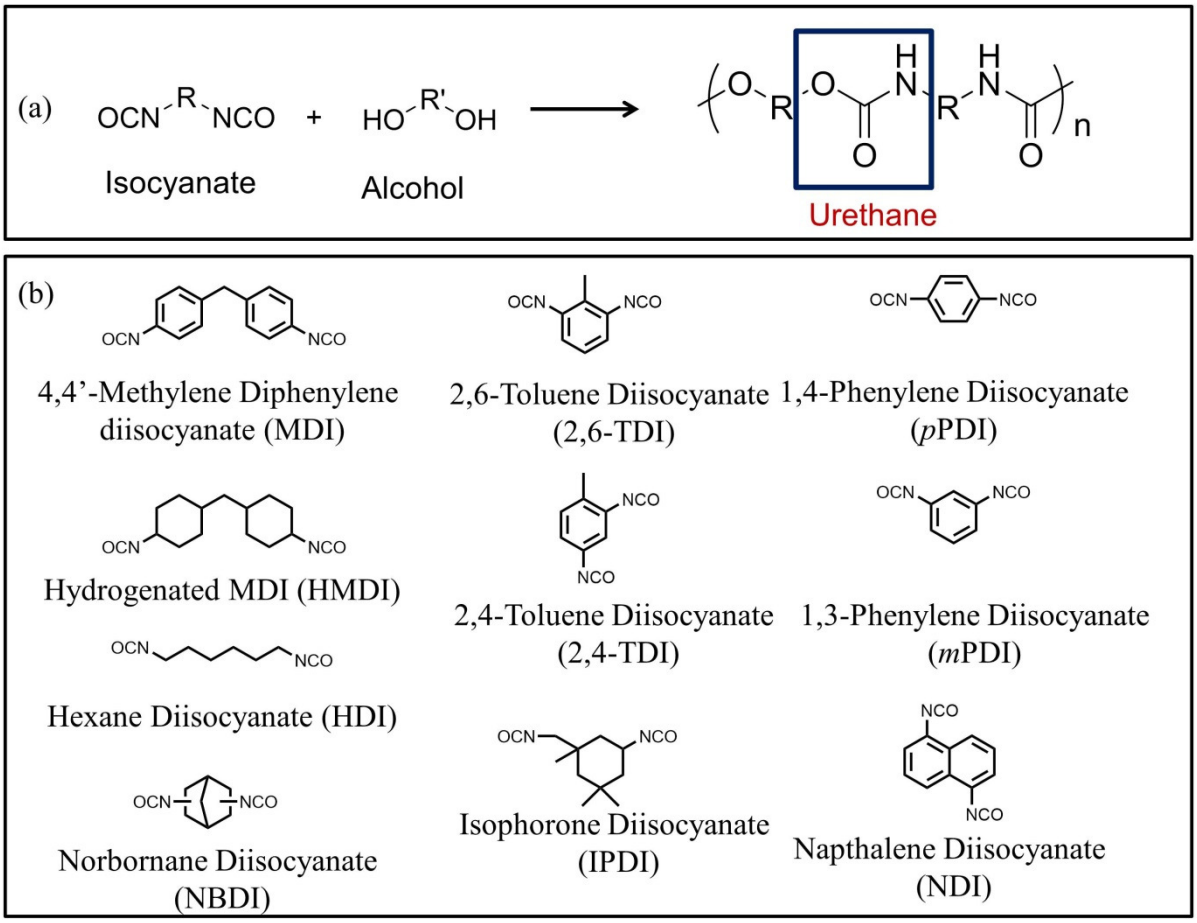

Figure 2.1: a) Reaction of isocyanate and alcohol to produce urethane linkage, b) structures of commonly used diisocyanates.

methylene diphenylene isocyanate (MDI), comprising of 4,4'-MDI and 2,4'-MDI (Oertel 1994, Engels 2013). Other, less commonly used, diisocyanates include 1,5-napthalene diisocyanate (NDI), hexane diisocyanate (HDI), isophorone diisocyanate (IPDI), hydrogenated MDI (HMDI), and norbornane diisocyanate (NBDI). (See Figure 2.1b for the chemical structures of diisocyanates employed in PU synthesis). Commonly used polyols include polyethylene oxide (PEO), polypropylene oxide (PPO), polytetramethylene oxide (PTMO), and polyesters with molecular weights ranging between 300-8000 g/mole. Other types of polyol such as polyhexamethylene oxide, polycarbonate, polybutadiene (PBD), and polydimethylsiloxane (PDMS) are also used. Due to the many possible combinations of starting materals in PU formulation, a broad range of accessible properties are attained. As such, PU can be tailored for broad range of uses including as rigid and flexible foams, elastomers, adhesives, coatings, films as well as biomedical materials.

About 66 % of raw materials that go into PU production are used to make foam (Engels 2013). During foam formation, isocyanate first reacts with water resulting in unstable carbamic acid, which decomposes into an amine and carbon dioxide. The amine further reacts with additional isocyanate resulting in urea while the CO_2 gas generated serve as a blowing agent. Additional blowing agents can also be used. Flexible foams are usually made with polyols having a functionality of three with a molar mass of 3000-4000 g/mole with a high propylene oxide content and low ethylene oxide content. The rigid foams are made with polyols having a functionality of three to six with molar mass of 400-12000 g/mole, with a lower propylene oxide and high ethylene oxide content.

PU elastomers occupy about 20 percent of global PU products, with 60 percent as footwear elastomer and the remaining 40 percent divided equally between thermoplastic PU elastomers (TPUs), synthetic leather, and elastomeric fibers (Engels 2013). PU as binders are widely employed as automative finishes, metal coatings for corrosion protection, wood, plastics,

as well as textile coatings. PU coatings can be formulated for water-borne or solvent-borne applications. PU is also combined with acrylate groups for UV-curable coatings formulation. PU adhesives also enjoyed widespread applications due to its ability to bond to a variety of substrates. PU adhesives are used in footwear, flexible packaging, construction and furniture as well as structural adhesives in transportation markets (Engels 2013).

2.3 Health Issues and Regulations on Isocyanate.

While PU has diverse range of applications, it is well-known that exposure to isocyanates can have undesirable effects on human health. Isocyanates are well-known dermal and respiratory sensitizers. Overexposure to isocyanates may cause sensitization and occupational asthma (OSHA 2013). Due to these health concerns, many regulatory bodies across the globe have taken actions to regulate the use, transport and handling of isocyanates and isocyanate-containing compounds. Regulatory pressure in the United States comes from the Environmental Protection Agency, which has issued action plans against TDI and MDI in 2011. In 2016, the EPA also issued significant new use rules under the Toxic Substance Control Act for prepolymer containing MDI and HDI, requiring persons or entities who intended to manufacture or process isocyanates to notify the EPA at least 90 days before commencing the activity (US EPA 2011, US EPA 2015, US EPA 2016). Within the European Union, REACH regulations also mandate that the content of isocyanate in the mixture supplied to the public should not exceed 0.1 wt% (Official Journal of European Union 2009). The increased awareness to the undesirable effects of isocyanates on human health and their increased regulations have prompted increasing investigations into alternative chemistries and precursors to produce PU and PU-like materials (Guan 2011, Blattmann 2014, Kathalewar 2013). There are two important alternative reactions to produce PU without using isocyanates: transurethanization and cyclic carbonate aminolysis (Blattmann 2014, Kathalewar 2013).

2.4 Transurethanization

An alternative route to produce PU without employing isocyanate precursor is transurethanization or transcarbamoylation process. In this reaction, an alcohol is condensed with a carbamate in a transurethane exchange reaction, releasing low-boiling-point alcohol as byproduct such as methanol or ethylene glycol. The carbamate monomer is produced from the reaction of an amine with a carbonate, thereby avoiding the use of phosgene and isocyanate in the synthesis. Figure 2.2a and 2.2b show the mechanism of a typical transurethanization reaction. This reaction is usually conducted at an elevated temperature above 150 °C with a catalyst, releasing small molecule alcohol as byproduct. The carbamate monomers can also be prepared through reaction of dialkylcarbonate with diamine resulting in dialkylcarbamate (see Figure 2.2c). Another route to generate carbamate monomer is through the reaction of diamine with cyclic carbonate such as ethylene carbonate and propylene carbonate, generating dihydroxyalkylcarbamate (see Figure 2.2d). The starting material can also be a heterebifunctional monomer bearing an amine and a carbamate group (see Figure 2.2e).

A number of studies have explored this approach for PU production (Ochiai 2013, Deng 2014, Li 2015, Wang 2016). Ochiai and Utsuno reacted hexamethylene diamine with ethylene carbonate to obtain 1,6-bis(hydroxyethyloxyl carbonyl amino)hexane (BHCH) (see Figure 2.2f). The BHCH monomer is subsequently polymerized with ethylene glycol in xylene at 150 °C for 6 hours with Bu_2SnO as catalyst (Ochiai 2012). Deng et al. also synthesized PU using a combination of BHCH, triethylene glycol and tetraethylene glycol. Reactions proceeded for 2 hours under nitrogen atmosphere, followed by 30 mmHg vacuum for 4 hours, and 2 mmHg vacuum until no further increase in viscosity was observed. The resulting polymers are semi-crystalline possessing tensile strengths ranging from 14 to 32 MPa and strain at break from few percent to 150 percent (Deng 2014). In another study, Li et al. used a similar approach to make

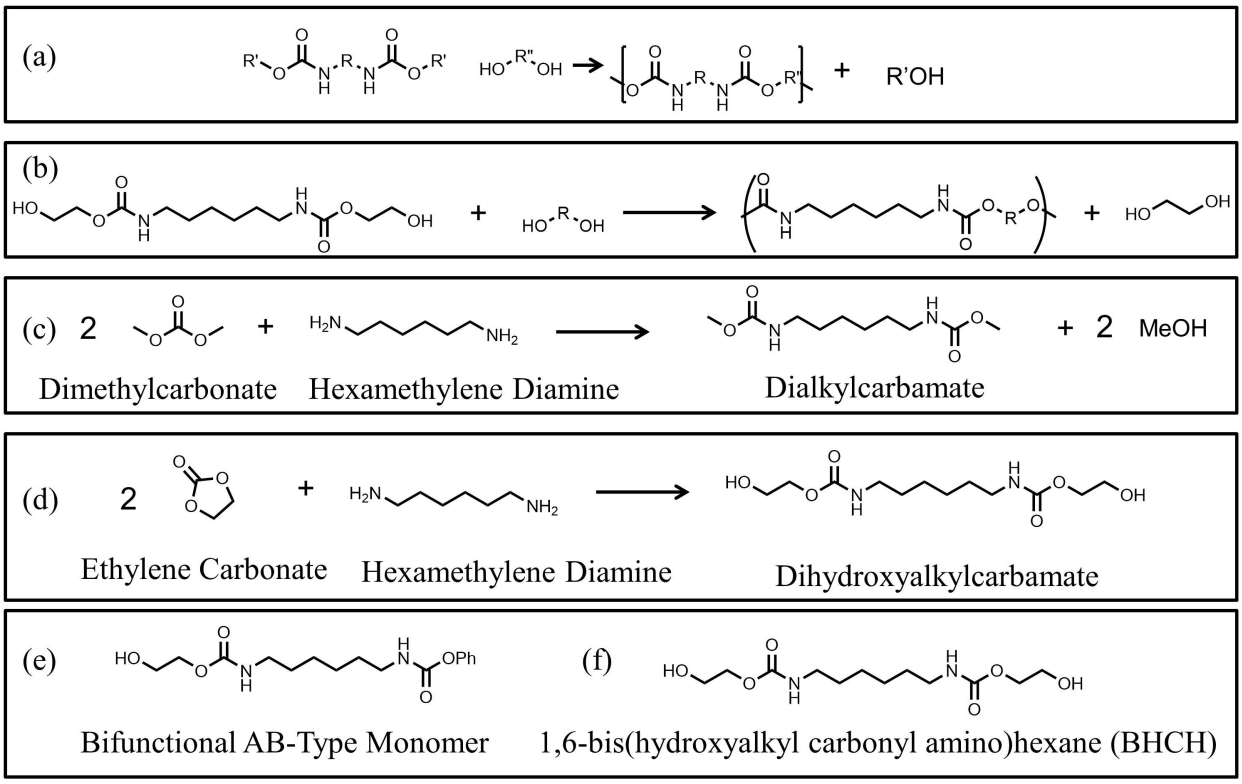

Figure 2.2: a) Transurethanization reaction between dicarbamate and diol generating urethane bond and alcohol byproduct, b) reaction of dihydroxylalkylcarbamate with diol generating urethane bond and ethylene glycol, c) reaction of dimethylcarbonate with diamine to generate dicarbamate monomer, d) ring opening of ethylene carbonate with diamine to obtaine dihydroxyalkylcarbamate monomer, e) structure of bifunctional monomer with alcohol and carbamate groups, f) structure of BHCH molecule.

segmented PUs using a di(hydroxypropyl)isophorone biscarbamate, obtained from reaction between propylene carbonate and isophorone diamine. PEO-based soft segments were used with molecular weights ranging from 400 to 4000 g/mole. Reactions were conducted at 170 °C for 1 to 6.5 h under vacuum to remove ethylene glycol byproduct. The resulting PUs had M_n ranging from 11.5 to 31.1 kDa and M_w ranging from 18.4 to 126 kDa. The tensile strengths of the resulting PUs were in the range of 5.8 to 24.4 MPa, and the elongation-at-break values ranged from 1 to 1380 percent (Li 2015). Wang et al. recently reported the synthesis of poly(ester urethane) using BHCH copolymerized with oxalic acid, hexanedioic acid, sebacic acid, itaconic acid, and terephthalic acid. The resulting polymers were semicrystalline possessing tensile strength of 9 to 17.9 MPa with strain at break of 35 to 235 % (Wang 2016).

2.5 Cyclic Carbonate Aminolysis

Another very promising approach for the synthesis of non-isocyanate PU is cyclic carbonate aminolysis (see Figure 2.3). The reaction between an amine with five-, six-, seven-, and eight-membered ring carbonates produce a urethane bond and a hydroxyl group at the beta carbon of the urethane moiety (Guan 2011, Kathalewar 2013, Blattmann 2014, Maisonneuve 2015, Cornille 2016). Depending on the structure of carbonates, a mixture of primary and secondary hydroxyl groups can be expected. In addition to bypassing isocyanate precursors, the production of cyclic carbonate monomers offers a route for CO_2 utilization, a potentially environmentally-friendly approach for monomer synthesis. Investigations into cyclic carbonate aminolysis in the last three decades have focused on the synthesis of linear PHUs, crosslinked PHUs, and reaction catalysis with very little emphasis on segmented, nanophase-separated PHUs (Guan 2011, Kathalewar 2013, Blattmann 2014, Maisonneuve 2015, Cornille 2016).

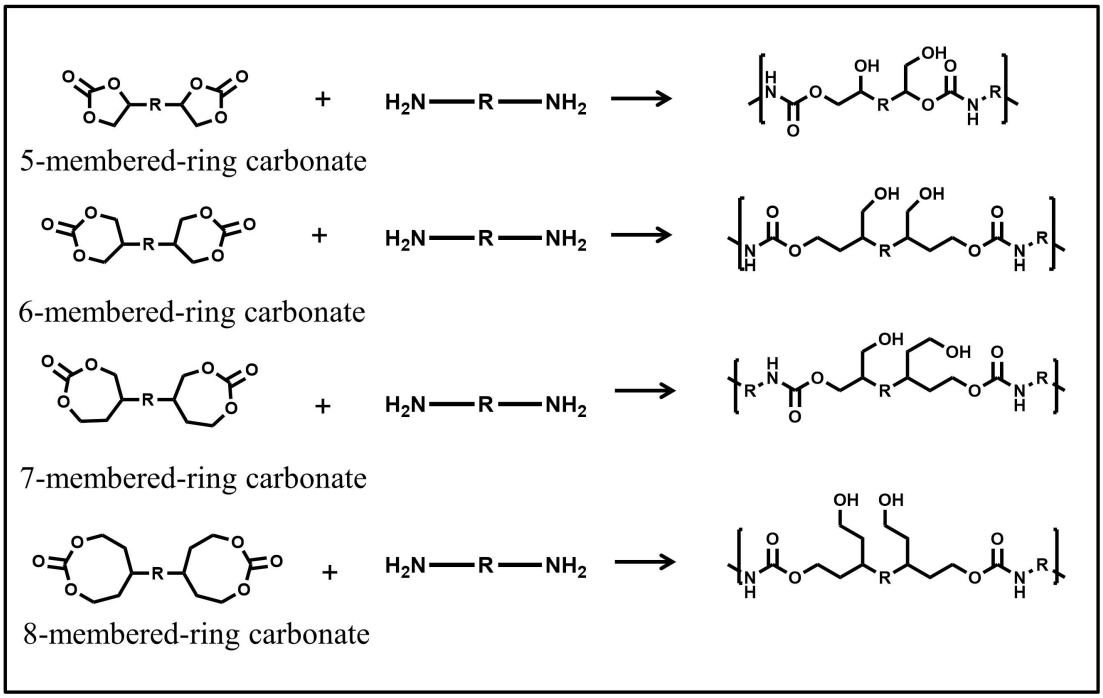

Figure 2.3: Reactions of five-, six-, seven-, and eight-membered-ring carbonates with diamine to obtain PHUs.

2.5.1 Synthesis of Linear PHUs

The synthesis and properties of linear PHUs were extensively studied by Endo and coworkers since more than two decades ago (Ochiai 2005a, Ochiai 2005b, Ochiai 2005c, Tomita 2001a, Tomita 2001b, Tomita 2001c, Tomita 2001d, Tomita 2001e, Steblyanko 2008). Kihara et al. synthesized a series of PHUs from cyclic carbonate derived from bisphenol A diglycidyl ether, hydroquinone diglycidyl ether, butanediol diglycidyl ether (see Figure 2.4a-c) with a series of aliphatic diamine and m-xylylene diamine. Reactions were performed at 70-100 °C and PHUs with molecular weight of 14-28 kDa were obtained. One of the polymers exhibits single glass transition temperature (T_g) of 34 °C. They also demonstrated the feasibility of using the hydroxyl groups for subsequent crosslinking reaction using hexamethylene diisocyanate as crosslinker in DMAc and THF (Kihara 1993). Tomita et al. also compared the reactivity of five-membered- and six-membered-ring cyclic carbonates with diamine. Both starting monomers were produced from thiol-ene addition into ene-functionalized five- and six-membered carbonate (see Figure 2.4d-e). It was found that six-membered-ring carbonate reacts faster than five membered carbonate. Increase in ring size increases the exothermic heat of reaction, indicating reactivity increases with increasing ring size (Tomita 2001a; Tomita 2001c). Tomita et al. also elucidated the detailed structure of a model PHU obtained from model single functional compounds. A variety of NMR techniques such as DEPT, COSY, ^{13}C NMR, ^{1}H NMR were used. The proportion of primary alcohol and secondary alcohols depends on the structure of amine, and solvent as well as temperatures at which the reactions were conducted (Tomita 2001b).

Tomita et al. also investigated the impact of substituents on reactivity and selectivity of five-membered-ring carbonates with amines in two different solvents using model single functional molecules. Five substituents (CF_3, $PhOCH_2$, Ph, H, and Me) were investigated and the two solvents were toluene and DMSO. Electron withdrawing substituents like CF3 were found to accelerate the reaction while solvent was found to have no impact on reactivity (Tomita 2001d).

Ochiai et al. investigated the role of several salt additives as catalyst for cyclic carbonate aminolysis. They found that lithium chloride and lithium fluoride can accelerate the reaction as interpreted from the higher conversion of cyclic carbonate attained in the presence of lithium salts (Ochiai 2005a). Later, in a one pot synthesis, Ochiai et al. synthesized PHUs by first converting bisphenol A diglycidyl ether to bisphenol A dicyclocarbonate, followed by reaction with 1,12-dodecaneamine. They also functionalized the hydroxyl groups by reacting them with acetyl chloride, benzoyl chloride, and t-butyldimethylsilyl chloride in DMF (Ochiai 2005b).

Tomita et al. also reported the synthesis of seven-membered-ring carbonate and its subsequent polymerization with small molecule diamines. The seven-membered-ring carbonate (see Figure 2.4f) was found to be more reactive than six- and five-membered-ring carbonates. Density functional theory calculations found that the ring strain energy decreases with decreasing ring size. The values of heat of reaction for model cyclic carbonate with methyl amine are 8.56, 5.58, 2.74 kcal/mole for seven-, six- and five-membered-ring carbonates, respectively (Tomita 2001e). Although seven-membered-ring carbonate has higher reactivity toward amine, the synthesis of seven-membered-ring carbonate requires the use of triphosgene and multi-step synthesis. Although triphosgene was touted to be a safer substitute to phosgene as it is a solid crystal at room temperature, its toxicity is the same as that of phosgene because triphosgene decomposes into phosgene upon heating and reaction with nucleophiles. Even a trace of moisture can lead to phosgene formation (Damle 1993).

Maisonneuve et al. (Maisonneuve 2014b) also synthesized PHUs from six-membered-ring carbonate obtained from fatty acid precursor in a four-step synthesis (see Figure 2.4g). The polymerization was conducted in DMF at room temperature and 50 °C. Kinetics studies reveal that the six-membered-ring carbonate reacts 30 times faster than the five-membered-ring carbonate equivalent. They also found that gelation occurs after the mixture was reacted for 24 hours at 50 °C. They attributed the gel formation to side reactions between hydroxyl group and

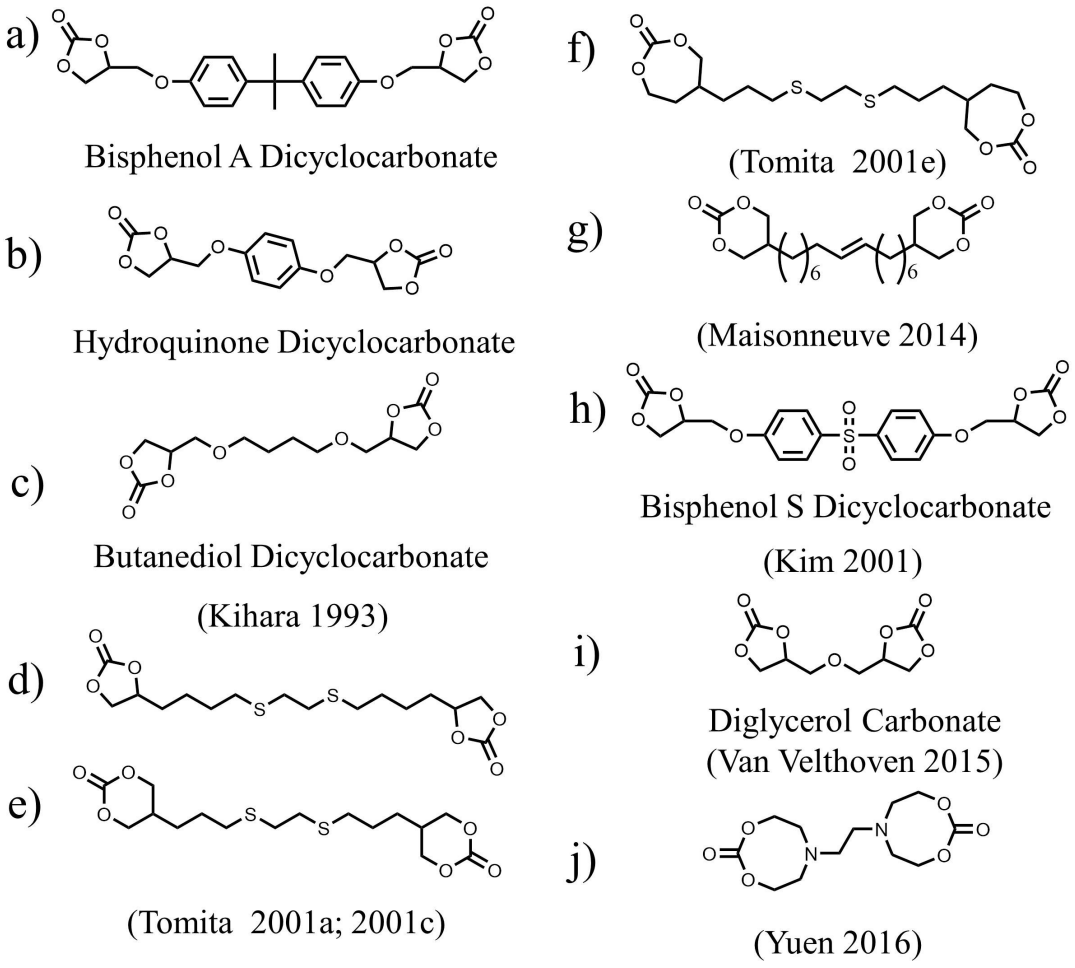

Figure 2.4: Chemical structures of carbonate monomers investigated in PHU synthesis.

cyclic carbonate resulting in carbonate linkage. After the gel was reacted with excess hexylamine, the gel became soluble again. MALDI-TOF MS analysis of the mixture confirmed that the side reaction occurred (Maisonneuve 2014b).

Other researchers have also investigated the formation of linear, single-phase PHUs. Kim et al. synthesized PHUs from bis-carbonate obtained from diglycidyl ether of bisphenol S (see Figure 2.4h) with aliphatic, cycloaliphatic and aromatic diamines (Kim 2001). The resulting PHUs have molecular weight ranging from 4.9 to 12.9 kDa, with T_gs of 55 to 102 °C. The T_gs are higher than the T_gs of PHUs reported by Endo and coworkers likely due to polar interaction between sulfone groups (Tomita 1993; Tomita 2001a; Tomita 2001b; Tomita 2001c; Tomita 2001d; Tomita 2001e). Van Velthoven et al. reported the synthesis of PHUs from diglycerol dicarbonate (see Figure 2.4i) and several (potentially) renewable aliphatic diamines such as diaminobutane, isoiodide diamine, nonanediamine, pentane diamine, and fatty acid dimer diamine. The resulting PHUs are single-phase polymers with T_g ranging from -7 to 66 ° (Van Velthoven 2015).

Very recently, Yuen et al. also described the synthesis of linear PHUs using eight-membered-ring carbonates (see Figure 2.4j). The eight-membered-ring carbonate requires multiple steps and triphosgene in its synthesis. The eight-membered-ring carbonate is much more reactive than five- or six-membered carbonates at room temperature. The molecular weights of PHUs obtained from reaction performed at room temperature with small molecule diamines range from 20 to 47 kDa (Yuen 2016). However, gelation was observed when the polymerization was conducted at 50 °C and 80 °C, which was thought to arise from possible side reaction between the pendant hydroxyl groups and the cyclic carbonate, in agreement with observation by Cramail and coworkers for six-membered-ring cyclic carbonate (Yuen 2016, Maisonneuve 2014b). Based on these studies, it is evident that although six- and higher-membered-ring carbonates are more reactive than their five-membered-ring counterpart, they suffers from side

reactions with the hydroxyl groups, which make the synthesis of linear PHUs prohibitive and more problematic.

2.5.2 Synthesis of Cross-linked PHUs

A significant number of studies also investigated the formation of networked PHU using custom-made monomers and renewable bio-based resources. Several examples are reviewed in this section.

Matsukizono and Endo synthesized networked PHU films containing positively charged moieties for potential application as antimicrobial films. They employed a six-membered-ring carbonate obtained from reaction of di(trimethylolpropane) with diphenyl carbonate. The resulting monomer was further reacted with a series of aliphatic diamine in DMF. The hydroxyl groups in these PHUs were further reacted with chloroacetyl chloride and N,N-dimethyl-n-octylamine resulting in quarternary-ammonium-chloride-functionalized PHU networked films. They also used N,N,N',N'-tetramethyl-1.6-diaminohexane to perform the quarternization reaction, simultaneously forming networked PHU films (Matsukizono 2015).

In a subsequent study, Matsukizono and Endo described another route to obtain bis(six-membered cyclic carbonate) from di(trimethylolpropane) with diphenyl carbonate. By varying the reaction condition, they were able to obtaine bifunctional cyclic carbonate monomer with carbonate in the center of the molecule. This monomer were used to form poly(carbonate hydroxyurethane). The hydroxyl groups obtained from the aminolysis of the cyclic carbonates were further reacted with succinic anhydride yielding carboxylic-acid-functionalized PHU. The resulting material is not soluble in aqueous media. To improve their solubility, the polymers were neutralized with sodium carbonate to improve their solubility. They also performed chain extension reaction of the oligomers with isothiocyanate. The reported molecular weights of these polymers were less than 10 kDa (Matsukizono 2016a).

Using trimethylolpropane, Matsukizono and Endo synthesized six-membered-cyclic carbonate molecules. This molecule contains one hydroxyl group and one 6-membered cyclic carbonate. The hydroxyl group is subsequently reacted with terepthaloyl chloride and trimesyl chloride to create difunctional and trifunctional cyclic carbonate molecules. The trifunctional carbonate and the difunctional carbonate were combined in several molar ratios and subsequently reacted with diaminopropane, diaminohexane, and diaminododecane to yield networked PHUs in DMF. The resulting films possess tensile strength ranging from 8.6 to 24.3 MPa with elongation at break ranging from 50 to 400 % (Matsukizono 2016b).

Mülhaupt and coworkers described the synthesis of cyclic carbonate monomers from glycerol in five steps. The sorbitol tricarbonate (see Figure 2.5a) is crystalline and needs to be milled for homogenization prior to reaction. The resulting sorbitol tricarbonate was cured with biobased diamine (Priamine™ 1074) and isophorone diamine at various molar ratios at 16 hours at 80 °C to get crosslinked PHUs with Young's modulus ranging from 12-630 MPa, with elongation at break ranging from as low as 0.3 to 250%. This work presents fully bio-based NIPU materials (Schmidt 2016).

Dichtel and coworkers synthesized crosslinked PHUs from the reaction of six-membered-ring cyclic carbonate obtained from di(trimethylolpropane) (see Figure 2.5b) with trifunctional tris(2-aminoethyl) amine. These crosslinked PHUs were demonstrated to be reprocessible via transurethane exchange reactions during annealing at 160 °C. The resulting materials are brittle, with tensile strength of 70 MPa, and strain-at-break of 5 %. Deterioration of properties was observed after several cycles. No catalyst was used for transcarbamoylation exchange reaction (Fortman 2015).

Soybean oil has been employed to make crosslinked PHUs in several studies (Tamami 2004; Javni 2008; Javni 2013). Wilkes and coworkers obtained carbonated soybean oil (CSBO) from epoxidized soybean oil (ESBO), and cured it with hexamethylene diamine, ethane diamine,

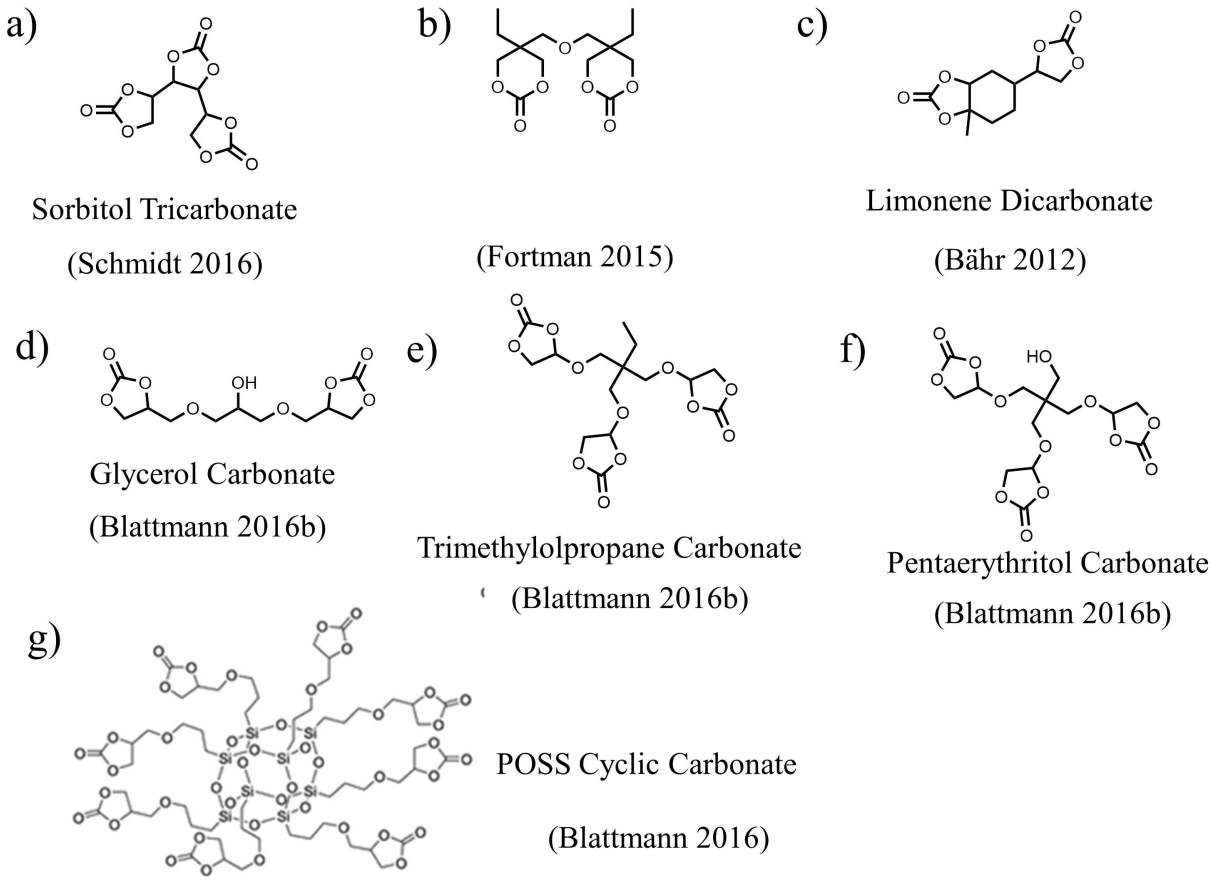

Figure 2.5: Chemical structures of carbonate monomers used in the synthesis of crosslinked PHUs.

and tris(2-aminoethyl) amine to obtain crosslinked thermosets. The resulting materials have tensile strengths ranging from 0.4 to 1.6 MPa and elongation at break from 40 to 200 % (Tamami 2004). Petrovic and coworkers also used CSBO with a series of diamines at several amine-to-carbonate ratios to synthesize crosslinked, elastomeric PHU. Due to the presence of an ester linkage in CSBO, side reaction of amine with ester resulting in amide formation was observed. This led to incomplete conversion of carbonate. The tensile strength of PHUs obtained ranges from 0.5 to 5.8 MPa (Javni 2008). Later, they employed cyclic isophorone diamine, m-xylylene diamine, and p-xylylene diamine to cure CSBO, resulting in PHUs with tensile strength ranging from 0.3 to 11.1 MPa with variable elongation at break from 3 to 200 % (Javni 2013).

Bähr and Mülhaupt used CSBO and carbonated linseed oil, isophorone diamine, diaminobutane, and ethylene diamine to synthesize crosslinked PHUs. These PHUs exhibit a range of properties from brittle to ductile materials, with T_g ranging from 12 to 60 °C, tensile strengths from 2 to 17 MPa. Later, they converted glycerol glycidyl ether, trimethylolpropane, and pentaerythritol glycidyl ether to carbonate via high pressure CO_2 synthesis (see Figure 2.5d-f). These carbonates were cured with hexamethylene diamine and citric acid amino-acid diamine. The resulting networked materials had T_gs ranging from 20 to 56 °C (Bähr 2012b). In another study, Bähr and Mülhaupt use utilize limonene to be converted into epoxide-functionalized limonene which is further converted into limonene dicarbonate (See Figure 2.5c). The resulting PHUs were brittle thermosets having tensile strength from 7 to 21 MPa and T_g from 55 to 70 °C (Bähr 2012b).

Blattmann and Mülhaupt use glycidyl-ether-functionalized polyhedral oligomeric silsequioxanes to be converted into POSS cyclic carbonate (see Figure 2.5g). By mixing it with glycerol carbonate, trimethylolpropane cyclic carbonate, and pentaerythritol cyclic carbonate (see Figure 2.5d-f), they further cured it with isophorone diamine and hexamethylene diamine to create hybrid organic/inorganic thermosets. The resulting thermosets were generally brittle

materials with elongation at break of less than 10 % with tensile strengths ranging from 10 to 90 MPa. They also demonstrated the utility of the synthesized materials in coating application (Blattman 2016b).

Poussard et al. also employed CSBO to make crosslinked PHUs. The CSBO was cured with amino-telechelic oligoamide. The PHU networks have Young's modulus ranging from 2 to 200 MPa, tensile strengths ranging from 2.5 to 3.3 MPa, and elongation at break from 13 to 350 percent. The PHUs also exhibited melt transition in the range of 77 to 85 °C due to the presence of amine-telechelic amide chain extender (Poussard 2016).

2.5.3 Synthesis of Segmented PHUs.

Since the commencement of research efforts documented in this thesis, there are only two published reports in the open literature on the synthesis of segmented PHUs. Nanclares et al. reported the synthesis of segmented PHUs using 1000 g/mole cyclic-carbonate-terminated PTMO, bisphenol A dicarbonate, and m-xylylene diamine. The hard-segment contents investigated were 30, 50 and 70 wt %. PHU with 30 wt% hard-segment is phase-mixed, single-phase PHU. PHU at 50 wt% hard-segment content exhibit elastomeric-like while PHU at 70 wt% hard-segment content is brittle. The impact of hydroxyl group on nanophase separation was not investigated and the reversibility of extension in their PHU samples was not demonstrated. An attempt was made to compare the properties of one of their PHUs with PU synthesized with MDI, PTMO and 1,4-butanediol (1,4-BDO) as chain extender. However, this comparison was done using PU with 70 wt% hard-segment, which is a glassy material and thus unsuitable for thermoplastic elastomer application (Nanclares 2015).

Long and coworkers reported the synthesis of segmented poly(hydroxyurethane amide) using Jeffamine THF-1000 (a copolymer of propylene oxide and tetramethylene oxide with M_n = 1000 g/mole), 1,12-diaminododecane as the chain extender, and 9,10-cyclic carbonate-methyl

undecanoate as the hard segment. The resulting polymers have alternating hydroxyurethane and amide bonds. The phase separation is driven by crystallization of the hard segment facilitated by hydrogen bonding of amide groups. PHUs with hard-segment content ranging from 33 to 90 % possessed nanophase-separated morphology as verified by small-angle X-ray scattering (SAXS) and atomic force microscopy (AFM). The hard domain was crystalline as verified by wide-angle X-ray diffraction (WAXD) and differential scanning calorimetry (DSC). These polymers had tensile strengths of 2.1 to 5.7 MPa and elongation at break values below 60 %. These elongation at break values are significantly lower than those of conventional thermoplastic polyurethane elastomer and other TPEs. Similar to the report by Nanclares et al., Long and coworkers did not demonstrate the reversibility of extension of their materials (Zhang 2016).

It is evident that there is a very limited understanding on the properties of segmented, nanophase-separated PHU, the influence of hydroxyl groups on nanophase separation, as well as how to control and tune the properties of segmented PHU.

2.6 Thermoplastic Polyurethane Elastomers, Hydrogen Bonding and Nanophase Separation

Thermoplastic elastomers (TPEs) are a class of polymeric materials which combine the processing characteristics of thermoplastics with the physical properties of crosslinked rubbers. The defining feature of TPEs is their phase-separated structure, with hard domains dispersed in a soft rubbery matrix. Unlike vulcanized rubber where the chains are held together by covalent crosslinks, the hard domains in TPEs are physical crosslinks, which soften upon heating at elevated temperatures. The ability of TPEs to become fluid on heating and solidify upon cooling allows them to possess rubber-like characteristics and to be processed with common thermoplastic processing equipment such as injection molding, extruders, etc. (Holden 2004).

TPEs generally possess two types of chemical structure: A-B-A or $(A\text{-}B)_n$ where A

represents the hard phase and B represents the soft phase. A wide range of chemical structures and molecular architectures made up TPEs. These include styrenic block copolymer, polyolefin block copolymer or multiblock polyolefin copolymer, segmented PU, segmented polyester, segmented polyamide, ionomers, polyacrylate-based block copolymers etc. Common examples of styrenic thermoplastic elastomers are styrene-butadiene-styrene (S-B-S) and styrene-isoprene-styrene (S-I-S) triblock copolymers made using anionic polymerization. These block copolymers have two T_gs because of strong phase separation between the polystyrene and polydiene phase. Polyolefins are also used to make TPEs. Their structure consists of blocks of crystalline and amorphous chain. For example, random stereoblock polypropylene with an alternating noncrystalline atactic polypropylene block and a crystalline isotactic polypropylene block. Other examples include random block copolymers of ethylene-propylene, ethylene-α olefin, or propylene-α olefin. Segmented PU, polyamide and polyesters are $(A\text{-}B)_n$ type of copolymers having alternating sequences of low T_g segment and high T_g amorphous or high T_m crystalline segments. Although TPEs exhibit elastomeric character like crosslinked rubber, they often exhibit hysteresis, permanent set, and softening in their cyclic stress-strain responses. This can be attributed to the breakage and reformation of hard domains. In nanophase-separated, thermoplastic PU elastomer, the hard domains are held together by interurethane hydrogen bonding.

According to IUPAC, hydrogen bonding is an attractive interaction between a hydrogen atom from a molecule or a molecular fragment X-H in which X is a highly electronegative atom, and an atom or a group of atoms in the same or a different molecule. Hydrogen bond may be depicted as X-H---Y-Z, where X-H represents the hydrogen bond donor, and Y-Z represents the hydrogen bond acceptor. X is usually highly electronegative atoms such as oxygen, fluorine, or nitrogen. In some cases, X and Y are the same atoms (Arunan 2011). Hydrogen bonding plays an important role in nanophase separation of segmented PUs. Interurethane hydrogen bonding holds

the hard segment of segmented PU together. The hydrogen bond donor in PU is the NH group in the urethane bond. The hydrogen bond acceptors can be a urethane carbonyl, C=O, or an ether oxygen, C-O-C and an ester carbonyl, C=O in the soft segment. Infrared analysis has revealed that a significant fraction (ranging from 60-80 %) of carbonyl groups in TDI-based PU are hydrogen bonded to the urethane NH groups (Sung 1975; Sung 1977; Sung 1978; Seymour 1970; Yilgor 2006).

A significant fraction of PUs is segmented copolymer, the structure of which contains alternating sequences of hard and soft domains. As such, a significant fraction of PUs exhibit nanophase-separated morphology with nano-sized domain. The degree and kinetics of phase separation in segmented PUs has been the subject of extensive investigations for many decades (Bonart 1974, Choi 2009, Castagna 2012, Abouzahr 1981, Chu 1992, Li 1992a, Li 1992b). A number of experimental techniques can be used to probe nanophase separation in segmented PUs including differential scanning calorimetry, SAXS, infrared spectroscopy, dynamic mechanical analysis, and microscopy techniques such as transmission electron microscopy and atomic force microscopy (Bonart 1974, Choi 2009, Castagna 2012, Abouzahr 1981, Chu 1992, Li 1992a, Li 1992b).

SAXS is used to provide assessment of nanophase separation in the bulk material morphology. Analysis of the degree of phase separation can be obtained through comparison of experimentally observed electron density variance with theoretical electron density variance calculated by assuming complete phase separation, using the method by Bonart and Muller (Abouzahr 1982, He 2014, Bonart 1974, Li 1992a, Li 1992b, Li 1993, Li 1994). Infrared spectroscopy was often used to analyze the degree and kinetics of phase separation in various PU systems. This technique relies on the presence of distinct spectral bands associated with mixed and phase-separated states. For example, hydrogen-bonded carbonyl group gives rise to the band at ~1700 cm^{-1} whereas free, non-hydrogen bonded carbonyl give rise to the band at ~1730 cm^{-1}.

Relative proportion of free and hydrogen-bonded carbonyl gives a measure of phase separation. Analysis of degree of phase separation with DSC typically employs comparison of the value of soft-segment T_g location relative to the T_g of pure soft-segment homopolymer. Comparisons of hard-segment T_g relative to its pure hard-segment homopolymer is less commonly used due to difficulties in observing hard-segment T_g by DSC. Another approach of assessing the amount of phase separation is by calculating the specific heat capacity increase of soft-segment domain relative to the soft-segment homopolymer. AFM phase imaging has also been used to demonstrate the presence of nanophase separation. TEM can also be used if enough contrast between phases could be obtained.

The aminolysis of cyclic carbonate produce a urethane linkage and a hydroxyl groups. The hydroxyl group is a hydrogen donor. It is capable of forming hydrogen bonding within the hard-segment domain and potentially to the soft segment. At the commencement of research documented in this thesis, there has been no investigation on the synthesis of segmented PHUs. As such, the role of hydroxyl group in controlling nanophase separation in segmented PHU and its effect on the properties of segmented PHU are unknown. Consequently, there was a lack of understanding of how to control their properties.

2.7 Structure-Property-Relationships in Segmented PUs

Segmented PUs are synthesized from a combination of hard segment, soft segment and chain extender. The physical properties of segmented PUs are significantly controlled by their molecular structures of components used in the synthesis and their relative compositions. In this section, past studies on structure-property-relationships of segmented PUs are reviewed.

2.7.1 Influence of Diisocyanate Hard-Segment Structure

Hard-segment structure plays a significant role in controlling the nanophase separation

and the resulting thermal and mechanical properties of segmented PUs as shown by many studies. Sheth et al. investigated the role of diisocyanate symmetry on the properties of segmented PU and segmented polyurea. The copolymers were synthesized using hydroxyl-terminated PTMO for PU or aminopropyl-terminated PTMO (M_n 1000 g/mole) for polyurea, and 1,4-phenylene diisocyanate (*p*PDI) or 1,3-phenylene diisocyanate (mPDI) as the hard segment. No chain extender was used in their study. The PU and polyureas were characterized with DMA, DSC, tensile testing, and WAXD. PU made with mPDI was phase-mixed with flow temperature of 0 °C, whereas that made with *p*PDI was nanophase-separated and possessed a wide rubbery plateau region with a flow temperature (T_{flow}) of 50 °C. The hard segment of PU made with *p*PDI was crystalline as confirmed by DSC and WAXD. When the urethane bond with monodentate hydrogen bonding was replaced by urea with bidentate hydrogen bonding, both diisocyanates led to nanophase-separated polymers. However, polyurea made with mPDI had a significantly narrower rubbery plateau region and lower T_{flow} than its *p*PDI counterpart. This study demonstrated the important role of hard-segment molecular symmetry on PU properties. The symmetrical nature of *p*PDI allows for better hard-segment association and therefore better interurethane hydrogen bonding resulting in better properties than its mPDI counterpart (Sheth 2005).

The effect of hard-segment symmetry on the extent of hydrogen bonding was also investigated by Sung and Schneider using IR spectroscopy (Sung 1975, Schneider 1975). Sung and Schneider compared PUs made with PTMO (M_n 1000 g/mole) as soft segment, 2,4-TDI or 2,6-TDI as hard segment, and 1,4-BDO as chain extender at several hard-segment contents. Investigation of urethane carbonyl stretching vibration at ~1730 cm^{-1} (free carbonyl) and at ~1700 cm^{-1} (hydrogen-bonded carbonyl) indicated that PU with the more symmetric 2,6-TDI had a higher fraction of hydrogen bonded carbonyl (~ 80 %) in comparison to PU with 2,4-TDI (~50 %) (Sung 1975). The two PUs also exhibited different thermal properties. Using

thermomechanical analysis (TMA), Schneider and coworkers showed that 2,4-TDI PU exhibited three thermal transitions whereas 2,6-TDI PU exhibited only two thermal transitions. The middle transition in 2,4-TDI was thought to arise from the glass transition of amorphous hard segment of 2,4-TDI. The absence of midpoint transition for 2,6-TDI PU was thought to be caused by its highly ordered structure. WAXD study indicated that PU with 2,4-TDI showed no indication of crystallinity whereas PU with 2,6-TDI possessed crystalline hard domains. Using DSC measurement, they showed that the soft-segment T_g increases with increasing hard-segment content in 2,4-TDI PU series whereas the soft-segment T_g remained invariant with increasing hard-segment content in 2,6-TDI PU series, indicating a better degree of nanophase separation in 2,6-TDI PU series (Schneider 1975).

Lee and Tsai investigated a series of PUs made from PTMO soft segment (M_n = 2000 g/mole), 1,4-BDO as chain extender and a series of diisocyanates: MDI, 2,4-TDI, hydrogenated MDI (HMDI), isophorone diisocyanate (IPDI) and 1,6-hexane diisocyanate (HDI) with a 40 wt% hard-segment content. Diisocyanate structure has a significant influence on the tensile properties. They showed that MDI-based PU exhibited the highest tensile strength and IPDI-based PU the lowest tensile strength (Lee 2000). The relatively high tensile strength of the MDI-based material was attributed to the more symmetrical molecular structure of MDI which allows for better association, organization and packing of the hard domain. DSC characterization showed that MDI-based PU and other PUs with aromatic diisocyanate have higher soft-segment T_gs compare to PUs with aliphatic diisocyanate. Higher soft-segment T_g is often associated with a lower degree of nanophase separation, but, in this study, MDI-based PU showed the highest tensile strength in comparison to other PUs made with aliphatic diisocyanate suggesting that tensile strength might not be correlated with the strength of nanophase separation.

Kojio et al. investigated a series of PUs prepared from PTMO (M_n = 2000 g/mole), 1,4-BDO, and several diisocyanates including norbornane diisocyanate (NBDI), HDI, HMDI, and

IPDI. The tensile strength decreased as follows: HDI > NBDI > HMDI > IPDI. The HDI-based and HMDI-based PU possessed crystalline hard segments whereas the hard segments of other PUs are amorphous. The HDI-based PU exhibited the highest Young's modulus, tensile strength and elongation at break, which were thought to arise from a highly crystalline hard segment and strong nanophase separation. In this study, HDI-based PU also exhibited the lowest soft-segment T_g by DSC and a higher proportion of hydrogen-bonded carbonyl by IR, in agreement with a higher degree of nanophase separation (Kojio 2007).

Seefried et al. investigated the effect of diisocyanate structures on the properties of PU made with polycaprolactone diol (M_n 2100 g/mole), and 1,4-BDO with MDI and TDI as hard segments (Seefried 1975a). Three hard-segment contents were investigated. In the TDI-based system, the increase in hard-segment content increases soft-segment T_g as observed via the peak in DMA loss modulus. In the MDI-based system, no change in soft-segment T_g was observed with increasing hard-segment content. The invariance of soft-segment T_g with increasing hard-segment content is consistent with a high degree of nanophase separation (Brunette 1981a, Brunette 1981b, Schneider 1979, Bengston 1985). Seefried et al. noted that the amorphous nature of TDI-based hard segment may result in considerable intermixing with the soft-segment domain, whereas the MDI-based system has a more perfect domain organization due to its crystalline nature. In two of the three hard-segment contents investigated, MDI-based PUs possessed higher tensile strengths than TDI-based PUs (Seefried 1975a).

Wingborg compared the tensile properties of PBD-based PUs made with IPDI and HMDI hard segments at several hard-segment contents made using two chain extenders: 1,4-BDO and 1,3-cyclohexanedimethanol. The tensile strengths of HMDI-based PUs were superior to IPDI-based PUs at all hard-segment contents investigated with both chain extenders, probably due to the more symmetrical structure of HMDI molecule. The tensile strengths of PBD-based PU are lower in comparison to other PUs with polyether or polyester-based soft-segment (Wingborg

2002, Schneider 1979, Bengston 1985, Lee 2000, Kojio 2007).

2.7.2 Influence of Soft-Segment Structure

Segmented PUs can be synthesized from a variety of soft-segments including polyether (such as PEO, PPO, PTMO etc.), polyester (polycaprolactone, polybutylene adipate, poly hexamethylene adipate etc.), polybutadiene, polyisobutylene, and polydimethysiloxane. The soft-segment structure dictates the degree of nanophase separation in segmented PU and can influence the resulting thermal and mechanical properties.

Korley et al. studied the influence of soft-segment structure on properties of segmented PUs made with HDI. The soft segments studied were PEO with M_n of 1000 and 4000 g/mole, and PEO-PPO-PEO copolymer with M_n of 1900 g/mole. All soft segments studied produced nanophase-separated materials as confirmed via SAXS and AFM. The PEO-PPO-PE PUs exhibited a higher degree of nanophase separation relative to PEO-based PUs. This claim was based on observation that PEO-PPO-PEO-based PUs had higher hard-segment crystallinity (with higher hard-domain melting temperature and enthalpy of fusion) than PEO-based PUs. The PPO block was thought to improve the degree of nanophase separation in PEO-PPO-PEO-based PU (Korley 2006). This was further verified in a subsequent study by Waletzko et al. using AFM (Waletzko 2009). The PEO-based PUs also exhibited superior tensile strengths than PEO-PPO-PEO-containing PUs. This was explained in terms of the presence of soft-segment crystalline ordering in PEO-based PU, serving as additional reinforcing fillers which act as stress-bearing components during tensile deformation. Soft-segment crystallization was suppressed in PEO-PPO-PEO-based PU due to presence of a PPO midblock (Korley 2006).

Chu and coworkers studied the impact of soft-segment structures on the degree of phase separation using SAXS by comparing PEO/PPO- and PTMO-based soft segments. The segmented PUs were made with MDI hard segment and 1,4-BDO as chain extender. The ratio of

experimentally-determined integrated scattered intensity or invariant to theoretical value of invariant gives an estimate of the degree of phase separation. The degree of phase separation was higher in the PTMO-based system compared to the PEO/PPO-based system (Chu 1992). Using a similar treatment to SAXS data, Fragiadakis and Runt also compared the degree of phase separation in MDI/BDO segmented PUs with a more extensive set of soft segments, namely PTMO, polyhexamethylene oxide (PHMO), poly(1,6-hexyl-1,2-ethyl carbonate) diol (PHCE), and polydimethylsiloxane. The degree of nanophase separation decreases in the following order: PDMS > PHMO > PTMO > PHEC. This observation can be rationalized using a progressive decrease in the density of hydrogen bond acceptor (ether oxygen in PHMO and PTMO or carbonate carbonyl in PHEC), moving from PHMO-, PTMO- to PHEC-based systems to a PDMS soft segment is highly incompatible with urethane hard segment (Fragiadakis 2013).

Cooper and coworkers also investigated the effects of soft-segment structure on the degree of nanophase separation in PUs made with monodisperse MDI-BDO hard segments. The soft segments investigated were PEO, PPO, PTMO with M_n ~ 1000 g/mole and PBD with M_n of 2000 g/mole. By comparison of carbonyl stretching vibration using IR spectroscopy, they found that the fraction of hydrogen-bonded carbonyl to free carbonyl decreases in the order PBD > PTMO > PPO > PEO, which is consistent with a decrease in the degree of nanophase separation in the same order. From DSC measurements, it was also found that the elevation of the soft-segment T_gs relative to the T_gs of their corresponding soft-segment homopolymers increases in the order PBD < PTMO < PPO < PEO, respectively, suggesting increasing level of phase mixing in the same order (Hwang 1984).

Nonpolar soft segments such as PBD, polyisobutylene, and PDMS are known to produce segmented PUs with the highest degree of nanophase separation. DSC investigations of many PBD-based PUs showed that their soft-segment T_gs are elevated by only a few degrees from the T_g of PBD homopolymer (Bengston 1985, Brunette 1981, Fu 1986, Schneider 1975, Schneider

1979, Hwang 1984). The invariance of the soft-segment T_gs with increasing hard-segment content indicated that PBD-based PUs have a very high degree of nanophase separation. SAXS investigation by Chen-Tsai et al. showed that PBD-based segmented PU exhibited the lowest degree of interfacial mixing (or the highest degree of nanophase separation) as well as the sharpest domain interphase in comparison with polyether- and polyester-based segmented PUs (Chen-Tsai 1986). While a high degree of nanophase separation can be obtained by using nonpolar soft segments like PBD, polyisobutylene and PDMS, it can also lead to inferior mechanical properties. Strong nanophase separation can lead to sharp domain interphase with weaker interfacial adhesion resulting in poor stress transfer during uniaxial elongation and consequently, a lower tensile strength (Speckhard 1983, Speckhard 1985a, Speckhard 1985b, Speckhard 1986).

2.7.3 Influence of Chain Extender Structure

Chain extender structure can also be used to tune and control the properties of segmented PUs. Bae et al. studied a PU system made from PTMO (with M_n=1000 g/mole) and MDI with several aliphatic and cycloaliphatic chain extenders at a hard-segment content of 50 wt%. The chain extenders are 1,3-propanediol, 1,4-BDO, 1,5-pentanediol, 1,4-pentanediol, 2,5-hexanediol, 2,5-dimethyl-2,5-hexanediol, 1,4-cyclohexanediol, 1,4-cyclohexanedimethanol (Bae 1999). From DMA results, they found that cycloaliphatic chain extender increases the T_{flow} of PU. Within the series of aliphatic chain extender studied, PU chain extended with 1,4-BDO shows the highest upper softening temperature and highest room temperature storage modulus. This result is in agreement with results obtained by Adhikari et al. who investigated PU systems made from hydrogenated MDI and a soft segment involving a mixture of polydimethylsiloxane and polyhexamethylene oxide (Adhikari 1999). PU chain extended with BDO also yields the highest value of tensile strength and Young's modulus. Blackwell et al. showed that that BDO affords

the formation of crystalline hard domain due to its ability to adopt a low energy conformation resulting in better packing (Blackwell 1981). Chattopadhyay et al. investigated moisture-cured polyurethane-urea with a series of chain extenders and concluded that more bulky chain extenders promote better phase mixing than linear chain extender like BDO (Chattopadhyay 2005).

2.7.4 Studies on Diamine Diamide Chain Extender

Amide-based chain extenders have also been investigated in detail by Gaymans and coworkers in segmented PU synthesis. The use of amide-based chain extenders was expected to drive the phase separation through hard-segment crystallization (Van der Schuur 2006; Biemond 2008; De 2009; Biemond 2012). Van der Schuur et al. investigated segmented polyurethane-urea-amide (PUUA) copolymers using PPO (M_n 2000 g/mole), TDI and hexamethylene-terephthalate diamine diamide chain extender (6T6, see Figure 2.6a) (Van der Schuur 2006). The PUUA copolymers were synthesized in DMAc and exhibited very wide, temperature-independent rubbery plateau regions ranging from 128 °C to greater than 200 °C depending on the number of repeat units in the 6T6 chain extender. The T_{flow} values of the PUUA copolymers, associated with the melting points of the hard-segment domains, ranged from 103 to 264 °C. The tensile strength values of these copolymers ranged between 4 to 10 MPa, lower than values reported for PPO-based polyurethane-urea reported by O'Sickey et al. made without using amide-based chain extender (O'Sickey 2001). A control PU synthesized without 6T6 chain extender exhibited narrower, more temperature-dependent rubbery plateau region, non-crystalline hard segment and a lower T_{flow} of 150 °C.

Biemond et al. investigated hexamethylene-adipate diamine diamide chain extender (6A6, see Figure 2.6b), a variant of 6T6 chain extender based on adipic acid, in segmented PUs made from PTMO (M_n ~2000 g/mole) and three diisocyanates (MDI, TDI, and HDI) as hard

a)

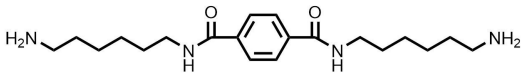

6T6 Chain Extender

b)

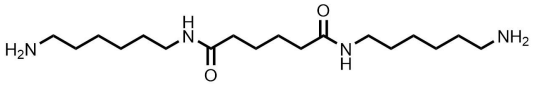

6A6 Chain Extender

Figure 2.6: Chemical structures of amide-based diamine diamide chain extenders.

segments (Biemond 2008). All the three PUUA copolymers exhibited very wide, relatively temperature-independent, rubbery plateau regions. The hard-segment crystallinity and melting points depends on the structure of diisocyanates. Melting points decrease in the following order TDI < MDI < HDI. DSC characterization from the second heating cycle revealed no crystallization or melting peaks in 2,4-TDI-based PUUA copolymer indicating that the crystallization was slower and the crystallinity was lower with 2,4-TDI. The PUUA copolymers in this study exhibited moderate tensile strengths, ranging from 5 to 11 MPa, lower than the values reported by Lee et al. and Kojio et al. for PTMO-based system synthesized without amide-based chain extender. (Lee 2001, Kojio 2007) Elongation at break values of the PUUA copolymers were not reported. (Biemond 2008)

De and Gaymans further investigated the 6T6 chain extender in PTMO-based soft segments having molecular weight ranging from 2250 to 6500 g/mole. The hard segment is a mixture of 2,4-TDI and 2,6-TDI (De 2009). Similar to the study by Van der Schuur et al., the hard segments of PUUA copolymers in this study are crystalline with melting points ranging from 166 to 197 °C. The tensile strength values of these PUUA copolymers range from 6 to 14 MPa and elongation at break ranges from 500 to 670 % (Van der Schuur 2006; De 2009). Biemond et al. systematically investigated a series of diamine-diamide, diamine-diol and diol-diester chain extenders in segmented PU based on HDI hard segment. Segmented PUs with diamine-diamide chain extenders with two urea groups, two urethane groups, and two amide groups have the highest number of hydrogen bonds and the highest melting temperatures (186-251 °C). Segmented PUs with diol-diamide chain extenders with four urethane groups and two amide groups, displayed lower melting temperatures (140-160 °C). Segmented PUs with diol-diester chain extenders containing four urethane groups displayed the lowest melting temperatures (80-100 °C) (Biemond 2012).

The abovementioned studies by Gaymans and coworkers showed that amide-based chain

extenders are useful in enhancing the thermal properties of segmented PUs through crystallization of hard segment, but not necessarily useful in enhancing their tensile properties. (Van der Schuur 2006; Biemond 2008; De 2009; Biemond 2012). The effects of these amide-based chain extenders on segmented PHU properties are not known, at present.

CHAPTER 3

Non-Isocyanate Thermoplastic Polyhydroxyurethane Elastomer Via Cyclic Carbonate Aminolysis

3.1 Introduction

Thermoplastic polyurethane elastomers (TPUs) are commonly produced by reaction of isocyanate-terminated prepolymers with low molecular weight (MW) diols; the prepolymers are formed by reaction of a long-chain polyol with an excess of diisocyanate and subsequently chain extended with small molecule diol. The final material possesses nanophase-separated morphology with hard segments dispersed in a rubbery soft-segment matrix. The hard segments act as physical crosslinks which promote elastomeric character (Oertel 1994, Holden 2004). Although these materials are commonly referred to as elastomers, hysteresis is usually observed in reversible elastomeric response (Qi 2005, Kim 1999). Global polyurethane (PU) production is expected to reach 18 million tons in 2016 (Nohra 2013), with TPUs accounting for 5% of the global PU market (Research and Markets 2013). Despite diverse and wide ranging applications of PUs, there has been increased regulatory scrutiny concerning the safe use and transport of isocyanates (US EPA 2011, OSHA 2014). Consequently, research into alternative pathways to PU or PU-like materials has intensified with aminolysis of 5-membered-ring cyclic carbonates to produce polyhydroxyurethane (PHU) being one of the most promising chemistries (Guan 2011, Kathalewar 2013, Blattmann 2014, Maisonneuve 2015).

Polyhydroxyurethane is analogous to PU with the exception of primary or secondary alcohol groups adjacent to the urethane linkage. Much focus within this research area has centered on production of cyclic-carbonate-functional monomers (Kim 2001, Pyo 2011, Comerford 2015, Kihara 1993a), reaction catalysis (Ochiai 2005a, Lombardo 2015, Lambeth

2013), and syntheses of single-phase linear PHU (Kihara 1993b, Tomita 2001d, Tomita 2001b) and of cross-linked PHU via renewable and other resources (Bähr 2012, Firdaus 2013, Javni 2008, Fleischer 2013, Blattmann 2016). No study has yet investigated the effects of the hydroxyl groups present in PHU on the development of elastomeric-like character or compared properties of PHUs to those of structurally analogous PUs. Nanclares et al. (Nanclares 2015) published the first and only study in which phase-separated, segmented thermoplastic PHUs were synthesized. They used a polytetramethylene oxide (PTMO)-based soft segment, bisphenol A dicarbonate, and *m*-xylylenediamine. Only one of three formulations studied by Nanclares et al. (Nanclares 2015) exhibited elastomeric-like tensile response (with 50% hard-segment content); there was no examination of reversibility of extension, and the resulting PHUs exhibited mechanical properties inferior to traditional PUs (Oertel 1994, Holden 2004). In only one case did they compare PHU to PU; the comparison was made with 70% hard-segment PHU, resulting in a glassy, brittle polymer exhibiting 6% elongation at break. Furthermore, the comparison PU was structurally very different from the PHU. Regarding their PU/PHU comparison, Nanclares et al. stated, "The effect of hydroxyl groups on mechanical properties is not clear because other structural differences are large." (Nanclares 2015) In order to determine the effects of hydroxyl groups in thermoplastic PHUs on the development of nanophase separation and elastomeric-like character, a comparison is needed between structurally analogous PU and PHU in which the hard segment does not constitute the majority of the polymer.

In this chapter, we present the synthesis and characterization of segmented, thermoplastic PHU elastomer. We also present the first comparison of a segmented, thermoplastic PU with elastomeric-like character to a structurally analogous (with the exception of hydroxyl groups) PHU.

3.2 Experimental

3.2.1 Materials

1,3-diaminopropane (Sigma-Aldrich, 99%), 1,3-phenylene diisocyanate (Sigma-Aldrich, 95%), 1,4-phenylene diisocyanate (Sigma-Aldrich), 1,3-cyclohexanebis(methylamine) (Sigma-Aldrich, 99%), *m*-xylylenediamine (Sigma-Aldrich, 99%), tetrabutylammonium iodide (Sigma-Aldrich, 98%),di amine-terminated polyethylene oxide (PEO) (Huntsman, Elastamine HE-1700), and diamine-terminated PTMO (Huntsman, Elastamine HT-1700) were used as received. Poly(ethylene glycol) (Polysciences, Inc., M_n ~1000) and 1,3-propanediol (Sigma-Aldrich, 98%) were heated to 110 °C in round bottom flasks with a dry N_2 purge for 12 hr prior to use to remove any residual water. Dibutyltin dilaurate (Sigma-Aldrich, 95%) was placed on activated 4Å molecular sieves prior to use. Polypropylene glycol (PPG) diglycidyl ether (Sigma-Aldrich, average M_n ~640), poly(ethylene glycol) diglycidyl ether (Polysciences, Inc., M_n ~1000), and 1,4-di(oxiran-2-yl)benzene (Divinylbenzene dioxide (DVBDO) or Dow Epoxy-12) were each reacted with dry, high purity CO_2 in the presence of tetrabutylammonium iodide catalyst to produce cyclic-carbonate-terminated monomers in a procedure similar to Kihara et al. (Kihara 1993a, Kihara 1993b) N,N-Dimethylacetamide (Sigma-Aldrich, 99%), dichloromethane (Sigma-Aldrich), acetone (Sigma-Aldrich, 99.5%), N,N-dimethylformamide (Sigma-Aldrich, 99.8%), and toluene (Sigma-Aldrich, 99.5%) were used as received for the synthesis of carbonate-terminated monomers and PTMO-based PHUs.

3.2.2 Synthesis

3.2.2.1 Synthesis of 4,4'-(1,4-phenylene)bis(1,3-dioxolan-2-one), otherwise referred to as divinylbenzene dicyclocarbonate (DVBDCC)

To create the hard segment used in this study, a CO_2 insertion reaction was completed on 1,4-di(oxiran-2-yl)benzene (Dow Epoxy-12). This reaction produced a difunctional cyclic

carbonate monomer with a backbone structurally identical to an isomeric mixture (67% 1,3-isomer, 33% 1,4-isomer) of phenylene diisocyanate. In a typical synthesis, 1,4-di(oxiran-2-yl)benzene (DVBDO) (39.3 mL, 308 mmol) and tetrabutylammonium iodide (TBAI) (11.4 g, 30.8 mmol) were added to a round bottom flask along with a stir bar and septa. The reaction flask was flushed with CO_2. Then, a balloon of CO_2 gas was fitted to the septa, and the reaction flask was heated to 80 °C. After 5 days, 15 mL of dimethylacetamide (DMAc) was added to the solid and the mixture was left to react until completion. The reaction progress was monitored by ^{1}H NMR until completion (disappearance of epoxide and formation of cyclic carbonate). Upon completion, 50 mL dichloromethane (DCM) was added to the reaction mixture followed by 50 mL water. The slurry was concentrated to remove DCM. The aqueous mixture remaining contained precipitated product, and after the aqueous solvent was decanted, 30 mL acetone was added to the solid. The mixture was stirred to form a slurry, and then 100 mL water was added to precipitate the product. The solvent was decanted, and the product was dried under vacuum.

3.2.2.2 Synthesis of Cyclic-Carbonate-Terminated PPG- and PEG-based Soft Segments

In order to create the analogous PHU for comparison to a traditional PEG-based PU, a carbonate-functional PEG-based soft segment had to be synthesized. A CO_2 insertion reaction into an epoxy moiety was used to create cyclic carbonate functionality. To examine the effects of soft-segment backbone on segmented PHU synthesis, PPG-based diglycidyl ether was also reacted with CO_2 to create the 730 g/mol PPG-based cyclic-carbonate-functional soft segment. In a typical synthesis, 640 g/mol PPG diglycidyl ether (50 g, 78 mmol) and TBAI (2.9 g, 7.8 mmol) were added to a round bottom flask equipped with magnetic stirring and septa. The reaction flask was flushed with dry CO_2, and a balloon of CO_2 was fitted into the septa. The reaction mixture was heated to 80 °C, and the CO_2 balloon was refilled as needed until complete disappearance of epoxy functionality was confirmed using ^{1}H NMR (typically 7 days of reaction). After complete

conversion of epoxy to cyclic carbonate was achieved, the material was dissolved in toluene to precipitate the TBAI catalyst. The catalyst was removed using multiple centrifugation steps. A rotovap was used to remove the remaining toluene from the cyclic-carbonate-functionalized PPG- and PEG-based soft segments.

3.2.2.3 Synthesis of Traditional PEG-based PU

To create the traditional PU depicted in Scheme 3.1 (PU-PEG/PDO/30), a prepolymer-based PU synthesis was completed. In a typical synthesis, 1,3-phenylene diisocyanate (9.0 g, 56 mmol) and 1,4-phenylene diisocyanate (4.4 g, 28 mmol) were charged into a round bottom flask equipped with a dry N_2 purge, overhead stirring, and an addition funnel. A mixture of isocyanate isomers was employed (67% 1,3-isomer, 33% 1,4-isomer) in order to directly compare to the PHU made with DVBDCC which exists as a mixture of 1,3 and 1,4 isomers. Following the isocyanate addition, 1000 g/mol dried PEG (40 g, 40 mmol) was added dropwise through the addition funnel. After complete addition of polyol the material was mixed for 30 min to create a uniform solution. After 30 min, dibutyltin dilaurate (0.01 wt%, 5.3 mg, 5.0 µL) was added, and the round bottom flask was placed in an oil bath at 80 °C. The reaction proceeded for 2 hr, and the resultant prepolymer was poured into Flacktek max 20 mixing cups and weighed. A 10% loss in isocyanate groups was assumed before calculating the amount of 1,3-propanediol chain extender to add. In a typical chain extension reaction, the prepolymer (14.5 g prepolymer, 11 mmol diisocyanate groups) was mixed with dry 1,3-propanediol (0.82 g, 11 mmol, 0.78 mL) and dibutyltin dilaurate (0.01wt%, 1.5 mg, 1.4 µL) using a FlackTek DAC 150.1 FVZ-K SpeedMixer™ at 3500 rpm for 30 sec. This reaction resulted in a material with a hard segment content of ~30%. The mixture was poured onto greased Kapton paper and pressed between two aluminum plates equipped with 1 mm spacers at 80 °C and 5 psi for 3 hr. Complete disappearance (within error) of isocyanate functionality was

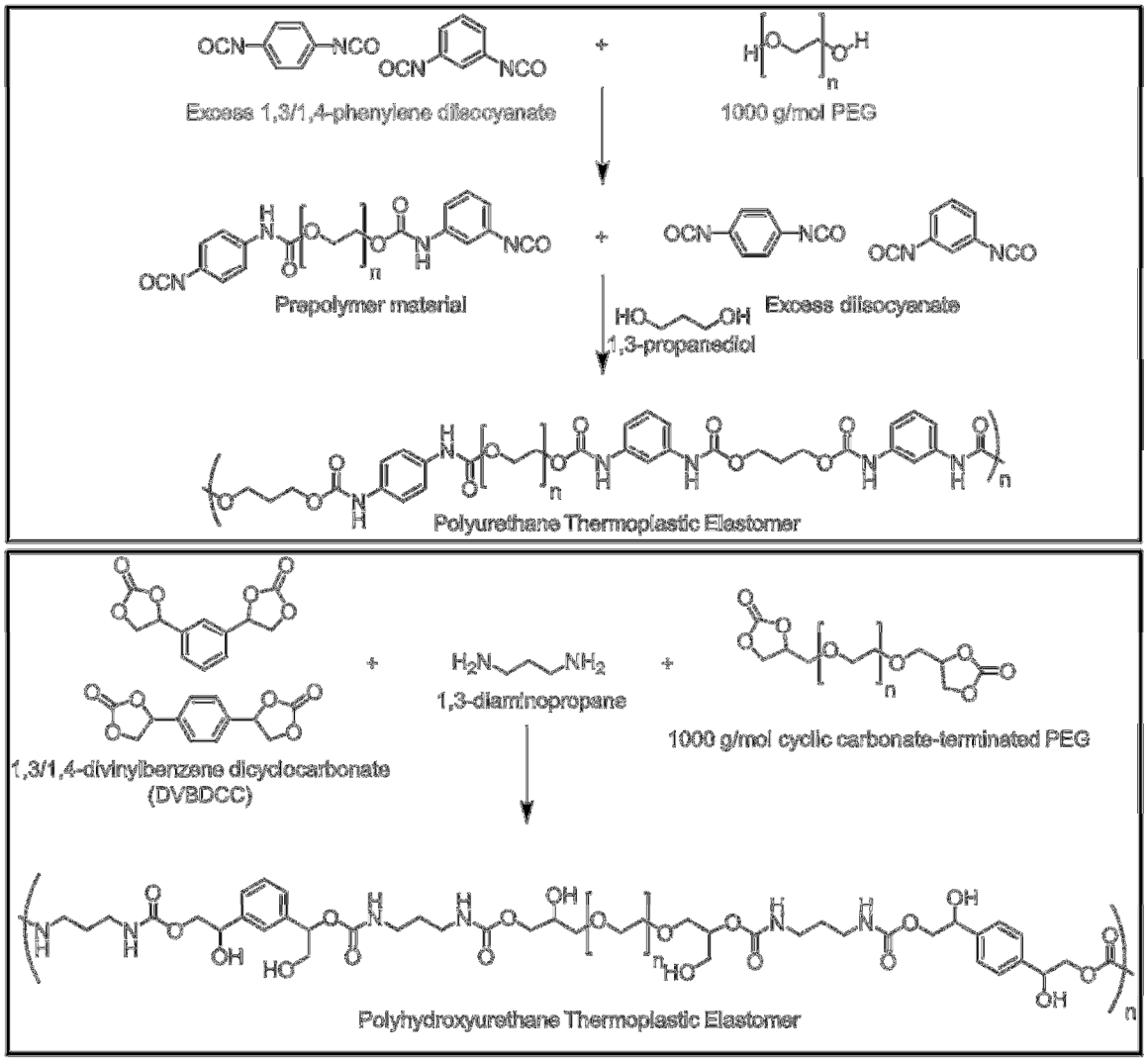

Scheme 3.1: Reaction schemes for the synthesis of PU-PEG/PDO/30 and an analogous PEG-based PHU (PEG1k/DP/30).

confirmed using a Bruker Tensor 37 FTIR with a MiD-IR diamond/ZnSe ATR attachment by monitoring the isocyanate peak at ~2200 cm^{-1}.

3.2.2.4 Synthesis of PEG-based PHU Analog

In order to examine the effects of the hydroxyl groups present in PHU, a PHU with a structurally analogous backbone to the PU in section 3.2.2.3 was synthesized from the 1000 g/mol PEG-based carbonate-functional soft segment, DVBDCC, and 1,3-diaminopropane (PEG1k/DP/30). This reaction is depicted in Scheme 3.1. In a typical synthesis, 1000 g/mol PEG dicyclocarbonate (8.0 g, 7.4 mmol), DVBDCC (1.6 g, 6.5 mmol), and 1,3-diaminopropane (1.0 g, 13.9 mmol) were combined in a max 20 Flacktek mixing cup and mixed using a FlackTek DAC 150.1 FVZ-K SpeedMixer™ at 3500 rpm for 5 min. After mixing, the cup was placed in an oven at 80 °C for at least 24 hr. Complete disappearance of cyclic carbonate functionality was confirmed using a Bruker Tensor 37 FTIR with a MiD-IR diamond/ZnSe ATR attachment by monitoring the cyclic carbonate peak at ~1800 cm^{-1}. The material was pressed into films using greased Kapton paper, aluminum plates, and 1 mm spacers at 120 °C and 5 psi for 5 min.

3.2.2.5 Synthesis of PEG/PPG-based PHUs

To further examine the effects of soft-segment backbone functionality on the development of elastomeric character in segmented PHUs, several additional formulations were synthesized using the 1000 g/mol cyclic-carbonate-functional PEG, 1700 g/mol amine-functional PEG, and 730 g/mol cyclic-carbonate-functional PPG. The materials and reaction schemes are depicted in Scheme 3.2. For the complete study on the effect of soft-segment backbone on segmented thermoplastic synthesis, the 1,3-diaminopropane chain extender used for the initial PU/PHU comparison was substituted with either 1,3-cyclohexanebis(methylamine) or *m*-xylylenediamine. In addition, the hard-segment contents investigated were increased to either

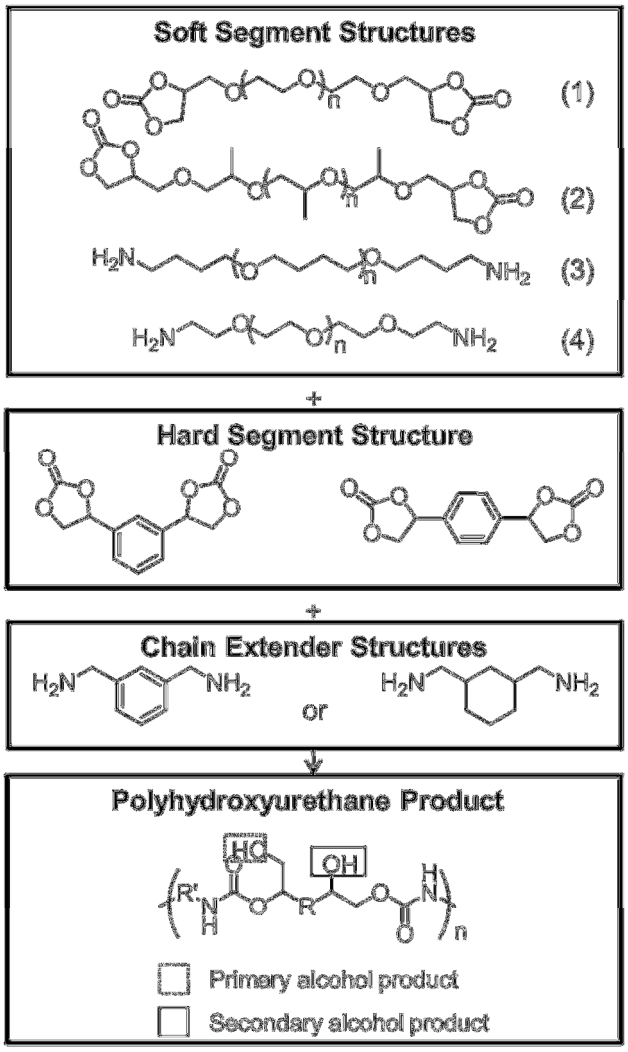

Scheme 3.2: Monomer structures and reaction scheme employed for the synthesis of segmented PHUs. The soft segments are (1) 1000 g/mol carbonate-terminated PEG, (2) 730 g/mol carbonate-terminated PPG, (3) 1700 g/mol amine-terminated PTMO, and (4) 1700 g/mol amine-terminated PEG. The hard segment exists as a mixture of 1,3- and 1,4- isomers of divinylbenzene dicyclocarbonate (DVBDCC). The amine chain extenders employed were *m*-xylylenediamine or 1,3-cyclohexanebis(methylamine). The PHU product is a simplified structure showing the two possible types of hydroxyurethane linkages created, primary and secondary; a mixture of these products is expected. Depending on the formulation, the R' group could represent the amine chain-extender backbone or the soft-segment backbone, and the R group could represent the hard-segment structure or the backbone of the soft segment.

40% or 50%. The aim of selecting a larger, more rigid chain extender, and increasing hard-segment content to strengthen the PHU materials synthesized resulting in robust mechanical responses. In a typical synthesis, 1000 g/mol PEG dicyclocarbonate (1.4 g, 1.3 mmol) was combined with DVBDCC (0.4 g, 1.7 mmol) and *m*-xylylenediamine (0.4 g, 3.0 mmol) in a max 10 FlackTek mixing cup. The material was mixed using a FlackTek DAC 150.1 FVZ-K SpeedMixer™ at 3500 rpm for 5 min and placed in an oven at 70 °C for at least 24 hr. Full conversion of cyclic carbonate was confirmed using a Bruker Tensor 37 FTIR with a MiD-IR diamond/ZnSe ATR attachment by observing the complete disappearance of the cyclic carbonate peak at ~1800 cm^{-1}. All PEG- and PPG-based materials depicted in Scheme 3.2 were synthesized following this procedure.

3.2.2.6 Synthesis of PTMO-based PHUs

In addition to synthesizing materials using PEG- or PPG-based soft segments, 1700 g/mol amine-terminated PTMO was used. Due to the waxy solid nature of the PTMO-based soft segment at room temperature, a solvent-based synthesis was completed to aid in the uniform dispersion of reactants. These materials were chain extended with either 1,3-cyclohexanebis(methylamine) or *m*-xylylenediamine at a hard-segment content of 40% or 50%. In a typical synthesis, DVBDCC (2.0 g, 8.0 mmol), Elastamine HT-1700 (4.1 g, 2.6 mmol), and 1,3-cyclohexanebis(methylamine) (0.8 g, 5.4 mmol) were combined in a FlackTek max 20 mixing cup. Following this, 6.3 mL of dimethylformamide (DMF) were added to adjust the concentration of reacting functional groups to 0.6 M. The solution was mixed in a FlackTek DAC 150.1 FVZ-K SpeedMixer™ for 5 min at 3500 rpm and reacted at70 °C for 24 hr. Upon reaction completion, the mixture was homogenized again in the FlackTek mixer for 5 min. The polymer was poured into a FlackTek max 100 cup and dried in an oven maintained at 70 °C for 24 hr. The FlackTek max 100 cup was selected for convenience in order to obtain dried films of

sufficient thickness for thermal and mechanical testing.

3.2.2.7 Calculation of Hard-Segment Content

For carbonate-terminated soft segments:

$$HS\% = 100 \times \frac{R \times A_{MW} + (R-1) \times DC_{MW}}{SS_{MW} + R \times A_{MW} + (R-1) \times DC_{MW}}$$

R = molar ratio of amine chain extender to soft segment

A_{MW} = Amine molecular weight

DC_{MW} = bis-carbonate hard-segment molecular weight

SS_{MW} = soft-segment molecular weight

For amine-terminated soft segments:

$$HS\% = 100 \times \frac{R \times DC_{MW} + (R-1) \times A_{MW}}{SS_{MW} + R \times DC_{MW} + (R-1) \times A_{MW}}$$

R = molar ratio of bis-carbonate hard segment to soft segment

A_{MW} = Amine molecular weight

DC_{MW} = bis-carbonate hard-segment molecular weight

SS_{MW} = soft-segment molecular weight

3.2.2.8 Synthesis of Pure Hard Segment Analog

To help determine the location of the hard-segment glass transition temperature (T_g) in the segmented PHU materials, single-phase materials were synthesized from the diamine chain extender (either 1,3-cyclohexanebis(methylamine) or *m*-xylylenediamine) and DVBDCC hard segment. The pure single-phase hard-segment polymers were prepared by reacting equimolar amounts of DVBDCC and chain extender in DMF. In a typical synthesis, DVBDCC (0.5 g, 2 mmol) and 1,3-cyclohexanebis(methylamine) (0.3 g, 2 mmol) were combined into 1.7 mL of DMF and reacted at 70 °C for 60 hr. The mixture was dried in an oven maintained at 90 °C for at

least 24 hr.

3.2.3 Characterizations

3.2.3.1 Conversion and Extent of Hydrogen Bonding Characterization

All PHU samples were analyzed for conversion of cyclic carbonate groups (~1800 cm^{-1}) and PU samples for conversion of isocyanate groups (~2200 cm^{-1}) with a Bruker Tensor 37 MiD IR FTIR spectrophotometer equipped with an attenuated total reflectance (ATR) diamond/ZnSe attachment. The PHUs were scanned at a resolution of 4 cm^{-1} and at least 16 scans were obtained in the 4000-600 cm^{-1} range for each spectrum. Figure A1 (see Appendix A) shows the spectra for all twelve PHU samples. In addition to examining conversion, the ATR-FTIR scans were also used to determine the extent to which urethane carbonyl groups were hydrogen bonded. The carbonyl peak examined to determine the extent of hydrogen bonding occurring was located at ~1700 cm^{-1}. A shift to lower wavenumbers indicated strong hydrogen bonding in the carbonyl urethane hard segments, while a shift to higher wavenumbers indicated a greater prevalence of free carbonyl groups. The examination of this absorbance to determine the extent of hard-segment segregation and hydrogen bonding is common practice in PU literature (Sheth 2005, Yilgor 2000).

3.2.3.2 ^{1}H NMR Characterization

^{1}H NMR spectra were recorded on a Bruker Avance III 500 MHz NMR spectrometer with a direct cryoprobe (500 MHz) at room temperature in deuterated chloroform ($CDCl_3$). Spectra are reported in parts per million relative to tetramethylsilane. NMR spectra and assignment of peaks are given for all PPG- and PTMO-based PHU samples in Figures A2 through A9 (see Appendix A).

3.2.3.3 Molecular Weight Characterization

The molecular weights (MWs) of PPG-based and PTMO-based PHUs were determined using gel permeation chromatography. Two Tosoh TSKgel Alpha-M columns (13 μm) were used. The eluent is DMF with 4g/L of $LiNO_3$ at 40 °C and the elution rate is 0.5 mL/min. The detector is Viscotek TDA 302 interface/Waters 2414 RI detector. Molecular weight values were reported relative to polyethylene oxide (PEO) standards. Agilent PEO/PEG EasiCal standards were used to construct the calibration curve.

3.2.3.4 Mechanical Property and Hysteresis Characterization

The mechanical properties of all materials were obtained under uniaxial tensile deformation according to ASTM D1708-10 with an MTS Sintech 20/G tensile tester. Dog bone-shaped samples (4.7 mm x 1.5 mm x 22 mm) were cut from pressed plaques using a Dewes-Gumbs die and subjected to an extension rate of 130 mm/min with a data acquisition frequency of 350 Hz. The Young's modulus, ultimate tensile strength, yield stress (where applicable), and strain at break were reported as an average value from at least 5 specimens. Hysteresis testing was also completed on select PTMO-based materials. The previously described dog bone-shaped samples were stretched to 100% strain at a cross-head speed of 130 mm/min and returned to 0% strain. Ten cycles with a 5 min interval between cycles were performed.

3.2.3.5 Thermal Property Characterization

All polymers were examined for their thermal properties using a combination of dynamic mechanical analysis (DMA) and differential scanning calorimetry (DSC). Dynamic mechanical analysis measurements were performed on as-pressed samples in tensile mode with a TA Instruments Rheometrics Stress Analyzer-GIII equipped with a liquid N_2 cooling system and a 3500 gf transducer. Specimens measuring approximately 30 mm x 7 mm x 1 mm were quenched

to -100 °C and subjected to a temperature sweep to 100 °C or until the material slips out of the grip at a heating rate of 3 °C/min. The measurement was conducted under tension at a dynamic frequency of 1 Hz and a strain of 0.03 %. The storage modulus (*E'*), loss modulus (*E"*) and the mechanical loss factor/loss tangent (tan δ) were recorded. The flow temperature (T_{flow}) (indicative of the hard-segment T_g) is defined as the onset temperature of inconsistent tan δ data. A Mettler Toledo DSC 822e was used for DSC thermal analysis. The pure hard-segment analog samples were heated to 200 °C at 10 °C/min, annealed for 5 min, and cooled to 0 °C at 40 °C/min. The DSC scans were collected on second heating at 10 °C/min. The PPG- and PEG-based materials were heated from -85 °C to 200 °C at a heating rate of 10 °C/min without previous thermal treatment. The PTMO-based materials were also tested using this method, but the soft-segment T_g occurred outside the temperature range of the cooler, and the hard-segment T_g was not visible using DSC methods. Note: Attempts were also made to probe the thermal transitions of PPG- and PTMO-based PHUs on second heating after annealing and cooling the samples at 40 °C/min without success.

3.2.3.6 Characterization of Phase Separation

The presence of nanophase or microphase separation in segmented PHU was determined using small-angle X-ray scattering (SAXS) or atomic force microscopy (AFM). Small-angle X-ray scattering experiments were performed on as-synthesized materials using a Rigaku S-MAX 3000 SAXS system emitting X-rays with a wavelength of 0.154 nm (Cu-Kα). The sample-to-detector distance was 1640 mm with a silver behenate calibration. The 2D scattering patterns were azimuthally averaged to produce a 1-D plot of intensity versus scattering vector q, where $q = 4\pi\sin\theta/\lambda$ where θ is one half of the scattering angle and λ is the X-ray wavelength. Atomic force microscopy samples were prepared by drop casting 15 wt% solutions of PHU in methanol onto glass cover slides. Surface characterization of the PPG-based samples was performed by a

Dimension FastScan Atomic Force Microscope (Bruker) using the tapping mode.

3.3 Results and Discussion

The traditional PU was synthesized using 1000 g/mol hydroxyl-terminated polyethylene glycol (PEG), 1,3/1,4-phenylene diisocyanate, and 1,3-propanediol (PDO) at a ~30% hard-segment content. The analogous PHU was produced using cyclic-carbonate-terminated 1000 g/mol PEG, 1,3/1,4-divinylbenzene dicyclocarbonate (DVBDCC), and 1,3-diaminopropane (DP) at 80 °C with a ~30% hard-segment content. The naming convention for PHU materials in this study is soft segment/chain extender/hard-segment content; e.g., the previously described PHU is denoted as PEG1k/DP/30. (All PHUs are synthesized using DVBDCC as hard segment.) The reactants and products for the comparison are depicted in Scheme 3.1. Unlike the traditional PU material which exhibited an elastomeric-like response, the analogous PHU flows under the force of gravity. In particular, the PU (PU-PEG/PDO/30) was mechanically robust, exhibited significant reversibility of extension, and had tensile properties characteristic of TPUs (2.5 MPa Young's modulus, 2.0 MPa tensile strength, and a 550% elongation at break) (Oertel 1994, Holden 2004). A qualitative assessment of the PU elastomeric-like reversibility and an example tensile curve are shown in Figure 3.1a-d. The PU exhibited a soft-segment T_g of about -20 °C by differential scanning calorimetry (DSC) and a flow temperature by dynamic mechanical analysis (DMA) at a value exceeding 160 °C (Figure 3.2c); in contrast, the PHU exhibited a single T_g at about -20 °C and a melting peak associated with the PEG-based soft segment (Figure 3.2b). The DMA results were similar; the PU was robust and had a rubbery plateau at temperatures above the soft-segment T_g whereas the PHU flowed and slipped from the testing grips shortly after passing through the single T_g. (See Figure 3.2a-c for DSC and DMA curves.)

We hypothesized that hydroxyl groups in PHU cause major phase mixing by hydrogen

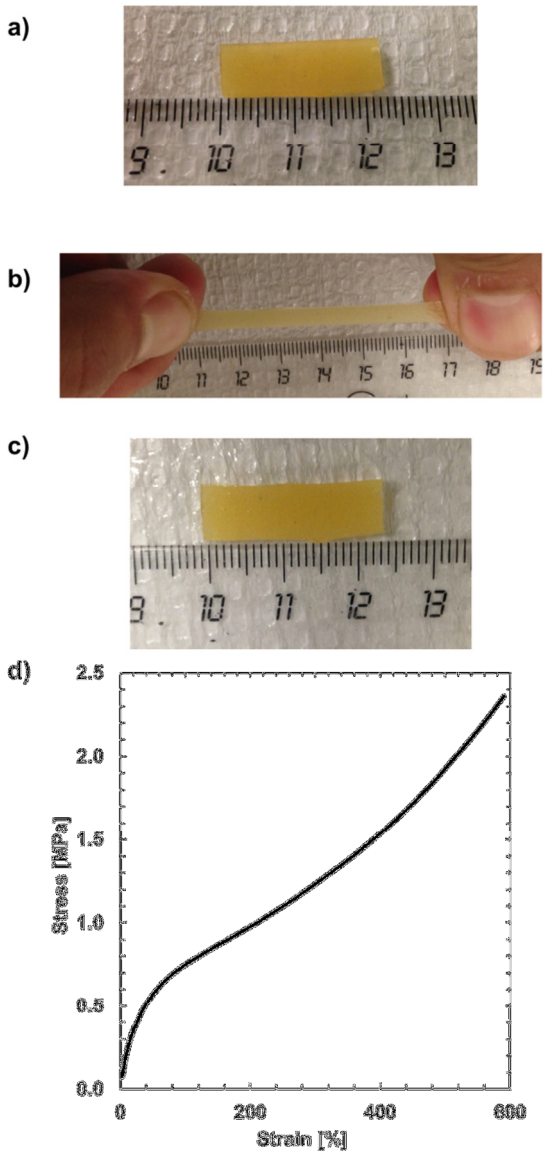

Figure 3.1: Mechanical behavior of the traditional segmented PU, PU-PEG/PDO/30. a) Segmented PU material previous to extension. b) Segmented PU material during extension. c) Segmented PU material after release of extensive force. d) Example tensile curve obtained for PU-PEG/PDO/30.

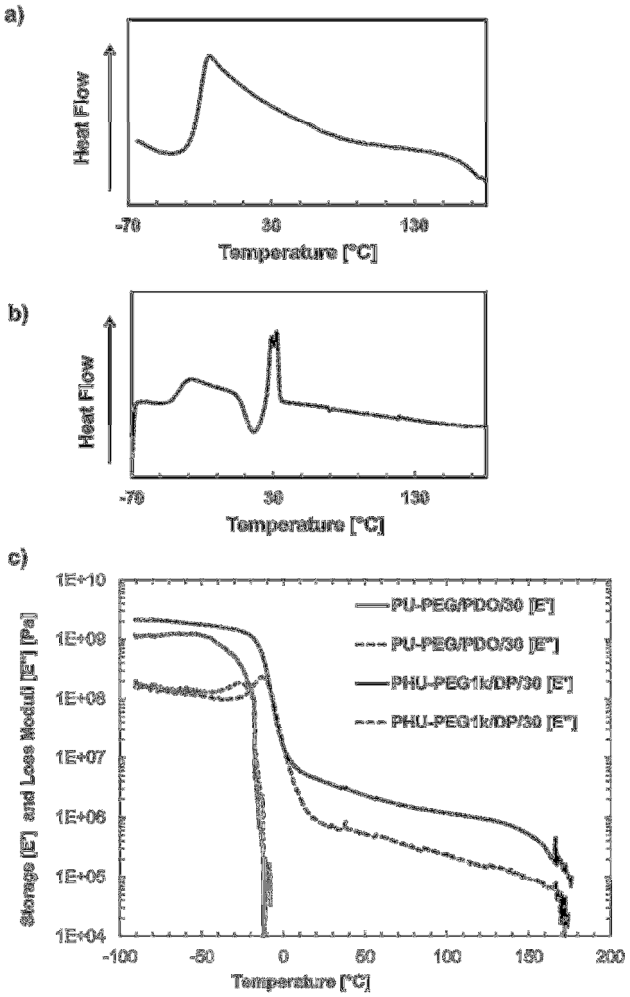

Figure 3.2: Thermal property characterization of analogous PEG-based PU (PU-PEG/PDO/30) and PHU (PHU-PEG1k/DP/30) materials. a) Representative DSC curve for PU-PEG/PDO/30. The soft-segment T_g is relatively narrow at about -20 °C while the hard-segment T_g is broad with a midpoint around 110 °C. b) Representative DSC curve for PHU-PEG1k/DP/30. This material exhibits a soft-segment T_g around -20 °C, a melting peak associated with the PEG-based soft segment, and no discernable hard-segment T_g. c) Representative DMA profiles for PU-PEG/PDO/30 and PHU-PEG1k/DP/30. The PU material exhibits a soft-segment T_g followed by a large rubbery plateau region, while the PHU material flows and slips from the testing grips shortly after passing through the soft-segment glass transition.

bonding to the soft-segment ether oxygen and preventing the segregation of urethane linkages into hard-segment domains. To test this hypothesis, additional PHUs were synthesized with PEG-based soft segments (both 1,000 and 1,700 g/mol), a 730 g/mol polypropylene glycol (PPG)-based soft segment (with sterically hindered ether oxygen relative to PEG), and a 1700 g/mol PTMO-based soft segment (with decreased ether oxygen content relative to PEG). In addition, the amine chain-extender structure was changed to 1,3-cyclohexanebis(methyl amine) (CYC) or m-xylylenediamine (XYL), and the hard-segment content was increased to 40 or 50 %. (See Scheme 3.2 and Table 3.1 for reaction schemes and formulations.)

After synthesizing numerous formulations with various soft segments, chain extenders, and hard-segment contents, all PEG-based PHUs flowed under the force of gravity (Figure 3.3a) while PPG- and PTMO-based PHUs were mechanically robust (Figure 3.3b). We used attenuated total reflectance-Fourier Transform Infrared (ATR-FTIR) spectroscopy to test the hypothesis of substantial hydrogen bonding of PHU hydroxyl groups to the soft segment in PEG-based PHUs. The hydroxyl group (-OH) peak cannot be evaluated using a mid-IR instrument because it overlaps with the peak associated with amide groups. In addition, the soft-segment ether oxygen peak is located in the fingerprint region, which differs across various soft-segment types, making comparisons of hydrogen bonding levels in different soft-segment types difficult, if not impossible. As a result, we chose to monitor the peak associated with the urethane carbonyl (C=O) (~1700 cm^{-1}) (Sheth 2005, Yilgor 2000). Significant hydrogen bonding between –OH groups and the soft-segment ether oxygens result in a decrease of hydrogen bonding between carbonyl groups and amide groups in the hard segments. The expected hydrogen bonding interaction in PU hard segments is depicted in Figure 3.3c, and the hypothesized hydroxyl group/soft-segment interaction in PEG-based PHUs is depicted in Figure 3.3d. Previous studies of hydrogen bonding in PUs have investigated shifts associated with carbonyl absorbance and concluded that absorbances at ~1700 cm^{-1} and ~1730 cm^{-1} are associated with hydrogen bonded

Table 3.1: Segmented PHU material formulations.

Material Name	Soft Segment	Chain Extender	HS wt%
PPG/XYL/40	720 g/mol PPG	*m*-Xylylenediamine	40
PPG/XYL/50			50
PPG/CYC/40		1,3-Cyclohexanebis(methylamine)	40
PPG/CYC/50			50
PTMO/XYL/40	1700 g/mol PTMO	*m*-Xylylenediamine	40
PTMO/XYL/50			50
PTMO/CYC/40		1,3-Cyclohexanebis(methylamine)	40
PTMO/CYC/50			50
PEG1k/XYL/40	1000 g/mol PEG	*m*-Xylylenediamine	40
PEG1k/CYC/40		1,3-Cyclohexanebis(methylamine)	40
PEG1.7k/XYL/40	1700 g/mol PEG	*m*-Xylylenediamine	40
PEG1.7k/CYC/40		1,3-Cyclohexanebis(methylamine)	40
PEG1k/DP/30	1000 g/mol PEG	1,3-diaminopropane	30
PU-PEG/PDO/30	1000 g/mol PEG	1,3-propanediol	30

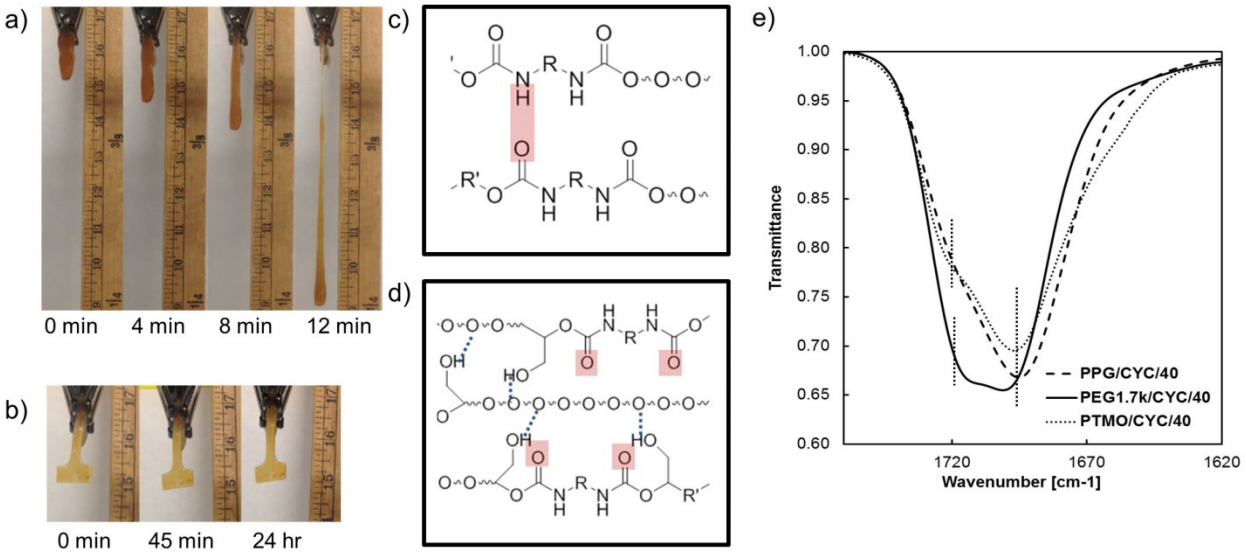

Figure 3.3: a) Room-temperature flow properties of PEG1k/XYL/40 PHU, b) room-temperature flow properties of PPG/XYL/40 PHU, c) representation of the expected hard-segment hydrogen bonding interaction between amide groups and carbonyl groups in traditional PU, d) representation of the hydrogen bonding interaction leading to phase mixing in PEG-based PHUs. (The urethane carbonyl appears non-bonded due to hydrogen bonding between adjacent hydroxyl groups and readily accessible soft segment ether oxygen.) e) ATR-FTIR spectra for PPG-, PEG-, and PTMO-based PHUs at 40% hard-segment content.

carbonyl and free carbonyl respectively (Sheth 2005, Yilgor 2000). As shown in Figure 3.3e, the level of hydrogen bonded carbonyl (~1700 cm^{-1}) was higher for the PPG- and PTMO-based PHUs whereas the free carbonyl (shoulder at ~1720 cm^{-1}) was much more evident in the spectrum of the PEG-based PHUs. Both the 1000 g/mol and 1700 g/mol PEG-based PHUs exhibited this behavior. (The apparent shift of the free carbonyl peak in PHU relative to PU is likely due to small differences in the chemical environment of their hard segments.)

All mechanically robust PHUs were evaluated by tensile testing. Representative stress-strain curves for several PHUs are shown in Figure 3.4a; average tensile properties are given in Table 3.2. A yield point is observed in all PPG-based PHUs, followed by strain hardening. In contrast, the majority of PTMO-based PHUs exhibited no yield point, with modest tensile strength and high elongation at break. (See Figure 3.4a and Figure 3.5a.) The differences between PPG- and PTMO-based PHUs are attributed to the relatively low MW of the PPG soft segment; decreasing the soft-segment MW decreases the elastomeric character in PU (Petrovic 1991).

TPUs do not exhibit perfect elastomeric recovery, and hysteresis is commonly observed (Qi 2005, Kim 1999). The PTMO/CYC/40 PHU was subjected to ten cycles of 100% strain to evaluate hysteresis of elastomeric recovery. Figure 3.4b shows that PTMO-based PHUs manifest elastomeric response with hysteresis like TPUs.

How do the properties of our PPG- and PTMO-based PHUs compare to related PUs? Several comparisons can be drawn to outline the similarities in mechanical properties. The PPG-based PHUs exhibited tensile properties comparable to similar PU systems cited in the literature (Petrovic 1991). PPG/XYL/50 exhibited a modulus of 180 MPa, tensile strength of 3.6 MPa and an elongation at break of 230% (see Table 3.2); a similar PU studied by Hourston et al. (Hourston 1997) exhibited a 4.4 MPa tensile strength and a 260% elongation at break. The PTMO-based PHUs exhibited Young's moduli ranging from 60 to 90 MPa with tensile strengths

Table 3.2: Tensile and thermal properties of segmented PHUs and a comparison PU.

Material Name	Young's Modulus [MPa]	Yield Stress [MPa]	Tensile Strength [MPa]	Strain at Break [%]	Soft Segment T_g [°C][a]	Hard Segment T_{flow} [°C][b]
PPG/XYL/40	47 ± 13	0.5 ± 0.2	0.5 ± 0.2	1800 ± 340	17	58
PPG/XYL/50	180 ± 40	3.6 ± 0.6	3.6 ± 0.6	230 ± 70	21	69
PPG/CYC/40	43 ± 6	0.5 ± 0.1	0.8 ± 0.1	1500 ± 240	19	60
PPG/CYC/50	230 ± 70	4.3 ± 0.6	4.3 ± 0.6	10 ± 20	27	69
PTMO/XYL/40	68 ± 12	None	3.0 ± 1.1	900 ± 230	-67	67
PTMO/XYL/50	68 ± 22	3.9 ± 1.4	4.4 ± 2.0	320 ± 130	-64	80
PTMO/CYC/40	59 ± 6	None	1.4 ± 0.3	> 2000	-66	80
PTMO/CYC/50	89 ± 18	None	4.2 ± 1.9	670 ± 160	-66	89
PEG1k/XYL/40	Not testable. Flows at room temperature.					
PEG1k/CYC/40						
PEG1.7k/XYL/40						
PEG1.7k/CYC/40						
PEG1k/DP/30						
PU-PEG1k/PDO/30	2.5 ± 0.3	None	2.0 ± 0.4	550 ± 70	-14	164

[a] Soft-segment T_g is determined from the peak in the dynamic loss modulus (E'') using DMA.
[b] Hard-segment T_{flow} is determined from the onset of inconsistent tan δ data using DMA.

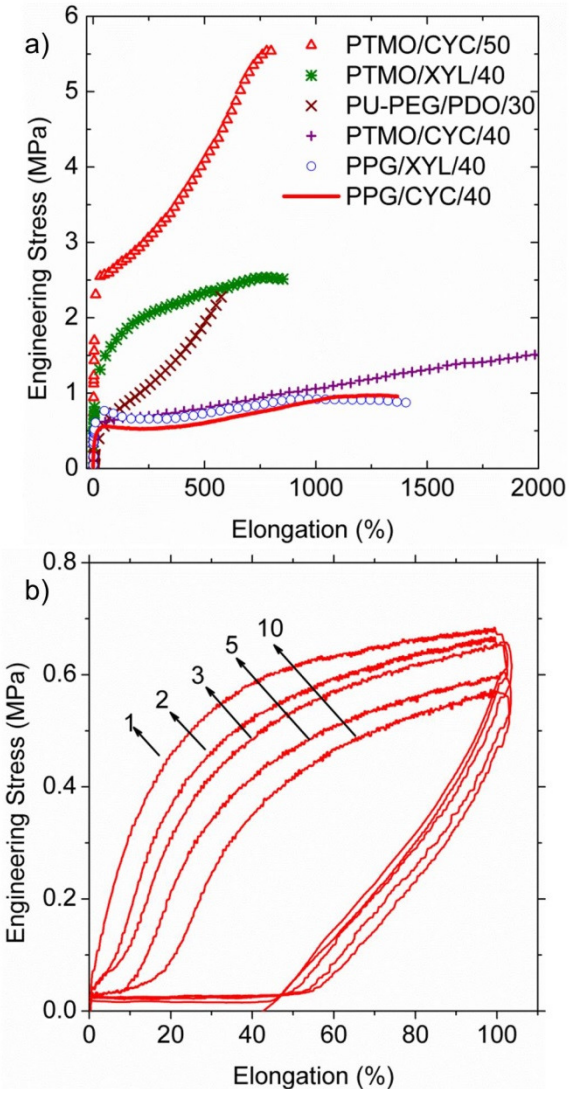

Figure 3.4: a) Representative tensile curves for segmented PU and PHUs which exhibit a robust elastomeric response. (See Figure 3.5b for response between 0-300% elongation.) b) Hysteresis of reversible elastomeric recovery exhibited by the PTMO/CYC/40 PHU. Data were collected in the tensile geometry by stretching to 100% strain at 130 mm/min. Samples were returned to 0% strain, and 10 cycles were completed.

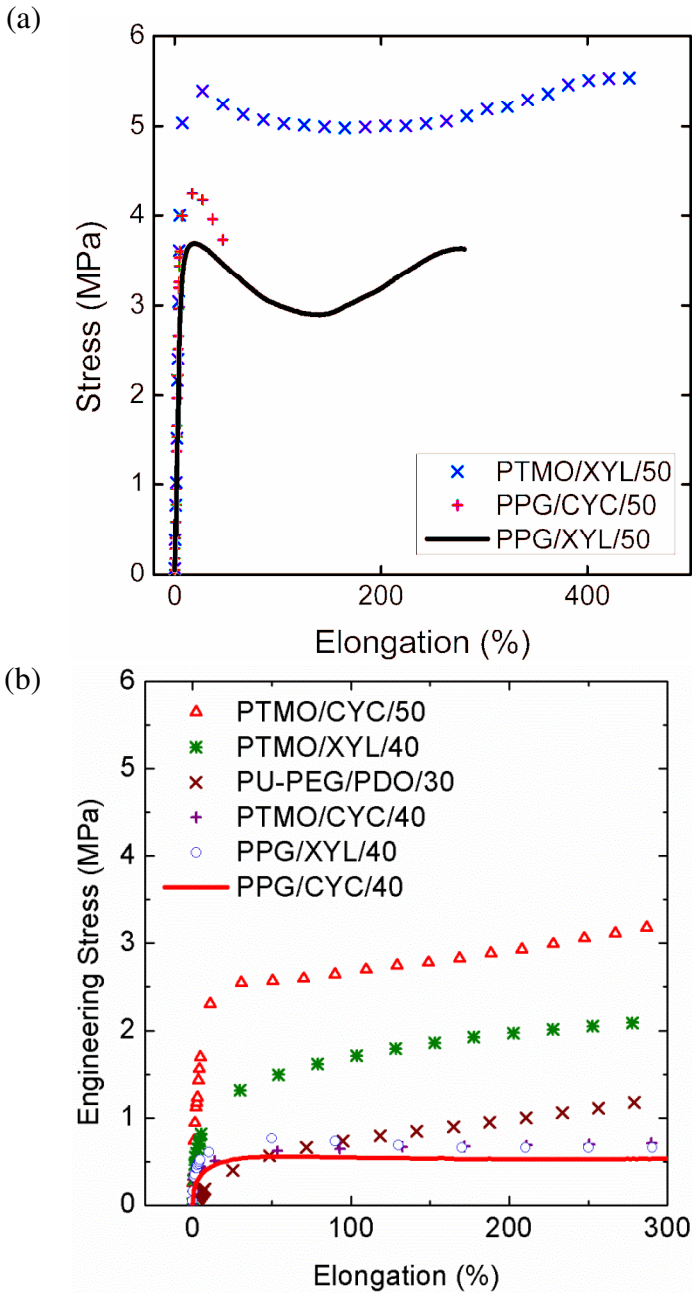

Figure 3.5: a) Representative tensile curves of materials which show yield points, b) representative tensile curves for segmented PU and PHUs which exhibit a robust elastomeric response between 0 to 300% elongation at break.

from 1.4 to 4.4 MPa and elongation-at-break values from 320 to >2000%. Except for some tensile strengths, these values are comparable to similar traditional PUs (Klinedinst 2012, Fu 1986). As compared to similar PUs, the PHUs exhibited lower tensile strength which can be attributed to several factors. First, the carbonyl group of the urethane linkage in PU can potentially hydrogen bond with the amide hydrogen on an adjacent linkage; in PHUs this interaction may be slightly hindered because of the presence of the hydroxyl group. Second, the urethane linkage in our PHU was separated from the aromatic ring by at least one or two methylene units, thereby making the hard domain more flexible, whereas in traditional PUs the urethane linkage is located adjacent to the aromatic ring. Lastly, the previously mentioned PUs (Klinedinst 2012, Fu 1986) were produced from monodisperse, symmetric *para*-phenylene diisocyanate (Klinedinst 2012) or pure 2,4-toluene diisocyanate (Fu 1986), whereas the bis-carbonate used here for PHU synthesis is a mixture of isomers. Although the PHU tensile strengths are lower, we note that slight changes in formulation can yield properties possessed by traditional PUs. By increasing the hard-segment content in PTMO-based PHUs from 40% to 50%, there is a marked increase in tensile strength, in the same range as PUs with slightly lower hard-segment content.

The robust mechanical properties and elastomeric character of the PPG- and PTMO-based PHUs are consequences of nanophase separation. Small-angle X-ray scattering (SAXS) and atomic force microscopy (AFM) were used to evaluate phase separation. Figure 3.6 shows SAXS patterns obtained for PTMO-based PHUs. Single interference peaks were observed, characteristic of nanophase separation. Interdomain spacing (d) is quantified from $d = 2\pi/q_{max}$, where q_{max} is the magnitude of the scattering vector at maximum intensity, with d = 12-15 nm. No interference peak is observed in PPG-based PHUs, likely because the interdomain spacing is at a length scale not amenable to SAXS or consists of many length scales. AFM phase imaging (see Figure A10a-d in Appendix A) indicates the presence of hard and soft domains in the PPG-

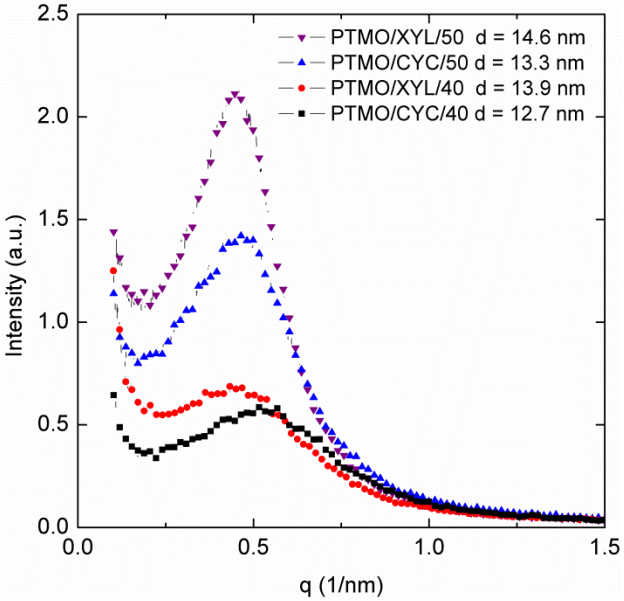

Figure 3.6: SAXS patterns for PTMO-based PHUs; peaks are indicative of nanophase separation. Interdomain spacings are indicated in the figure legend.

based PHUs.

It is interesting to note that nanophase separation occurs in both PPG- and PTMO-based PHUs even though the apparent MWs are relatively modest in comparison with conventional PUs. Besse et al. (Besse 2015) have recently discussed why PHU synthesized via cyclic carbonate aminolysis usually results in low MW products; possible reasons involve side reactions leading to urea formation and oxazolidinone as well as dehydration products. The highest apparent M_n value achieved in our PHUs was 10 kg/mole and apparent M_w values ranged from 12 to 40 kg/mole. (See Table 3.3 for information on apparent MW averages and measurement by gel permeation chromatography.)

Thermal transitions of PPG- and PTMO-based PHUs were characterized using DSC and DMA. Due to slight phase mixing and heterogeneity, hard-segment T_gs could not be determined by traditional DSC methods. The inability to discern the hard-segment T_g is a common problem seen with traditional TPUs (Kojio 2007). In order to help elucidate hard-segment T_gs, pure hard-segment materials were synthesized and characterized by DSC. (See Figure A11 in Appendix A for DSC thermograms.)

Figure 3.7 shows typical DMA results of PTMO-based samples. (See Figures A13 and A14 in Appendix A for other DMA profiles.) Nanophase separation was verified by the presence of a soft-segment T_g below room temperature and a flow temperature (T_{flow}) above room temperature. The T_{flow} determined from DMA can be associated with the upper end of a broad hard-segment glass transition region; these values agree well with the T_gs of pure hard-segment analogs as determined by DSC (see Figure A12 in Appendix A). The values of soft-segment T_g and hard-segment T_{flow} (related to the upper end of a very broad glass transition region) are summarized in Table 3.1. The hard-segment T_g values correlate well with similar traditional PUs which have hard-segment T_gs in the range of 50 to 100 °C (Sheth 2005, Schneider 1975, O'Sickey 2002). The soft-segment T_gs of -65 °C for PTMO-based PHUs correlate well to those

Table 3.3: Apparent Molecular Weight Averages of PHUs.

Material Name	**Apparent M_n (kg/mol)**	**Apparent M_w (kg/mol)**
PPG/XYL/40	3.8	20.6
PPG/XYL/50	3.0	12.2
PPG/CYC/40	4.1	23.9
PPG/CYC/50	3.0	11.9
PTMO/XYL/40	4.0	35.8
PTMO/XYL/50	3.4	15.8
PTMO/CYC/40	10.0	40.0
PTMO/CYC/50	6.4	23.3

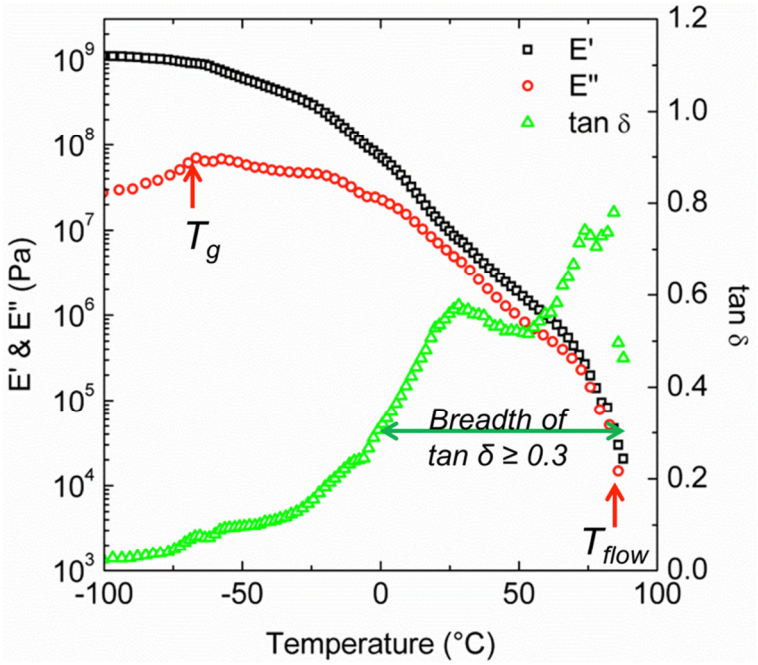

Figure 3.7: Representative DMA profile of the PTMO/CYC/40 PHU. Sample exhibits tan δ ≥ 0.3 over an 81 °C temperature range, which is desirable for acoustic and vibrational damping.

reported for similar systems in the literature (Sheth 2005, Schneider 1975, O'Sickey 2002). The soft-segment T_gs of PPG-based PHUs are in the range of 17 to 27 °C (as determined by DMA loss modulus (E") peaks) and are elevated as compared to neat PPG due to the soft-segment MW; with decreasing soft-segment MW, the observed T_g often shifts to higher temperature due to slight phase mixing (Petrovic 1991, Klinedinst 2012, O'Sickey 2002).

The data in Figure 3.7 also reveal that PTMO-based PHUs can serve as excellent acoustic and vibration damping materials over a very broad range of temperature, a function not achieved by traditional TPUs. (A survey of PU literature indicates that TPUs typically exhibit very good nanophase separation. This is manifested in sharp tan δ peaks over a narrow range of temperature typically at temperatures several tens of degrees above DSC-determined glass transitions of the soft and hard domains. To achieve high and continuous tan δ values over a broad temperature range, TPUs are incorporated into crosslinked interpenetrating polymeric networks with other polymers (Chern 1999, Qin 2004, Mok 2008).) The PTMO/CYC/40 PHU exhibits a very gradual decrease in storage modulus (E') with temperature above the soft-segment T_g and high tan δ (≥ 0.3) from -1 to 80 °C, a range of 81 °C. Tan δ ≥ 0.3 is widely used as a criterion for excellent damping properties of polymeric materials (Chern 1999, Qin 2004, Mok 2008). By analogy with a gradient copolymer study (Mok 2008), such response indicates that this PHU is a nanophase-separated system with unusually broad interphases and a wide range of local composition. This result is a consequence of partial phase mixing resulting from hydrogen bonding of some of the PHU hydroxyl groups to the PTMO-based soft segment. In contrast, TPUs exhibit two sharp drops in E' with increasing temperature as well as sharp tan δ peak centered over a narrow temperature range (see Figure 3.2c), consistent with the fact that TPUs are unsuitable for damping applications. In fact, when TPUs are incorporated in damping materials, it is a part of an interpenetrating polymeric network with secondary polymeric components to broaden the tan δ response (Qin 2004, Mok 2008). This work shows that the hydroxyl groups in PHU, while

detrimental in formulating nanophase-separated elastomers with PEG-based systems, are advantageous in PTMO-based systems and enable novel properties not achieved with traditional TPUs.

3.4 Conclusions

In summary, we demonstrated that hydroxyl groups in PHU play a critical role in the development of elastomeric-like character; the hydroxyl groups can undergo hydrogen bonding to soft segments with accessible ether oxygen resulting in phase mixing, and in the case of a PEG-based soft segment, a total loss of robust mechanical response. This interaction can be suppressed by using soft segments with sterically hindered ether oxygen (PPG) or decreased ether oxygen content (PTMO), resulting in robust, nanophase-separated PHUs despite their relatively low MWs. The PTMO-based PHUs exhibited reversible elastomeric extension with hysteresis and also displayed potential as broad-temperature-range acoustic and vibrational damping materials. Notably, the latter behavior results from the partial phase mixing associated with hydroxyl groups in PHUs and is not observed in TPUs.

APPENDIX A

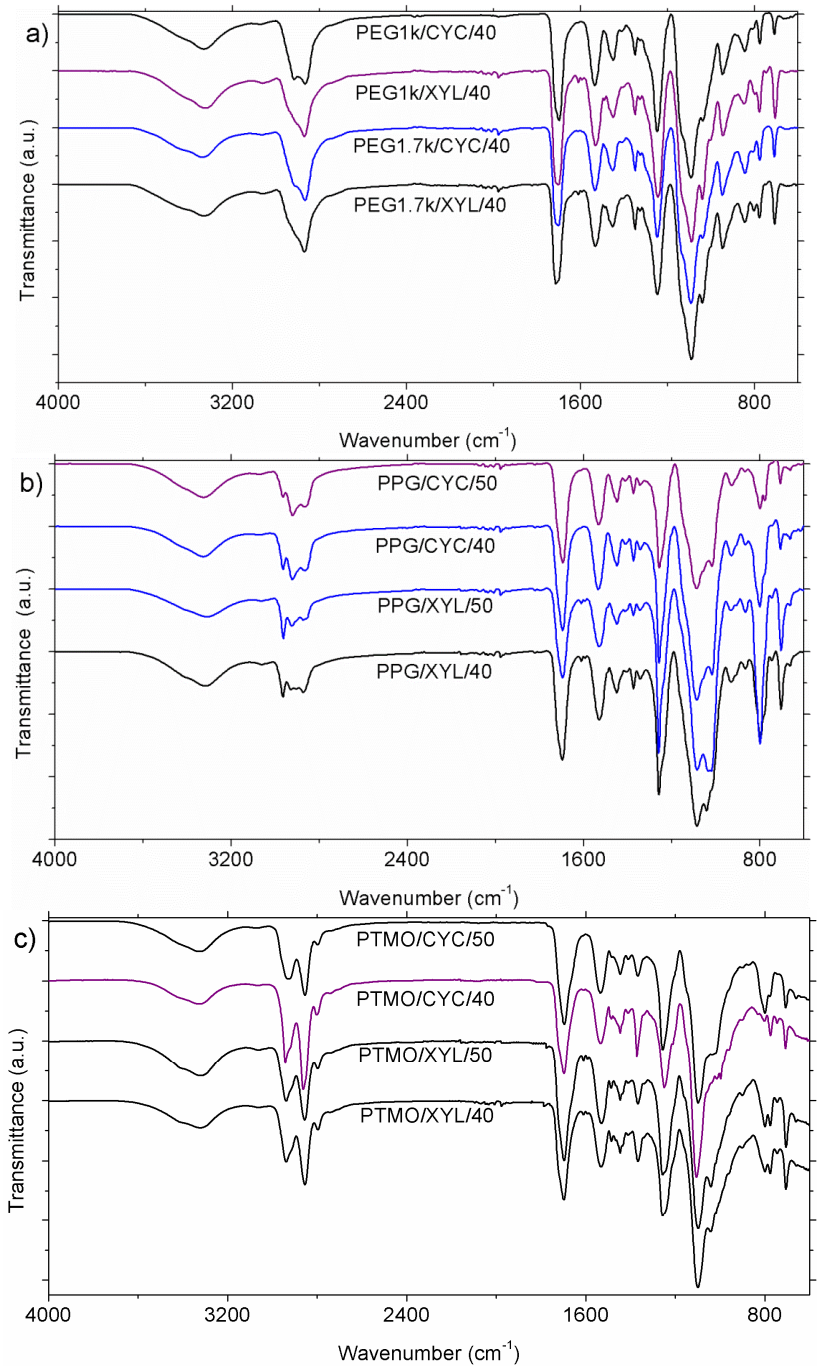

Figure A1: FTIR spectra of a) PEG-based PHUs, b) PPG-based PHUs, and c) PTMO-based PHUs. FTIR (ν, cm^{-1}): 3500-3300 (N-H), 3500-3100 (O-H), 3100-3000 (=C-H and aromatics), 1730-1700 (C=O), 1570 (N-H), 1300-1000 (C-O). (Note: An absorbance band at ~1800 cm^{-1} associated with DVBDCC is absent in all of the synthesized polymers.)

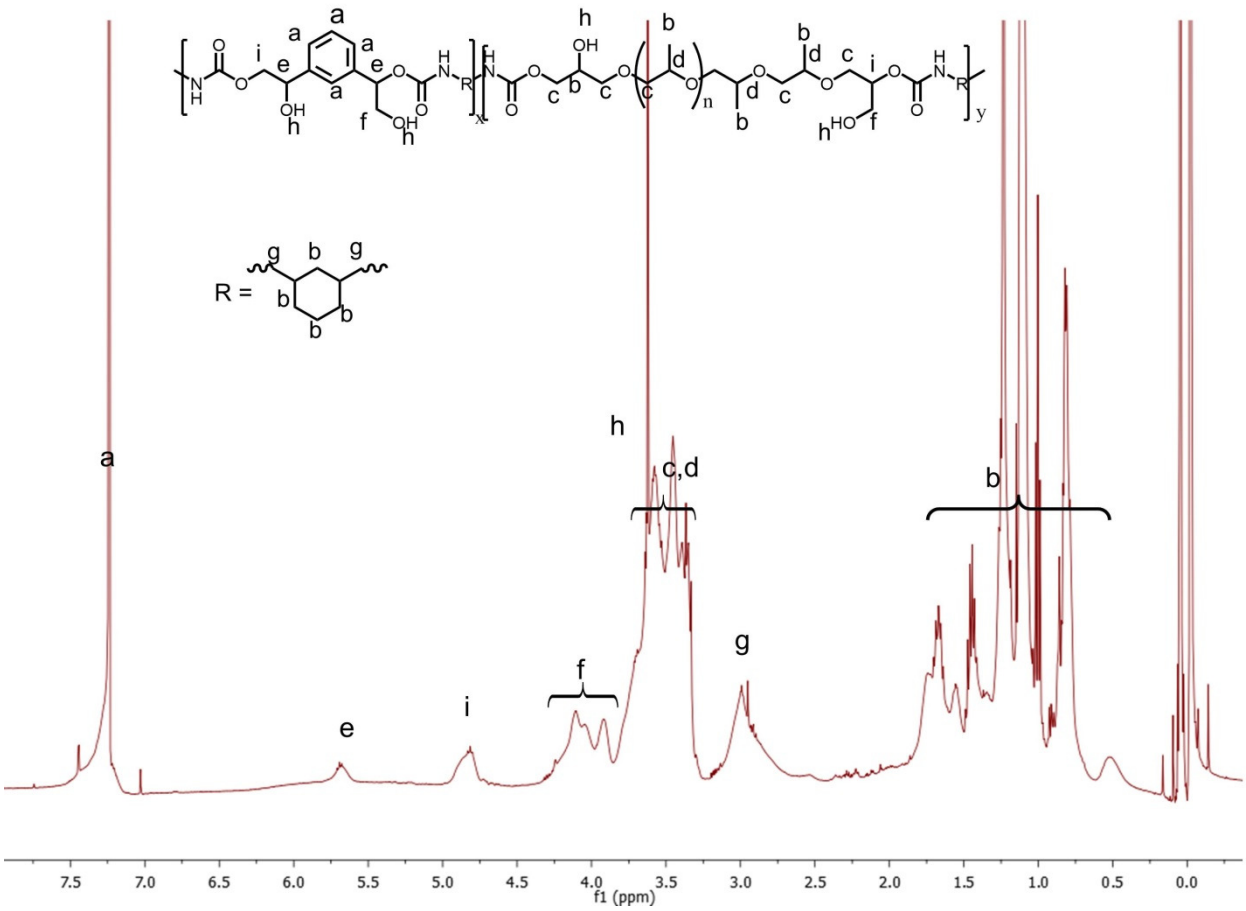

Figure A2: ^{1}H NMR Spectra of PPG/CYC/40 PHU in $CDCl_3$.

PPG/CYC/40. ^{1}H NMR (CDCl3, 500 MHz), δ (ppm): 0.5-2.0 (3H, $OCH_2CH(C\boldsymbol{H}_3)O$), 10H $NHCH_2(C\boldsymbol{H}C\boldsymbol{H}_2C\boldsymbol{H}_2C\boldsymbol{H}_2C\boldsymbol{H}C\boldsymbol{H})CH_2NH$), 2.7-3.2 (1H, $C\boldsymbol{H}_2NHC(=O)O$), 3.3-3.8 (2H, $OC\boldsymbol{H}_2CH(CH_3)O$, 1H, $OCH_2C\boldsymbol{H}(CH_2OH)O$, 1H, $O\boldsymbol{H}$), 3.8-4.2 (2H, $C\boldsymbol{H}_2OH$), 4.8-5.0 (1H, $C\boldsymbol{H}OC(=O)NH$), 5.6-5.7 (1H, $PhC\boldsymbol{H}(CH_2OH)O$), 7.0-7.5 (Ph).

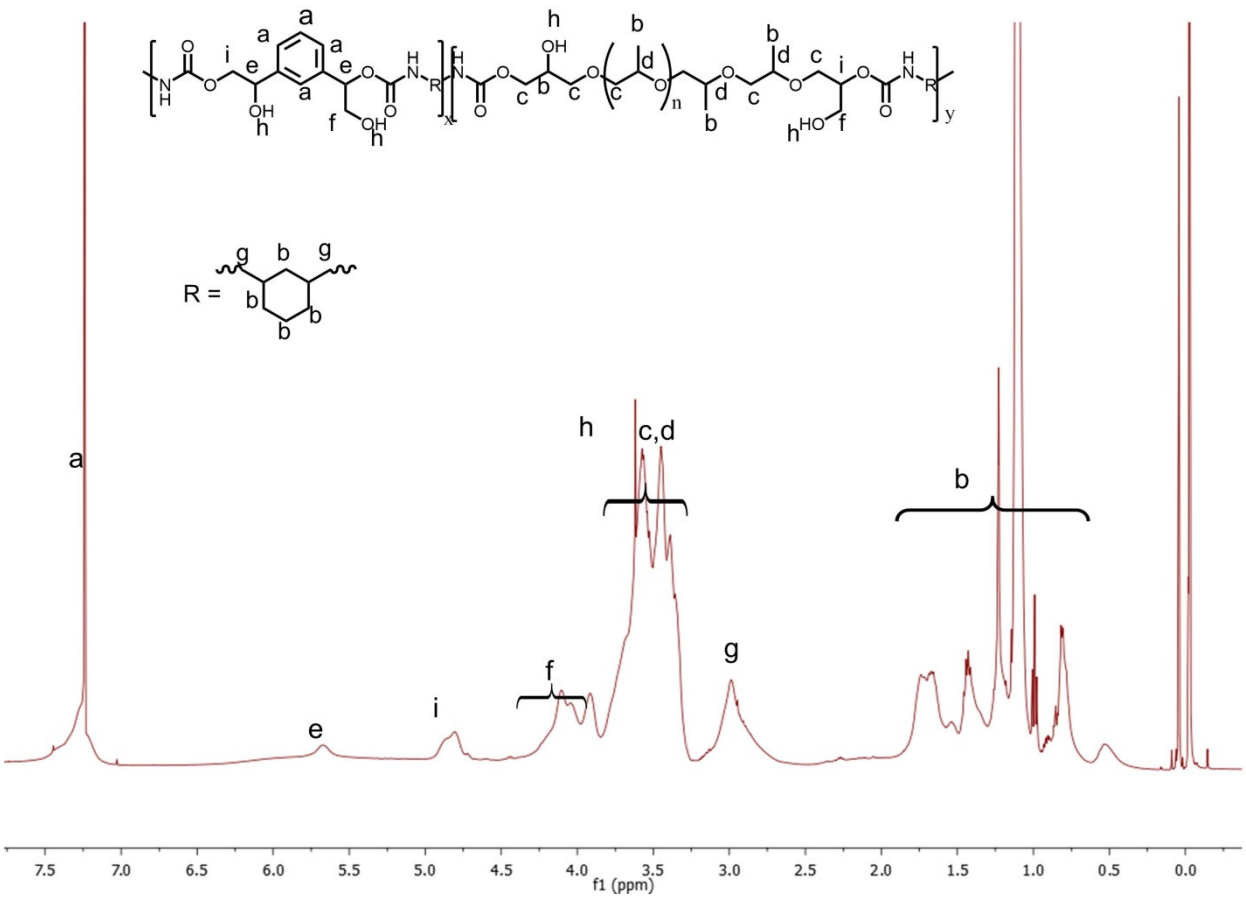

Figure A3: ^{1}H NMR Spectra of PPG/CYC/50 PHU in $CDCl_3$.

PPG/CYC/50. ^{1}H NMR (CDCl3, 500 MHz), δ (ppm): 0.5-2.0 (3H, $OCH_2CH(C\boldsymbol{H}_3)O$), 10H $NHCH_2(C\boldsymbol{H}C\boldsymbol{H}_2C\boldsymbol{H}_2C\boldsymbol{H}_2C\boldsymbol{H}C\boldsymbol{H})CH_2NH$), 2.7-3.2 (1H, $C\boldsymbol{H}_2NHC(=O)O$), 3.3-3.8 (2H, $OC\boldsymbol{H}_2CH(CH_3)O$, 1H, $OCH_2C\boldsymbol{H}(CH_2OH)O$, 1H, $O\boldsymbol{H}$), 3.8-4.2 (2H, $C\boldsymbol{H}_2OH$), 4.8-5.0 (1H, $C\boldsymbol{H}OC(=O)NH$), 5.6-5.7 (1H, $PhC\boldsymbol{H}(CH_2OH)O$), 7.0-7.5 (Ph).

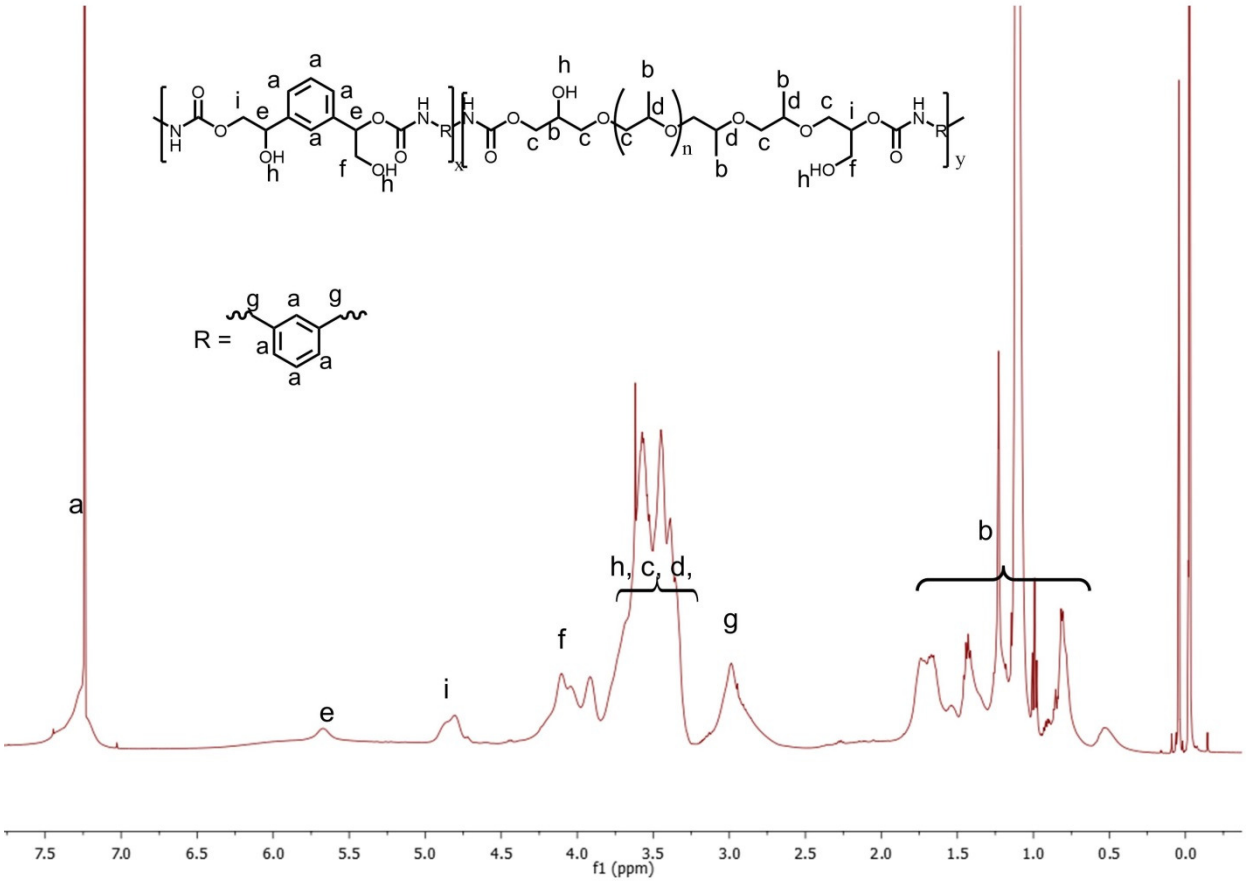

Figure A4: ^{1}H NMR Spectra of PPG/XYL/40 PHU in $CDCl_3$.

PPG/XYL/40. ^{1}H NMR (CDCl3, 500 MHz), δ (ppm): 0.5-2.0 (3H, $OCH_2CH(C\boldsymbol{H}_3)O$) , 2.7-3.2 (1H, $C\boldsymbol{H}_2NHC(=O)O$), 3.3-3.8 (2H, $OC\boldsymbol{H}_2CH(CH_3)O$, 1H, $OCH_2C\boldsymbol{H}(CH_2OH)O$, 1H, $O\boldsymbol{H}$), 3.8-4.2 (2H, $C\boldsymbol{H}_2OH$), 4.8-5.0 (1H, $C\boldsymbol{H}OC(=O)NH$), 5.6-5.7 (1H, $PhC\boldsymbol{H}(CH_2OH)O$), 7.0-7.5 (Ph).

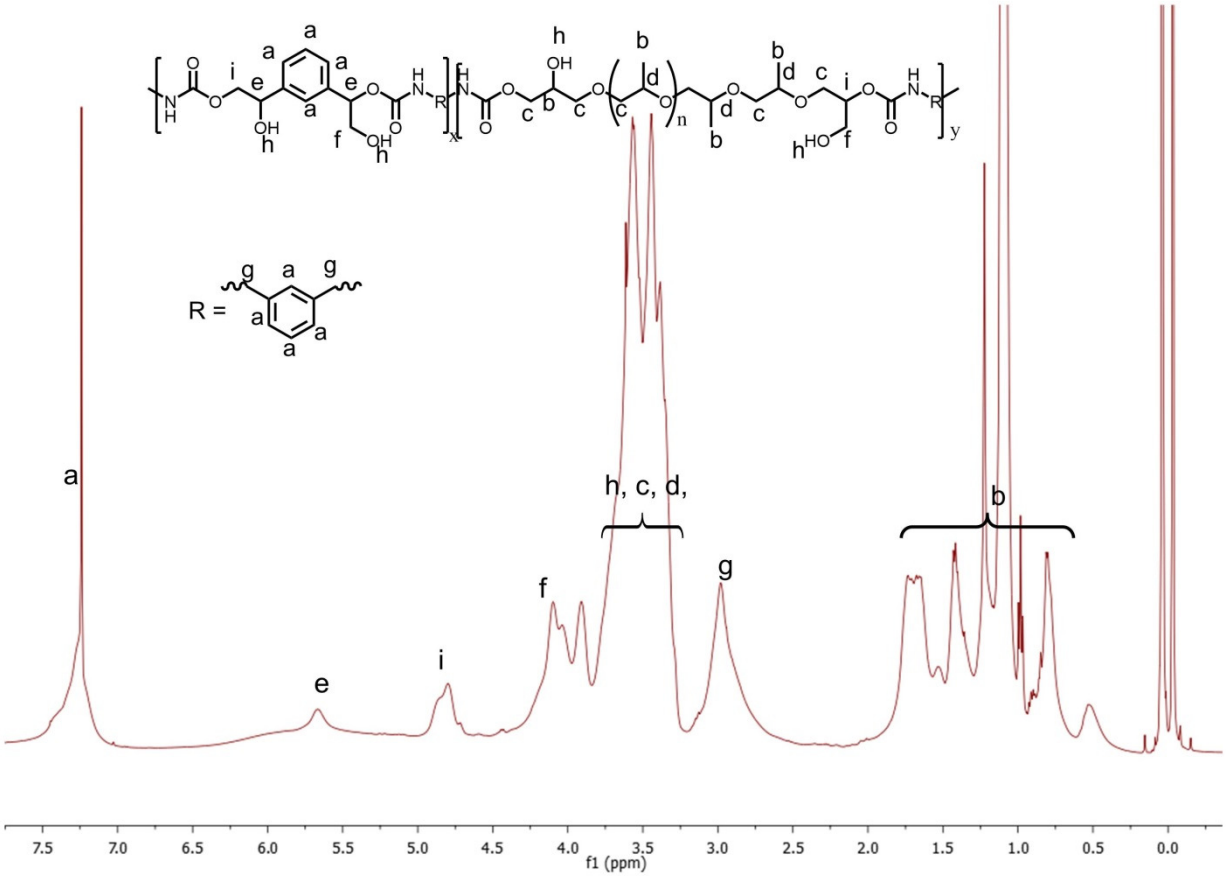

Figure A5: ^{1}H NMR Spectra of PPG/XYL/50 PHU in $CDCl_3$.

PPG/XYL/50. ^{1}H NMR (CDCl3, 500 MHz), δ (ppm): 0.5-2.0 (3H, $OCH_2CH(C\boldsymbol{H}_3)O$) , 2.7-3.2 (2H, $C\boldsymbol{H}_2NHC(=O)O$), 3.3-3.8 (2H, $OC\boldsymbol{H}_2CH(CH_3)O$, 1H, $OCH_2C\boldsymbol{H}(CH_2OH)O$, 1H, $O\boldsymbol{H}$), 3.8-4.2 (2H, $C\boldsymbol{H}_2OH$), 4.8-5.0 (1H, $C\boldsymbol{H}OC(=O)NH$), 5.6-5.7 (1H, $PhC\boldsymbol{H}(CH_2OH)O$), 7.0-7.5 (Ph)).

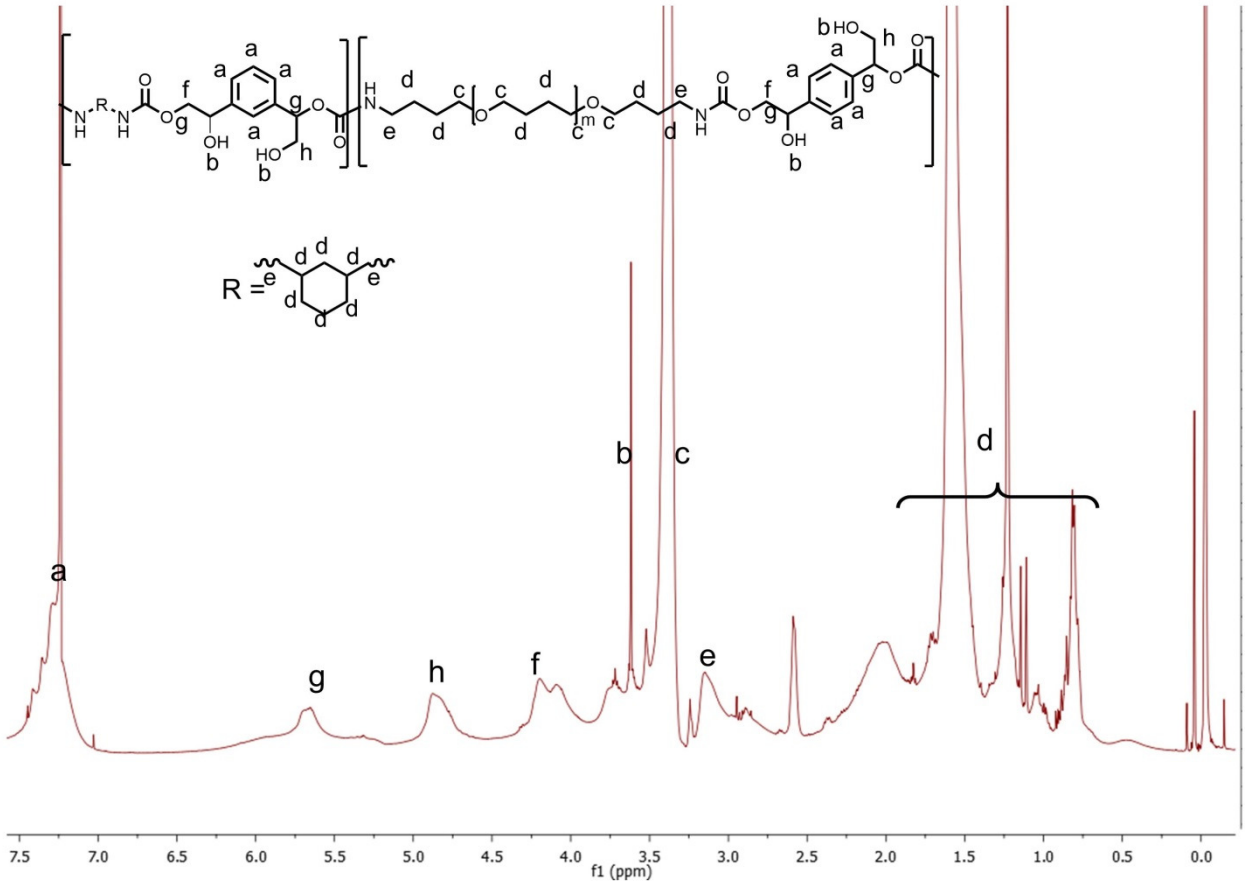

Figure A6: ^{1}H NMR Spectra of PTMO/CYC/40 PHU in $CDCl_3$.

PTMO/CYC/40. ^{1}H NMR (CDCl3, 500 MHz), δ (ppm): 0.5-2.0 (8H, $OCH_2C\boldsymbol{H}_2C\boldsymbol{H}_2CH_2O$, $NHCH_2C\boldsymbol{H}_2C\boldsymbol{H}_2CH_2O$, $NHCH_2(C\boldsymbol{H}C\boldsymbol{H}_2C\boldsymbol{H}_2C\boldsymbol{H}_2C\boldsymbol{H}C\boldsymbol{H})CH_2NH$), 2.8-3.2 (1H, $NHC\boldsymbol{H}_2CH_2CH_2CH_2O$, $NHC\boldsymbol{H}_2$), 3.3-3.5 (4H, $C\boldsymbol{H}_2OC\boldsymbol{H}_2$, $NHC(=O)OC\boldsymbol{H}_2$), 3.6-3.7 (1H, O***H***), 3.9-4.2 (2H, $C\boldsymbol{H}_2OC(=O)NH$), 4.7-5.0 (2H, $C\boldsymbol{H}_2OH$), 5.5-5.6 (1H, $PhC\boldsymbol{H}(CH_2OH)O$), 7.0-7.5 (4H, Ph).

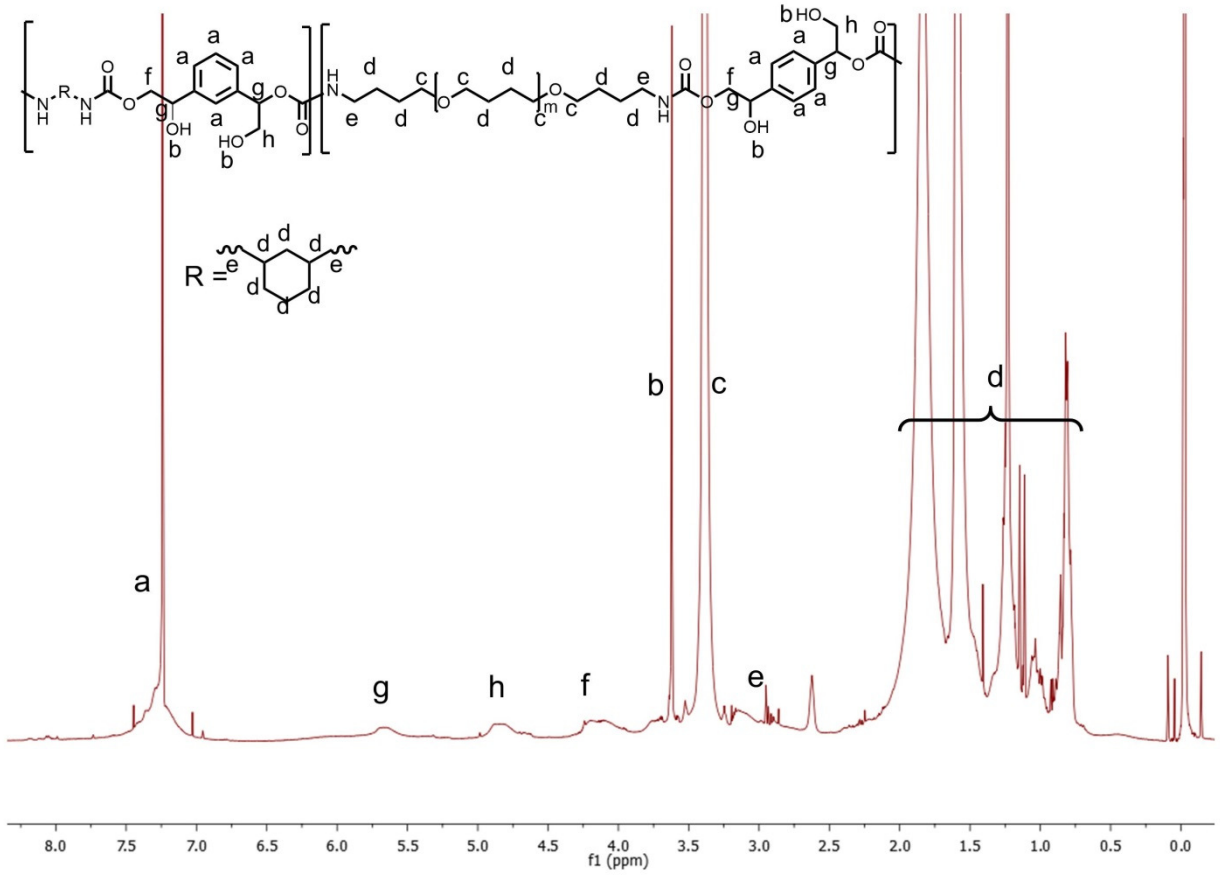

Figure A7: ^{1}H NMR Spectra of PTMO/CYC/50 PHU in $CDCl_3$.

PTMO/CYC/50. ^{1}H NMR (CDCl3, 500 MHz), δ (ppm): 0.5-2.0 (8H, $OCH_2C\boldsymbol{H}_2C\boldsymbol{H}_2CH_2O$, $NHCH_2C\boldsymbol{H}_2C\boldsymbol{H}_2CH_2O$, $NHCH_2(C\boldsymbol{H}C\boldsymbol{H}_2C\boldsymbol{H}_2C\boldsymbol{H}_2C\boldsymbol{H}C\boldsymbol{H})CH_2NH$), 2.8-3.2 (1H, $NHC\boldsymbol{H}_2CH_2CH_2CH_2O$, $NHC\boldsymbol{H}_2$), 3.3-3.5 (4H, $C\boldsymbol{H}_2OC\boldsymbol{H}_2$, $NHC(=O)OC\boldsymbol{H}_2$), 3.6-3.7 (1H, O***H***), 3.9-4.2 (2H, $C\boldsymbol{H}_2OC(=O)NH$), 4.7-5.0 (2H, $C\boldsymbol{H}_2OH$), 5.5-5.6 (1H, $PhC\boldsymbol{H}(CH_2OH)O$), 7.0-7.5 (4H, Ph).

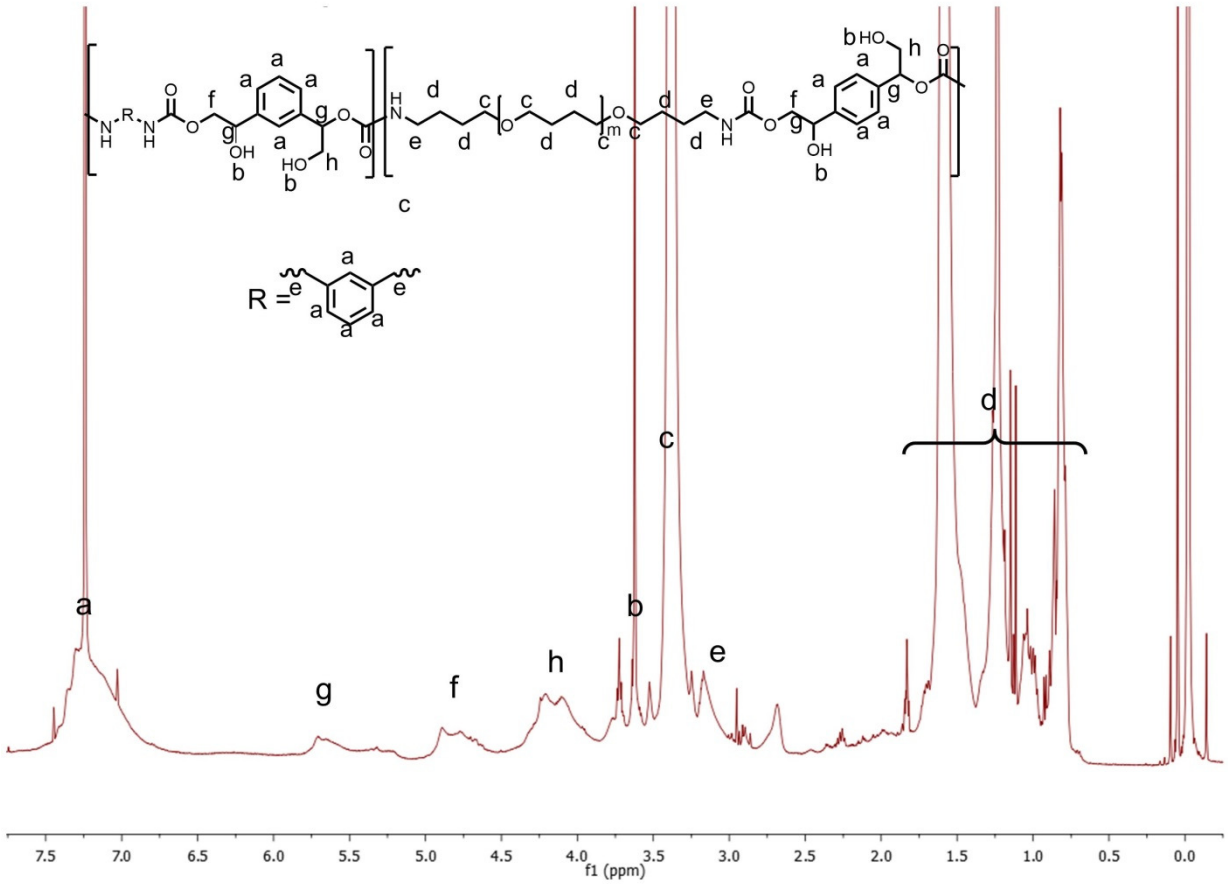

Figure A8: ^{1}H NMR Spectra of PTMO/XYL/40 in $CDCl_3$.

PTMO/XYL/40. ^{1}H NMR (CDCl3, 500 MHz), δ (ppm): 0.5-2.0 (8H, $OCH_2C\boldsymbol{H}_2C\boldsymbol{H}_2CH_2O$, $NHCH_2C\boldsymbol{H}_2C\boldsymbol{H}_2CH_2O$, 2.8-3.2 (1H, $NHC\boldsymbol{H}_2CH_2CH_2CH_2O$, $NHC\boldsymbol{H}_2$), 3.3-3.5 (4H, $C\boldsymbol{H}_2OC\boldsymbol{H}_2$, $NHC(=O)OC\boldsymbol{H}_2$), 3.6-3.7 (1H, O***H***), 3.9-4.2 (2H, $C\boldsymbol{H}_2OC(=O)NH$), 4.7-5.0 (2H, $C\boldsymbol{H}_2OH$), 5.5-5.6 (1H, $PhC\boldsymbol{H}(CH_2OH)O$), 7.0-7.5 (4H, Ph).

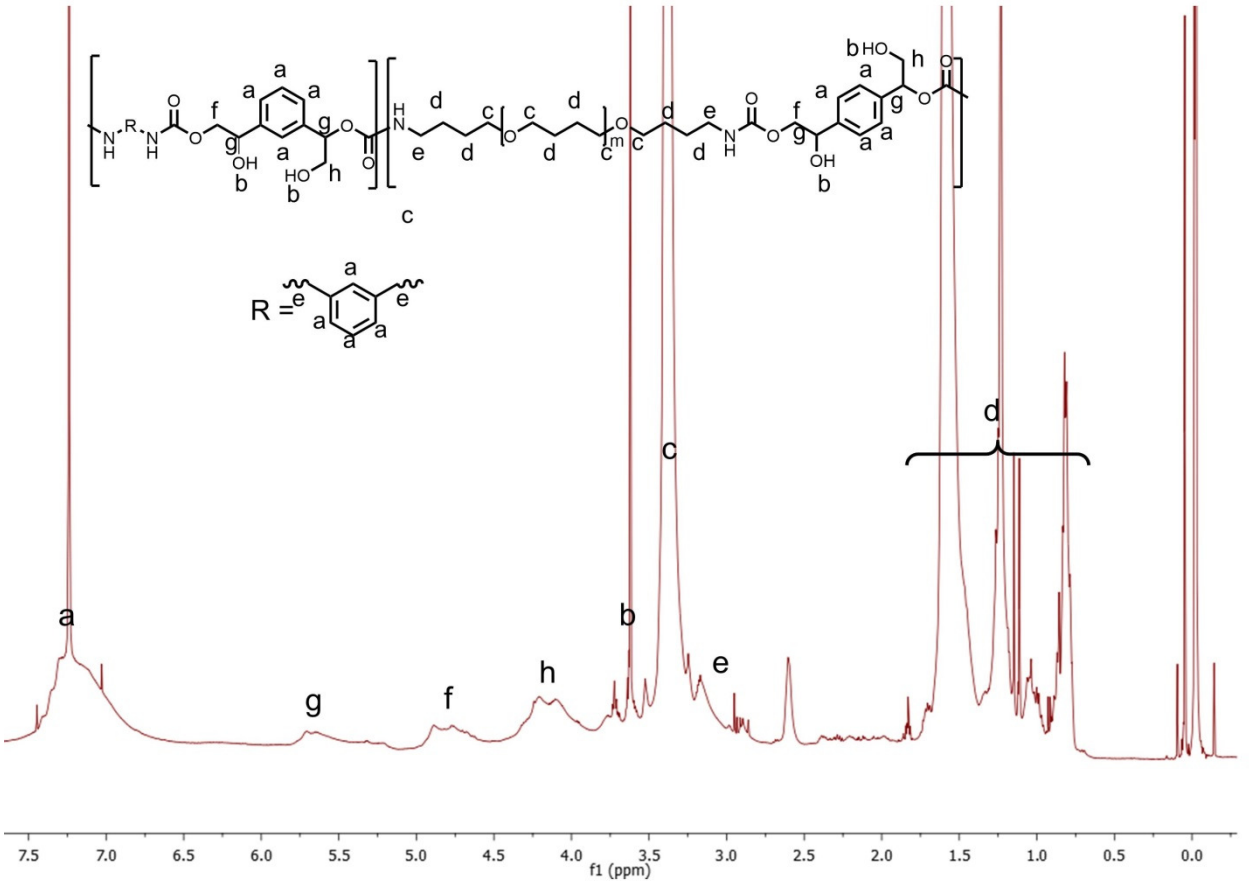

Figure A9: ^{1}H NMR Spectra of PTMO/XYL/50 in $CDCl_3$.

PTMO/XYL/50. ^{1}H NMR (CDCl3, 500 MHz), δ (ppm): 0.5-2.0 (8H, $OCH_2C\boldsymbol{H}_2C\boldsymbol{H}_2CH_2O$, $NHCH_2C\boldsymbol{H}_2C\boldsymbol{H}_2CH_2O$, 2.8-3.2 (1H, $NHC\boldsymbol{H}_2CH_2CH_2CH_2O$, $NHC\boldsymbol{H}_2$), 3.3-3.5 (4H, $C\boldsymbol{H}_2OC\boldsymbol{H}_2$, $NHC(=O)OC\boldsymbol{H}_2$), 3.6-3.7 (1H, O***H***), 3.9-4.2 (2H, $C\boldsymbol{H}_2OC(=O)NH$), 4.7-5.0 (2H, $C\boldsymbol{H}_2OH$), 5.5-5.6 (1H, $PhC\boldsymbol{H}(CH_2OH)O$), 7.0-7.5 (4H, Ph).

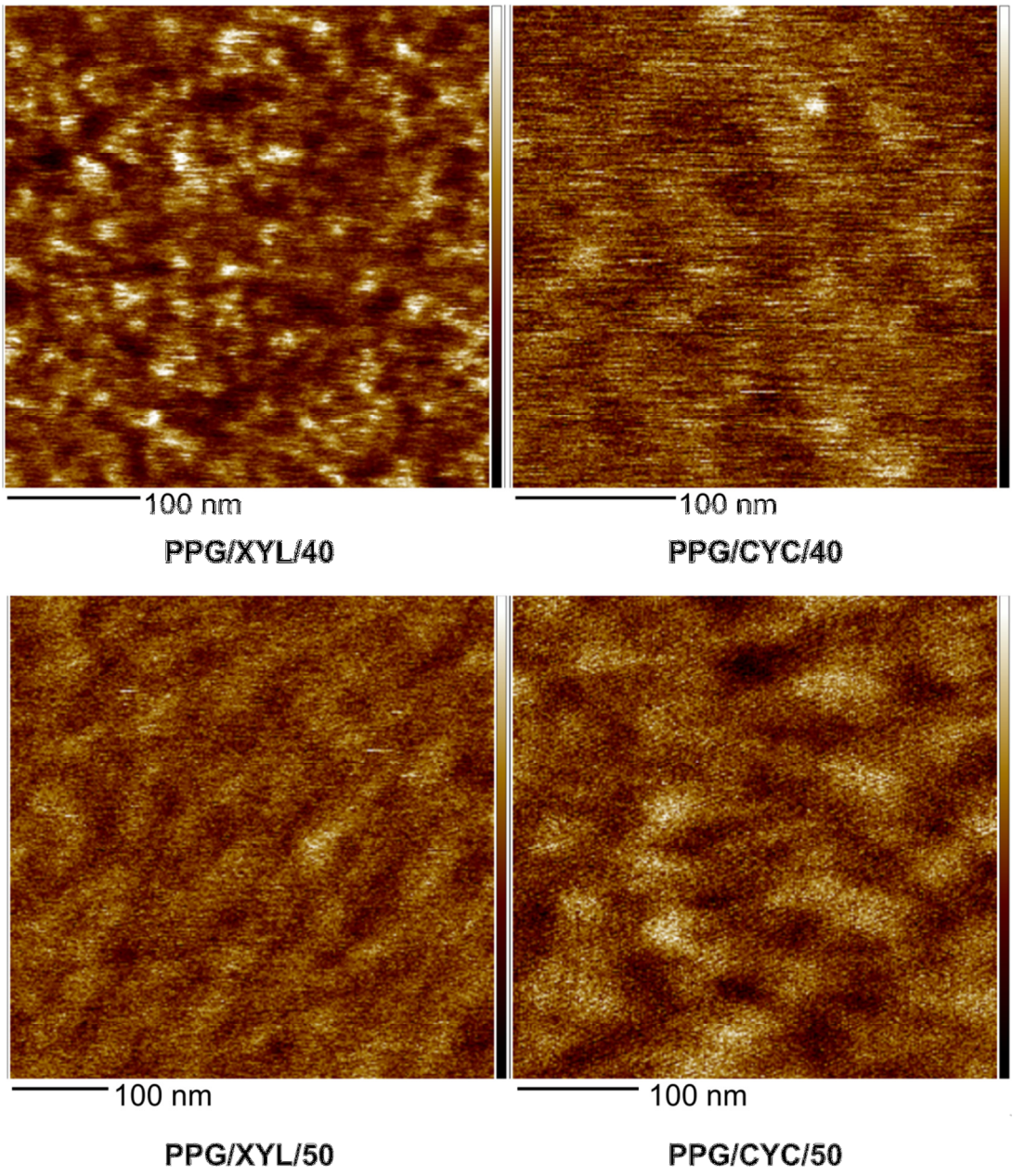

Figure A10:. Atomic force microscopy (AFM) phase images of the PPG-based PHUs. Phase separation is evident by the presence of dark and bright regions on the AFM images. Images were obtained using a Bruker Dimension FastScan Atomic Force Microscope in tapping mode.

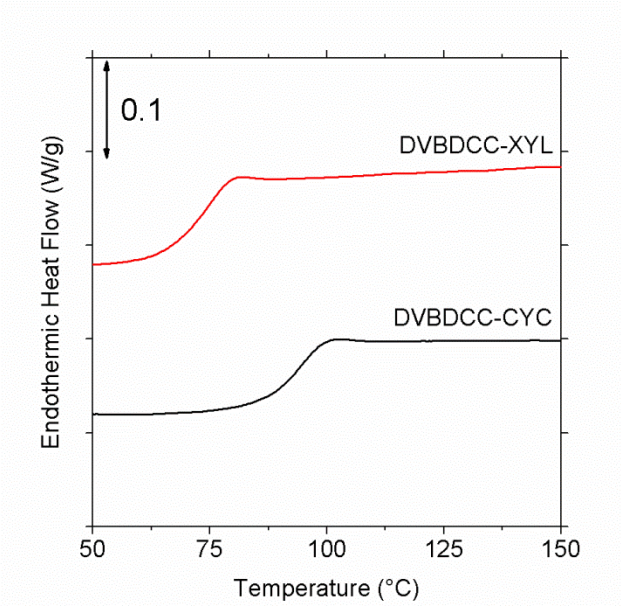

Figure A11: Differential scanning calorimetry heat flow curves for pure hard segment single-phase PHUs. The T_gs at ½ Δ C_p are 93 °C for DVBDCC/CYC and 72 °C for DVBDCC/XYL.

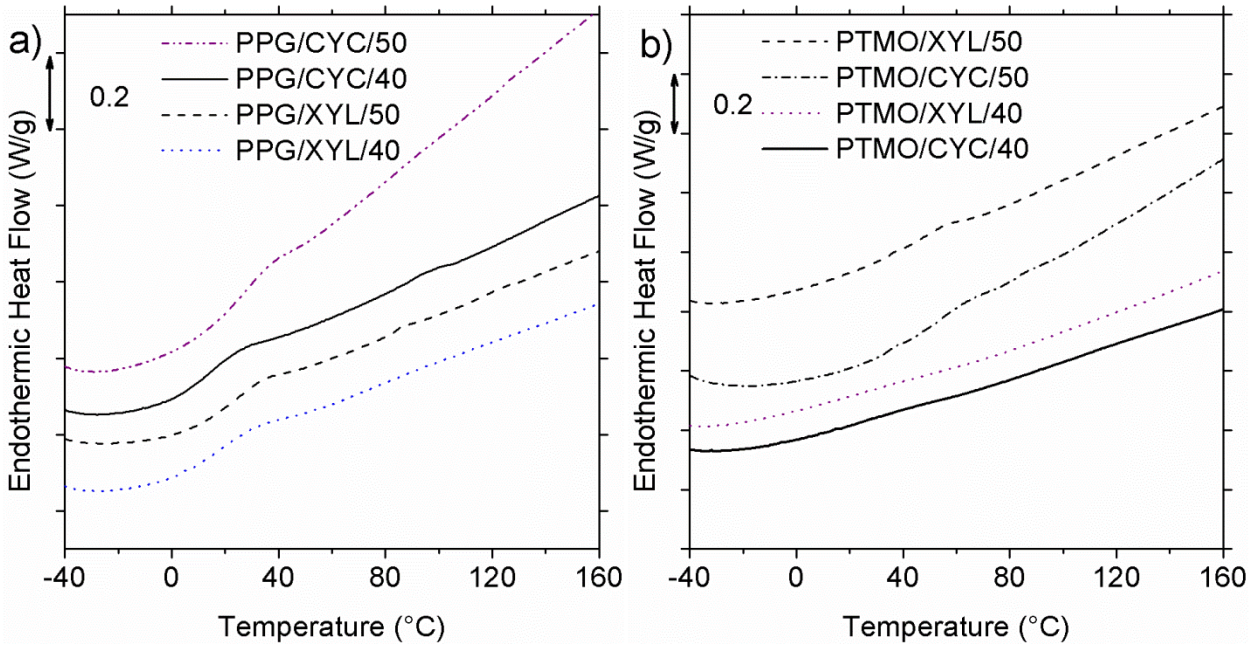

Figure A12: DSC Thermograms of a) PPG-based PHUs and b) PTMO-based PHUs.

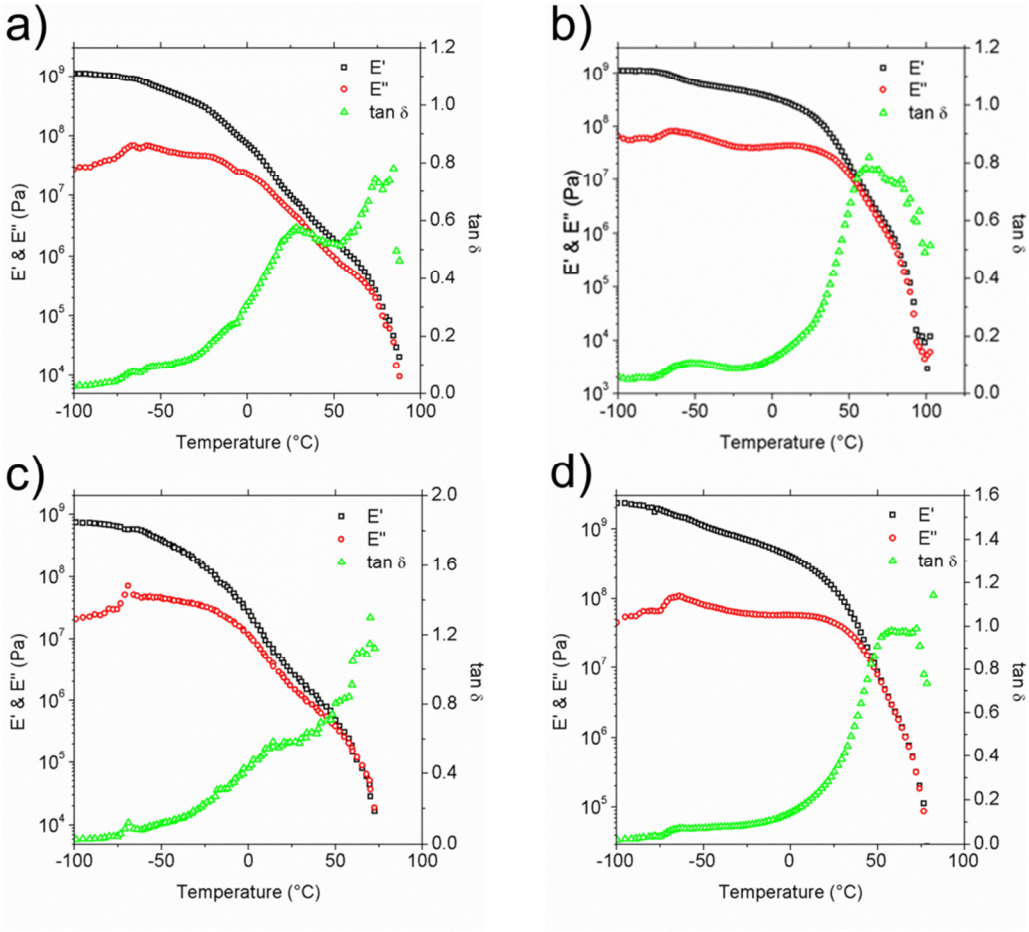

Figure A13: DMA profiles of PTMO-based PHU formulations: a) PTMO/CYC/40, b) PTMO/CYC/50, c) PTMO/XYL/40, d) PTMO/XYL/50.

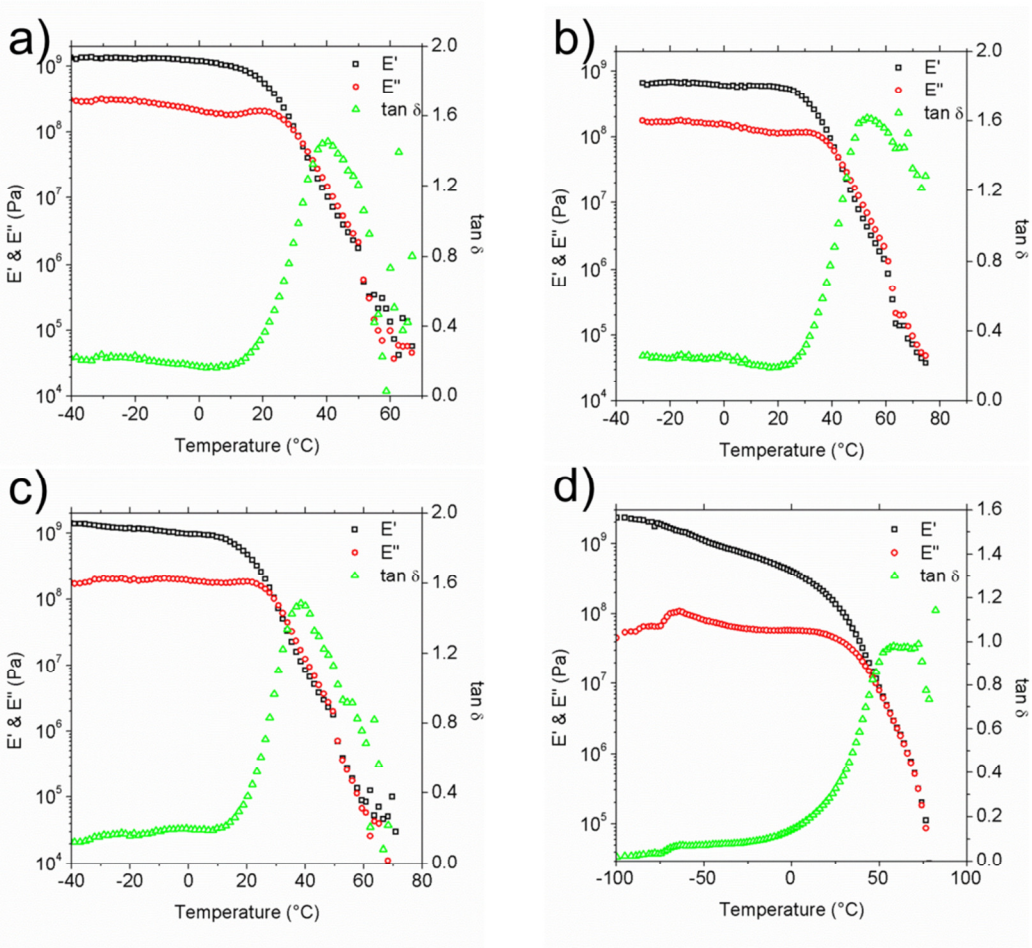

Figure A14: DMA profiles of PPG-based PHU formulations: a) PPG/CYC/40, b) PPG/CYC/50, c) PPG/XYL/40, d) PPG/XYL/50.

CHAPTER 4

Novel Thermoplastic Polyhydroxyurethane Elastomers as Effective Damping Materials over Broad Temperature Ranges

4.1 Introduction

Polyurethane is one of the most important commodity polymers in the world with an estimated world-wide production of 18 million tons in 2016 (Nohra 2013). It is used in a wide range of applications, including flexible and rigid foams, coatings, adhesives, elastomers and biomedical implants (Nohra 2013, Oertel 1994, Delebecq 2013, Engels 2013). It is produced from a step growth reaction between isocyanate and alcohol with relatively fast reaction kinetics. Despite its wide-ranging applications, in recent years there have been increasing constraints on the use, transport and handling of isocyanate from various regulatory bodies such as the United States Environmental Protection Agency and the European Union (Official Journal of European Union 2009, US EPA 2011, US EPA 2015, US EPA 2016). These constraints have fueled significant efforts from both academic and industrial research communities to develop alternatives to PU materials that are synthesized without employing isocyanate-based chemistry.

Cyclic carbonate aminolysis has emerged as one of the most promising chemistries to produce PU-like material without using isocyanate (Guan 2011, Kathalewar 2013, Blattmann 2014, Maisonneuve 2015). This chemistry relies on the ring opening of five-, six-, seven-, or eight-membered-ring cyclic carbonates by amine moieties to produce polyhydroxyurethane (PHU) that is analogous to PU with the exception of an additional primary or secondary hydroxyl group adjacent to the urethane linkage (Oertel 1994, Guan 2011, Kathalewar 2013, Blattmann 2014, Maisonneuve 2015, Yuen 2016). Five-membered-ring cyclic carbonates can be easily obtained from a carbon dioxide insertion reaction into an epoxy ring enabling the

generation of carbonate monomers from various epoxy precursors (Besse 2013b). In recent years, numerous studies have investigated PHU synthesis with strong emphasis on the production of single-phase PHUs, crosslinked PHU networks, reaction catalysis and the synthesis of carbonate monomers (Yuen 2016, Besse 2013b, Kihara 1993, Steblyanko 2000, Ochiai 2005, Tomita 2001b, Tomita 2001a, Tomita 2001c, Tomita 2001e, Tomita 2001d, Ochiai 2005a, Ochiai 2005b, Kim 2001, Figovsky 2002, Birukov 2012, Van Velthoven 2015, Duval 2015, Tryznowski 2015, Lambeth 2015, Lombardo 2015, Blain 2014, Bähr 2012, Tamami 2004, Javni 2008, Javni 2013, Bähr 2012, Fleischer 2013, Besse 2013b, Kathalewar 2014, Lee 2015, Fortman 2015, Matsukizono 2015, Cornille 2015, Benyahya 2011, Maisonneuve 2014a, Tang 2011, Lebarbe 2014, Sheng 2015, Maisonneuve 2014b, Lamarzelle 2016). For example, Endo and coworkers (Kihara 1993, Steblyanko 2000, Ochiai 2005, Tomita 2001b, Tomita 2001a, Tomita 2001c, Tomita 2001e, Tomita 2001d, Ochiai 2005a), as well as others (Ochiai 2005b, Kim 2001, Figovsky 2002, Birukov 2012, Van Velthoven 2015, Duval 2015), synthesized PHUs from carbonated epoxy resins (such as Bisphenol A diglycidyl ether, hydroquinone diglycidyl ether, and butanediol diglycidyl ether) and small-molecule diamines (such as hexamethylene diamine) resulting in single-phase PHUs (Yuen 2016, Besse 2013b, Kihara 1993, Steblyanko 2000, Ochiai 2005, Tomita 2001b, Tomita 2001a, Tomita 2001c, Tomita 2001e, Tomita 2001d, Ochiai 2005a, Ochiai 2005b, Kim 2001, Figovsky 2002, Birukov 2012, Van Velthoven 2015, Duval 2015). The reaction kinetics of five-, six- (Tomita 2001b, Tomita 2001a, Maisonneuve 2014b), seven- (Tomita 2001c) and eight-membered ring carbonates (Yuen 2016), the influence of substituent on reactivity (Tomita 2001e, Lamarzelle 2016), and the effects of catalysts (Tomita 2001d, Blain 2014, Lambeth 2013, Lombardo 2015) were also characterized. Renewable resources such as carbonated soybean oil, linseed oil (Bähr 2012, Tamami 2004, Javni 2008, Besse 2013b, Kathalewar 2014), limonene (Bähr 2012), cellulose (Fleischer 2013), isosorbide (Besse 2013b), cashew nut shell liquid (Kathalewar 2014), and glycerol (Fleischer

2013) have been used to make crosslinked PHUs. Other investigators have studied various routes to generate cyclic carbonate monomers for synthesizing single-phase and crosslinked PHUs (Fortman 2015, Matsukizono 2015, Cornille 2015, Benyahya 2011, Benyahya 2012, Maisonneuve 2014a, Tang 2011, Lebarbe 2014) as well as the increased reactivity of eight-membered ring carbonates allowing room temperature synthesis without the aid of catalysts (Yuen 2016).

While extensive research has been done on PHU synthesis, relatively little work has focused on nanophase-separated PHUs as thermoplastic elastomer (Nanclares 2015, Leitsch 2016a). Only one study has contributed to understanding the role of hydroxyl groups in modifying the properties of thermoplastic PHU elastomer in comparison to analogous, isocyanate-based thermoplastic PU elastomers (TPUs) (Leitsch 2016a). TPUs are obtained from step-growth reactions between long-chain diol as the soft segment and diisocyanate with chain extender as the hard segment. The soft segment has a glass transition temperature (T_g) below room temperature whereas the hard segment has a T_g, or in some cases a melt temperature (T_m), above room temperature. The incompatibility between the two segments and the hydrogen bonding between polar urethane units result in nanophase separation in TPU; the hard domains dispersed in a rubbery matrix act as physical crosslinking sites, leading to elastomeric character (Hepburn 1992, Holden 1994).

TPUs typically exhibit very good nanophase separation with narrow T_g ranges of their respective components (Korley 2006, Klinedinst 2012, Das 2007, O'Sickey 2002b, O'Sickey 2002a, O'Sickey 2003, Yilgor 2015, Seefried 1975a, Seefried 1975b, Seefried 1975c, Seefried 1975d, Kojio 2009, Eceiza 2008). Dynamic mechanical analysis (DMA) of TPUs typically shows sharp transitions with well-defined loss tangent (tan δ) peaks over a narrow temperature range (Korley 2006, Klinedinst 2012, Das 2007, O'Sickey 2002b, O'Sickey 2002a, O'Sickey 2003, Yilgor 2015, Seefried 1975a, Seefried 1975b, Seefried 1975c, Seefried 1975d, Kojio 2009,

Eceiza 2008). A common criterion to identify effective, broad-temperature-range, acoustic and/or vibration damping materials is tan $\delta \geq 0.30$ over at least a 60 °C temperature range (Sophiea 1994, Huelck 1972a, Huelck 1972b, Hu 1997, Chern 1999, Qin 2004, Chen 1994, Yu 1999, Hourston 1996). Given its characteristic viscoelastic response, TPU by itself cannot serve as a broad-temperature-range acoustic damping material. To increase the T_g breadth, efforts have been made to combine TPUs with secondary polymeric components such as epoxy (Chern 1999), polyester (Qin 2004), polyacrylate (Chen 1994, Yu 1999), polystyrene (Hourston 1996), etc. into crosslinked interpenetrating polymeric network (IPN) structures. The intimate mixing created by an IPN structure produces microheterogenous domains with a range of local compositions and a broad tan δ profile (Sophiea 1994, Huelck 1972a, Huelck 1972b, Hu 1997, Chern 1999, Qin 2004, Chen 1994, Yu 1999, Hourston 1996).

In Chapter 3, we described the synthesis and characterization of thermoplastic PHU elastomer from several polyether-based soft segments. We compared PU and PHU having analogous chemical structures and demonstrated that the hydroxyl groups in PHU play a critical role in the development of nanophase separation in segmented PHUs. When a polyethylene oxide (PEO)-based soft segment is used, significant phase mixing occurs due to the high density of oxygen atoms in PEO resulting in PHU that flows under the force of gravity; in contrast, an analogous TPU synthesized from PEO-based soft segment shows good mechanical properties (Leitsch 2016a, Korley 2006). This difference is due to hydrogen bonding of hard-segment hydroxyl groups in PHU to oxygen atoms in PEO soft segments. This hydrogen bonding can be suppressed by using polypropylene oxide (PPO)-based soft segments with sterically hindered oxygen atoms and polytetramethylene oxide (PTMO)-based soft segments with dilution of oxygen atom content relative to PEO-based soft segments. In a limited demonstration, it is showed that the hydroxyl groups can be advantageous in PTMO-based PHUs yielding good damping properties over a broad temperature range, a function not observed in isocyanate-based

TPUs (Korley 2006, Klinedinst 2012, Das 2007, O'Sickey 2002b, O'Sickey 2002a, O'Sickey 2003, Yilgor 2015, Seefried 1975a, Seefried 1975b, Seefried 1975c, Seefried 1975d, Kojio 2009, Eceiza 2008). The presence of some level of phase mixing results in materials with broad interphases having a wide range of local composition and therefore broad T_g responses. As viscoelastic polymeric materials possess the most effective damping properties near their T_gs, such responses allow PTMO-based PHUs to serve as acoustic damping materials over a broad range of use temperature without the need to produce IPN structures.

In this chapter, we describe a more complete study of PTMO-based segmented, thermoplastic PHUs as damping materials over broad and tunable temperature ranges without employing IPN structures. The tunability of temperature range for good damping performance can be achieved through variation in hard-segment content and chain-extender structure. We synthesized and characterized a series of PHUs with three different chain extenders at four different hard-segment contents. Small-angle X-ray scattering (SAXS) demonstrates the presence of nanophase-separated morphology within these materials. Tensile tests demonstrates elastomeric-like material responses with tunable mechanical properties. DMA demonstrates that these materials exhibit high tan δ values (≥ 0.30) over broad and tunable temperature ranges of at least 60 °C. The thermoplastic nature of these broad-temperature-range, PHU damping materials allow them to be molded and shaped into various forms to suit multiple needs.

4.2 Experimental

Materials. Diamine-terminated PTMO (XTJ-548, M_n = 1700 g/mol) was supplied by Huntsman Corporation. Hydroxyl-terminated PTMO (M_n = 2000 g/mol), 2,4-tolylene diisocyanate (2,4-TDI, 95%), 1,4-cyclohexanedimethanol (mixture of cis and trans isomers, 99%), 1,6-hexanediol (99%), dibutyltindilaurate (DBTDL), 1,4-butanediol (BDO, 99%), 1,3-cyclohexanebis(methyl amine) (CYCDA, mixture of isomers, 99%) and hexamethylene diamine (HMDA, 98%) were

purchased from SigmaAldrich and used as received. *p*-xylylene diamine (pXDA, 99%) was purchased from TCI America and used as received. Dimethylformamide (DMF) was purchased from Fischer Scientific and used as received. Divinylbenzene dicyclocarbonate (DVBDCC) was synthesized according to the procedure outlined in Chapter 3 (Leitsch 2016a).

Synthesis of Thermoplastic PHU Elastomer. All PHUs were synthesized following Scheme 4.1. Material formulations were varied by adjusting molar ratios of reacting components according to Table 4.1. The hard-segment content is defined by (weight of DVBDCC + weight of chain extender)/(weight of DVBDCC + weight of chain extender + weight of XTJ-548). The naming convention for PHUs in this study is CYCDA-XX, HMDA-XX, and pXDA-XX for PHUs chain extended with 1,3-cyclohexanebis(methyl amine), hexamethylene diamine and *p*-xylylene diamine, respectively, whereas XX indicates the hard-segment content in the material. For example, CYCDA-40 is synthesized with 1,3-cyclohexanebis(methyl amine) as the chain extender with 40 wt% hard-segment content. In a typical synthesis of CYCDA-40, 2 g (8 mmol) of DVBDCC, 4.152 g (2.59 mmol) of XTJ-548 and 0.77 g (5.41 mmol) of 1,3-cyclohexanebis(methyl amine) were combined in a FlackTek max 20 cup. Then, 6.3 mL of DMF were added to adjust the concentration of reacting functional groups to 0.60 M. The mixture was then homogenized in a FlackTek SpeedMixer™ for 5 min at 3500 rpm. Then, it was reacted at 70 °C for 24 hr. Upon completion of reaction, the mixture was homogenized again for 5 min. The mixture was poured into a FlackTek max 50 cup and dried in an oven maintained at 70 °C for at least 24 hr to remove solvent. The dried materials were hot-pressed into a 1-mm-thick sheet at ~100 °C using a PHI (Model 0230C-X1) press with 5 ton ram force.

Synthesis of Thermoplastic PU Elastomer. The analogous TPUs used in this study were synthesized with hydroxyl-terminated PTMO, 2,4-TDI, 1,4-cyclohexanedimethanol and 1,6-hexanediol at 30 wt% hard-segment content. The hydroxyl-terminated PTMO was first dried by bubbling through nitrogen at 130 °C overnight prior to use. In a typical synthesis of TPU chain

Table 4.1: Composition, thermal properties as determined from dynamic mechanical analysis, interdomain spacings determined from SAXS and temperature range with good damping performance of PTMO-based PHUs. HS: hard segment, CE: chain extender, SS: soft segment.

Sample Name	Molar Ratio (HS/CE/SS)	HS Content (wt %)	*d*-spacing (nm)[a]	SS T_g (°C)[b]	T_{flow} (°C)[c]	T (tan δ ≥ 0.30) (°C)	ΔT (°C)
CYCDA-30	2.1/1.1/1	30	11.7	-61	51	-27 – 51	78
CYCDA-40	3.1/2.1/1	40	12.7	-66	80	-1 – 80	81
CYCDA-50	4.4/3.4/1	50	13.3	-66	89	32 – 89	57
CYCDA-60	6.5/5.5/1	60	16.4	-67	92	38 - 92	54
HMDA-30	2.2/1.2/1	30	14.7	-63	40	-33 – 40	73
HMDA-40	3.2/2.2/1	40	15.0	-65	48	-9 – 48	57
HMDA-50	4.7/3.7/1	50	15.2	-66	54	10 – 54	44
HMDA-60	6.9/5.9/1	60	16.4	-65	64	16 – 64	48
pXDA-30	2.1/1.1/1	30	12.4	-62	50	-31 – 50	81
pXDA-40	3.1/2.1/1	40	14.6	-66	75	0 – 75	75
pXDA-50	4.5/3.5/1	50	14.6	-63	80	10 – 80	70
pXDA-60	6.6/5.6/1	60	17.2	-66	90	26 - 90	64

[a] Interdomain spacing is calculated using $d = 2\pi/q_{max}$.

[b] Determined from the peak in the loss modulus (E") curves in DMA on heating from -100 °C to 150 °C at a rate of 3 °C/min, frequency of 1 Hz, and strain of 0.03%.

[c] T_{flow} is defined as the temperature at which the material starts to irreversibly deform; this is often reported as the temperature prior to inconsistent tan δ data, close to the temperature at which the sample is no longer mechanically robust.

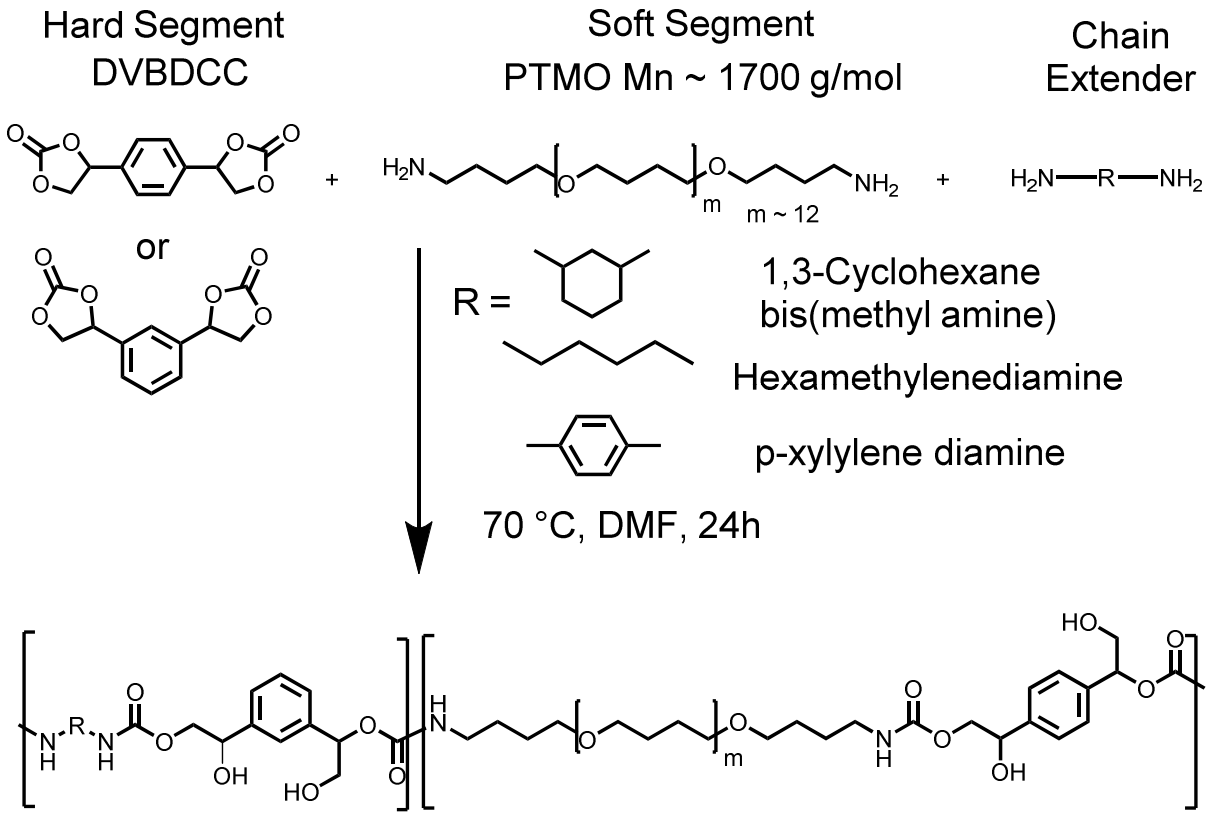

Scheme 4.1: Reaction scheme for the formation of segmented PHUs from DVBDCC, PTMO and chain extenders. The PHUs can either possess a 1° or 2° hydroxyl group; a mixture of these products is expected.

extended with 1,6-hexanediol, 10 g (5 mmol) of PTMO were reacted with 2.91 g (16.7 mmol) of 2,4-TDI in a three-necked flask equipped with overhead stirrer at 60 °C for 2 hr with 10 μL of DBTDL as catalyst. The resulting prepolymer was transferred into a mixing cup, and 1.38 g (11.7 mmol) of 1,6-hexanediol were added and mixed for 30 s at 3500 rpm in a FlackTek mixer. The mixture was poured into a mold and cured at 60 °C for 2 hr. A similar procedure was used to synthesize PU chain extended with 1,4-cyclohexanedimethanol at 30 wt% hard-segment content.

Attenuated Total Reflectance-Fourier Transform Infrared (ATR-FTIR) Spectroscopy. All PHUs were analyzed for complete conversion of carbonate groups with a Bruker Tensor 37 Mid IR FTIR spectrometer equipped with an ATR diamond/ZnSe attachment. Dried materials were scanned at a resolution of 4 cm^{-1}; 32 scans were obtained in the 4000-600 cm^{-1} range for each spectrum.

^{1}H NMR Spectroscopy. ^{1}H NMR spectra were recorded on a Bruker Avance III 500 MHz NMR spectrometer with a direct cryoprobe at room temperature in deuterated chloroform ($CDCl_3$). Spectra are reported in parts per million relative to tetramethylsilane.

Molecular Weight Characterization. The molecular weights (MWs) of PHUs were determined using gel permeation chromatography. A Waters 2695 separation module and two Tosoh TSKgel Alpha-M columns (13 μm) in series were used. The eluent was DMF with 4 g/L of $LiNO_3$ at 40 °C; the elution rate was 0.5 mL/min. The detector was a Viscotek TDA 302 interface/Waters 2414 RI detector. Molecular weight values were reported relative to polyethylene oxide (PEO) standards. Agilent PEO/PEG EasiCal standards were used for calibration.

Small-Angle X-Ray Scattering. SAXS experiments were performed using a Rigaku S-MAX 3000 SAXS system emitting X-rays with a wavelength of 0.154 nm (Cu-Kα). The sample-to-detector distance was 1640 mm with silver behenate calibration. The 2D scattering patterns were azimuthally averaged to produce 1-D plots of intensity versus scattering vector q, where $q = 4\pi\sin\theta/\lambda$; θ is one-half of the scattering angle, and λ is the X-ray wavelength.

Tensile Testing. Tensile properties were obtained according to ASTM D1708 standard with an MTS Sintech 20/G tensile tester. Dog bone-shaped samples (4.7 mm x 1.0 mm x 22 mm) were cut using a Dewes-Gumbs die from dried sheets and subjected to an extension rate of 130 mm/min. Tensile tests were performed approximately 2-3 days after the samples were compression molded. The Young's modulus, tensile strength and elongation at break were reported as average values of five specimens. The Young's Modulus values were determined from the initial slope of the stress-strain curves in the linear region.

Differential Scanning Calorimetry (DSC). DSC experiments were performed with a Mettler Toledo DSC 822e. Samples were tested from 30 to 250 °C at a heating rate of 10 °C/min.

Dynamic Mechanical Analysis. DMA experiments were performed with a TA Instruments Rheometrics Stress Analyzer-GIII. Rectangular specimens measuring 8 mm in width and 0.9 mm in thickness were cooled with N_2 gas to -100 °C and subjected to a temperature sweep from -100 °C to 120 °C at a heating rate of 3 °C/min. The measurements were conducted in tensile mode with frequency of 1 Hz and strain of 0.03%. The storage modulus (E'), loss modulus (E'') and loss tangent (tan δ) were recorded. The soft-segment T_g was identified from the peak maximum in E''; the flow temperature was defined as the onset of inconsistent tan δ data, close to the temperature at which the sample was no longer mechanically robust.

4.3 Results and Discussion

Synthesis and Characterization

All PHUs were synthesized according to Scheme 4.1. Table 4.1 lists the formulation of starting materials. Three chain-extender molecules were used, and four hard-segment contents for each chain extender structure were studied. The hard-segment contents were varied by adjusting the molar ratios of DVBDCC hard segment and chain extender relative to that of PTMO soft segment. The progress of synthesis was monitored using ATR-FTIR spectroscopy

via the disappearance of the carbonyl stretching band at ~1800 cm^{-1} originating from DVBDCC. Figure B1a-c (see Appendix B) reports typical FTIR spectra of all PHUs along with the spectrum of DVBDCC. The peak associated with the carbonate group disappeared in the final materials indicating a complete conversion of carbonate functional groups into hydroxyurethane linkages within experimental error. The appearance of urethane peaks at 1730-1700 cm^{-1} confirms successful PHU formation. These peaks represent contributions from free, non-hydrogen bonded (~1730 cm^{-1}) and hydrogen bonded (~1700 cm^{-1}) urethane units. In addition, peaks associated with N-H, O-H, C-O, C=C, and C-H bonds from various segments in the polymer chain were also present. The chemical structures of the resulting polymers were also analyzed using ^{1}H NMR spectroscopy. Figures B2-B4 (see Appendix B) show typical spectra of (three of the twelve) PHUs produced in this study: CYCDA-40, HMDA-40, and pXDA-40, respectively. Signals from various protons along the polymer chain were identified and assigned accordingly as indicated.

The apparent MWs of these PHUs were characterized using GPC and are reported in Table B1 (see Appendix B). The apparent M_n values of these PHUs range from 3.1 to 10.0 kg/mol whereas the apparent M_w values range from 12.2 to 48.3 kg/mol. The challenge in obtaining high MW polymers from aminolysis of 5-membered ring carbonate is commonly observed (Benyahya 2011, Benyahya 2012, Lamarzelle 2016, Besse 2015). The origin of the low MW values associated with PHU is not fully resolved in the literature. One possible reason could be due to the presence of side reactions leading to urea formation and oxazolidinone as well as dehydration products as outlined by Besse et al. (Besse 2015). Further studies are needed to investigate the origin of this phenomenon and to improve the MW range attainable in PHU synthesis. Recent work by Sardon and coworkers (Yuen 2016) on PHU synthesis at room temperature using 8-membered ring carbonate achieved M_n in excess of 40 kg/mol. Synthesis of segmented PHUs using organic catalyst such as 1,5,7-triazabicyclo[4,4,0] undec-5-ene (TBD)

also merits further investigation.

Small-Angle X-Ray Scattering

The nanophase-separated morphology in TPUs arises from the thermodynamic incompatibility of the hard and soft segments. SAXS is a powerful technique to probe the presence of nanophase-segregated structures, quantify interdomain distances, and evaluate the degree and kinetic of phase separation in TPUs (Wilkes 1981, Li 1992a, Li 1992b). Figure 4.1 shows the SAXS patterns of CYCDA samples. (See Figure B5a-b in Appendix b for SAXS patterns of HMDA and pXDA samples, respectively.) All PHUs show single interference peaks centered at specific scattering vector locations indicating the presence of nanophase-separated morphology. The interdomain spacing can be calculated using $d = 2\pi/q_{max}$ where q_{max} is the magnitude of the scattering vector at maximum intensity. The interdomain spacings are 10-20 nm and increase with increasing hard-segment content. See Table 4.1 for *d*-spacings of all PHUs produced in this study.

Tensile Properties

The nanophase separation in segmented PHUs produces elastomeric material character. Previously, Torkelson and coworkers (Leitsch 2016a) have shown that thermoplastic PHU elastomers exhibit elastomeric response with some level of hysteresis, qualitatively similar to that observed in TPUs (Sarva 2007). The tensile properties of the PHUs were analyzed via uniaxial tensile deformation. Figure 4.2 shows representative tensile stress-strain curves of CYCDA samples. (See Figure B6a-b in Appendix B for representative stress-strain curves of HMDA and pXDA samples.) Samples with 30 to 50 wt% hard-segment content show elastomeric responses whereas samples with 60 wt% hard-segment content exhibit yield points, which can be attributed to the change in nanostructure of the materials. As the hard-segment content is increased to 60 wt%, the nanostructure changes from hard segments dispersed in a rubbery matrix to continuous, interconnected hard domains. This yield point can be attributed to

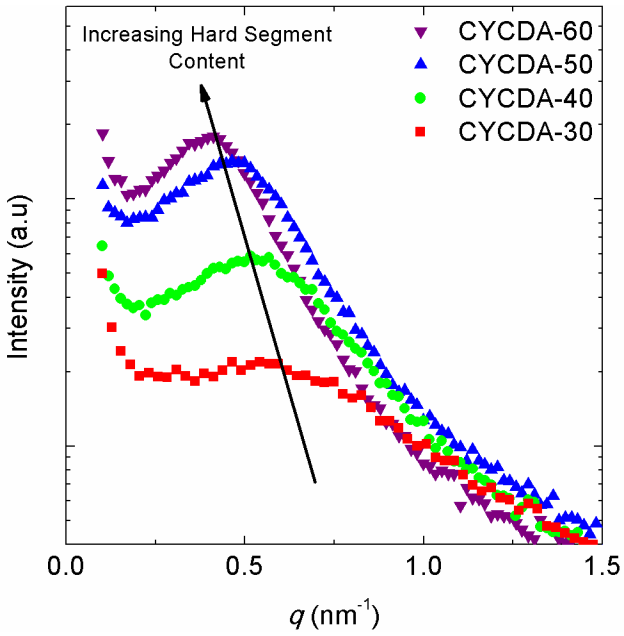

Figure 4.1: SAXS patterns of PHUs chain extended with (a) 1,3 cyclohexane bis(methyl amine), CYCDA-30 through CYCDA-60.

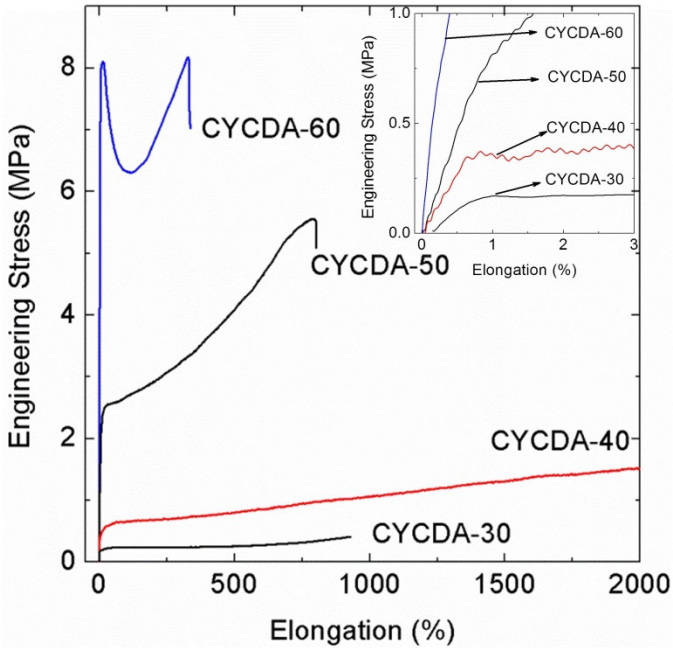

Figure 4.2: Representative stress-strain curves of PHUs chain extended with 1,3-cyclohexane bis(methyl amine) with hard-segment content of 30 to 60 wt%. Inset: Representative stress-strain curves of CYCDA samples at low elongation.

the breakage of interconnected, well-percolated hard domains throughout the soft-segment matrix. Sheth et al. (Sheth 2005) also observed yield points in tensile stress-strain responses of segmented polyureas which they attributed to the presence of a well-percolated hard domain, and they supported this claim with evidence from AFM phase imaging. We also note that TPUs and polyurea elastomers may display yield points in their stress-strain curves when tested at a very high strain rate (> 1000 s^{-1}). Yi et al. (Yi 2006) and Sarva et al. (Sarva 2007) performed uniaxial compressive testing at several strain rates on polyurea and polyurethane elastomers and observed yield point at strain rates exceeding 1000 s^{-1}, but Roland et al. (Roland 2007) did not observe any yield point when performing the test in tension mode. Given that the strain rate used in our experiments is low, yield points observed in samples with 60 wt% hard-segment content can be attributed to their continuous, well-percolated hard-segment morphology and not to the strain rate used for testing.

Table 4.2 summarizes the Young's modulus, tensile strength, and elongation at break for all PTMO-based PHUs. The mechanical properties of these PHUs can be tuned by varying the compositions of soft and hard segments. An increase in the hard-segment content leads to increases in Young's modulus and ultimate tensile strength as a direct consequence of increased physical crosslinking sites. Increasing the hard-segment content also leads to a concomitant decrease in elongation at break. Young's modulus values ranged from 27 to 200 MPa, tensile strength values from 0.3 to 9.7 MPa, and elongation at break values from 110% to greater than 2000%. The tensile strengths of pXDA samples are generally higher than CYCDA and HMDA samples, likely due to the symmetric and aromatic structure of *p*-xylylene diamine.

The tensile properties of PHUs produced in this study can be compared to those obtained with conventional TPUs. Schneider and coworkers (Fu 1986) synthesized a series of TPUs from 2,4-TDI, PTMO with M_n = 2000 g/mol, and 1,4-butanediol as chain extender. They reported tensile strength values ranging from 0.5 to 7.7 MPa and elongation at break values from 1100 to

Table 4.2: Mechanical properties of PTMO-based PHUs at various hard-segment contents produced with three different chain extenders.*

Sample Name	Young's Modulus, E (MPa)	Ultimate Tensile Strength (MPa)	Elongation at Break ϵ_B (%)
CYCDA-30	27 ± 5	0.40 ± 0.04	850 ± 110
CYCDA-40	59 ± 6	1.4 ± 0.3	No Break
CYCDA-50	89 ± 18	4.2 ± 1.9	670 ± 160
CYCDA-60	186 ± 55	6.2 ± 2.8	220 ± 100
HMDA-30	27 ± 5	0.88 ± 0.27	680 ± 30
HMDA-40	49 ± 5	0.50 ± 0.12	No Break
HMDA-50	51 ± 6	5.1 ± 0.8	1100 ± 50
HMDA-60	110 ± 46	5.5 ± 2.4	530 ± 230
pXDA-30	29 ± 16	0.3 ± 0.1	No Break
pXDA-40	74 ± 17	2.4 ± 0.5	1400 ± 160
pXDA-50	121 ± 14	5.3 ± 0.5	440 ± 180
pXDA-60	200 ± 27	9.7 ± 1.3	110 ± 30

*Values are reported as average of five specimens. Error represents one standard deviation.

2100 %. The tensile strength values of PHUs in this study are comparable to those obtained by Schneider and coworkers in TPU (Fu 1986). However, they are lower than those obtained by Wilkes and coworkers (Klinedinst 2012) who studied PTMO-based TPUs synthesized using symmetric *para*-phenylene diisocyanate (*p*PDI); they obtained Young's modulus values ranging from 9 to 31 MPa, tensile strength values from 8 to 20 MPa and elongation at break values from 900 to 1500 %. Their tensile strength values are higher than those we obtained, likely due to the symmetric structure of *p*PDI and its monodispersity which can lead to a better hard segment association. The DVBDCC molecule employed in our study contains a mixture of *meta* and *para* isomers. The urethane linkages in our PHU materials are also placed at least two methylene units away from the aromatic ring as opposed to being directly adjacent to the aromatic ring, as in isocyanate-based TPU. The hydroxyl groups may also cause some steric hindrance to packing or a tight association of the urethane linkages in the hard segment. These hydroxyl groups are also capable of forming hydrogen bonds with the soft segment. This intersegmental hydrogen bonding can lead to some level of phase mixing which can contribute to weaker material strength. However, this slight phase mixing in PTMO-based PHUs results in wide compositional heterogeneity and therefore broad glass transition response that may prove beneficial for application in acoustic or vibrational damping. This aspect will be discussed in the following section.

Dynamic Mechanical Analysis

The temperature dependences of viscoelastic properties including E', E'' and tan δ of CYCDA-30, HMDA-30 and pXDA-30 samples are shown in Figure 4.3a-c, respectively. (See Figures B7-B9 in Appendix B for DMA profiles of other PHUs.) Figure 4.3a-c provides further support for the presence of nanophase separation in these materials as indicated by two thermal transitions: the soft-segment T_g as determined from the peak maximum in E'' and the flow temperature (T_{flow}), indicative of the upper end of hard-segment T_g. Table 4.1 lists the location of

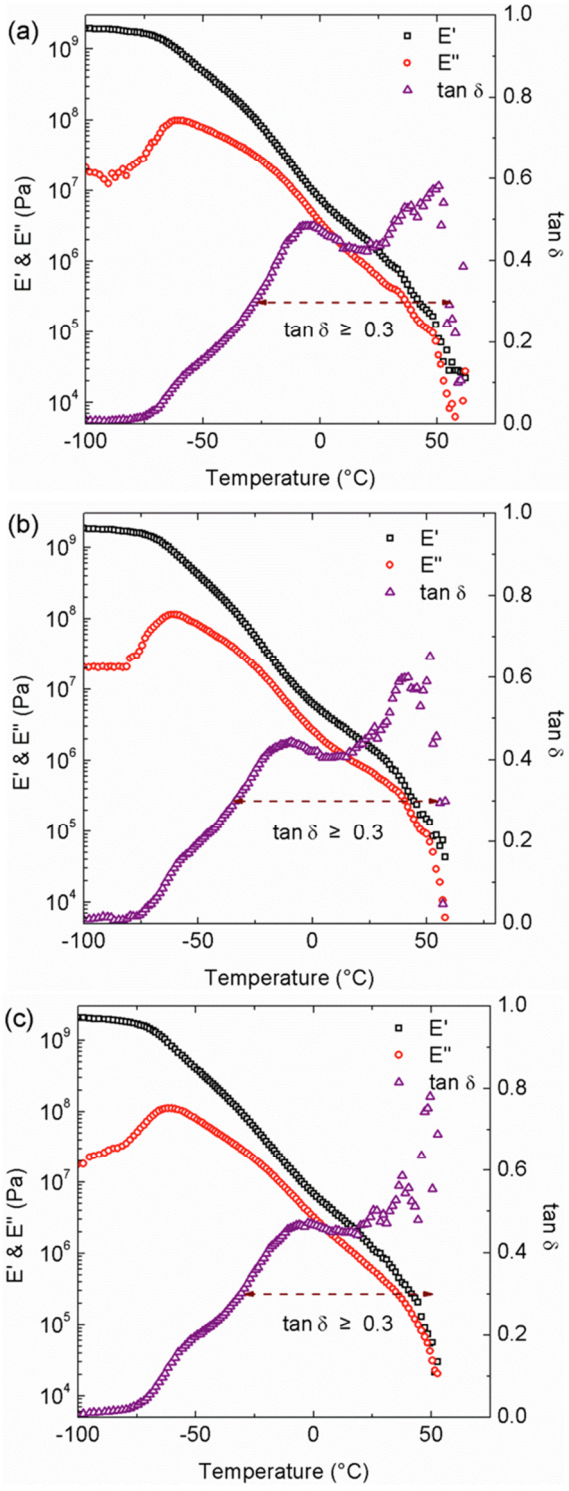

Figure 4.3: Temperature dependences of tensile storage modulus (*E*'), loss modulus (*E*"), and tan δ of (a) CYCDA-30, (b) HMDA-30, and (c) pXDA-30 PHUs.

the soft-segment T_g and T_{flow} values for all PHUs. The soft segment T_gs are -60 to -70 °C. The T_{flow} values range between 51 and 92 °C for CYCDA samples, from 50 to 90 °C for pXDA samples, and from 40 to 64 °C for HMDA samples. The higher T_{flow} in CYCDA and pXDA samples can be attributed to the more rigid structure of 1,3-cyclohexanebis(methyl amine) and *p*-xylylene diamine in comparison to the more flexible structure of aliphatic hexamethylene diamine. In all series, T_{flow} increases with increasing hard-segment content, indicating improved nanophase separation and a more perfected hard domain with increasing hard-segment interdomain spacing. DSC characterization reveals no evidence of crystallinity via a melting peak in the hard segment of our PHUs.

Figure 4.3a-c also demonstrates that the DMA results for PTMO-based PHUs are qualitatively very different from those observed in PTMO-based TPUs. The *E*' in PTMO-based PHUs exhibits a very gradual decrease with respect to temperature above their soft segment T_gs. The tan δ-temperature profile also shows high values over a broad temperature range. (See Figures B7-B9 in Appendix B for the DMA profiles of other PHUs which manifest similar behavior.) No rubbery plateau region similar to that obtained in TPUs is present in any of the PTMO-based PHUs. For comparison, we synthesized two TPUs with very similar chemical structures and compositions to CYCDA-30 and HMDA-30 PHUs by using 2000 g/mol hydroxyl-terminated PTMO, 2,4-TDI, 1,4-cyclohexanedimethanol and 1,6-hexanediol as chain extenders at 30 wt% hard-segment content. The DMA results of these TPUs are shown in Figure 4.4a-b. In contrast to those exhibited by PHUs, the *E*'-temperature profiles of these TPUs show two distinct drops at two specific locations corresponding to glass transitions of the soft and hard segments. The sharp drop in *E*' near the soft-segment T_g is followed by a relatively temperature-independent rubbery plateau region which extends tens of degree before exhibiting another drop as the sample approaches its hard-segment T_g. The corresponding tan δ-temperature profiles of these TPUs show sharp and narrow peaks at two locations corresponding to the soft- and hard-

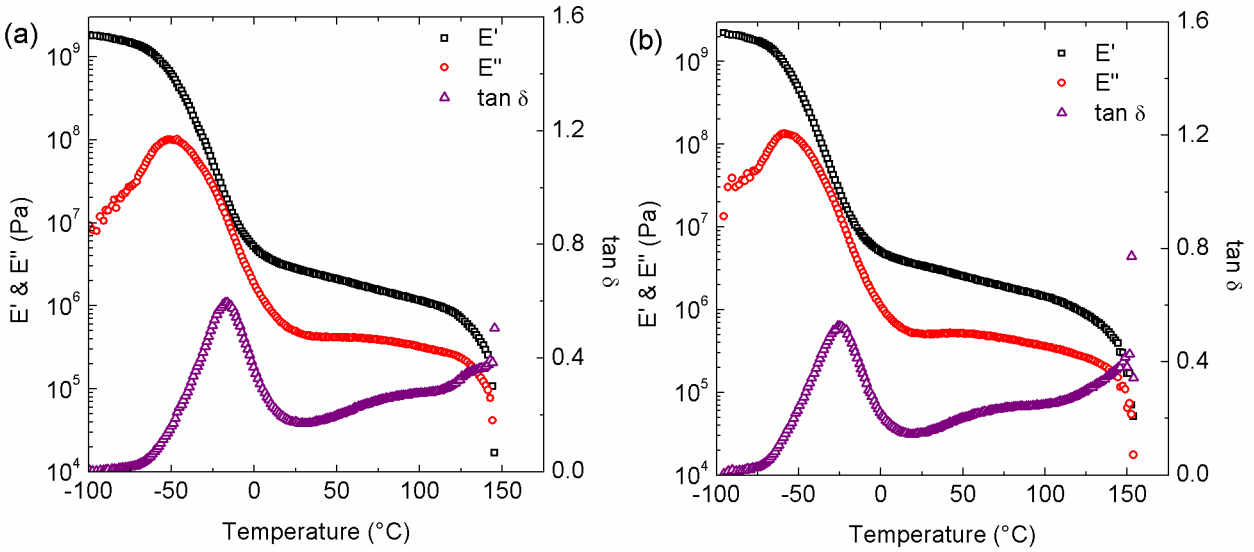

Figure 4.4: Temperature dependences of tensile storage modulus (E'), loss modulus (E'), and tan δ of (a) analogous PU made with PTMO (M_n = 2000 g/mol), 2,4 TDI and 1,4-cyclohexane dimethanol and (b) analogous PU made with PTMO (M_n = 2000 g/mol), 2,4 TDI and 1,6-hexanediol at 30 wt% hard-segment content.

segment T_gs. The temperature ranges where the tan δ continuously exceeds 0.30 in these TPUs are only about 10 °C. Similar DMA results have also been reported in PTMO-based TPUs as well as other TPUs employing soft segments such as polyester or polycarbonate (Korley 2006, Klinedinst 2012, Das 2007, O'Sickey 2002b, O'Sickey 2002a, O'Sickey 2003, Yilgor 2015, Seefried 1975a, Seefried 1975b, Seefried 1975c, Seefried 1975d, Kojio 2009, Eceiza 2008).

The step change in *E*' and sharp tan δ peaks observed in TPUs are consequences of very good nanophase separation. Due to the strong hydrogen bonding within hard-segment urethane units, the nanophase separation produces sharp interphases between the hard and soft domains. By contrast, the *E*' and tan δ profile of PTMO-based PHUs (Figure 4.3a-c) are characteristic of nanophase-separated systems having broad interphases with a wide range of local composition (Mok 2008). This is a result of some level of phase mixing due to hydrogen bonding between the hard-segment hydroxyl groups and the soft-segment oxygen atoms. Such profiles are analogous to those seen in gradient copolymer systems known to possess nanophase separation with broad interphase regions and broad ranges of T_gs (Mok 2008, Mok 2009, Mok 2010, Kim 2006, Karaky 2006, Karaky 2007, Karaky 2008). Mok et al. (Mok 2008) compared DMA results of block and gradient copolymers of styrene/n-butyl acrylate and styrene/hydroxystyrene. They observed that block copolymers showed two distinct transitions in *E*' with sharp and narrow tan δ peaks whereas gradient copolymers showed a very gradual decrease in *E*' and high tan δ values over broad temperature ranges. Their observations concur with results from Karaky et al.(Karaky 2006, Karaky 2007, Karaky 2008) and theoretical predictions by Hashimoto et al. (Hashimoto 1983) for tapered block copolymer systems with sinusoidal composition variation. Mok et al. (Mok 2008) and Hashimoto et al. (Hashimoto 1983) indicated that gradient copolymer systems are good for damping applications. By analogy to gradient copolymer systems, PTMO-based PHUs are advantageous for acoustic and vibration damping applications over a wide range of use temperature.

Sound and vibration damping are important in aircraft, automobiles, and machinery as well as in structural applications for noise reduction and prevention of fatigue failures. In practical damping application, utility over wide ranges of temperature and frequencies is often required. Thus, high tan δ values over a broad temperature window are desired good damping performance. Typically, tan $\delta \geq 0.30$ over a temperature range of ≥ 60 °C is desired (Sophiea 1994, Huelck 1972a, Huelck 1972b, Hu 1997, Chern 1999, Qin 2004, Chen 1994, Yu 1999, Hourston 1996). We have used the same criterion to evaluate our PHUs. We use T_{flow} as the upper limit of service temperature for good damping because characterization of loss factor beyond T_{flow} is not possible; DMA experiments were performed in tensile mode, and the materials are no longer mechanically robust beyond T_{flow}.

Figure 5a-c shows the temperature dependences of tan δ for CYCDA, HMDA, and pXDA samples, respectively, at all hard-segment contents. Table 4.1 summarizes the temperatures and the breadths of regions for which tan $\delta \geq 0.30$. As shown in Table 4.2, all PHUs exhibit good damping character spanning at least ~44 °C with tunable temperature range depending on their compositions. In particular, all pXDA samples exhibit good damping characteristics over temperature range of 64 to 81 °C whereas CYCDA-30, 40, and 50 exhibit similar damping behavior over temperature ranges of 78, 81, and 57 °C, respectively. Likewise, HMDA-30 and HMDA-40 show good damping characteristics over temperature ranges of 73 and 57 °C. These temperature ranges are tunable depending on hard-segment content and chain extender structure. For example, the good damping range for pXDA-30 PHU spans temperatures from -31 to 50 °C. Increasing the hard-segment content to 40 wt%, 50 wt% and 60 wt% shifts the good damping regions to 0 to 75 °C, 10 to 80 °C, and 26 to 90 °C, respectively. Similar trends were observed in CYCDA and HMDA samples. Generally, increasing the hard-segment content increases the hard-segment domain size and favors better segregation of the hard domain. The latter outcome results in a shift of the glass transition range to higher temperature. Chain

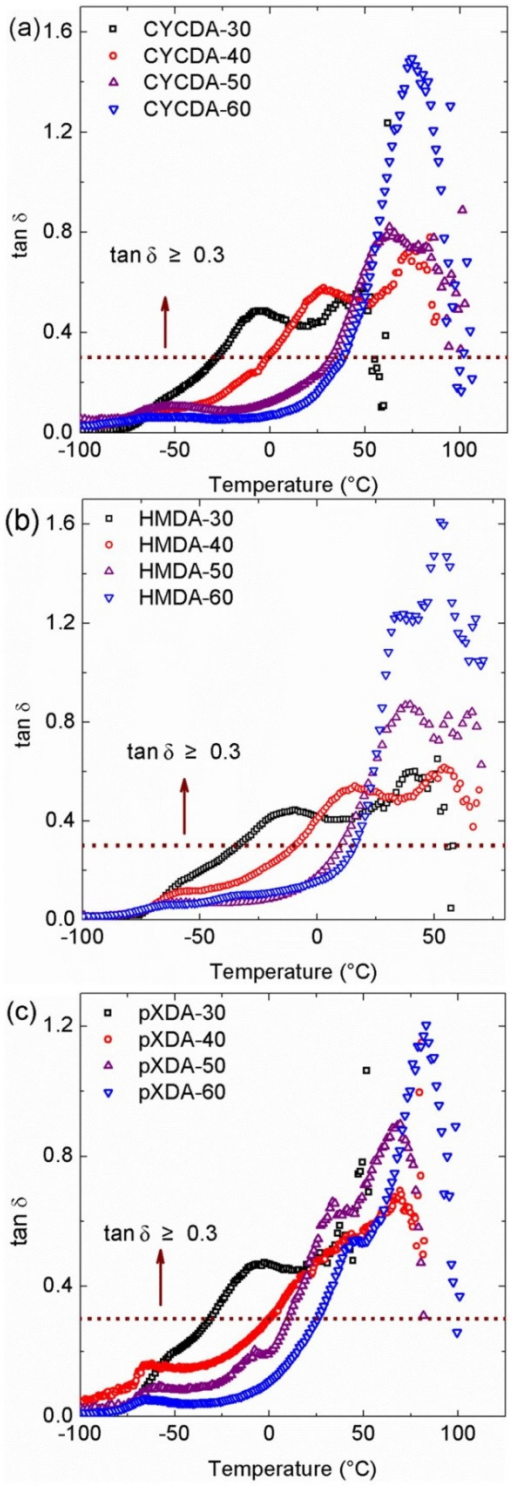

Figure 4.5: Temperature dependences of tan δ of (a) CYCDA-30 through CYCDA-60, (b) HMDA-30 through HMDA-60 and (c) pXDA-30 through pXDA-60.

extender structure also impacts the good damping range in these materials. The T_{flow} values of HMDA samples are lower due to the more flexible structure of the hexamethylene diamine molecule. The breadths of the temperature range with good damping performance are generally similar across samples with similar hard-segment content.

Our results demonstrate that PTMO-based PHUs can be excellent damping materials over broad ranges of use temperature, a function not observed in conventional TPUs. The temperature range for good damping performance can be easily tuned through compositional variation in hard-segment content as well as chain extender structure. We note that polyurethane has previously been investigated for damping applications. To achieve broad-temperature-range damping capability, TPUs are incorporated into IPNs with secondary polymeric components such as epoxy (Chern 1999), polyester (Qin 2004), polyacrylate (Chen 1994, Yu 1999), polystyrene (Hourston 1996), etc. The IPN structure consists of networks of at least two polymers that are catenated or topologically interlocked by covalent crosslinks resulting in intimate mixing between the two components. This intimate mixing produces microheteregeneous or nanoheteregenous morphology with a broad range of local composition and broad T_gs resulting in high tan δ response useful for acoustic damping application. As demonstrated from our DMA results in Figure 4.4a-b and by others in a variety of reports (Korley 2006, Klinedinst 2012, Das 2007, O'Sickey 2002b, O'Sickey 2002a, O'Sickey 2003, Yilgor 2015, Seefried 1975a, Seefried 1975b, Seefried 1975c, Seefried 1975d, Kojio 2009, Eceiza 2008), TPU by itself is unable to serve as a broad-temperature-range damping material due to narrow peaks in tan δ response. In contrast, our PTMO-based PHUs show high tan δ values over broad temperature ranges without the need to employ an IPN structure.

The extraordinarily broad temperature ranges with tan $\delta \geq 0.30$ in PTMO-based PHUs are direct consequences of the hard-segment hydroxyl groups forming hydrogen bonds with oxygen atoms in the soft segment. The partial miscibility due to some level of phase mixing results in

nanophase-separated systems possessing broad interphases having a wide range of local composition. The PTMO-based PHUs have high tan δ values over broad temperature ranges that are easily tunable via material compositions making them useful as broad-temperature-range acoustic and vibration damping materials. These PHU materials are also thermoplastics, and thus can be easily processed and molded into a range of shapes or forms to tailor to different applications. Future studies are warranted to consider other applications for which PHUs may possess advantages over conventional polyurethanes, including as adhesives (Leitsch 2016b).

4.4 Conclusions

Non-isocyanate-based thermoplastic PHU elastomers were synthesized with cyclic carbonate aminolysis using PTMO as the soft segment and DVBDCC with three different chain extenders as the hard segment. Hard-segment contents were varied from 30 to 60 wt%. FTIR results demonstrate the complete disappearance (within error) of carbonate peaks, indicating successful PHU synthesis at high conversion. SAXS measurements demonstrate that these PHUs possess nanophase-separated morphology with 10-20 nm interdomain spacings as a result of the nanophase separation. PHUs with 30 to 50 wt% hard-segment content exhibit elastomeric material responses with tunable tensile properties. DMA results reveal that these PTMO-based PHUs possess very different nanophase separation behavior than that exhibited by isocyanate-based TPUs; this difference is a result of some level of phase mixing caused by hydrogen bonding between hard-segment hydroxyl groups and oxygen atoms in the PTMO soft segment. Notable features include a gradual decrease in E' with temperature and high tan δ values (≥ 0.30) over broad temperature ranges, indicative of a system with a wide range of local composition. Using the criterion of tan $\delta \geq 0.30$, we demonstrate that these PHUs can serve as effective damping materials over extraordinary temperature ranges as large as 80 °C, a function not present in conventional TPUs. We also demonstrate that the damping temperature ranges are

tunable via simple variation of hard-segment content and chain extender structure.

APPENDIX B

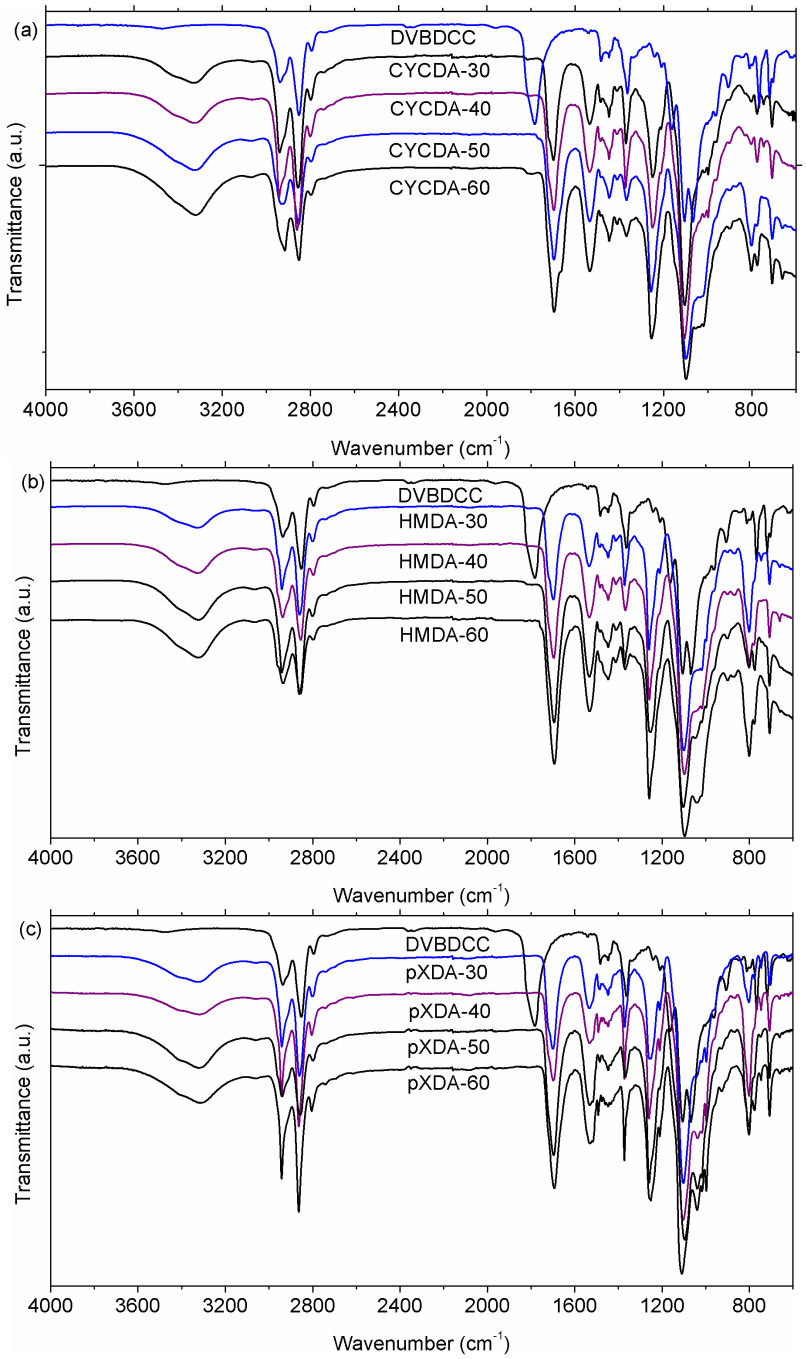

Figure B1: FTIR spectra of a) CYCDA-30 to CYCDA-60, b) HMDA-30 to HMDA-60, and c) pXDA-30 to pXDA-60 PHUs plotted with the spectrum of DVBDCC. FTIR (ν, cm^{-1}): 3500-3300 (N-H), 3500-3100 (O-H), 3100-3000 (=C-H and aromatics), 1730-1700 (C=O), 1570 (N-H), 1300-1000 (C-O). (Note: An absorbance band at ~1800 cm^{-1} associated with DVBDCC is absent in all of the synthesized polymers.)

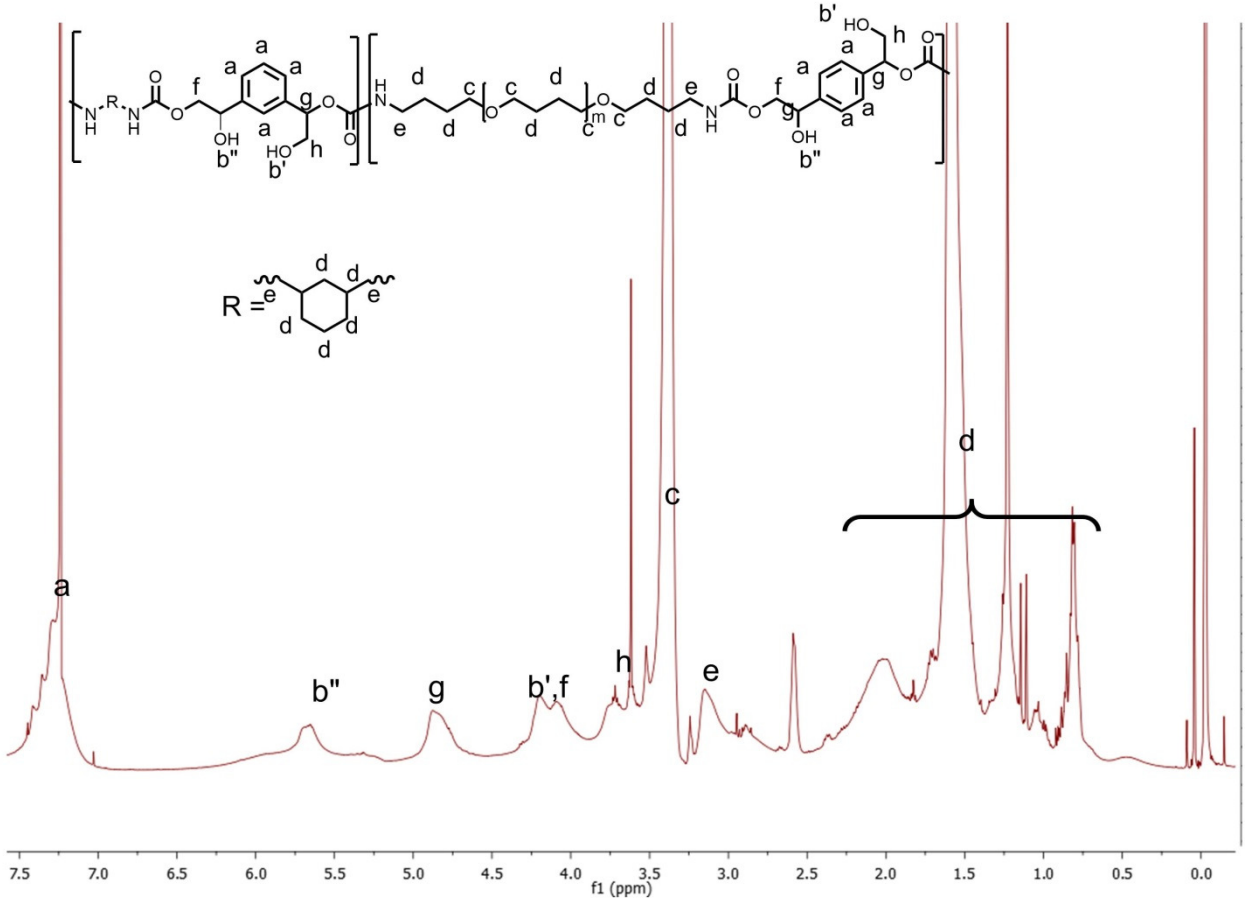

Figure B2: ^{1}H NMR Spectra of CYCDA-40 PHU in $CDCl_3$.

PHU CYCDA-40. ^{1}H NMR ($CDCl_3$, 500 MHz), δ (ppm): 0.5-2.3 (8H, $OCH_2C\boldsymbol{H}_2C\boldsymbol{H}_2CH_2O$, $NHCH_2C\boldsymbol{H}_2C\boldsymbol{H}_2CH_2O$, $NHCH_2(C\boldsymbol{H}C\boldsymbol{H}_2C\boldsymbol{H}_2C\boldsymbol{H}_2C\boldsymbol{H}_2C\boldsymbol{H})CH_2NH$), 2.8-3.2 (4H, $NHC\boldsymbol{H}_2CH_2CH_2CH_2O$, $NHC\boldsymbol{H}_2$), 3.3-3.5 (6H, $C\boldsymbol{H}_2OC\boldsymbol{H}_2$, $NHC(=O)OC\boldsymbol{H}_2$), 3.6-3.7 (1H, $C\boldsymbol{H}_2OH$), 4.0-4.2 (2H, $C\boldsymbol{H}_2OC(=O)NH$), 4.2-4.3 (1H, $CH_2O\boldsymbol{H}$), 4.8-5.0 (1H, $PhC\boldsymbol{H}(OH)CH_2$), 5.5-5.7 (1H, $PhCH(O\boldsymbol{H})CH_2$), 7.0-7.5 (4H, Ph).

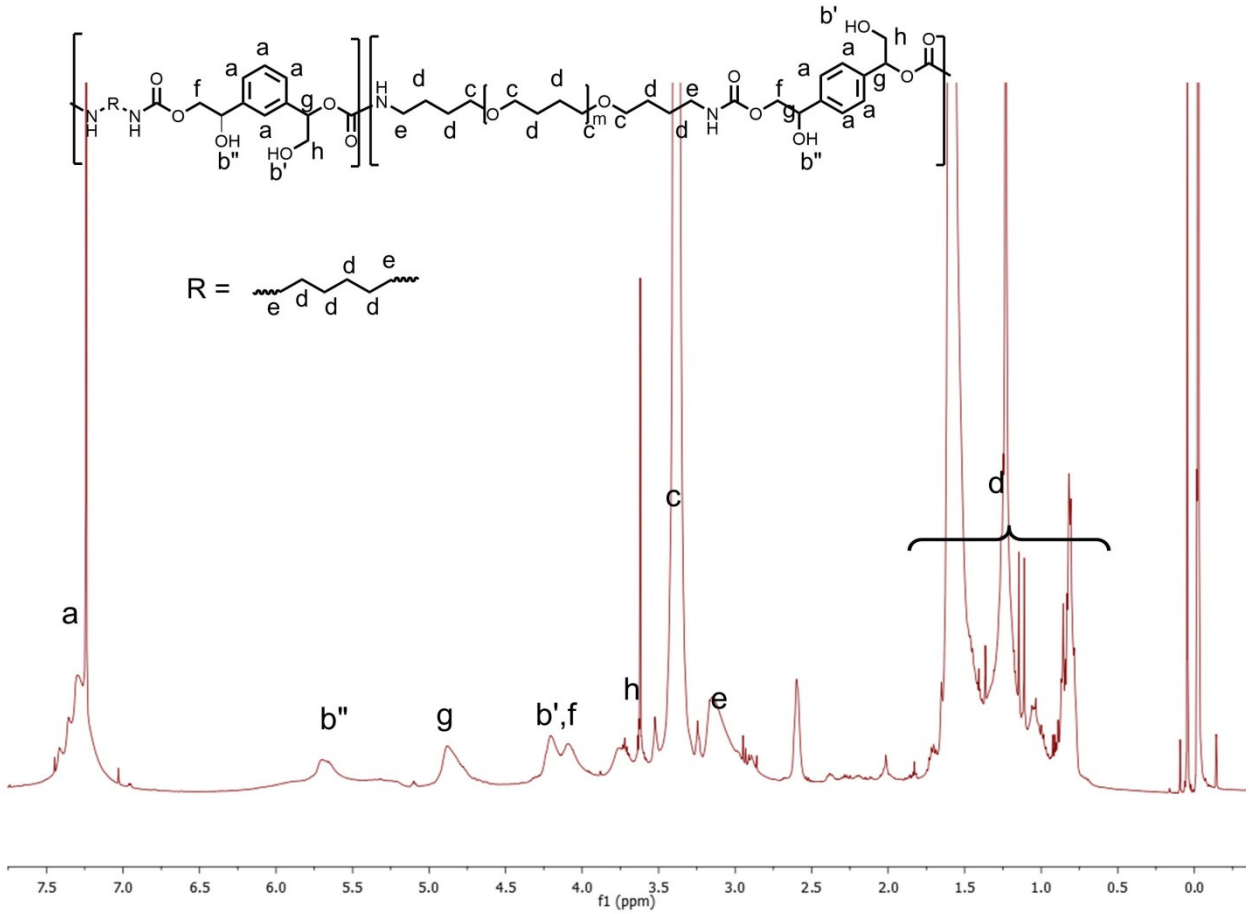

Figure B3: ^{1}H NMR Spectra of HMDA-40 PHU in $CDCl_3$.

PHU HMDA-40. ^{1}H NMR ($CDCl_3$, 500 MHz), δ (ppm): 0.5-2.0 (16H, $OCH_2C\boldsymbol{H}_2C\boldsymbol{H}_2CH_2O$, $NHCH_2C\boldsymbol{H}_2C\boldsymbol{H}_2CH_2O$, $NHCH_2C\boldsymbol{H}_2C\boldsymbol{H}_2C\boldsymbol{H}_2C\boldsymbol{H}_2CH_2NH$), 2.8-3.2 (4H, $NHC\boldsymbol{H}_2CH_2CH_2CH_2O$, $NHC\boldsymbol{H}_2$), 3.3-3.5 (6H, $C\boldsymbol{H}_2OC\boldsymbol{H}_2$, $NHC(=O)OC\boldsymbol{H}_2$), 3.6-3.7 (1H, $C\boldsymbol{H}_2OH$), 4.0-4.2 (2H, $C\boldsymbol{H}_2OC(=O)NH$), 4.2-4.3 (1H, $CH_2O\boldsymbol{H}$), 4.8-5.0 (1H, $PhC\boldsymbol{H}(OH)CH_2$), 5.5-5.7 (1H, $PhCH(O\boldsymbol{H})CH_2$), 7.0-7.5 (4H, Ph).

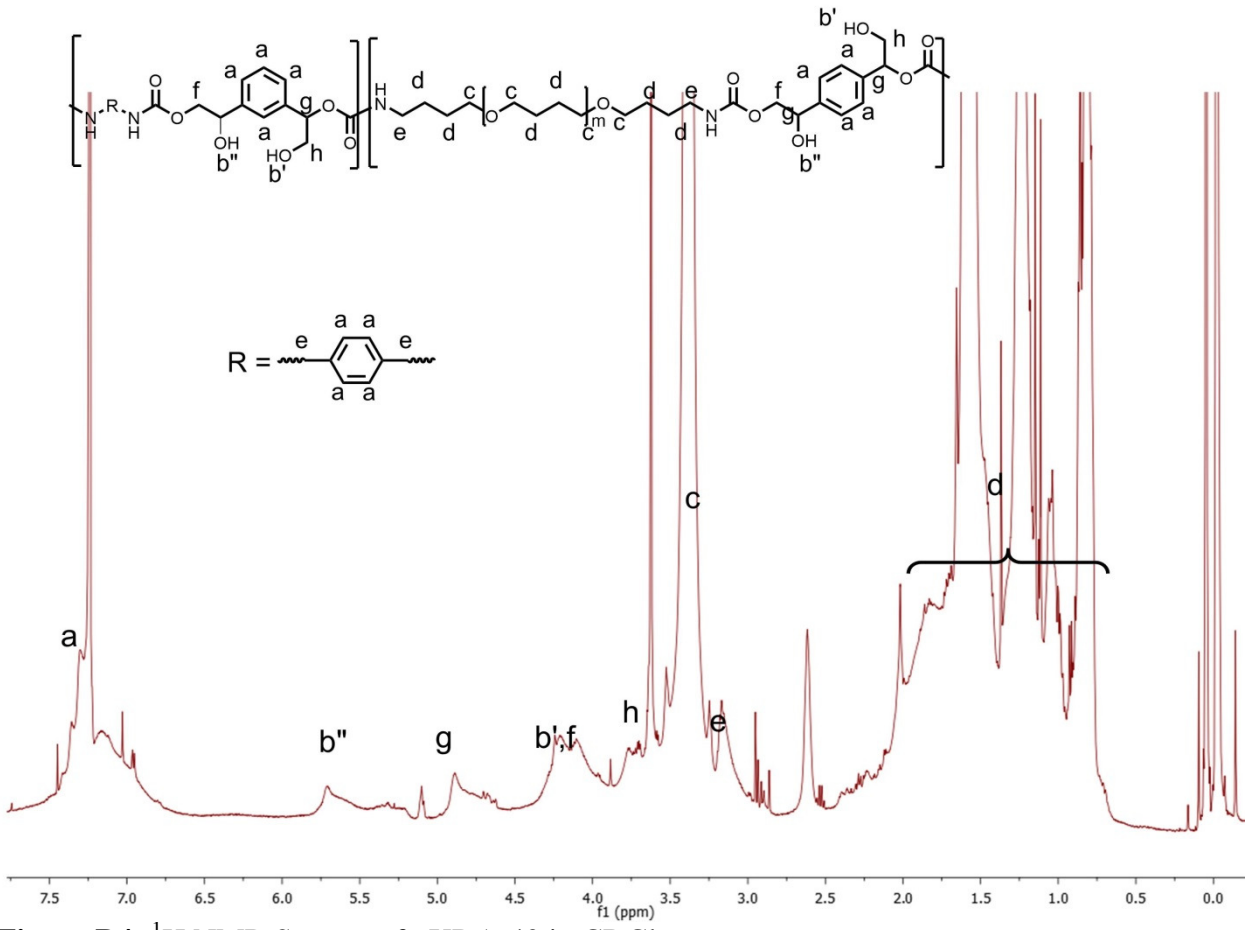

Figure B4: ^{1}H NMR Spectra of pXDA-40 in $CDCl_3$.

PHU pXDA-40. ^{1}H NMR ($CDCl_3$, 500 MHz), δ (ppm): 0.5-2.5 (8H, $OCH_2C\boldsymbol{H}_2C\boldsymbol{H}_2CH_2O$, $NHCH_2C\boldsymbol{H}_2C\boldsymbol{H}_2CH_2O$, 2.8-3.2 (4H, $NHC\boldsymbol{H}_2CH_2CH_2CH_2O$, $NHC\boldsymbol{H}_2$), 3.3-3.5 (6H, $C\boldsymbol{H}_2OC\boldsymbol{H}_2$, $NHC(=O)OC\boldsymbol{H}_2$), 3.6-3.7 (1H, $C\boldsymbol{H}_2OH$), 4.0-4.2 (2H, $C\boldsymbol{H}_2OC(=O)NH$), 4.2-4.3 (1H, $CH_2O\boldsymbol{H}$), 4.8-5.0 (1H, $PhC\boldsymbol{H}(OH)CH_2$), 5.5-5.7 (1H, $PhCH(O\boldsymbol{H})CH_2$), 7.0-7.5 (4H, Ph).

Table B1: Apparent molecular weight averages of PHUs characterized by gel permeation chromatography.

Material Name	Apparent Mn (kg/mol)	Apparent Mw (kg/mol)
CYCDA-30	7.7	44.4
CYCDA-40	10.0	40.1
CYCDA-50	6.4	23.2
CYCDA-60	3.1	14.1
HMDA-30	8.8	41.1
HMDA-40	7.8	29.0
HMDA-50	5.2	17.2
HMDA-60	3.3	12.2
pXDA-30	8.4	48.3
pXDA-40	8.7	44.8
pXDA-50	6.1	23.6
pXDA-60	5.1	17.4

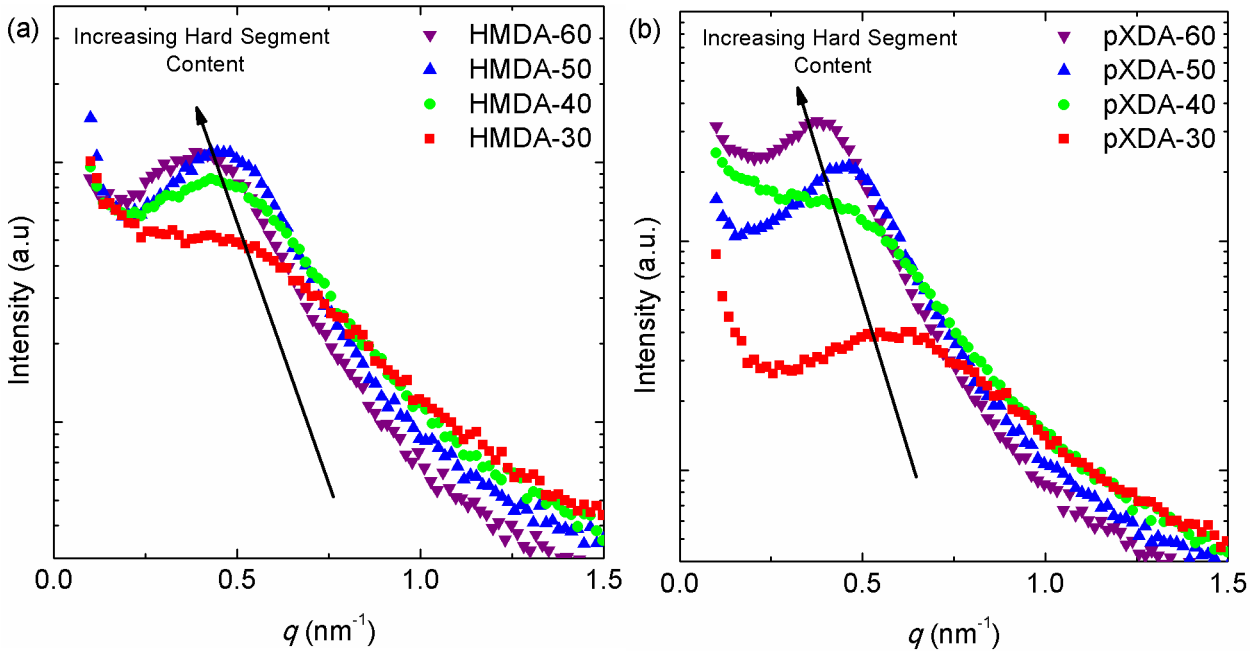

Figure B5: SAXS patterns of PHUs chain extended with (a) hexamethylene diamine, HMDA-30 through HMDA-40, (b) p-xylylene diamine, pXDA-30 through pXDA-60.

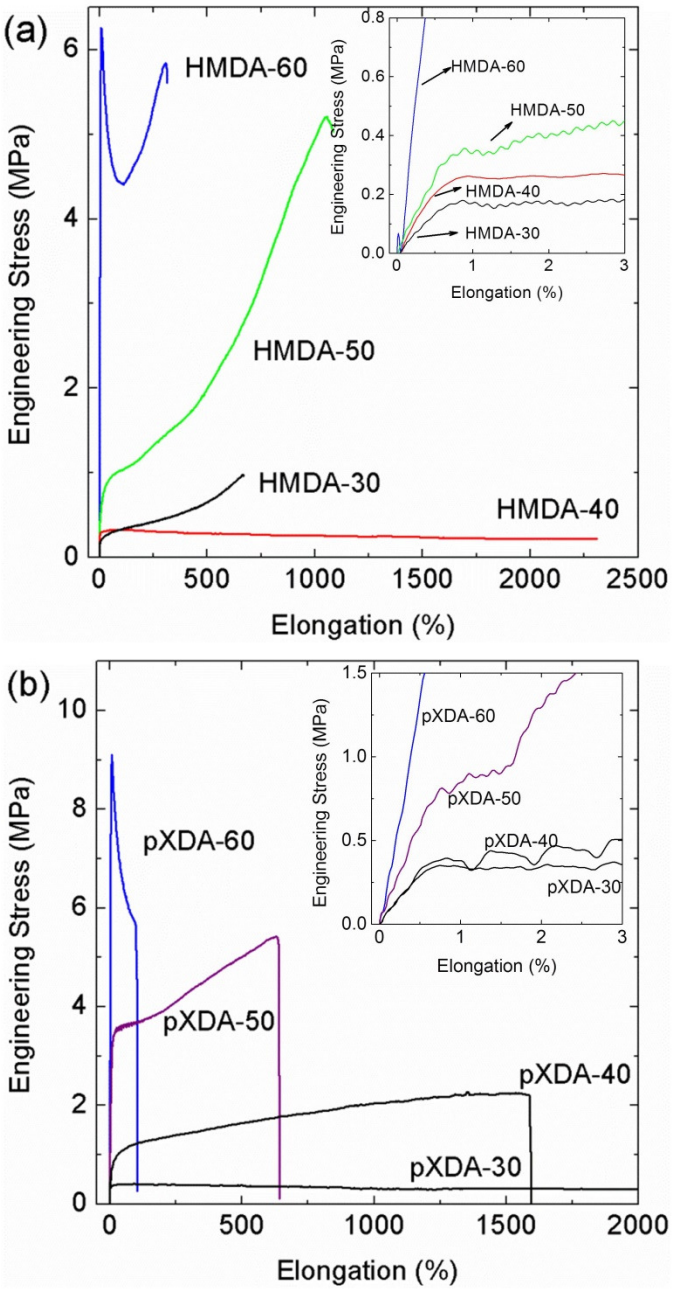

Figure B6: Representative stress-strain curves of PHUs chain extended with (a) hexamethylene diamine, and (b) *p*-xylylene diamine at hard-segment content of 30 to 60 wt%.

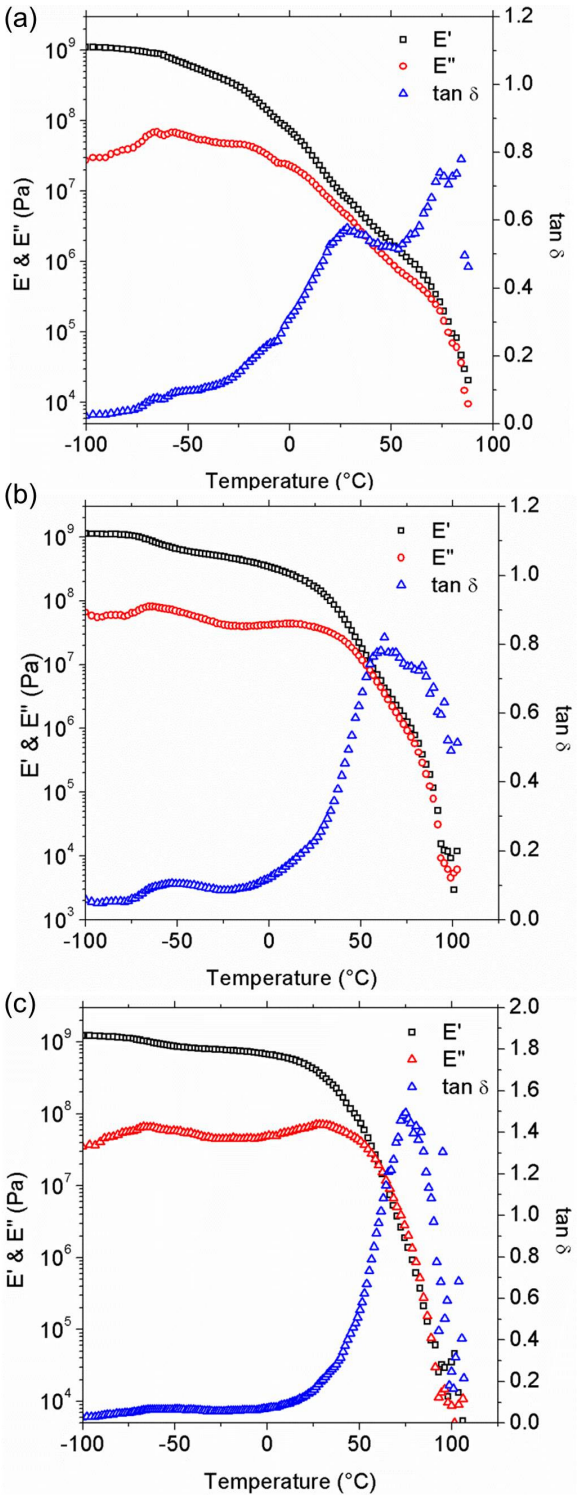

Figure B7: Temperature dependences of tensile storage modulus (E'), loss modulus (E'), and tan δ of (a) CYCDA-40, (b) CYCDA-50, and (c) CYCDA-60 PHUs.

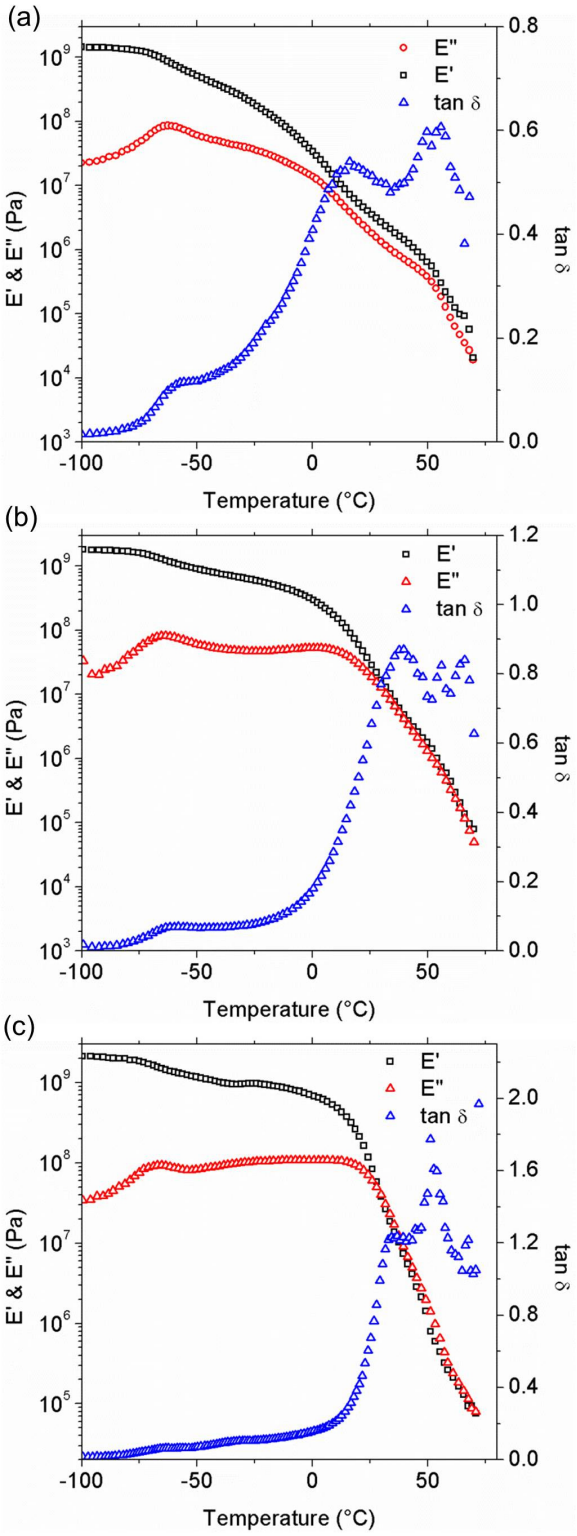

Figure B8: Temperature dependences of tensile storage modulus (E'), loss modulus (E'), and tan δ of (a) HMDA-40, (b) HMDA-50, and (c) HMDA-60 PHUs.

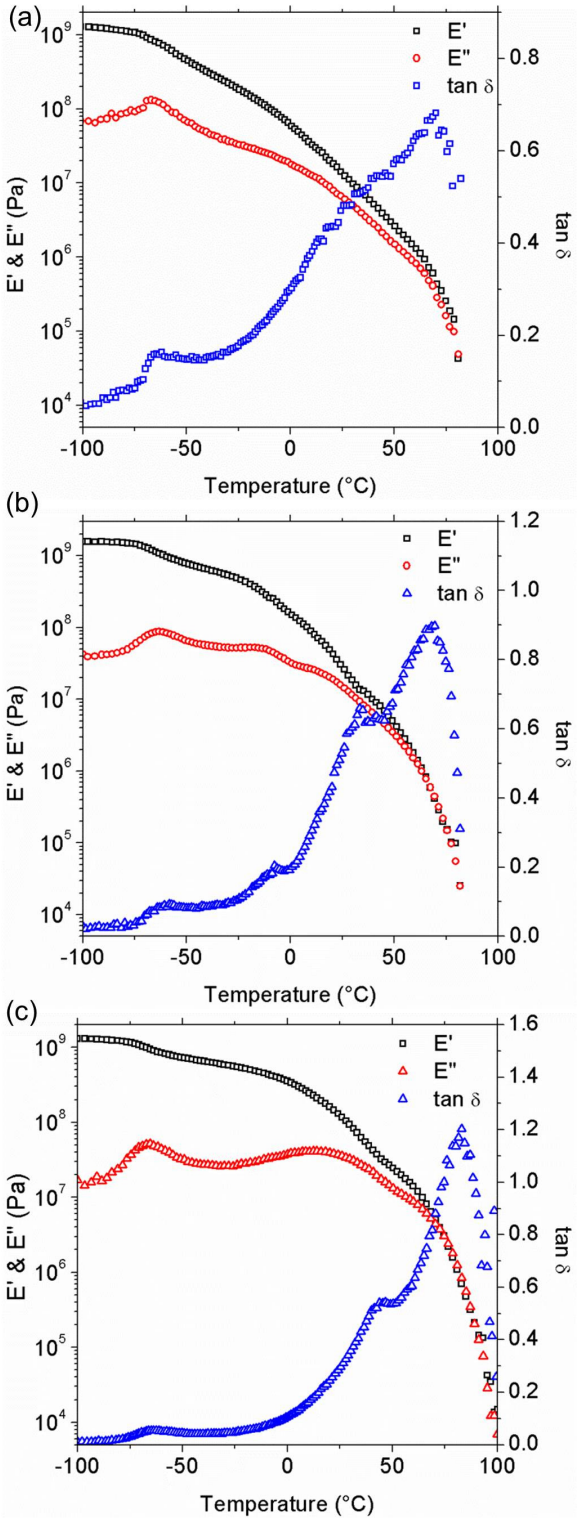

Figure B9: Temperature dependences of tensile storage modulus (E'), loss modulus (E'), and tan δ of (a) pXDA-40, (b) pXDA-50, and (c) pXDA-60 PHUs.

CHAPTER 5

Tuning Nanophase Separation Behavior in Segmented Polyhydroxyurethane via Judicious Choice of Soft Segment

5.1 Introduction

Polyurethane (PU) is an important class of commodity polymer with wide-ranging applications (Nohra 2013, Oertel 1994, Delebecq 2013, Engels 2013). It is produced from a step-growth reaction between isocyanates and alcohols with relatively fast reaction kinetics. There has been increasing regulatory scrutiny regarding the safe use, transport and handling of isocyanates, which has led to investigations into alternative chemistries to produce PU or PU-like materials without employing isocyanates (Official Journal of European Union 2009, US EPA 2011, US EPA 2015). Cyclic carbonate aminolysis resulting in polyhydroxyurethane (PHU) is a most promising chemistry to produce non-isocyanate polyurethane-like (NIPU) materials (Guan 2011, Kathalewar 2013, Blattmann 2014, Maisonneuve 2015, Besse 2013a). Although there have been many studies on single-phase PHUs, cross-linked PHUs, reaction catalysis, and cyclic carbonate synthesis (Guan 2011, Kathalewar 2013, Blattmann 2014, Maisonneuve 2015, Besse 2013b, Kihara 1993, Steblyanko 2000, Ochiai 2005, Tomita 2001a, Tomita 2001b, Tomita 2001c, Tomita 2001d, Tomita 2001e, Ochiai 2005a, Ochiai 2005b, Kim 2001, Figovsky 2002, Birukov 2012, Van Velthoven 2015, Duval 2015, Tryznowski 2015, Lambeth 2013, Lombardo 2015, Blain 2014, Bähr 2012, Tamami 2004, Javni 2008, Javni 2013, Bähr 2012, Fleischer 2013, Besse 2013, Kathalewar 2014, Lee 2015, Fortman 2015, Matuskizono 2015, Cornille 2015, Benyahya 2011, Benyahya 2012, Maisonneuve 2014a, Tang 2011, Lebarbe 2014, Sheng 2015, Maisonneuve 2014b, Lamarzelle 2016), few studies have focused on segmented, nanophase-separated PHUs (Nanclares 2015, Leitsch 2016a, Beniah 2016, Zhang 2016).

Segmented PU is a class of linear, multiblock copolymer composed of alternating sequences of soft and hard blocks. Depending on the block composition, segmented PU can exhibit properties ranging from those of soft elastomers to hard plastics while retaining the processing characteristics of thermoplastics. The soft blocks are typically long, flexible molecules with a glass transition temperature (T_g) below room temperature whereas the hard blocks, composed of diisocyanate condensed with small molecule diol, have a T_g above room temperature (Holden 2015, Hepburn 1992). Segmented PUs typically exhibit excellent nanophase separation due to the incompatibility of soft and hard domains. The hydrogen bonding between polar urethane units reinforces the hard domain. Temperature-dependent dynamic mechanical studies of many segmented PUs show two stepwise transitions in storage modulus (E') with two distinct peaks in tan δ at temperatures related to the T_gs of the soft and hard segments. This behavior is consistent with features observed in nanostructured block copolymers with a sharp interphase and in immiscible polymer blends. Varying degrees of nanophase separation are expected depending upon the structures of diisocyanate, soft segment, and chain extender employed in the synthesis of segmented PU as well as the overall material composition.

Segmented PHUs with additional primary and secondary hydroxyl groups adjacent to the urethane linkages manifest very different nanophase separation behavior because of the ability of hard-segment hydroxyl groups to undergo intersegmental hydrogen bonding with hydrogen bond acceptors in the soft segment (Leitsch 2016a, Beniah 2016). Torkelson and coworkers recently reported the synthesis and characterization of segmented PHUs using several polyether-based soft segments (Leitsch 2016a). They showed that the hydroxyl groups caused major phase mixing in PHUs with polyethylene oxide (PEO)-based soft segment due to a high degree of intersegmental hydrogen bonding from the hard-segment hydroxyl groups to ether oxygen in the soft segment. This hydrogen bonding can be suppressed with polypropylene glycol (PPG)-based soft segments which sterically hinder access to the oxygen atoms and polytetramethylene oxide

(PTMO)-based soft segments which dilute the oxygen atom content relative to PEO-based soft segments. Tunable mechanical properties can be achieved by the extent to which intersegemental hydrogen bonding is suppressed. In PTMO-based PHUs, the hydrogen bonding is partially suppressed but not eliminated (Beniah 2016). This results in the formation of nanophase-separated PHU with broad interphases having a wide range of local compositions and potential application as broad-temperature-range damping materials (Beniah 2016, Mok 2008). Long and coworkers reported on segmented poly(amide-hydroxyurethane) systems composed of crystallizable hard segments and PTMO-based soft segments (Zhang 2016). They observed that phase mixing is dominant in nanophase-separated structures of such segmented PHUs. While the foregoing studies have successfully synthesized and characterized segmented PHUs, no study has yet demonstrated the ability to tune nanophase separation behavior in segmented PHU close to the level obtained in segmented PU.

The soft segment plays a critical role in controlling the degree of nanophase separation in segmented PUs (Yilgor 2015, Choi 2009, Castgana 2012, Klinedinst 2005, Ertem 2012, Martin 1996, Korley 2006, Zou 2016, Brunette 1981a, Brunette 1981b, Schneider 1979, Bengston 1985, Cuvé 1991, Cuvé 1992, Chen-Tsai 1986, Li 1988, Siegmann 1987, Maglio 1994, Krakovský 1997a, Krakovský 1997b, Hood 2010, Tang 2014, Sheth 2004). Among many soft segments studied, polybutadiene-based soft segments have been reported to exhibit a very high degree of nanophase separation relative to those conferred by polyether- and polyester-based soft segments (Brunette 1981a, Brunette 1981b, Schneider 1979, Bengston 1985, Cuvé 1991, Cuvé 1992, Chen-Tsai 1986, Li 1988, Siegmann 1987, Maglio 1994). This result can be attributed to the non-polar nature of and the lack of hydrogen bond acceptor in polybutadiene-based soft segments, limiting hydrogen bonding to occur only within the hard segment. The suppression of intersegmental hydrogen bonding produces PU with a high degree of nanophase separation. Schneider and coworkers studied a segmented PU system composed of polybutadiene, toluene

diisocyanate, and chain extenders (Brunette 1981a, Brunette 1981b, Schneider 1979, Bengston 1985). Their differential scanning calorimetry (DSC) results showed that the soft-segment T_g is only slightly elevated from the T_g of pure polybutadiene soft-segment starting material with its value invariant with respect to PU hard-segment content. They attributed this effect to an almost complete segregation of hard and soft segments (Brunette 1981a, Brunette 1981b, Schneider 1979, Bengston 1985). Similar observations were made by Boiteux and coworkers in other polybutadiene-based systems (Cuvé 1991, Cuvé 1992). Chen-Tsai et al. studied several polybutadiene-based PU systems using small-angle X-ray scattering (SAXS) (Chen-Tsai 1986). They found that polybutadiene-based segmented PU possesses the lowest degree of interfacial mixing (highest degree of nanophase separation) as well as the sharpest domain interphase in comparison with polyether- and polyester-based segmented PUs.

In this chapter, we demonstrate that segmented PHU exhibits significant tunability in nanophase separation behavior through judicious choice of soft segment. A series of PHUs were synthesized using PTMO- and polybutadiene-co-acrylonitrile (PBN)-based soft segments, with the latter strongly suppressing the potential for hydrogen bonding between hard and soft segments relative to the former. These PHUs were characterized by DMA, DSC, atomic force microscopy (AFM), FTIR and tensile testing. All PHUs synthesized in this study exhibit nanophase-separated structures in their bulk morphology via SAXS. The PTMO-based PHUs exhibit nanophase separation behavior characteristic of a material with broad interphases and thus a wide range of local compositions whereas the PBN-based PHUs exhibit nanophase separation with sharper domain interphases characteristic of nanophase-separated, isocyanate-based PUs and conventional block copolymer. FTIR reveals a higher proportion of hydrogen-bonded carbonyl in PBN-based PHUs than in PTMO-based PHUs, consistent with the absence and presence of intersegment hydrogen bonding in PBN-based PHUs and PTMO-based PHUs, respectively. This study demonstrates that the choice of soft segment can significantly tune the

state of nanophase separation in segmented PHUs, in some cases resulting properties that are qualitatively similar to those of nanophase-separated, isocyanate-based PUs.

5.2 Experimental

5.2.1 Materials

Polybutadiene-co-acrylonitrile with 18 wt% acrylonitrile (Hypro™ 1300X42 ATBN), subsequently referred to as PBN18, was supplied by Emerald Performance Materials® CVC Thermoset Specialties. It contains oligomers of Dytek-A-terminated polybutadiene-co-acrylonitrile (18 wt% acrylonitrile) with M_n = 3800 g/mol and excess Dytek-A. The amine equivalent weight is 427 g/mol. Polybutadiene-co-acrylonitrile with 10 wt% acrylonitrile, subsequently referred to as PBN10, is an experimental variant of Hypro™ 1300X42 ATBN. It contains oligomer of Dytek-A-terminated polybutadiene-co-acrylonitrile (10 wt% acrylonitrile) with M_n = 3800 g/mol and excess Dytek-A. The amine equivalent weight is 634 g/mol. Diamine-terminated polytetramethylene oxide with M_n = 1700 g/mol (Elastamine HT-1700 or also known as XTJ-548) was supplied by Huntsman Corporation and used as received. Additional 1,5-diamino-2-methylpentane/Dytek-A (99%) was purchased from SigmaAldrich and used as received. Dimethylformamide (DMF) was purchased from Fisher Scientific and used as received. Divinylbenzene dicyclocarbonate (DVBDCC) was synthesized as described by Torkelson and coworkers (Leitsch 2016a).

5.2.2 Synthesis of PHUs

All PHUs were synthesized according to Scheme 5.1. The naming convention for PHUs in this study is soft segment-XX where the soft segments can be PBN18, PBN10, and PTMO, respectively, whereas XX denotes the hard-segment content in the material. The hard-segment content is defined by [(weight of DVBDCC + weight of chain extender)/(weight of DVBDCC +

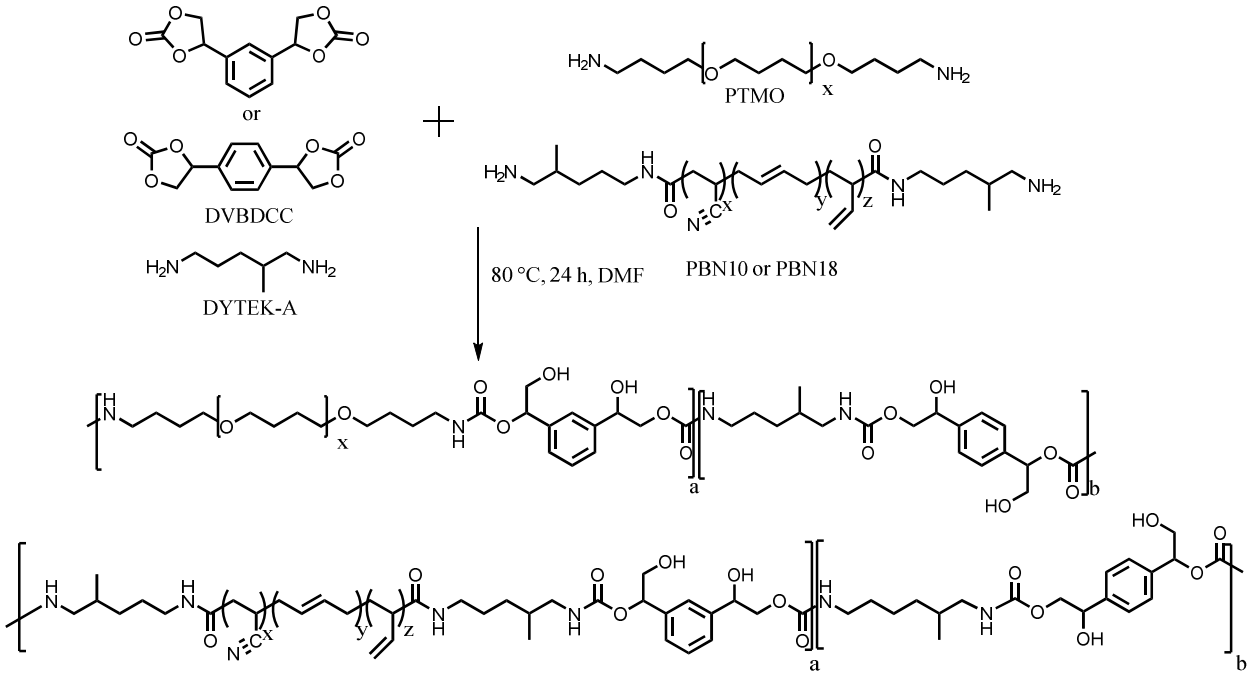

Scheme 5.1: Reaction schemes for synthesis of PTMO-based and PBN-based PHUs.

weight of chain extender + weight of soft segment)] x 100 %. In a typical synthesis of PBN18-30, 3.0 g of PBN18 (comprised of 0.70 mmol of Dytek-A-terminated polybutadiene-co-acrylonitrile oligomers and 2.81 mmol Dytek-A), and 0.88 g (3.51 mmol) of DVBDCC were combined into a Max20 cup (FlackTek™). Then, 2.0 mL of DMF were added to solubilize the mixture and to bring the concentration of reacting groups to ~0.50 M. The mixture was homogenized in a FlackTek SpeedMixer™ for 1.0 min and transferred to a 20-mL vial where it reacted at 80 °C for 24 h with stirring. In a typical synthesis of PBN10-30, 3.0 g of PBN10 (comprised of 0.70 mmol of Dytek-A-terminated polybutadiene-co-acrylonitrile oligomers and 1.66 mmol of DYTEK-A), 0.88 g (3.51 mmol) of DVBDCC and 0.13 g (1.14 mmol) of Dytek-A were combined into a Max20 cup. Then, 2.3 mL of DMF were added to solubilize the mixture and to bring the concentration of reacting groups to ~0.50 M. The mixture was homogenized in a FlackTek SpeedMixer™ for 1.0 min and transferred to a 20-mL vial and let to react at 80 °C for 24 h with stirring. In a typical synthesis of PTMO-30, 1.5 g (6.0 mmol) of DVBDCC, 4.37 g (2.77 mmol) of Elastamine HT-1700, 0.382 g (3.22 mmol of Dytek-A) and 3.7 mL of DMF were combined into a Max20 cup and homogenized. The mixture was transferred to a 20-mL vial where it reacted at 80 °C for 24 h with stirring.

5.2.3 Characterization of PHUs

Attenuated total reflectance-Fourier transform infrared (ATR-FTIR) spectroscopy was performed with a Bruker Tensor 37 MiD IR FTIR spectrophotometer equipped with a diamond/ZnSe attachment. All PHUs were scanned at a resolution of 4 cm^{-1} and 32 scans were collected in the 4000-600 cm^{-1} range. The conversion of the starting materials were determined by analyzing carbonate carbonyl groups of DVBDCC at ~1800 cm^{-1}.The urethane carbonyl peaks located at ~1730-1700 cm^{-1} were analyzed to determine the extent of hydrogen bonding in the urethane carbonyl regions. ^{1}H NMR spectra were recorded on a Bruker Avance III 500 MHz

NMR spectrometer with a direct cryoprobe at room temperature in deuterated chloroform ($CDCl_3$). Spectra were reported in parts per million relative to tetramethylsilane. The molecular weights (MWs) of PHUs were determined using gel permeation chromatography (GPC). A Waters 2695 separation module and two Tosoh TSKgel Alpha-M columns (particle size13 μm, mixed-bed, 30 cm long, P/N 0018334) in series were used with 4 cm guard column (TSK guardcolumn alpha, P/N 0018345. The eluent was DMF with 4.0 g/L of $LiNO_3$ at 40 °C; the elution rate was 0.5 mL/min. The detector was a Viscotek TDA 302 interface/Waters 2414 RI detector. Molecular weight values were reported relative to polyethylene oxide (PEO) standards. Agilent PEO/PEG EasiCal P/N 2080-0201/0202 was used for calibration.

SAXS experiments were performed using a Rigaku S-MAX 3000 SAXS system emitting X-rays with a wavelength of 0.154 nm (Cu-Kα). The sample-to-detector distance was 1640 mm with silver behenate calibration. The 2D scattering patterns were azimuthally averaged to produce 1-D plots of intensity versus scattering vector q, where $q = 4\pi\sin\theta/\lambda$; θ is one-half of the scattering angle, and λ is the X-ray wavelength.

AFM samples were prepared by drop casting 10 wt% solutions of PHU in DMF onto glass cover slides. Samples were dried for 24 h at 80 °C. AFM phase imaging was performed using a Bruker Dimension FastScan Atomic Force Microscope in tapping mode.

DMA experiments were performed with a TA Instruments Rheometrics Stress Analyzer-GIII. Rectangular specimens measuring 8.0 mm in width and 0.9 mm in thickness were cooled with N_2 gas to -100 °C and subjected to a temperature sweep from -100 °C to 120 °C at a heating rate of 3 °C/min. The measurements were conducted in tensile mode at a frequency of 1 Hz and a strain of 0.03%. The storage modulus (E'), loss modulus (E") and loss tangent (tan δ) were recorded. The soft-segment T_g was identified from the peak maximum in E"; the flow temperature was defined as the onset of inconsistent tan δ data, close to the temperature at which the sample was no longer mechanically robust. Differential scanning calorimetry was performed

using a Mettler Toledo DSC 822e. Samples were heated to a 100 °C and annealed for 5 minutes and subsequently quenched to -80 °C and heated a second time at 10 °C/min, with T_g values determined upon second heat via the onset method.

Tensile properties were obtained according to ASTM D1708 standard with an MTS Sintech 20/G tensile tester. Dog bone-shaped samples (4.7 mm x 1.0 mm x 22 mm) were cut using a Dewes-Gumbs die from dried sheets and subjected to an extension rate of 130 mm/min. The Young's modulus, tensile strength and elongation at break were reported as average values of five specimens. Error represents one standard deviation.

5.3 Results and Discussion

5.3.1 Synthesis and Characterization of PHU Molecular Structure

All PHUs were synthesized according to Scheme 5.1. The successful synthesis of PHU was confirmed by FTIR and NMR spectroscopy. Figure C1 (see Appendix C) shows FTIR spectra of all polymers along with the spectrum of the DVBDCC starting material. The carbonate peak at ~1800 cm^{-1} present in the DVBDCC sample is absent in all PHU samples, indicating complete conversion of carbonate functional groups into hydroxyurethane linkages within experimental error. The urethane carbonyl stretch (1730-1700 cm^{-1}), amide stretch (3500-3300 cm^{-1}), and hydroxyl stretch (3500-3100 cm^{-1}) were present in the spectra of these PHUs. The nitrile stretch (~2238 cm^{-1}) and ether (~1100 cm^{-1}) groups were present in PBN- and PTMO-based PHUs, respectively, indicating successful incorporation of soft-segment molecules into the polymer. The successful formation of PHUs was also confirmed by ^1H NMR spectroscopy. Figures C2-C7 (see Appendix C) show NMR spectra of all PHUs, with positions of various protons within the polymer assigned accordingly.

Apparent molecular weight (MW) averages of these PHUs were determined by GPC and are tabulated in Table C1 in Appendix C; all apparent MW averages are relatively low. The

achievement of relatively low MW during synthesis of PHUs was also reported in a recent study by Averous and coworkers (Carré 2016) who synthesized segmented PHUs using fatty-acid based diamine, terephthaloyl bis-carbonate and diamine-terminated polypropylene glycol (Jeffamine™ D2000); other studies have made related reports (Benyahya 2012, Benyahya 2012, Leitsch 2016, Beniah 2016, Lamarzelle 2016, Besse 2015). A recent study on segmented, PTMO-based PHU by Long and coworkers (Zhang 2016) also noted that the MWs of their PHUs might be low although no data were provided. Additionally, we consider it possible that PHUs undergo some GPC column interaction. Long and coworkers noted that column interaction was observed in their system, even for PHU with the lowest hard-segment content (with the lowest amount of hydroxyurethane and amide linkages) (Zhang 2016). Future study is needed to produce higher MW PHU, possibly by using more reactive six- or eight-membered-ring carbonates or via the aid of organic catalysts (Lambeth 2013, Lombardo 2015).

5.3.2 SAXS

The hard and soft segments in segmented PUs are thermodynamically incompatible resulting in segregation of hard segments into nanosized-domains dispersed within a rubbery matrix. The hydrogen bonding between the urethane units and the vitrification of the hard domains reinforce the nanophase-separated structures in segmented PUs. SAXS is commonly used to probe the existence, degree and kinetics of nanophase separation in PU (Elwell 1996a, Elwell 1996b, Ryan 1991, Ryan 1992). The SAXS patterns of PBN-based and PTMO-based PHUs are shown in Figure 5.1. Nanophase separation is evident from the peak in scattered intensity for each PHU. The interdomain spacing (*d*) can be determined from the peak location in scattered intensity. For all PHUs, *d* values are ~ 9-16 nm (see Table 5.1), with the 40 wt% hard-segment content PHUs exhibiting larger *d* values than their 30 wt% analogues, consistent with larger hard-segment domains being present at higher hard-segment content. At equal hard-

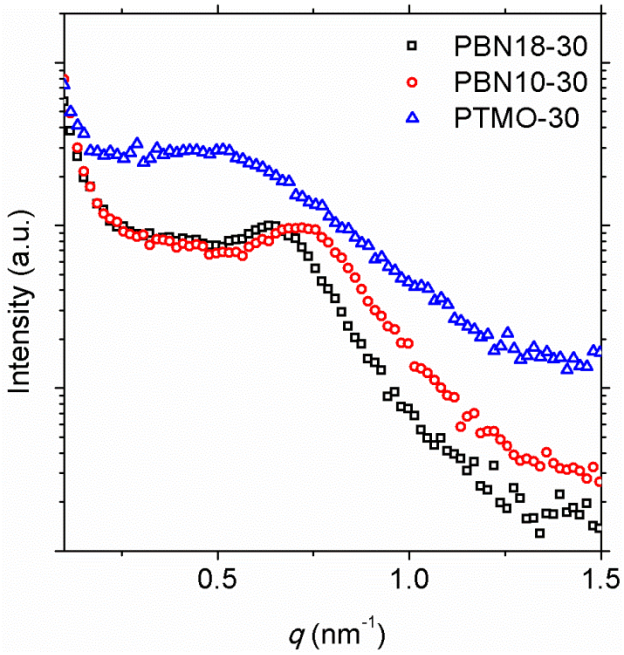

Figure 5.1:. Small-angle X-ray scattering patterns of PTMO-30, PBN18-30 and PBN10-30.

segment content, PTMO-based PHUs have larger *d* values than the PBN-based PHUs even though the PTMO-based soft segment is of lower MW than those of the PBN-based soft segments. The origin for this difference as a function of soft-segment species warrants further study.

5.3.3 DMA

The thermomechanical properties of PHUs synthesized in this study were analyzed using DMA. Consistent with the presence of nanophase-separated structures, all PHUs show two thermal transitions corresponding to T_gs of the soft and hard segments. The soft-segment T_g is identified from the peak in loss modulus (*E*") located well below ambient temperature. As determined by DMA, in PTMO-based PHUs the soft-segment T_gs are ~ -67 °C whereas in PBN-based PHUs the soft-segment T_gs are ~ -54 and ~ -67 °C for PBN18 and PBN10 soft segments, respectively. The T_{flow} values, related to the hard-segment domain undergoing a transition from a glassy state to a liquid state upon heating, resulting in loss of any mechanical robustness, are above room temperature. Table 5.1 summarizes the thermal transition values obtained by DMA.

The general shapes of DMA profiles for PTMO-based and PBN-based PHUs differ significantly, testifying to the different nanophase separation behavior obtained as a function of soft-segment choice in segmented PHUs. Figure 2a shows the temperature dependences of *E*', *E*" and tan δ of PTMO-30. The value of log *E*' shows a very gradual decrease with temperature above the soft-segment T_g. The tan δ-temperature profile of PTMO-30 shows high values exceeding 0.30 over a temperature range of more than 70 °C in breadth. The profiles obtained with PTMO-based PHUs are consistent with nanophase-separated systems with broad interphases having a wide range of local composition; such materials may serve as highly effective, broad-temperature-range damping materials (Beniah 2016).

Figure 5.2b shows the temperature dependences of *E*', *E*" and tan δ of a typical PBN-based PHU, PBN18-30. In contrast to PTMO-30, PBN18-30 manifests two distinct, roughly

Table 5.1: Summary of interdomain spacing, thermal and mechanical properties of PTMO- and PBN-based PHUs.

Material	*d*-spacing (nm)	SS T_g (DSC) (°C)[a]	SS T_g (DMA) (°C)[b]	HS T_g (DSC) (°C)[c]	T_{flow} (DMA) (°C)[d]	Young's Modulus (MPa)	Tensile Strength (MPa)	Elongation at Break (%)
PBN18-30	10.1	-60 to -48	-46	17 to 49	52	48 ± 7	1.1 ± 0.2	900 ± 200
PBN18-40	13.4	-60 to -48	-48	35 to 50	65	53 ± 5	1.0 ± 0.3	300 ± 130
PBN10-30	9.6	-72 to -63	-62	8 to 48	43	56 ± 4	0.6 ± 0.1	720 ± 100
PBN10-40	10.7	-74 to -64	-57	38 to 58	73	61 ± 4	0.8 ± 0.1	100 ± 60
PTMO-30	12.6	-	-65	-	40	23 ± 6	0.4 ± 0.1	>2000
PTMO-40	16.1	-	-65	-	40	36 ± 3	0.8 ± 0.2	1600 ± 300

[a]The onset and endset of the soft-segment T_gs as determined by DSC using the first derivative method.

[b]Determined from the peak in dynamic loss modulus (*E*") in DMA.

[c]The onset and endset of the hard segment T_gs as determined by DSC using the first derivative method.

[d]Determined from the onset of inconsistent tan δ data using DMA, close to the temperature at which the sample is no longer mechanically robust.

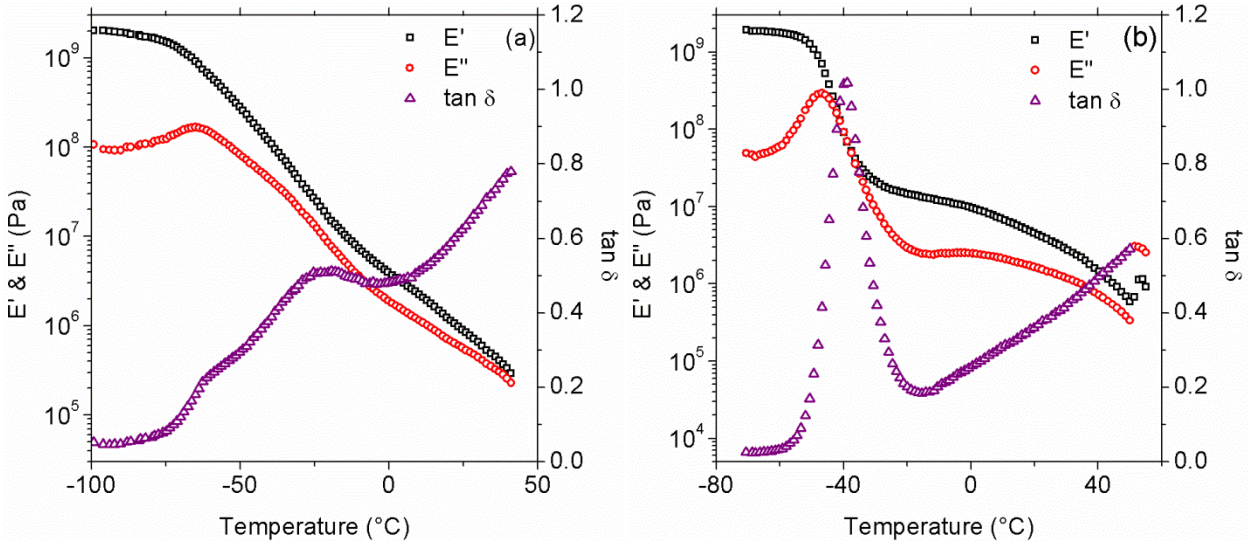

Figure 5.2: Temperature dependences of storage modulus (*E*'), loss modulus (*E*") and loss factor (tan δ) of PHUs synthesized with a) PTMO soft segment, PTMO-30, and b) polybutadiene-co-acrylontrile, 18 wt% acrylonitrile soft segment, PBN18-30.

stepwise transitions in its log *E*'-temperature curve with sharp, well-defined peaks in the tan δ-temperature curve. The first drop in log *E*' upon heating near the soft-segment T_g is followed by a rubbery plateau region which extends several tens of degrees prior to another drop in log *E*' due to the hard segment undergoing its glass transition to a liquid state. This profile is consistent with the behavior of a nanophase-separated system with sharp domain interphases such as those observed in conventional segmented PUs or conventional, nanostructured block copolymers. The difference in nanophase separation behavior in these PHUs is a direct result of hydrogen bonding. In PTMO-based PHUs, the hard-segment hydroxyl groups can undergo hydrogen bonding with oxygen atoms in the soft segment, causing some level of phase mixing. (Leitsch 2016a, Beniah 2016) This intersegmental hydrogen bonding then leads to interphase regions with a wide range of local composition. The switch to a PBN-based soft segment suppresses this intersegmental hydrogen bonding and leads to improved nanophase separation and sharper domain interphases.

Figure 5.3 shows the temperature dependences of *E*', *E*" and tan δ for PHUs synthesized with PBN18 and PBN10 at 30 wt% and 40 wt% hard-segment contents. Despite the difference in acrylonitrile content in the soft segments, both PHUs show similar thermomechanical responses, with only the values of the soft-segment T_gs changing significantly as a function of acrylonitrile content in the soft segment. Thus, for the PBN-based soft segments employed here, the soft-segment acrylonitrile content has little influence on the nanophase separation behavior.

Figure 5.3 also reveals that the rubbery plateau modulus and T_{flow} value increase with increasing hard-segment content. In PBN18-based PHUs, T_{flow} increases from 52 to 65 °C as hard-segment content increases from 30 wt% to 40 wt%. This effect can be attributed to increased physical crosslinking with increasing hard-segment content and a more perfected hard-segment domain. This interpretation is also supported by the fact that the interdomain spacing from SAXS measurements increases from 10.1 to 13.4 nm with increasing hard-segment content

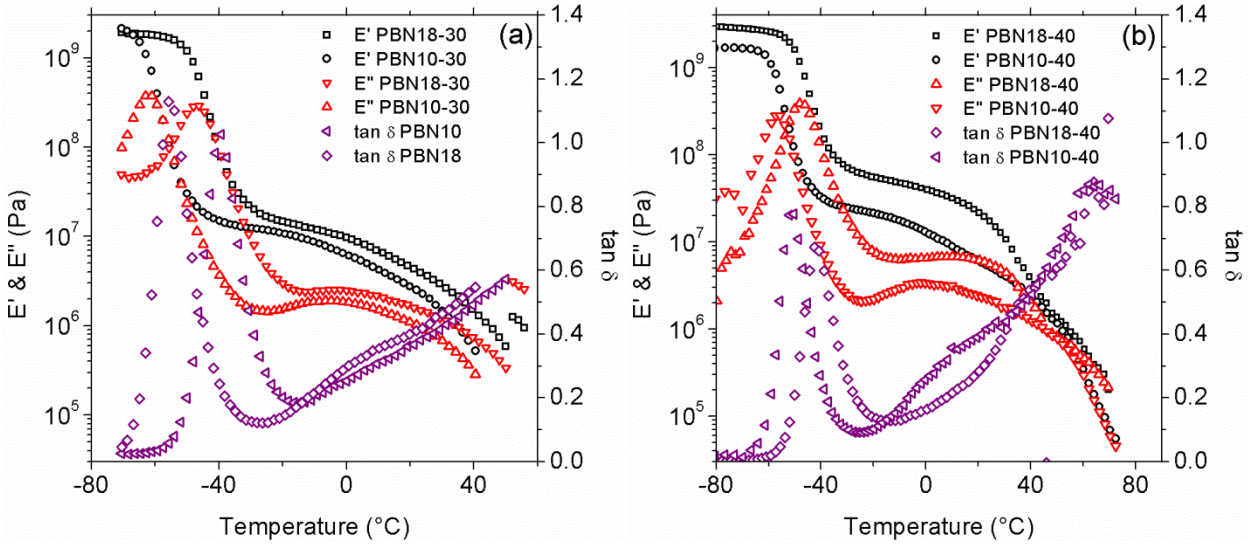

Figure 5.3: Temperature dependences of storage modulus (*E*'), loss modulus (*E*") and loss factor (tan δ) of PHUs synthesized with polybutadiene-co-acrylonitrile soft segments at a) 30 wt% hard-segment content (PBN18-30 and PBN10-30) and b) 40 wt% hard-segment content (PBN18-40 and PBN10-40).

in PBN18-based PHUs. This means that the size of the hard segment nanodomains are smaller in the 30 wt% hard-segment PHU, likely < 5 nm in diameter, leading to more imperfect phase separation and thus a lower hard–segment domain T_g.

As shown in Figure 5.3, the slope of the log *E*' vs. temperature curve in the "rubbery plateau" regime provides a qualitative measure of the degree and perfection of nanophase separation in segmented PUs. In some well phase-separated PU systems (Ertem 2012, Korley 2006, Maglio 1994, Tang 2014, Sheth 2004) the rubbery plateau regime is almost unchanging with temperature, i.e., the slope is nearly zero or only slightly negative. The slopes of the "rubbery plateau" regions in the PBN-based PHUs considered here are more temperature-sensitive, likely because some mixing of hard and soft segments still persists. Nevertheless, the nanophase separation is much sharper in PHUs with PBN-based soft segments relative to PHUs with PTMO-based soft segments. The dramatic difference observed in DMA results between PTMO-based PHUs and PBN-based PHUs demonstrates that nanophase separation behavior can be tuned significantly in segmented PHU by judicious choice of soft segment.

It is worth noting that the presence of acrylonitrile in the soft-segment of PBN-based PHUs does not result in extensive phase mixing. Previous studies have shown that nitrile groups are capable of forming hydrogen bonds with hydroxyl groups (Knoezinger 1975, Healy 1989, Lachat 2009). However, we observed that nanophase-separated PBN-based PHUs exhibit behavior consistent with sharper interphase regions than those of PTMO-based PHUs, which indicates that the acrylonitrile units are not interacting significantly with hydroxyl groups in the hard segment to cause phase mixing. We hypothesize that this behavior arises from acrylonitrile units that are self-associating in the soft domain instead of participating in hydrogen bonding with hydroxyl groups. Self-association of acrylonitrile units due to a strong dipole-dipole interaction is well studied in the literature (Alia 2007, Phadke 2005, Phadye 1985). This self-association is also supported by the location of nitrile peaks of PBN-based PHUs from FTIR

measurement (see Figure C8 in Appendix C). The nitrile peaks in PBN-based PHUs appear at ~2238 cm^{-1}, equivalent to acrylonitrile groups in bulk polyacrylonitrile. Studies by Lachat et al. (Lachat 2009) indicated that high temperature and pressure are needed to break nitrile-nitrile interactions and replace them with nitrile-hydroxyl interactions. In other words, under the conditions of our study, nitrile-hydroxyl interactions are insufficiently strong to disrupt nitrile-nitrile interactions. As a result of acrylonitrile self-association, the soft segment is reinforced and the hard segment is effectively excluded from the soft segment leading to better nanophase separation. We note that a study by Maglio and coworkers on PBN-based segmented PUs also indicated that there is no extensive phase mixing of soft and hard segments based on DSC and DMA characterization (Maglio 1994).

5.3.4 DSC

Figure 5.4a shows DSC heat flow curves of all PHUs. The PTMO-based PHUs do not exhibit distinct hard-segment thermal transitions, likely due, at least in part, to their broad interphases leading to very broad and hence weak T_g responses. The hard-segment hydroxyl groups can hydrogen bond with soft-segment ether oxygen atoms resulting in some level of phase mixing, thus making thermal transitions in PTMO-based PHUs difficult to discern by DSC. In contrast, two distinct thermal transitions below and above ambient temperature corresponding to the soft- and hard-segment T_gs are clearly observed in all PBN-based PHUs. The distinct thermal transitions observed by DSC in PBN-based PHUs indicate that PBN-based soft segments result in better nanophase separation and sharper domain interphases than PTMO-based soft segments and consequently more discernible thermal transitions of each domain.

To quantify further the transition breadths in these PHUs, we plot the first derivative heat flow curves in Figure 5.4b. First derivative heat flow curves have been useful in determining the glass transition responses of minor phases in materials or when there is only a small change in

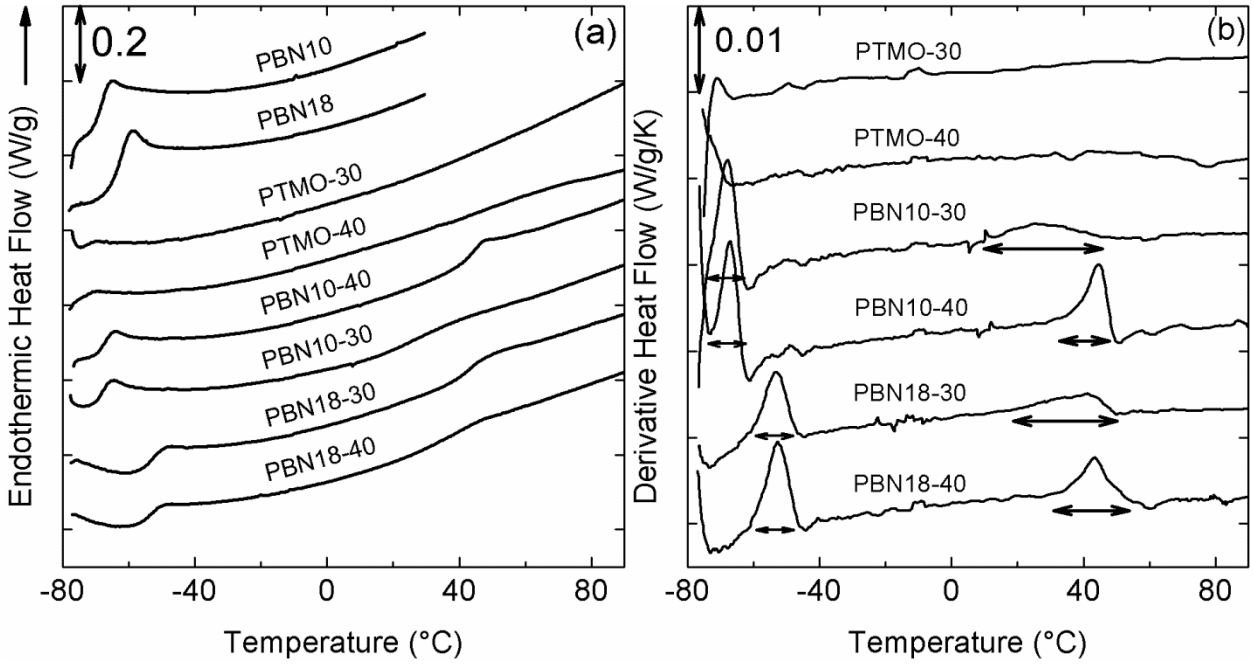

Figure 5.4: Thermal properties of PHUs as characterized by DSC. a) Representative heat flow curves of PHUs at a heating rate of 10 °C/min and, b) first derivative heat flow curves of PHUs.

heat capacity. Derivative heat flow curves also permit quantification of T_g breadth which is related to compositional heterogeneity or phase mixing (Kim 2006, Wong 2007, Mok 2009). The first derivative heat flow curves of PTMO-based PHUs do not show any discernible features, indicating that the thermal transition(s) in PTMO-based PHUs, easily apparent via DMA, are not be amenable to DSC characterization.

The derivative heat flow curves of PBN-based PHUs provide further information on thermal transition breadths in PBN-based PHUs. As shown in Figure 5.4b, the apparent soft-segment glass transition breadths for PBN18-30 and PBN10-30 span the ranges from -60 to -48 °C and -72 to -63 °C, respectively. These values are elevated only by ~10 °C from the T_gs of the corresponding pure soft-segment homopolymers, consistent with a high degree of nanophase separation in PBN-based PHUs. Increasing the hard-segment content to 40 wt% in the cases of PBN18-40 and PBN10-40 does not significantly alter the soft-segment domain T_gs. The proximity of the soft-segment domain T_g values to the T_g of its corresponding homopolymer and their invariance with respect to the hard-segment content indicate a high level of nanophase separation in PBN-based PHUs. These results agree with DSC characterization of several polybutadiene-based segmented PUs reported by Schneider and coworkers (Brunette 1981a, Brunette 1981b, Schneider 1979, Bengston 1985) as well as our DMA results on the same PBN-based PHUs.

Figure 5.4b also shows that PBN-based PHUs exhibit broader hard-segment T_g regions as hard-segment decreases from 40 to 30 wt%. The hard-segment glass transition regions for PBN18-40 and PBN10-40 span 35 to 50 °C and 38 to 58 °C, respectively, whereas those for PBN18-30 and PBN10-30 span 17 to 49 °C and 8 to 48 °C, respectively. The endset T_g reported by DSC is lower than T_{flow} by DMA, in accord with literature reports (Xu 2006. Hsu 1999, Van Ekeren 2011, Miller 1985). As described above regarding DMA results, the effect of decreasing hard-segment content on glass transition breadth can be attributed at least in part to the decrease

in size of hard-segment nanodomains, which likely leads to less perfect nanophase separation and thus a broader glass transition.

5.3.5 AFM

Surface morphological characterization of segmented PUs by AFM has been used to provide supporting evidence of nanophase separation (Klinedisnt 2005, Ertem 2012, Martin 1996, Korley 2006). Imaging of phase segregation in PTMO-based PHUs was met with limited success. The limitations may be caused by the low contrast between domains in PTMO-based PHUs as a result of their broad domain interphases. A similar limitation in imaging phase-segregated domains was previously reported in gradient copolymer systems which possesses broad interphases with a wide range of local composition (Mok 2012). AFM phase images from a recent study of PTMO-based segmented PHUs by Long and coworkers (Zhang 2016) provided relatively strong compositional contrasts between hard and soft domains. However, this response was likely caused by the ability of the hard segments to crystallize. Their polymers also possessed amide linkages and one-half the content of hydroxyl groups possessed by our PHUs. Long and coworkers also noted that there was significant phase mixing between domains in their PHUs as evidenced from DMA and DSC results (Zhang 2016).

Figure C9a-c in Appendix C compares AFM phase images of PBN18-40 and PBN10-40 with PTMO-30. For the PBN-based PHUs, the light regions correspond to hard domains and the dark regions to soft domains. Contrast between soft and hard domains is evident in PBN-based PHUs whereas little or no contrast is evident in PTMO-based PHUs. These results are consistent with less effective nanophase separation and the presence of substantial phase mixing in the PTMO-based PHUs, in agreement with DMA and DSC characterization.

5.3.6 FTIR

The level of nanophase separation in segmented PUs can be inferred from the strength of hydrogen bonding interaction in the hard segment. FTIR is commonly used to evaluate the degree and kinetics of nanophase separation by comparison of spectral bands associated with urethane carbonyl groups and amide groups (Yilgor 2009, Yilgor 2006, Sheth 2005a, Sheth 2005b, Lee 2000, Lee 2007, Garrett 2003, Lee 1988. Lee 1997). The carbonyl region may display two characteristics: one associated with free, non-hydrogen-bonded carbonyl presenting as a shoulder centered at ~1730 cm^{-1} and a second associated with hydrogen-bonded carbonyl presenting as a peak centered at ~1700 cm^{-1}. Figure 5.5 shows FTIR spectra in the carbonyl regions of all PHUs. Based on Figure 5.5, the PTMO-based PHUs exhibit the presence of both free, non-hydrogen bonded carbonyl and hydrogen bonded carbonyl; in contrast, the PBN-based PHUs exhibit no evidence of a shoulder at ~1730 cm^{-1}, consistent with well-hydrogen-bonded carbonyl. These results indicate that the lack of ether oxygen atoms as hydrogen bond acceptors in PBN-based soft segment limits hydrogen bonding to occur within the hard segment of PBN-based PHUs and thus nanophase separation to occur without substantial phase mixing. In contrast, in PTMO-based PHUs, the hard-segment hydroxyl groups can form hydrogen bonds with soft segment oxygen atoms giving rise to a distribution of free and hydrogen-bonded carbonyls.

The FTIR spectra of PBN-based PHUs also show carbonyl absorbance at ~1670 and ~1640 cm^{-1}. These bands are attributed to free and hydrogen-bonded amide groups which are located at the terminal units of PBN18 and PBN10 soft segments incorporated in the PHUs (Biemond 2007, Biemond 2008, Biemond 2012). Although the amide groups may participate in hydrogen bonding, we doubt that these amide groups contribute significantly to the apparent improvement in nanophase separation observed in PBN-based PHUs because they are present at much lower concentration than the hydroxyl groups. Future study is warranted to investigate the influence of such amide groups on nanophase separation.

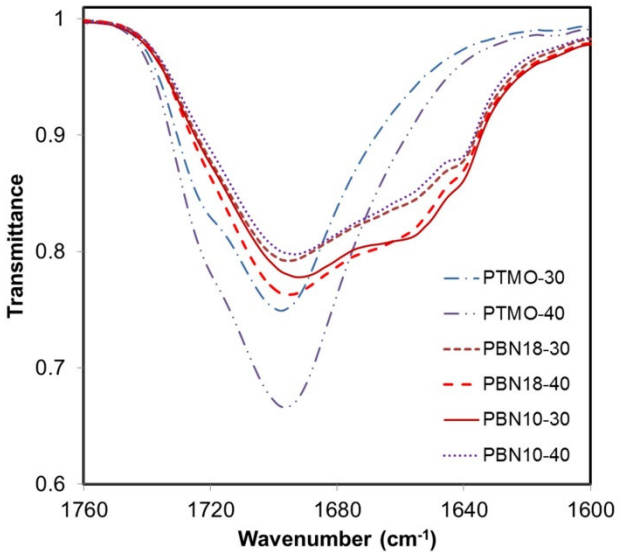

Figure 5.5: FTIR spectra of the carbonyl regions representing free, non-hydrogen bonded urethane carbonyl (~1730 cm^{-1}) and hydrogen bonded urethane carbonyl (~1700 cm^{-1}). PBN-based PHUs show peaks centered at ~1670 and 1640 cm^{-1}, associated with free and hydrogen bonded amide carbonyl in the soft segment.

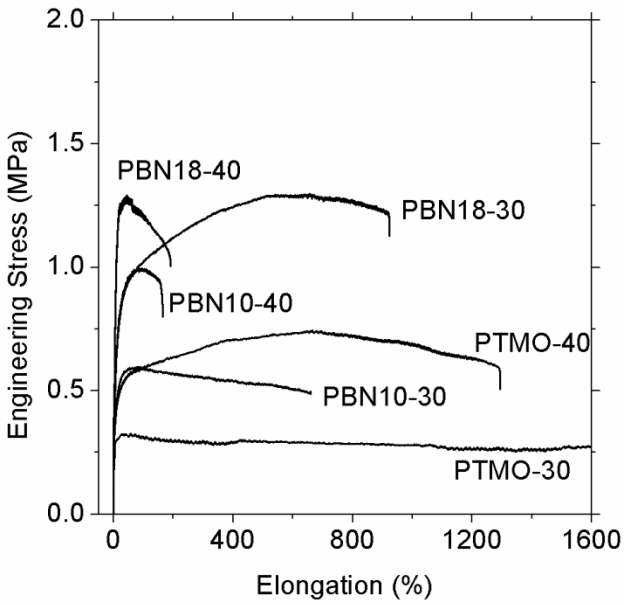

Figure 5.6: Representative stress-strain curves of PHUs characterized by uniaxial tensile testing.

5.3.7 Tensile Testing

Figure 5.6 displays representative stress-strain curves of all PHUs during tensile deformation. Table 1 lists average values of Young's Modulus, ultimate tensile strength, and elongation at break. The PTMO-based PHUs exhibit tensile strengths up to 0.8 MPa whereas PBN-based PHUs exhibit tensile strengths up to 1.1 MPa. Relative to PTMO-based PHUs, the PBN-based PHUs experience a larger reduction in elongation-at-break values with increasing hard-segment content. This result is in agreement with previous studies of segmented PUs with nonpolar soft segments such as polyisobutylene and polybutadiene, which show large reductions in elongation-at-break values with increasing hard-segment content (Brunette 1981a, Schneider 1979, Speckhard 1985a, Speckhard 1985b). Segmented PUs with nonpolar soft segments typically possess a very sharp domain interphase (Chen-Tsai 1986, Speckhard 1985a, Speckhard 1985b). Cooper and coworkers suggested that poor interfacial adhesion between the hard and soft segments and localization of shear stress in the hard segment might lead to lower elongation-at-break values with higher hard-segment content in PUs made with nonpolar soft segment (Speckhard 1986). This explanation is in accord with results from our study showing that PBN-based PHUs possess a much sharper domain interphase relative to PTMO-based PHUs.

In general, elongation-at-break and Young's modulus values of the PHUs in this study are similar to those obtained in conventional TPUs; however, the tensile strength values of the PHUs are inferior (Zou 2016, Brunette 1981a, Brunette 1981b, Schneider 1979). Further structure-property-relationship studies which consider the influences of hard-segment, chain-extender, and other soft-segment structures are warranted to obtain segmented PHUs with improved properties. Such studies are detailed in the next chapters.

5.4 Conclusion

Tunability of nanophase separation behavior in segmented PHU was demonstrated via a

simple change in soft-segment type. A series of PHUs were synthesized with PTMO- and PBN-based soft segments and characterized via SAXS, DMA, DSC, AFM, FTIR spectroscopy and tensile testing. SAXS results demonstrate the presence of nanophase-separated structures in all PHUs with interdomain spacings of 9-16 nm, independent of soft-segment type. DMA characterization shows that PTMO-based PHUs exhibit nanophase separation with broad interphases having a wide range of local composition. The broad interphases are a result of small to moderate levels of phase mixing originating from hard-segment hydroxyl groups undergoing hydrogen bonding with ether oxygen in the PTMO backbone. A change to PBN-based soft segments results in PHUs having sharper domain interphases due to a lack of hydrogen bonding between hard and soft segments. These interpretations are supported by FTIR spectroscopy which indicates that a substantial proportion of non-hydrogen-bonded carbonyl is present in PTMO-based PHUs but absent in PBN-based PHUs. The polar acrylonitrile units in PBN have no significant impact on the nanophase separation, likely due to their self-association. DSC and AFM results provide further support of the significantly different nanophase separation behavior in PTMO- and PBN-based PHUs. PHUs exhibited elongation-at-break and Young's modulus values generally in accord with conventional TPUs. However, tensile strengths were inferior to conventional TPUs, with values ranging from 0.6 to 1.1 MPa and PBN-based PHUs being better than PTMO-based PHUs.

APPENDIX C

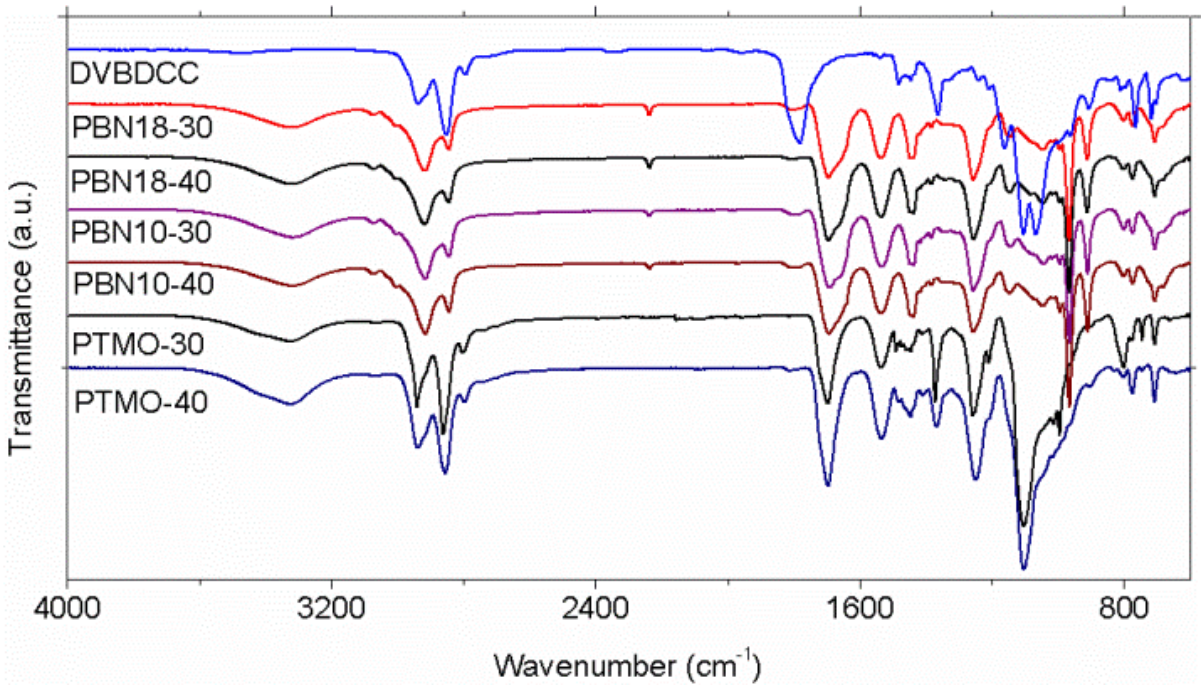

Figure C1: FTIR spectra of PTMO- and PBN-based PHUs plotted with the spectrum of DVBDCC starting materials.

FTIR: (ν = cm^{-1}): 3500-3300 (N-H), 3500-3100 (O-H), 3100-3000 (=C-H and aromatics), 1730-1700 (C=O, urethane), 1670-1640 (C=O, amide), 2250-2230 (C≡N), 1570 (NH), 1100 (C-O from PTMO).

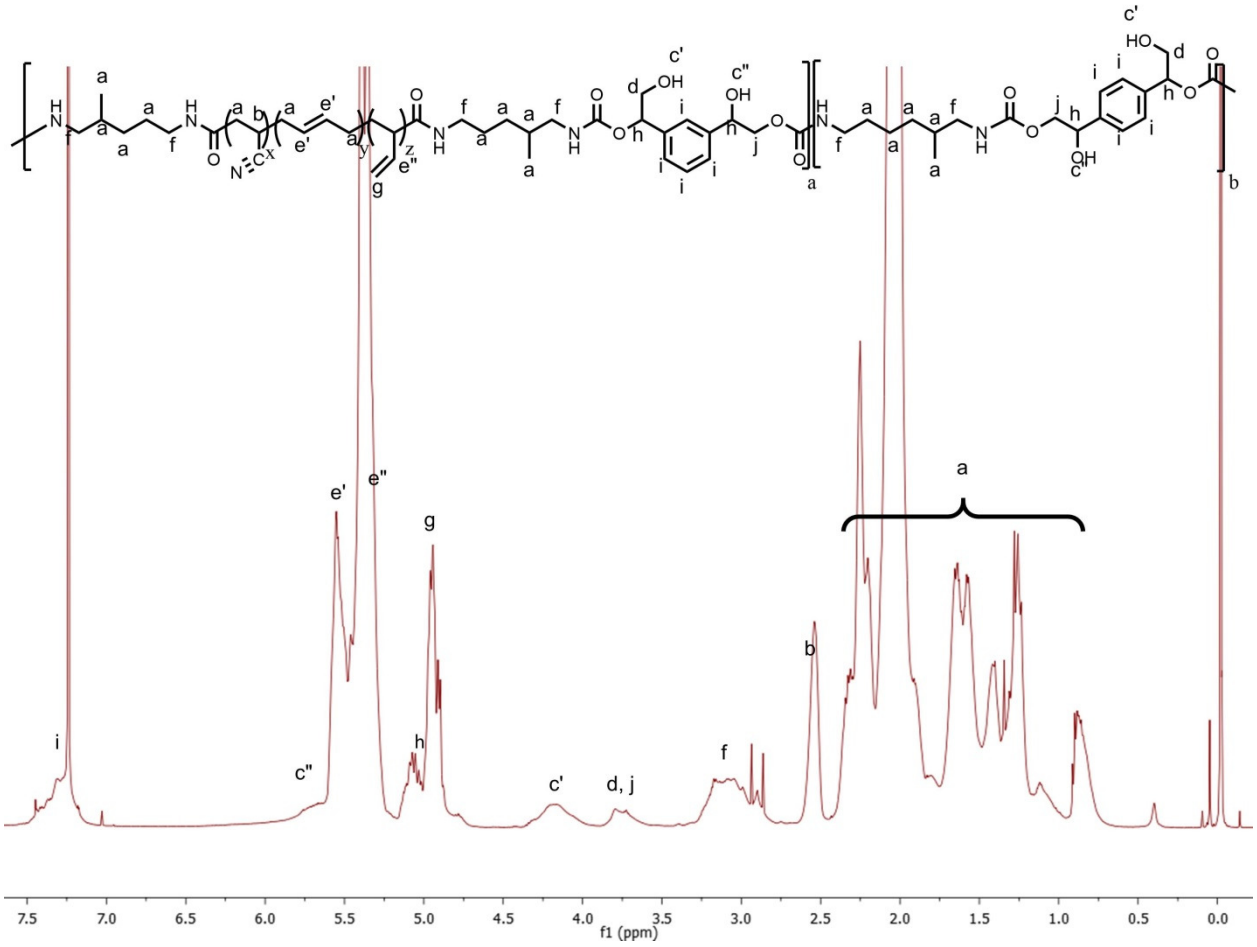

Figure C2:. ^{1}H NMR Spectra of PBN18-30.

PBN18-30. ^{1}H NMR ($CDCl_3$, 500 MHz), δ (ppm): 0.5-2.0 (15H, $NHCH_2C\boldsymbol{H}_2C\boldsymbol{H}_2C\boldsymbol{H}(C\boldsymbol{H}_3)CH_2NH$, $-C\boldsymbol{H}_2C\boldsymbol{H}(CH_2{=}CH_2)-$, $-C\boldsymbol{H}_2CH(CN)-$), 2.5-2.6 (1H, $-CH_2-C\boldsymbol{H}(CN)$), 3.0-3.3 (2H, $C\boldsymbol{H}_2NHC(=O)OCH_2$), 3.4-3.7 (3H, $C\boldsymbol{H}_2OH$, $C\boldsymbol{H}_2OC(-O)NH$) 4.2-4.3 (1H, $CH_2O\boldsymbol{H}$), 4.8-5.0 (2H, $CH(CH{=}C\boldsymbol{H}_2)$), 4.9-5.1 (1H, $PhC\boldsymbol{H}(OH)CH_2O$), 5.2-5.4 (1H, $CH(C\boldsymbol{H}{=}CH_2)$), 5.5-5.6 (2H, $CH_2C\boldsymbol{H}{=}C\boldsymbol{H}CH_2$), 5.7-5.8 (1H, $PhCH(O\boldsymbol{H})CH_2O$).

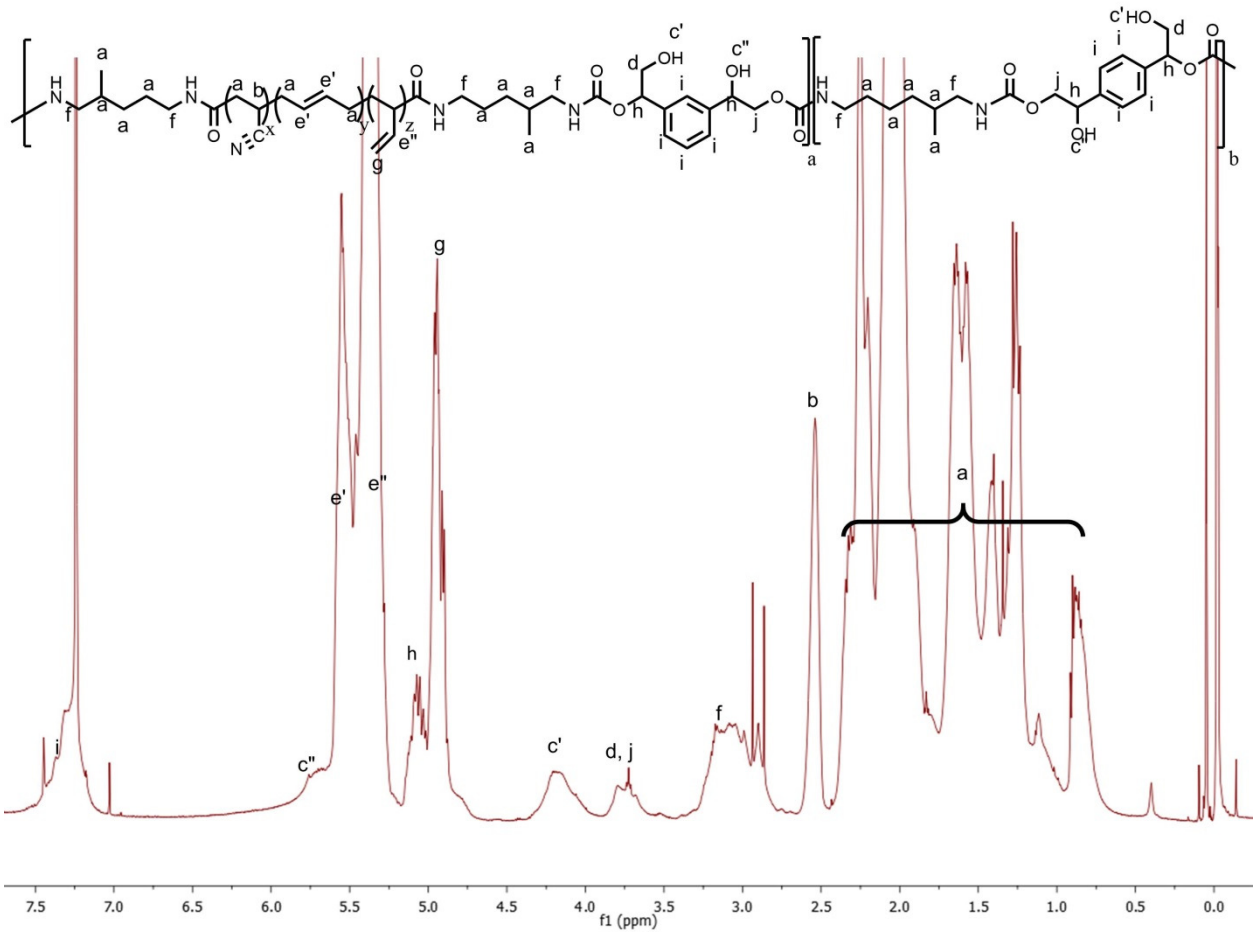

Figure C3: ^{1}H NMR Spectra of PBN18-40.

PBN18-40. ^{1}H NMR ($CDCl_3$, 500 MHz), δ (ppm): 0.5-2.0 (15H, $NHCH_2C\boldsymbol{H}_2C\boldsymbol{H}_2C\boldsymbol{H}(C\boldsymbol{H}_3)CH_2NH$, $-C\boldsymbol{H}_2C\boldsymbol{H}(CH_2{=}CH_2)-$, $-C\boldsymbol{H}_2CH(CN)-$), 2.5-2.6 (1H, $-CH_2-C\boldsymbol{H}(CN)$), 3.0-3.3 (2H, $C\boldsymbol{H}_2NHC(=O)OCH_2$), 3.4-3.7 (3H, $C\boldsymbol{H}_2OH$, $C\boldsymbol{H}_2OC(-O)NH$) 4.2-4.3 (1H, $CH_2O\boldsymbol{H}$), 4.8-5.0 (2H, $CH(CH{=}C\boldsymbol{H}_2)$), 4.9-5.1 (1H, $PhC\boldsymbol{H}(OH)CH_2O$), 5.2-5.4 (1H, $CH(C\boldsymbol{H}{=}CH_2)$), 5.5-5.6 (2H, $CH_2C\boldsymbol{H}{=}C\boldsymbol{H}CH_2$), 5.7-5.8 (1H, $PhCH(O\boldsymbol{H})CH_2O$).

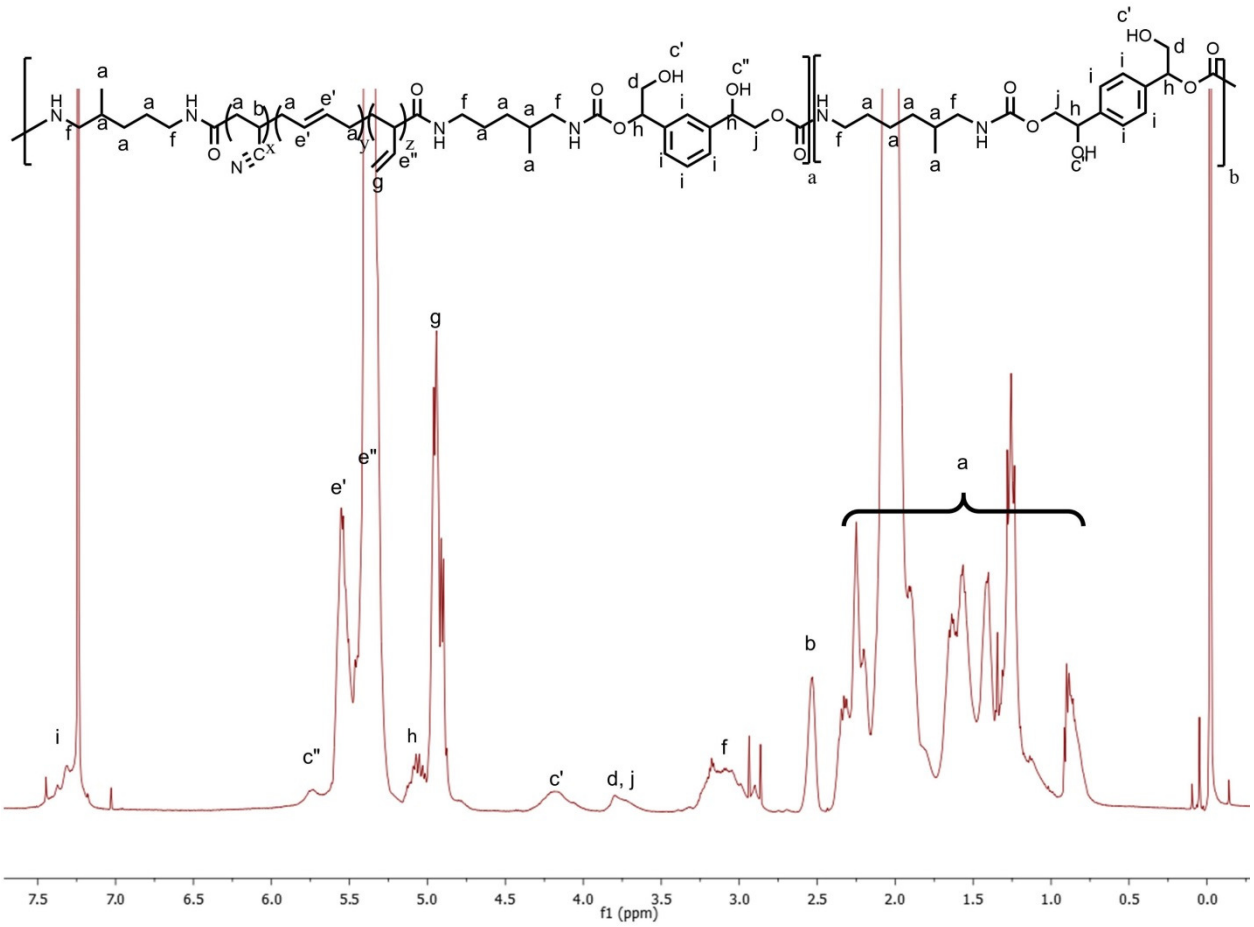

Figure C4: ^{1}H NMR Spectra of PBN10-30.

PBN10-30. ^{1}H NMR ($CDCl_3$, 500 MHz), δ (ppm): 0.5-2.0 (15H, $NHCH_2C\boldsymbol{H}_2C\boldsymbol{H}_2C\boldsymbol{H}(C\boldsymbol{H}_3)CH_2NH$, $-C\boldsymbol{H}_2C\boldsymbol{H}(CH_2{=}CH_2)-$, $-C\boldsymbol{H}_2CH(CN)-$), 2.5-2.6 (1H, $-CH_2-C\boldsymbol{H}(CN)$), 3.0-3.3 (2H, $C\boldsymbol{H}_2NHC(=O)OCH_2$), 3.4-3.7 (3H, $C\boldsymbol{H}_2OH$, $C\boldsymbol{H}_2OC(-O)NH$) 4.2-4.3 (1H, $CH_2O\boldsymbol{H}$), 4.8-5.0 (2H, $CH(CH{=}C\boldsymbol{H}_2)$), 4.9-5.1 (1H, $PhC\boldsymbol{H}(OH)CH_2O$), 5.2-5.4 (1H, $CH(C\boldsymbol{H}{=}CH_2)$), 5.5-5.6 (2H, $CH_2C\boldsymbol{H}{=}C\boldsymbol{H}CH_2$), 5.7-5.8 (1H, $PhCH(O\boldsymbol{H})CH_2O$).

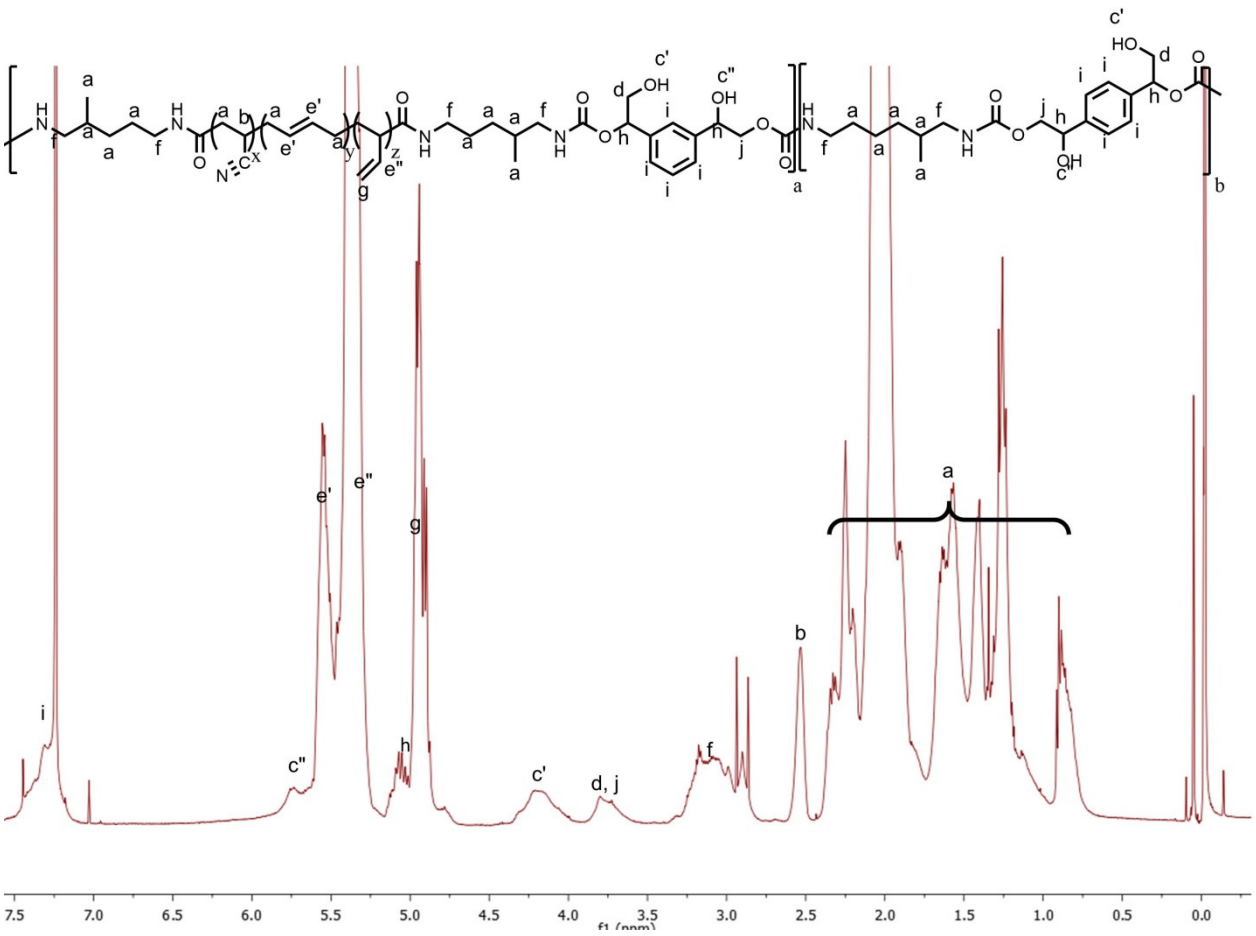

Figure C5: ^{1}H NMR Spectra of PBN10-40.

PBN10-40. ^{1}H NMR ($CDCl_3$, 500 MHz), δ (ppm): 0.5-2.0 (15H, $NHCH_2C\boldsymbol{H}_2C\boldsymbol{H}_2C\boldsymbol{H}(C\boldsymbol{H}_3)CH_2NH$, $-C\boldsymbol{H}_2C\boldsymbol{H}(CH_2{=}CH_2)-$, $-C\boldsymbol{H}_2CH(CN)-$), 2.5-2.6 (1H, $-CH_2-C\boldsymbol{H}(CN)$), 3.0-3.3 (2H, $C\boldsymbol{H}_2NHC(=O)OCH_2$), 3.4-3.7 (3H, $C\boldsymbol{H}_2OH$, $C\boldsymbol{H}_2OC(-O)NH$) 4.2-4.3 (1H, $CH_2O\boldsymbol{H}$), 4.8-5.0 (2H, $CH(CH{=}C\boldsymbol{H}_2)$), 4.9-5.1 (1H, $PhC\boldsymbol{H}(OH)CH_2O$), 5.2-5.4 (1H, $CH(C\boldsymbol{H}{=}CH_2)$), 5.5-5.6 (2H, $CH_2C\boldsymbol{H}{=}C\boldsymbol{H}CH_2$), 5.7-5.8 (1H, $PhCH(O\boldsymbol{H})CH_2O$).

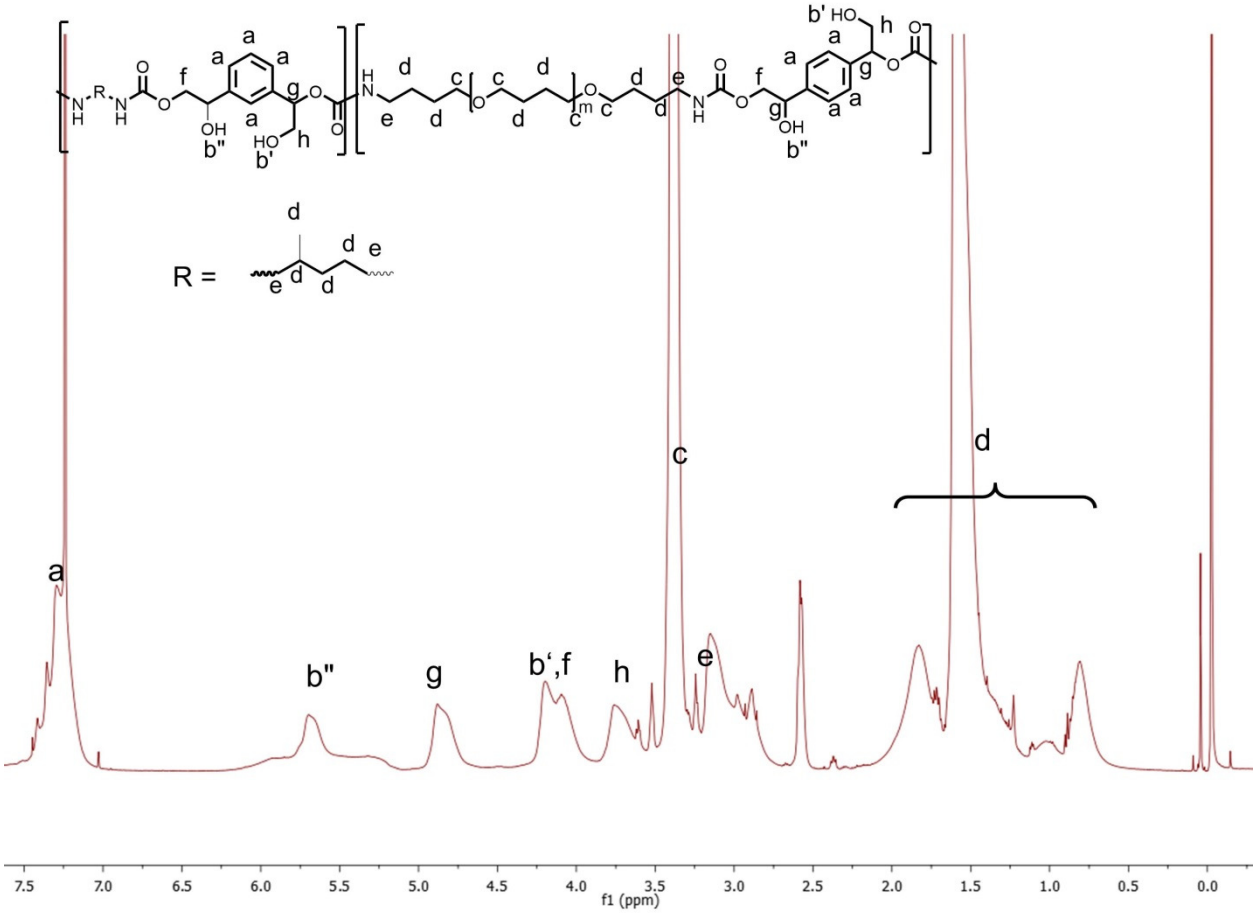

Figure C6: ^{1}H NMR Spectra of PTMO-30.

PTMO-30. ^{1}H NMR ($CDCl_3$, 500 MHz), δ (ppm): 0.5-2.0 (16H, $OCH_2C\boldsymbol{H}_2C\boldsymbol{H}_2CH_2O$, $NHCH_2C\boldsymbol{H}_2C\boldsymbol{H}_2CH_2O$, $NHCH_2C\boldsymbol{H}_2C\boldsymbol{H}_2C\boldsymbol{H}(C\boldsymbol{H}_3)CH2NH$), 2.8-3.2 (4H, $NHC\boldsymbol{H}_2CH_2CH_2CH_2O$, $NHC\boldsymbol{H}_2$), 3.3-3.5 (6H, $C\boldsymbol{H}_2OC\boldsymbol{H}_2$, $NHC(=O)OC\boldsymbol{H}_2$), 3.6-3.7 (1H, $C\boldsymbol{H}_2OH$), 4.0-4.2 (2H, $C\boldsymbol{H}_2OC(=O)NH$), 4.2-4.3 (1H, $CH_2O\boldsymbol{H}$), 4.8-5.0 (1H, $PhC\boldsymbol{H}(OH)CH_2$), 5.5-5.7 (1H, $PhCH(O\boldsymbol{H})CH_2$), 7.0-7.5 (4H, Ph).

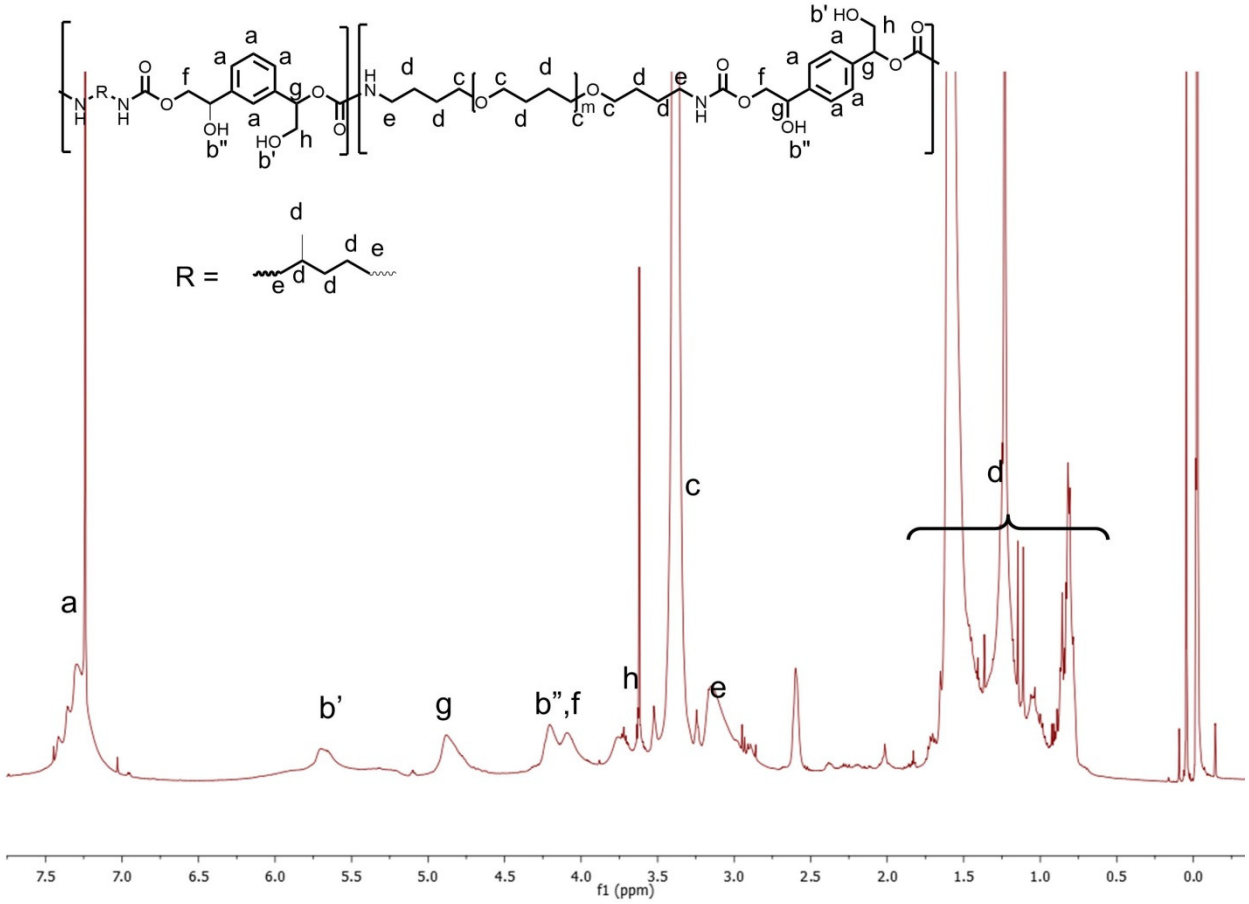

Figure C7: ^{1}H NMR Spectra of PTMO-40.

PTMO-40. ^{1}H NMR ($CDCl_3$, 500 MHz), δ (ppm): 0.5-2.0 (16H, $OCH_2C\boldsymbol{H}_2C\boldsymbol{H}_2CH_2O$, $NHCH_2C\boldsymbol{H}_2C\boldsymbol{H}_2CH_2O$, $NHCH_2C\boldsymbol{H}_2C\boldsymbol{H}_2C\boldsymbol{H}(C\boldsymbol{H}_3)CH2NH$), 2.8-3.2 (4H, $NHC\boldsymbol{H}_2CH_2CH_2CH_2O$, $NHC\boldsymbol{H}_2$), 3.3-3.5 (6H, $C\boldsymbol{H}_2OC\boldsymbol{H}_2$, $NHC(=O)OC\boldsymbol{H}_2$), 3.6-3.7 (1H, $C\boldsymbol{H}_2OH$), 4.0-4.2 (2H, $C\boldsymbol{H}_2OC(=O)NH$), 4.2-4.3 (1H, $CH_2O\boldsymbol{H}$), 4.8-5.0 (1H, $PhC\boldsymbol{H}(OH)CH_2$), 5.5-5.7 (1H, $PhCH(O\boldsymbol{H})CH_2$), 7.0-7.5 (4H, Ph).

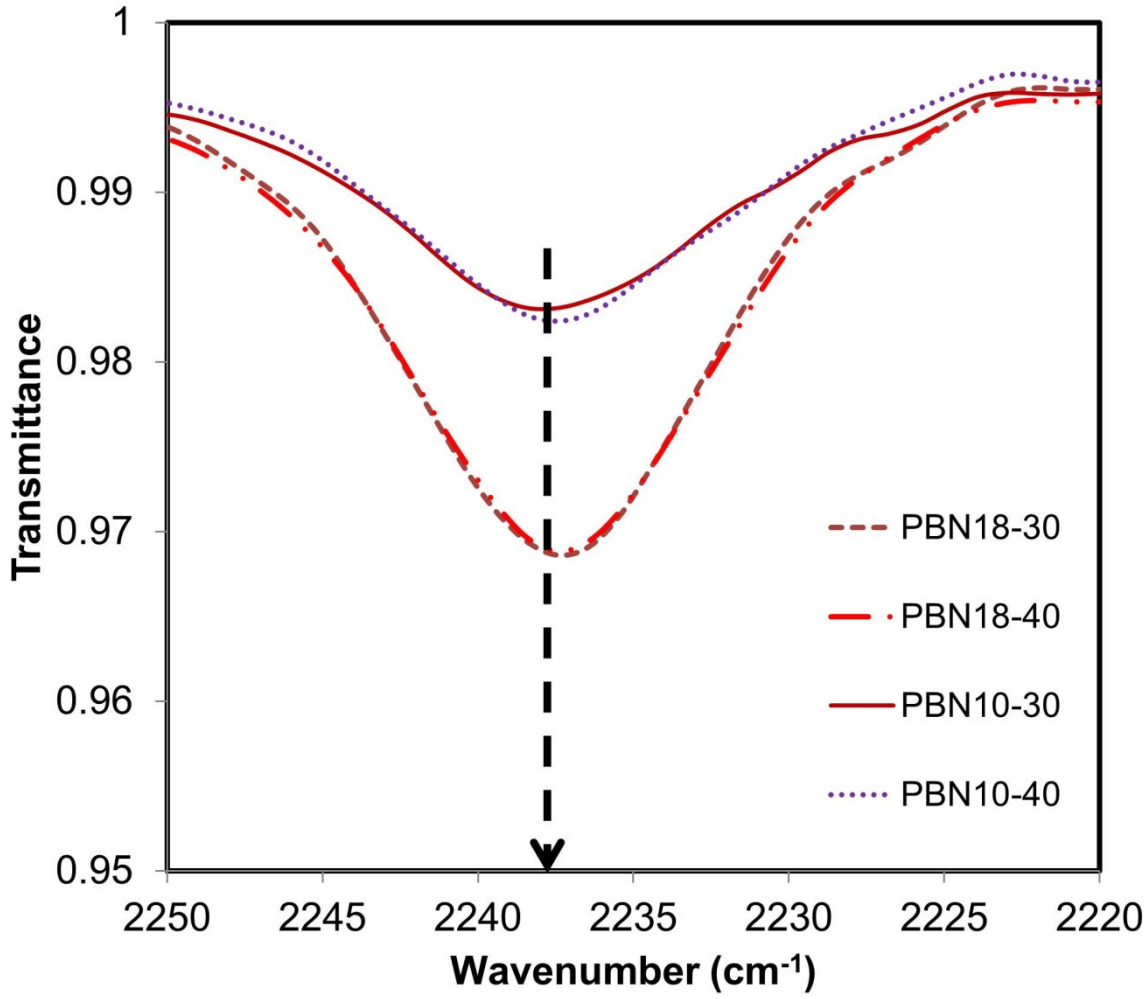

Figure C8: FTIR spectra in of PBN-based PHUs. Acrylonitrile stretch is centered at ~ 2238 cm^{-1}.

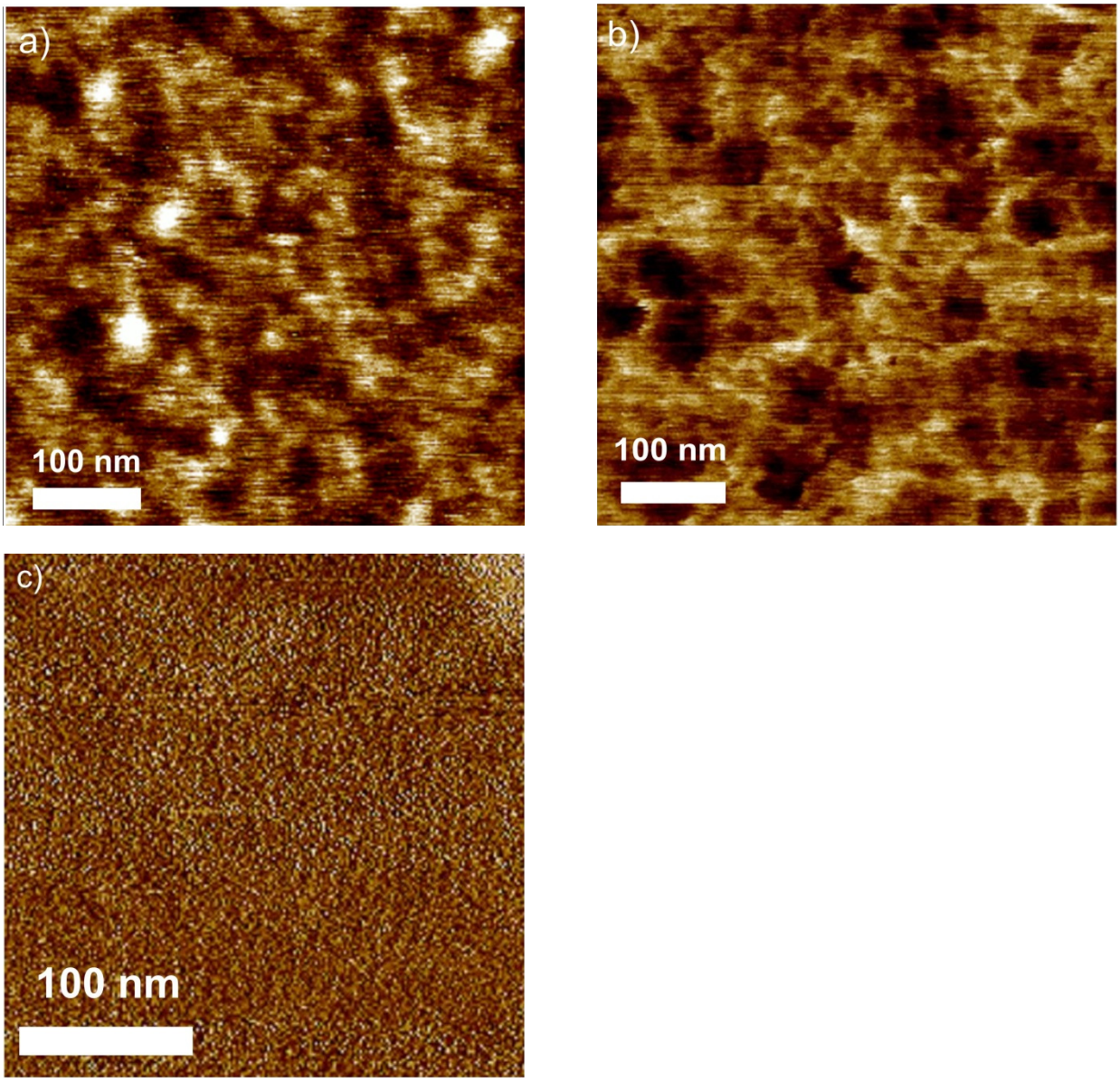

Figure C9: Surface morphology of a) PBN18-40, b) PBN10-40, and c) PTMO-30 characterized by AFM phase imaging in tapping mode.

Table C1: Apparent Molecular Weight Averages of PHUs.*

Sample	M_n (kg/mole)	M_w (kg/mole)	PDI
PTMO-30	5.5	24.4	4.0
PTMO-40	4.6	19.4	4.3
PBN10-30	2.2	8.5	3.9
PBN10-40	2.8	9.9	3.6

* We consider it possible that PHUs undergo some GPC column interaction. Long and coworkers noted that column interaction was observed in their system, even for PHU with the lowest hard-segment content (with the lowest amount of hydroxyurethane and amide linkages). See K. Zhang, A. M. Nelson, S. J. Talley, M. Chen, E. Margaretta, A. G. Hudson, R. B. Moore, T. E. Long, Green Chem. 18 (2016) 4667-4681.

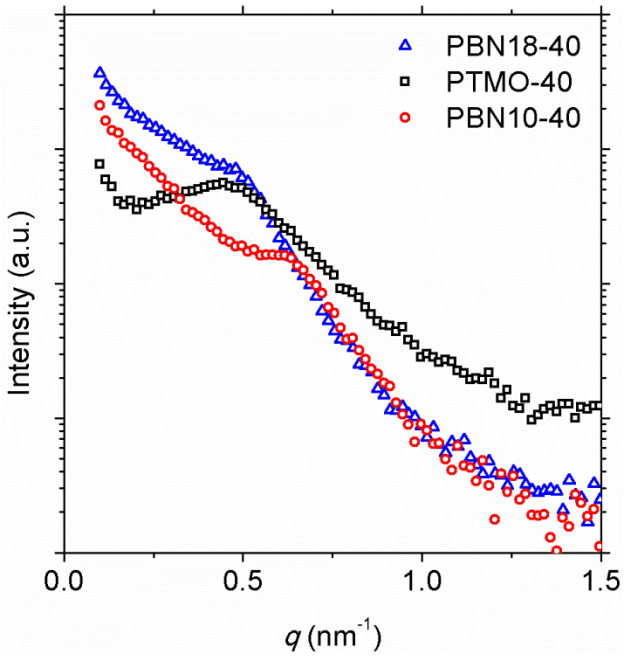

Figure C10: SAXS patterns of PTMO-40, PBN18-40 and PBN10-40.

CHAPTER 6

Combined Effects of Carbonate and Soft-Segment Molecular Structures on the Nanophase Separation and Properties of Segmented Polyhydroxyurethane

6.1 Introduction

Polyurethanes (PUs) are broadly used as foams, elastomers, coatings, films, and adhesives (Oertel 1994, Delebecq 2013, Engels 2013, Nohra 2013). Annual worldwide production was estimated to be 18 million tons in 2016 (Delebecq 2013), ranking sixth among all polymers. Traditional PU synthesis relies on isocyanate starting materials, which face increasing scrutiny from various regulatory bodies such as the United States Environmental Protection Agency and from European Union REACH regulations (Official Journal of European Union 2009, US EPA 2011, US EPA 2015). As a result, efforts to find alternative routes to PU or PU-like materials have intensified in recent years. Cyclic carbonate aminolysis offers a route to PU-like materials without employing isocyanates in the synthesis (Guan 2011, Kathalewar 2013, Blattmann 2014, Maisonneuve 2015). The aminolysis of five-, six-, seven- and eight-membered ring carbonates results in polyhydroxyurethane (PHU), which contains urethane linkages with additional primary and/or secondary hydroxyl groups (Kihara 1993, Steblyanko 2000, Tomita 2001a, Tomita 2001b, Tomita 2001c, Tomita 2001d, Tomita 2001e, Yuen 2016).

Most literature reports on PHU synthesis have focused on cyclic carbonate monomer synthesis (Kihara 1993, Steblyanko 2000, Tomita 2001a, Tomita 2001b, Tomita 2001c, Tomita 2001d, Tomita 2001e, Yuen 2016, Carre 2016, Mazurek-Budzynska 2016, Cornille 2016, Matsukizono 2015, Fortman 2015, Blattmann 2016a, Blattmann 2016b, Cornille 2016, Van Velthoven 2015, Rix 2016, Duval 2016, Cornille 2016, Poussard 2016), its subsequent polymerization into single-phase thermoplastics (Kihara 1993, Steblyanko 2000, Tomita 2001a,

Tomita 2001b, Tomita 2001c, Tomita 2001d, Tomita 2001e, Yuen 2016, Carre 2016) and cross-linked thermosets (Mazurek-Budzynska 2016, Cornille 2016, Matsukizono 2015, Fortman 2015, Blattmann 2016a, Blattmann 2016b, Cornille 2016, Van Velthoven 2015, Rix 2016, Duval 2016, Cornille 2016, Poussard 2016), as well as reaction catalysis (Lombardo 2015, Lambeth 2013, Blain 2014). Few reports have focused on the synthesis of segmented, nanophase-separated PHUs and developing an understanding of their structure-property relationships (Nanclares 2015, Leitsch 2016a, Beniah 2016, Zhang 2016, Beniah 2017). Torkelson and coworkers recently reported the synthesis of segmented PHUs as potential thermoplastic elastomers from several polyether-based soft segments (Leitsch 2016a, Beniah 2016). The hydroxyl groups in the hard segment are critical in controlling nanophase separation because of their ability to form hydrogen bonds with ether oxygen in commonly used soft segments. Tuning this interaction by careful choice of soft segment results in thermoplastic PHU elastomer with elastomeric character qualitatively similar to conventional thermoplastic PU elastomer (TPU) (Leitsch 2016a). Additionally, polytetramethylene oxide (PTMO)-based PHUs can be nanophase-separated materials with broad interphases having a wide range of local composition due to significant phase mixing resulting from hydrogen bonding between hydroxyl groups in the hard segment and ether oxygen atoms in the PTMO soft segment. As a result, PTMO-based PHUs are potentially useful as broad-temperature-range acoustic and vibration damping materials (Beniah 2016). In contrast, when PHUs are synthesized using a polybutadiene-based soft segment, which eliminates the possibility of intersegmental hydrogen bonding, the nanophase separation is accompanied by sharp, narrow interphases and the materials have properties more like TPUs (Beniah 2017). Long and coworkers have reported the synthesis of poly(hydroxyurethane-amide) from bio-based precursors resulting in segmented PHU with crystallizable hard domains (Zhang 2016). None of the previous studies (Nanclares 2015, Leitsch 2016a, Beniah 2016, Zhang 2016) has investigated the effect of hard-segment carbonate molecular structure on property

development.

The hard-segment structure can significantly influence the properties of segmented PU (Lee 2000, Seefried 1975c, Kojio 2007, Park 2011, Wingborg 2002, Klinedinst 2012, Shin 2009, He 2014, Li 1993, Buckley 2010, Petrovic 1991, Li 1994, Huang 1997, Sheth 2005, Seefried 1975d). It is well known that differences in diisocyanate molecular architecture can yield significant differences in TPU tensile properties. For example, Lee and Tsai (Lee 2000) synthesized segmented PU containing PTMO-based soft segment with a series of diisocyanates including 4,4'-diphenyl methane diisocyanate (MDI), toluene diisocyanate (TDI), isophorone diisocyanate (IPDI), hydrogenated MDI (HMDI), and 1,6-hexane diisocyanate (HDI) with a 40 wt% hard-segment content. They showed that MDI-based PU exhibited the highest tensile strength and IPDI-based PU the lowest tensile strength. The relatively high tensile strength of the MDI-based material was attributed to the more symmetrical molecular structure of MDI which allows better association, organization and packing in the hard domain (Lee 2000, Seefried 1975a). Kojio et al. (Kojio 2007) also compared PU made from norbornane diisocyanate (NBDI), HMDI, HDI, and IPDI, with tensile strength decreasing as follows: HDI > NBDI > HMDI > IPDI. Although many studies have investigated the influence of hard-segment structure on segmented PU properties, no study has yet investigated the influence of carbonate molecular architecture on segmented PHU properties. Such a study is needed to advance the understanding of PHU properties in light of the rising need for competitive non-isocyanate PU (NIPU) materials and because the presence of hydroxyl groups in PHU hard segments can alter the phase behavior and properties of PHU relative to those of analogous PU (Leitsch 2016a, Beniah 2016). Structure-property relationship studies focused on PHUs will enable the design and synthesis of PHU with improved properties, potentially leading to the development of PHUs that are competitive with commercially available PUs.

In this chapter, we consider the influence of hard-segment carbonate structure on the

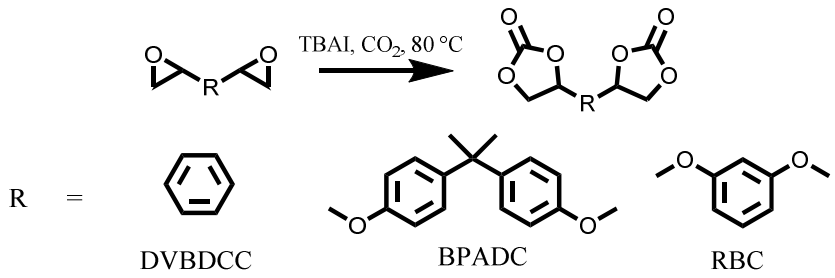

Scheme 6.1: Formation of bis-carbonate monomers.

morphology and properties of segmented PHUs. Three carbonate structures with structural motifs similar to common diisocyanates (see Scheme 6.1) were synthesized from epoxy precursors: divinylbenzene dicyclocarbonate (DVBDCC), bisphenol A dicarbonate (BPADC) and resorcinol bis-carbonate (RBC). These carbonates were formulated with one of two soft segments: a polytetramethylene oxide (PTMO)-based soft segment, where some intersegmental hydrogen bonding occurs between hard-segment hydroxyl groups and soft-segment ether oxygens, and a polybutadiene-co-acrylonitrile (PBN)-based soft segment, where intersegmental hydrogen bonding is absent. The hard-segment content is maintained at 40 wt% for all PHUs. This ensures that the soft segment forms the major phase and that the segmented PHUs would have the potential to be used for thermoplastic elastomer application if there is appropriate nanophase separation. Characterization via small-angle X-ray scattering (SAXS), dynamic mechanical analysis (DMA), and tensile testing reveals both hard-segment and soft-segment structures cooperatively influence the resulting morphology and properties of segmented PHUs. Unlike segmented PU, where, with few exceptions (Li 1994, Sheth 2005), any diisocyanate used in synthesis generally leads to well nanophase-separated materials, some hard-segment and soft-segment molecular structures do not lead to well nanophase-separated segmented PHU. In PTMO-based formulations with 40 wt% hard segment, BPADC results in fully phase-mixed PHU whereas DVBDCC and RBC result in nanophase-separated PHUs with relatively broad interphase regions. By suppressing intersegmental hydrogen bonding via the use of PBN-based soft segment, all three hard segments employed in this study lead to well nanophase-separated PHU at 40 wt% hard segment with relatively pure domain compositions and narrow interfaces. The PBN-based PHUs also exhibit reversible extension with hysteresis characteristic of conventional TPU.

6.2 Experimental

6.2.1 Materials

Divinyl benzene dioxide was supplied by The Dow Chemical Company, Freeport, TX. Resorcinol diglycidyl ether, Bisphenol A diglycidyl ether, tetrabutylammonium iodide (TBAI, reagent grade, 98%), 1,5-diamino-2-methylpentane (Dytek-A, 99%), and 1,5,7-triazabicyclo[4,4,0]dec-5-ene (TBD, 98%) were purchased from SigmaAldrich. Diamine-terminated polytetramethylene oxide (PTMO; M_n = 1700 g/mole) or Elastamine HT-1700 (also known as XTJ-548) was supplied by The Huntsman Corporation. Polybutadiene-co-acrylonitrile with 18 wt% acrylonitrile (Hypro™ 1300X42 ATBN), subsequently referred to as PBN18, was supplied by Emerald Performance Materials® CVC Thermoset Specialties. The PBN18 contains oligomers of Dytek-A-terminated polybutadiene-co-acrylonitrile (18 wt% acrylonitrile) with M_n = 3800 g/mol and excess Dytek-A. The amine equivalent weight is 427 g/mol.

6.2.2 Synthesis of *Bis*-Carbonate Monomers

Synthesis of Divinyl Benzene Dicyclocarbonate (DVBDCC). Synthesis followed the procedure outlined by Torkelson and coworkers (Leitsch 2016a) with a slight modification. In a typical synthesis, divinylbenzene dioxide (25 g, 15.4 mmol) and TBAI (5.69 g, 1.54 mmol) were added to a round bottom flask along with a stir bar and a septum, and the mixture was heated to 80 °C. Then, CO_2 gas was bubbled through the mixture until it turned solid (typically ~24-36 h). 15 mL of DMAc was added to dissolve the solid, and CO_2 was continuously bubbled until the reaction reached completion (typically after ~12 h). Reaction progress was monitored via ^{1}H NMR spectroscopy by the disappearance of protons associated with the epoxy moiety. Upon completion, 50 mL CH_2Cl_2 was added to the mixture followed by 50 mL water. The CH_2Cl_2 was removed by rotary evaporation and the product precipitated. The aqueous mixture was decanted, and the precipitated product was washed with 30 mL acetone and precipitated with 100 mL

water to remove TBAI. The slurry was filtered, and the pure solid product was collected and dried.

Synthesis of Bisphenol A Dicyclocarbonate (BPADC). Bisphenol A diglycidyl ether (20 g, 58.8 mmol) and TBAI (2.17 g, 5.88 mmol) were added to a round bottom flask along with a stir bar and a septum, and the mixture was heated to 80 °C. Then, CO_2 gas was bubbled through the mixture until it turned solid (~24-36 h). 15 mL DMAc was added to this solid, and CO_2 gas was continuously bubbled until the reaction reached completion (typically after ~12 h). Reaction progress was monitored by ^{1}H NMR spectroscopy via the disappearance of protons associated with the epoxy moiety. Upon completion, 50 mL CH_2Cl_2 was added to the reaction mixture followed by 50 mL water. The CH_2Cl_2 was removed by rotary evaporation and the product precipitated. The aqueous mixture was then decanted. The precipitated product was washed with 30 mL acetone. The slurry was filtered, and the pure solid product was collected and dried.

Synthesis of Resorcinol bis-Carbonate (RBC). Resorcinol diglycidyl ether (30 g, 135 mmol) and TBAI (4.99 g, 13.50 mmol) were added to a round bottom flask along with a stir bar and septum. Then, CO_2 gas was bubbled through the mixture until it turned solid (typically 24 h). 15 mL DMAc was added to this solid, and CO_2 gas was continuously bubbled until the reaction reached completion. The reaction progress was monitored by ^{1}H NMR spectroscopy as evidenced by the disappearance of protons associated with the epoxy moiety. Upon completion, 50 mL CH_2Cl_2 was added to the reaction mixture followed by 50 mL water. The CH_2Cl_2 was removed using rotary evaporation and the product precipitated. The aqueous solution was then decanted. The precipitated product was washed with 30 mL acetone and precipitated with 100 mL water to remove TBAI. The slurry sat at room temperature for 24 h to allow the product to crystallize. The slurry was then filtered, and the pure solid product was collected and dried.

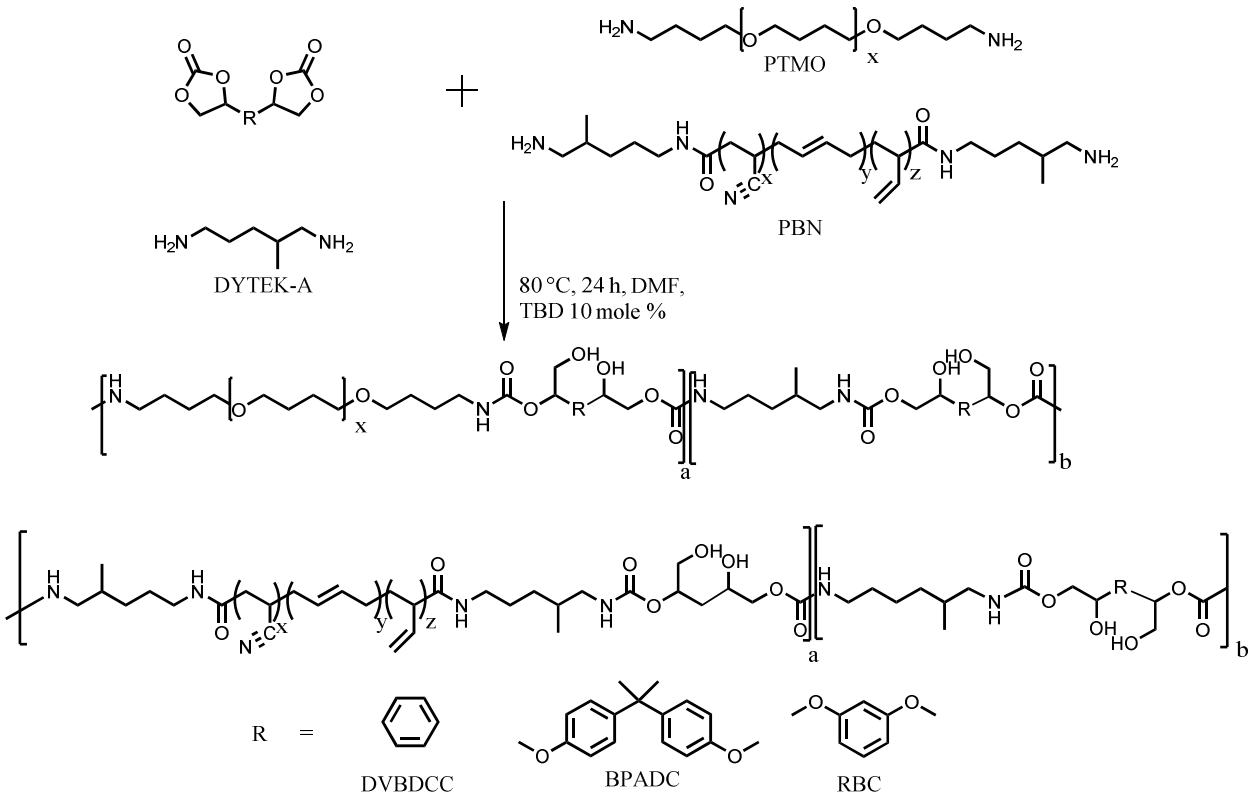

Scheme 6.2: Reaction scheme for the synthesis of segmented PHUs with different hard-segment carbonate and soft-segment structures.

6.2.3 Synthesis of PHUs

All PHUs were synthesized following Scheme 6.2. The naming convention for these samples is soft segment-hard segment, where the soft segment is PBN or PTMO and the hard segment is RBC, BPADC or DVBDCC. The hard-segment content is defined by (weight of carbonate + weight of chain extender)/(total weight of material) and is maintained at 40 wt% for all PHUs. In a typical synthesis of PBN-RBC, 3.00 g PBN18 (containing 0.70 mmol of Dytek-A-terminated polybutadiene-co-acrylonitrile oligomers and 2.81 mmol Dytek-A), 1.36 g RBC (4.37 mmol), and 99.7 mg Dytek-A (0.86 mmol) were added to a 20 mL scintillation vial. Then, 6.8 mL anhydrous dimethylformamide (DMF) was added to dissolve the reactants and adjust the carbonate concentration to 0.40 M. After solubilization, 60.8 mg (0.437 mmol) TBD was added, and the mixture was reacted for 24 h at 80 °C with stirring. In a typical synthesis of PTMO-RBC, 3.00 g Elastamine HT-1700 (1.90 mmol), 1.62 g RBC (5.20 mmol), and 384.1 mg Dytek-A (3.30 mmol) were added to a 20 mL scintillation vial. Then, 3.7 mL anhydrous DMF was added to dissolve the reactants and adjust the carbonate concentration to 0.60 M. After complete solubilization, 72.5 mg (0.52 mmol) TBD was added, and the mixture was reacted for 24 h at 80 °C with stirring.

6.2.4 Characterization

Attenuated total reflectance-Fourier transform infrared (ATR-FTIR) spectroscopy was done with a Bruker Tensor 37 MiD IR FTIR spectrophotometer equipped with a diamond/ZnSe attachment. All PHUs were scanned at a resolution of 4 cm^{-1}; 32 scans were collected in the 4000-600 cm^{-1} range. The conversion of the starting materials was determined by analyzing carbonate group conversion at ~1780 cm^{-1}. ^{1}H NMR spectra were obtained using a Bruker Avance III 500 MHz NMR spectrometer with a direct cryoprobe at room temperature and deuterated chloroform ($CDCl_3$) as solvent. Spectra were reported in parts per million relative to

tetramethylsilane. Proton-decoupled ^{13}C NMR spectra were obtained using a Bruker Avance 500 MHz w/ direct cryoprobe (126 MHz) spectrometer and are reported in ppm using solvent as an internal standard ($CDCl_3$ at 77.0 ppm). Mass spectra data were obtained using an Agilent 7890A/5975C GCMS System. Apparent molecular weight averages of PHUs were determined by gel permeation chromatography (GPC), using a Waters 2695 separation module and two Tosoh TSKgel Alpha-M columns (13 μm) in series. The eluent was dimethyl formamide with 4 g/L of $LiNO_3$ at 40 °C; the elution rate was 0.5 mL/min. The detector was a Malvern OmniFACE analog-to-digital interface/Waters 2414 RI detector. Molecular weight values are relative to polyethylene oxide standards (Agilent PEO/PEG EasiCal standards).

SAXS experiments were performed using a Rigaku S-MAX 3000 SAXS system emitting X-rays with a wavelength of 0.154 nm (Cu-Kα). The SAXS system was calibrated with silver behenate. The sample-to-detector distance was 1640 mm. The 2D scattering patterns were collected and azimuthally averaged using Fit2D software (from the European Synchrotron Radiation Facility website) to produce 1-D plots of intensity versus scattering vector q, where $q = 4\pi\sin\theta/\lambda$; θ is one-half of the scattering angle, and λ is the X-ray wavelength.

The DMA results were obtained using a TA Instruments Rheometrics Stress Analyzer-GIII. Rectangular specimens measuring 8.0 mm in width and 0.9 mm in thickness were cooled with N_2 gas to -100 °C for PTMO-based PHU and to -80 °C for PBN-based PHU. Temperature sweep experiments were conducted from 120 °C at a heating rate of 3 °C/min or until the sample flowed out of the grips. Measurements were conducted in tensile mode at a frequency of 1 Hz and a strain of 0.03%, resulting in characterization of storage modulus (E'), loss modulus (E") and loss tangent (tan δ). The soft-segment T_g was identified from the peak maximum in E"; the flow temperature was defined as the onset of inconsistent tan δ data, close to the temperature at which the sample was no longer mechanically robust.

Tensile testing was performed at room temperature (~22 °C) according to ASTM D1708

using an MTS Sintech 20/G tensile tester. Dog bone-shaped samples (4.7 mm x 1.0 mm x 22 mm) were cut using a Dewes-Gumbs die from dried sheets and an extension rate of 130 mm/min. The Young's modulus, tensile strength and elongation at break were reported as average values of five specimens. Error represents one standard deviation. Hysteresis testing was performed on PBN-based PHUs. Dog bone-shaped samples were stretched to 100% strain at a cross-head speed of 130 mm/min and returned to 0% strain. Ten cycles were performed with a 5-min interval between cycles.

6.3 Results and Discussion

6.3.1 Synthesis

Three carbonate monomers were synthesized from corresponding epoxy precursors using CO_2 insertion reactions with a catalytic amount of TBAI. Because of the increased mass transfer rate with CO_2 bubbling, the time to reach reaction completion was significantly reduced in comparison with our previous report (of DVBDCC synthesis) (Leitsch 2016a). The three hard-segment structures were selected based on structural similarities to diisocyanates commonly used in PU synthesis and the availability of the corresponding epoxy starting materials. DVBDCC and RBC have structures similar to phenylene diisocyanate whereas BPADC is somewhat similar to MDI. The successful syntheses of carbonate monomers were confirmed using ^{1}H NMR, ^{13}C NMR, and FTIR spectroscopy. Figures D1, D3, and D5 (see Appendix D) show ^{1}H NMR spectra and peak assignments of the carbonate monomers. The epoxy groups were fully converted into carbonate groups as evidenced by the disappearance within error of protons associated with the epoxy moiety and the appearance of protons associated with carbonate moiety. Figures D2, D4, and D6 (see Appendix D) show ^{13}C NMR spectra and peak assignments of the carbonate monomers. The FTIR spectra in Figure D7 in Appendix D show a strong peak associated with the carbonate carbonyl stretching band at ~1780 cm^{-1}.

The successful synthesis of PHU was confirmed by FTIR and NMR spectroscopy. The FTIR spectra of RBC, BPADC, DVBDCC and all PHU samples are shown in Figure D8. The disappearance of carbonate peak at ~1780 cm^{-1} indicates the complete conversion within error of carbonate functional groups into urethane linkages. The presence of the urethane carbonyl stretch (1730-1700 cm^{-1}) and hydroxyl stretch (3500-3100 cm^{-1}) verify formation of hydroxyurethane groups. The nitrile stretch (~2238 cm^{-1}) in PBN-based PHUs and ether stretch (~1100 cm^{-1}) in PTMO-based PHUs demonstrate the successful incorporation of soft-segment moieties into polymer chains. Figures D9-D14 show the ^{1}H NMR spectra of all PHUs with the assigned positions of different protons demonstrating the successful formation of PHUs. Gel permeation chromatography yielded apparent weight average molecular weights of 31 to 38 kg/mol for PTMO-based PHUs and 22 to 37 kg/mole for PBN-based PHUs. (See Table D1 for molecular weight averages of all PHUs.)

6.3.2 Influence of Hard-Segment Structure in PTMO-based PHUs

Using DVBDCC as hard segment and different sets of chain extender, we previously synthesized segmented PHUs from PTMO-based soft segment and evaluated their potential for applications as thermoplastic elastomer and/or damping materials (Leitsch 2016a, Beniah 2016). Here, we compare the physical properties of PTMO-based PHUs synthesized with three different hard-segment structures. The hard-segment structure has a significant impact on macroscopic properties of the resulting PHUs. The PTMO-BPADC sample is a soft, sticky solid at room temperature; the PTMO-RBC and PTMO-DVBDCC samples are stiffer and much more mechanically robust.

Figure 6.1 shows the room-temperature SAXS characterization of the PTMO-based PHUs. The PTMO-BPADC sample exhibits no scattering peak, consistent with the absence of significant nanophase separation; in contrast, PTMO-RBC and PTMO-DVBDCC show single,

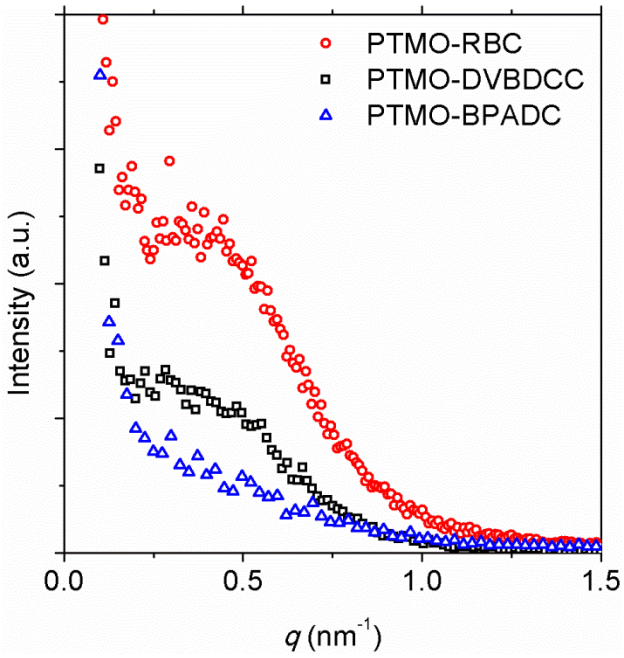

Figure 6.1: Small-angle X-ray scattering patterns of PTMO-based PHUs.

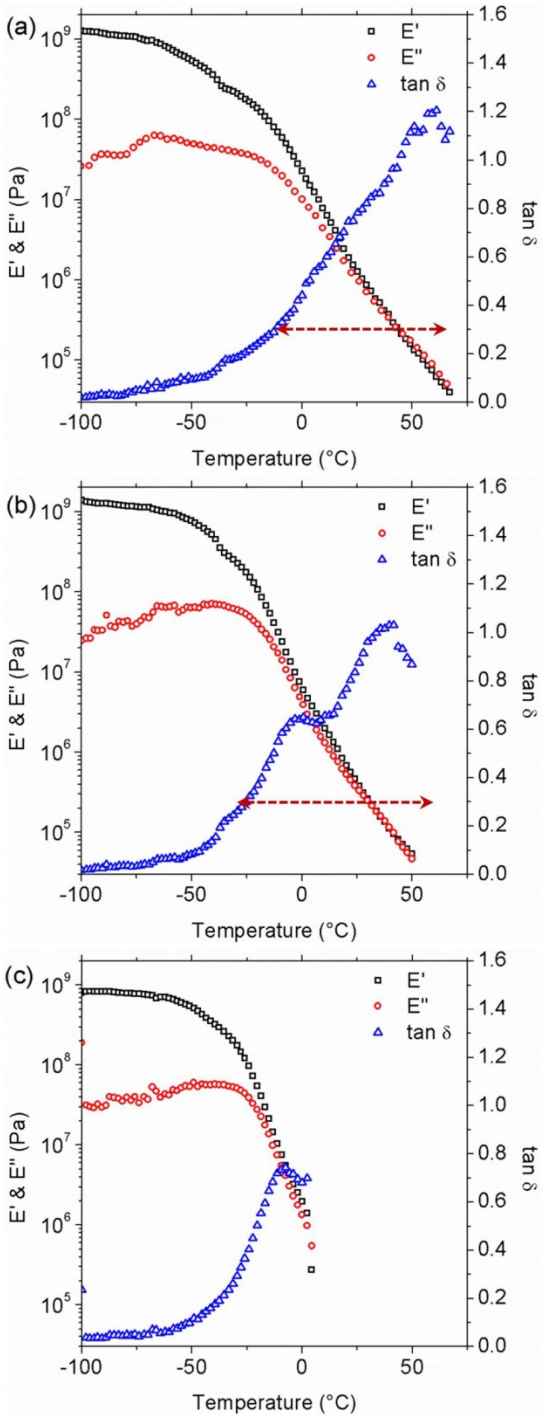

Figure 6.2: Temperature dependences of storage modulus (*E*'), loss modulus (*E*") and loss factor (tan δ) of a) PTMO-DVBDCC, b) PTMO-RBC, and c) PTMO-BPADC. Arrows indicate region in which tan $\delta \geq 0.3$.

broad SAXS peaks consistent with significant nanophase separation. The interdomain spacings (*d*-spacings) of PTMO-DVBDCC and PTMO-RBC are ~16.8 and ~15.6 nm, respectively. For PTMO-BPADC, the soft and sticky nature and the absence of a SAXS peak are indicative of a relatively homogenous single-phase material with T_g below room temperature. The SAXS data shown in Figure 6.1 clearly reflect the effect of different carbonate structure on PHU nanophase separation in PTMO-based PHUs.

As shown in Figure 6.2, the carbonate molecular architecture has a significant influence on the thermomechanical properties of the PTMO-based PHUs as characterized by DMA. First, at the lowest temperature (-100 °C) where all three samples are fully glassy, PTMO-BPADC exhibits an *E'* value that is approximately one-half the values for PTMO-DVBDCC and PTMO-RBC. This difference may be associated with the mechanical robustness of the hard-segment domains present in the two nanophase-separated samples. Such domains, which are absent in the phase-mixed PTMO-BPADC sample, have significant interurethane hydrogen bonding which could contribute to an enhanced modulus. Second, PTMO-BPADC remains sufficiently mechanically robust for meaningful DMA testing only up to ~0 °C whereas PTMO-RBC and PTMO-DVBDCC remain sufficiently robust up to ~51 °C and ~65 °C, respectively. We refer to these temperatures as flow temperatures (T_{flow}), above which the DMA samples no longer remain consolidated samples but instead flow out of the DMA grips. In the case of PTMO-RBC and PTMO-DVBDCC, the T_{flow} values are related to the hard-segment glass transition temperatures; for PTMO-BPADC, T_{flow} is related to (and above) the glass transition of the phase-mixed system.

Notably, none of the PTMO-based PHUs exhibits a quasi-rubbery plateau region characteristic of a general TPU. Furthermore, tan δ (= *E*"/*E'*) exceeds 0.30 only over a narrow range of temperature (~ -25 to ~0 °C) for PTMO-BPADC but over much broader (~75 °C in breadth) temperature ranges for PTMO-RBC (-25 to 51 °C) and PTMO-DVBDCC (-12 to 65 °C). From previous studies of PHUs (Leitsch 2016a, Beniah 2016) as well as gradient

copolymers (Mok 2008), these results are expected based on PTMO-BPADC being phase mixed and PTMO-RBC and PTMO-DVBDCC being nanophase separated but with a sufficient level of phase mixing to achieve broad interphases having a wide range of local composition. The temperature ranges over which PTMO-RBC and PTMO-DVBDCC exhibit tan $\delta \geq 0.30$ indicate that these materials have potential as broad-temperature-range vibration or acoustic damping materials (Mok 2008). The phase mixing achieved in these materials arises from the ability of hydroxyl groups in the PHU hard segment to undergo hydrogen bonding with ether oxygens in the PTMO soft segment (Leitsch 2016a, Beniah 2016).

The results with our 40 wt% hard-segment content PTMO-BPADC are consistent with those of Nanclares et al. (Nanclares 2015) who also used BPADC and PTMO (but a different chain extender, *m*-xylene diamine) to formulate segmented PHUs at 30, 50 and 70 wt% hard-segment content. Based on thermal and mechanical properties, they reported results consistent with single-phase PHU at 30 wt% hard segment but with nanophase-separated PHU at higher hard-segment content, with the extent of phase mixing being greater at 50 wt% hard segment than at 70 wt% (Nanclares 2015). Like Nanclares et al. (Nanclares 2015), we might have observed nanophase separation in our PTMO-BPADC if we had prepared samples with much greater hard-segment content, but that would eliminate the possibility of the PHUs to have potential use as thermoplastic elastomers.

We also evaluated the uniaxial tensile properties of our nanophase-separated PTMO-based PHUs. (The PTMO-BPADC sample was not tested because of its lack of mechanical integrity at room temperature owing to its single-phase nature with a glass transition significantly below room temperature.) Figure 6.3 shows representative stress-strain curves of PTMO-DVBDCC and PTMO-RBC, and Table 6.1 summarizes the average tensile properties. In comparison with TPUs, both of our tested PTMO-based PHUs exhibit very low tensile strengths, 0.40 MPa for PTMO-DVBDCC and 0.27 MPa for PTMO-RBC, and values of Young's modulus

Table 6.1: Summary of properties of PHUs.

Sample Name	*d*-spacing (nm)	SS T_g (°C)[a]	HS T_{flow} (°C)[b]	Young's Modulus (MPa)	Elongation at Break (%)	Tensile Strength (MPa)
PTMO-DVBDCC	16.8	-68	65	31.6 ± 3.6	750 ± 100	0.40 ± 0.06
PTMO-BPADC	-	-25[c]	-	-[d]	-[d]	-[d]
PTMO-RBC	15.6	-60	51	27.6 ± 3.4	830 ± 30	0.27 ± 0.05
PBN-DVBDCC	10.9	-44	65	31.9 ± 3.8	870 ± 180	1.6 ± 0.3
PBN-BPADC	15.5	-45	69	32.1± 3.1	1100 ± 560	1.0 ± 0.1
PBN-RBC	12.2	-44	64	27.3 ± 2.5	1500 ± 310	0.50 ± 0.01

[a] Determined from the peak in dynamic loss modulus (*E*") in DMA.

[b]Determined from the onset of inconsistent tan δ data using DMA, close to the temperature at which the sample is no longer mechanically robust.

[c]Only one T_g can be identified for PTMO-BPADC since it is a phase-mixed material.

[d]Sample is not robust enough for testing.

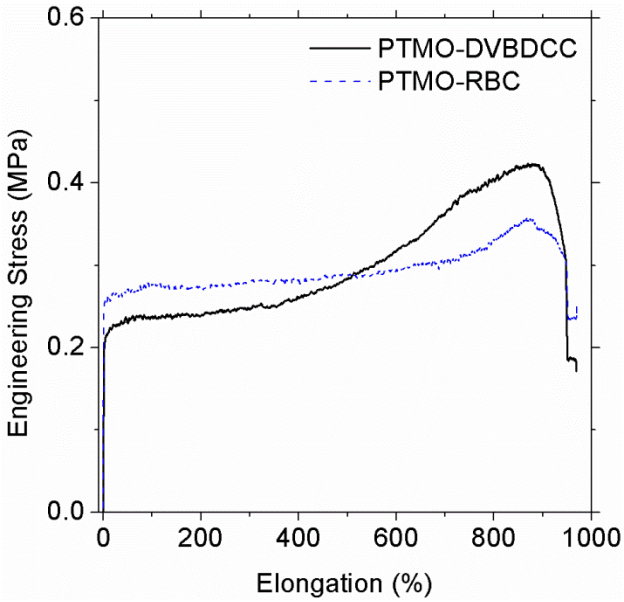

Figure 6.3: Representative stress-strain curves of PTMO-based PHUs.

and elongation at break in the range of typical TPUs. The low tensile strengths are consistent with some level of phase mixing in these nanophase-separated PHUs, including the broad interphase. In comparison with well phase-separated TPUs, the combined effects of some phase mixing with nanophase separation in PHUs would lead to less inter-urethane group hydrogen bonding in hard-segment domains as well as softening of these domains via the presence of soft segment.

6.3.2 Influence of Hard-Segment Structures in PBN-based PHUs

In PBN-based PHUs, hydrogen bonding of PHU hydroxyl groups to the soft segment is suppressed because of the absence of oxygen atoms in polybutadiene and the fact that acrylonitrile units undergo self-association (Alia 2007, Phadke 2005, Padhye 1985). In addition, the self-association of acrylonitrile units in PBN serves to reinforce the soft segment. Thus, unlike PTMO-based PHUs which exhibit either nanophase separation with substantial phase mixing or an apparent absence of nanophase separation, PBN-based PHUs formulated with DVBDCC-based hard segment exhibit nanophase separation with narrow interfaces, like that exhibited in TPUs. Here, we consider the effect of hard-segment molecular structure on the nanophase separation and properties of PHUs in the absence of significant intersegmental hydrogen bonding by comparing PBN-DVBDCC, PBN-RBC, and PBN-BPADC.

Figure 6.4 shows SAXS patterns of our 40 wt% hard-segment PBN-based PHUs. The effect of carbonate structure on PHU nanophase separation in PBN-based PHUs as reflected in Figure 6.4 is clearly very different from that in PTMO-based PHUs as shown in Figure 6.1. In contrast to SAXS results for 40 wt% hard-segment PTMO-based PHUs in Figure 6.1, each PBN-based PHU exhibits a single, relatively sharp SAXS peak, consistent with a well nanophase-separated morphology. Based on peak locations, the *d*-spacings are 10.9, 12,2 and 15.5 nm for PBN-DVBDCC, PBN-RBC, and PBN-BPADC, respectively, and increase with the size of the

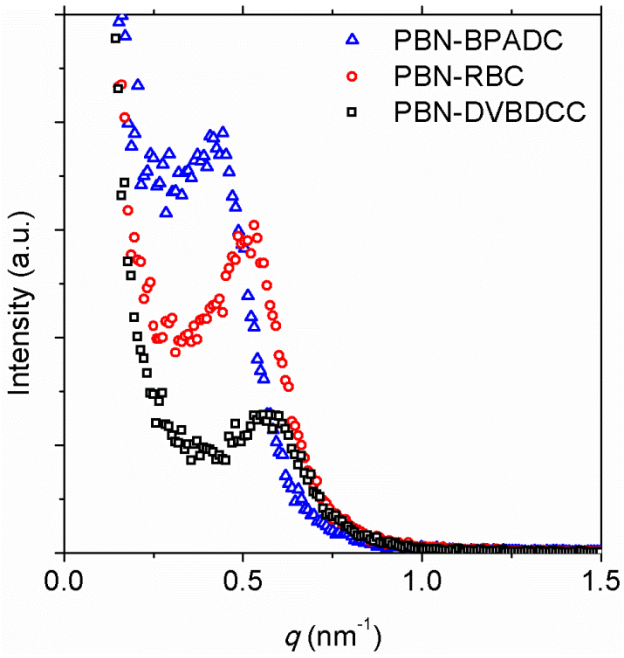

Figure 6.4: Small-angle X-ray scattering patterns of PBN-based PHUs.

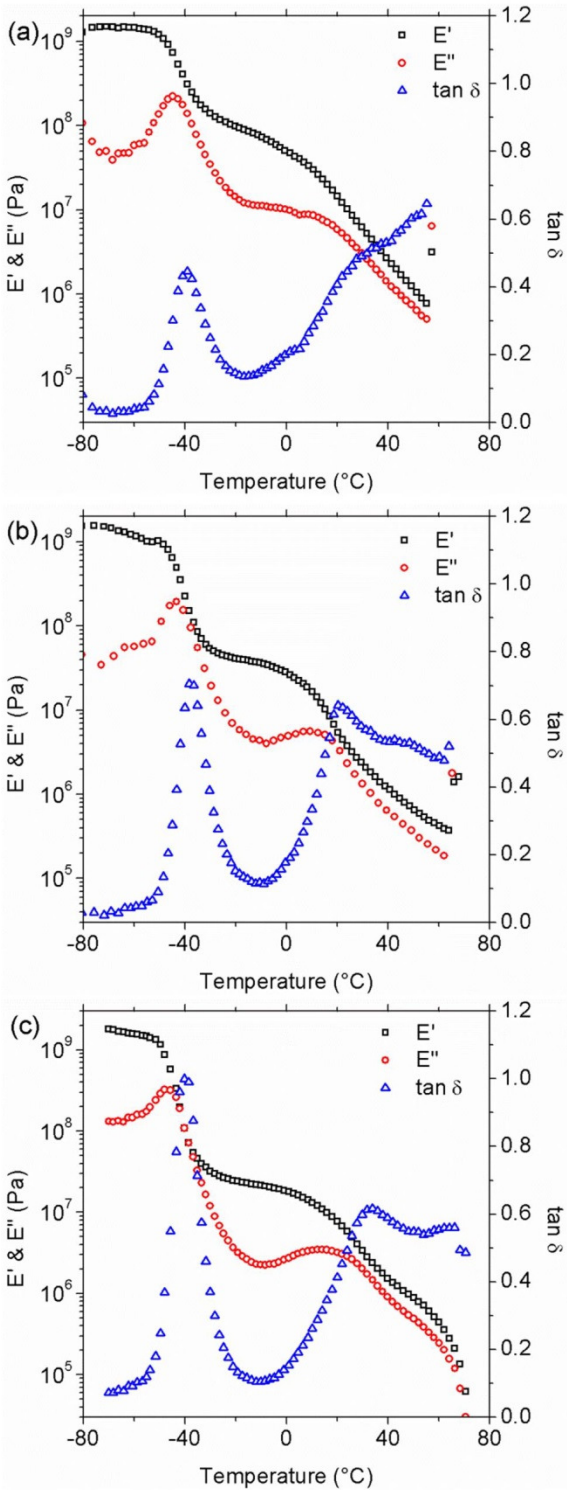

Figure 6.5: Temperature dependences of storage modulus (*E*'), loss modulus (*E*") and loss factor (tan δ) of a) PBN-DVBDCC, b) PBN-RBC, and c) PBN-BPADC.

carbonate molecule. These *d*-spacings indicate that the hard-segment domain cannot exceed several nanometers.

Figure 6.5 shows DMA results for PBN-DVBDCC, PBN-RBC, and PBN-BPADC; in each case, they are characteristic of well nanophase-separated systems. In each PBN-based PHU, the log *E*'-temperature profile exhibits two, roughly stepwise decreases. The first, sharper decrease is associated with the glass transition of the PBN soft domains, and the second broader decrease is associated with the glass transition of the hard domains. Directly reflecting the different kind of interphase (or phase-mixing) present in PTMO- and PBN-based PHUs, a quasi-rubbery plateau region in the *E*' data is evident for each PBN-based PHU but absent for each PTMO-based PHU (Figure 6.2). Likewise, the broad (~75 °C) temperature ranges associated with high tan δ values (≥ 0.30) that are evident for PTMO-DVBDCC and PTMO-RBC (Figure 6.2) are absent in each of the PBN-based PHUs. Instead, narrower temperature ranges (≤ 50 °C in breadth) over which tan δ ≥ 0.30 are evident in each of the PBN-based PHUs, which are associated with the breadth of glass transition responses of the hard-segment domains. The breadth of glass transition response is associated with the very small size, several nanometers in diameter based on *d*-spacing in Table 6.1, of the hard domain. Under such circumstances, even sharp interfaces (1 to 2 nm in width) between phases would result in the interface constituting a significant fraction of the hard domain. As identified from the peak in *E*", the soft-segment T_gs in the PBN-based PHUs are ~ -44 °C independent of hard-segment structure. These results indicate that the degree of nanophase separation in these PBN-based PHUs is similarly high regardless of the carbonate structure. The hard-segment T_{flow} values vary only slightly with carbonate structure, being 61, 64, and 69 °C for PBN-DVBDCC, PBN-RBC, and PBN-BPADC, respectively. These flow temperatures may be increased by using chain extenders that are more rigid than Dytek-A.

The mechanical properties of PBN-based PHUs were evaluated by room-temperature

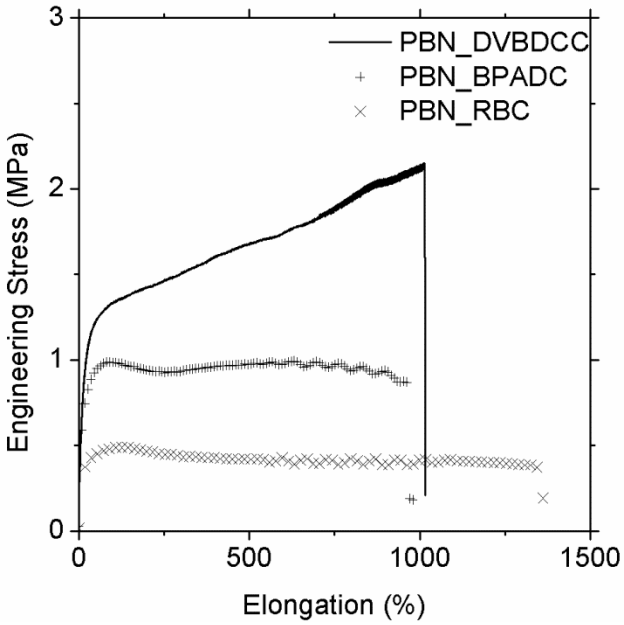

Figure 6.6: Representative stress-strain curves of PBN-based PHUs.

tensile testing. Figure 6.6 shows representative stress-strain curves of PBN-based PHUs, and Table 6.1 summarizes average tensile properties. Consistent with more effective nanophase separation in the PBN-based PHUs, the tensile strengths of all three PBN-based PHUs exceed the highest value for a PTMO-based PHU. Similarly, all PBN-based PHUs exhibit elongation at break values that equal (within error) or are considerably greater than those of PTMO-based PHUs.

Based on average values, PBN-DVBDCC exhibits the highest tensile strength at 1.6 MPa, followed by PBN-BPADC and PBN-RBC at 1.0 and 0.5 MPa, respectively. From the tensile responses of both PTMO-based and PBN-based PHUs, it is evident that DVBDCC yields PHUs with the best tensile properties in the series. This result is in accord with expectations because DVBDCC has the most rigid and compact structure of the three carbonates. Its compactness ensures that, among the three PBN-based PHUs, PBN-DVBDCC has the highest density of carbonyl and –NH groups present in hard-segment domains, which, along with the DVBDCC rigidity, should afford the highest density of inter-urethane group hydrogen bonding and thus aid in achieving the best tensile strength. The underlying cause(s) for PBN-BPADC exhibiting a tensile strength which is twice the value for PBN-RBC deserves further study.

Although the Young's modulus and elongation at break values of the PBN-based PHUs are within the range commonly exhibited by TPUs when evaluated at conditions associated with ASTM D1708), the tensile strength values are low by comparison (Lee 2000, Seefried 1975c, Wingborg 2002, Klinedinst 2012, Huang 1997, Sheth 2005). The difference is tensile strength values between well phase-separated TPUs and well phase-separated PBN-based PHUs may be understood to be, at least in part, a consequence of steric effects associated with the hydroxyl group in PHUs. These hydroxyl groups may be expected to perturb the packing efficiency of hard segments, reducing the density of inter-urethane group hydrogen bonds in PHUs relative to structurally similar TPUs. Thus, even in the absence of hydrogen bonding interactions between

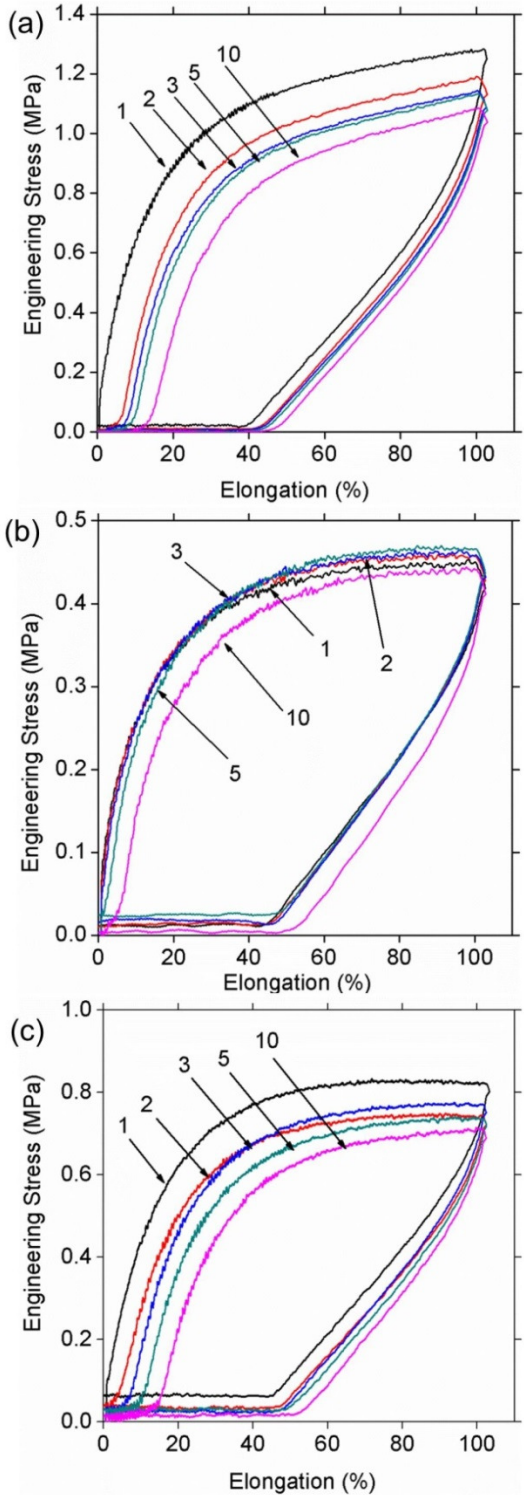

Figure 6.7: Hysteresis profile of (a) PBN-DVBDCC, (b) PBN-RBC, and (c) PBN-BPADC. Enlarged version of PBN-RBC profile can be found in Figure D16.

the hydroxyl group in the hard segment and atoms in the soft segment, hydroxyl groups in the hard segment can reduce the effectiveness of inter-urethane group hydrogen bonding in the hard-segment domains, which contributes to optimal tensile strengths in TPUs.

To further assess their potential as thermoplastic elastomers, the PBN-based PHUs were subjected to cyclic tensile testing. Figure 6.7 shows hysteresis profiles for each of the PBN-based PHUs. In general, these PHUs exhibit good recovery with slight softening and permanent sets increasing only slightly with increasing number of cycles. Such reversible elastomeric response is qualitatively similar to that manifested by conventional thermoplastic PU elastomer (Qi 2005), further supporting the potential of PBN-based PHUs as thermoplastic elastomers, albeit with somewhat reduced tensile strength relative to conventional TPUs.

Discussion on Combined Effects of bis-Carbonate and Soft-Segment Structures

To the best of our knowledge, this is the first investigation of the influence of hard-segment structure on the physical properties of segmented PHUs. Our results compare and contrast the effect of hard-segment structure in formulations with two soft-segment structures. Unlike studies of segmented PUs, which with few exceptions (Li 1994, Sheth 2005) show that diisocyanates used in synthesis of segmented PU generally lead to well phase-separated materials and associated properties (especially at such a high hard-segment content like 40 wt%), our study shows that in some cases there is a significant cooperativity between hard-segment and soft-segment structures in controlling segmented PHU phase separation and properties whereas in other cases there is little or no cooperativity.

When there is little or no potential for hydrogen bonding between a hard-segment hydroxyl group and atoms present in soft segments, as with PBN-based PHUs, there is little or no cooperative effect of carbonate and soft-segment structures on nanophase separation and associated properties. Highly effective nanophase separation can be generally achieved in these

systems with many macroscopic properties being similar to those of TPUs. An exception is tensile strength, with well nanophase-separated PHUs exhibiting lower values than those of typical TPUs. This difference is caused by the hydroxyl groups in the PHU hard segment, which by their mere presence reduce the density of carbonyl and –NH groups in the hard segment and interfere with packing efficiency, both of which tend to reduce inter-urethane group hydrogen bonding (relative to TPUs) which enhances tensile strength.

In contrast, when there is significant potential for hydrogen bonding between a hard-segment hydroxyl group and atoms such as ether oxygen present in soft segments, there is significant cooperativity regarding how hard- and soft-segments affect nanophase separation and properties in segmented PHUs. The potential for hydrogen bonding between hydroxyl groups in the hard segment and soft segment atoms competes against the potential for inter-urethane group hydrogen bond formation in the hard segment. This competition arises from the fact that each PHU hydroxyl group is located only three bonds away from a hard-segment urethane group; thus, having a hydroxyl group undergo hydrogen bonding with a soft segment atom strongly reduces the likelihood of the adjoining urethane group undergoing hydrogen bonding with another urethane group. When both types of hydrogen bonds are present in sufficient numbers, nanophase-separated PHUs with broad interphase regions and associated macroscopic properties result, as manifested by PTMO-DVBDCC and PTMO-RBC. However, when the competition for hydrogen bond formation is more significantly dominated by hydroxyl groups bonding to ether oxygen atoms in the soft segment, phase-mixed PHUs and associated macroscopic properties result, as manifested by PTMO-BPADC at 40 wt% hard-segment content.

Why is PTMO-BPADC so different from the other PTMO-based PHUs whereas PBN-BPADC is similar to the other PBN-based PHUs? The BPADC molecule is significantly larger than the other two bis-carbonates, thereby reducing the density of urethane groups formed in hypothetical hard-segment domains of BPADC-based PHUs relative to hard-segment domain of

PHUs made with DVBDCC and RBC. Additionally, based on its molecular structure BPADC is likely to exhibit more steric hindrance for effective packing than DVBDCC and RBC. Both factors should lead to a reduced likelihood for inter-urethane group hydrogen bonding in BPADC-based PHUs. In PBN-based PHUs which do not undergo hard-segment to soft-segment hydrogen bonding, BPADC is nevertheless able to undergo significant inter-urethane group hydrogen bonding in the hard-segment domain because there is nothing to compete with it. As a result, the three PBN-based PHUs are much more alike than the three PTMO-based PHUs.

With PTMO-based PHUs, the competition between hard-segment to soft-segment hydrogen bonding and inter-urethane group hydrogen is significant. Among the three PTMO-based PHUs, PTMO-BPADC has the least effective hard-segment structure for achieving inter-urethane hydrogen bonding at sufficiently high levels to enforce nanophase separation when there is competition for phase mixing caused by hard-segment to soft-segment hydrogen bonding. We employed FTIR spectroscopy to examine the intersegmental hydrogen bonding of hydroxyl groups to the soft segment. FTIR spectroscopy can be used to determine relative levels of non-hydrogen-bonded carbonyl (at ~1720 cm^{-1}) and hydrogen-bonded carbonyl (at ~1690-1700 cm^{-1}) in urethane groups present in the PHU hard segments (Leitsch 2016a). The hydroxyl group (-OH) peak cannot be evaluated because it overlaps with the peak associated with amide groups. Furthermore, the soft-segment ether oxygen peak is only present in PTMO-based PHUs making comparison with PBN-based PHUs impossible. Therefore, we chose to monitor the peak associated with the urethane carbonyl at 1720-1690 cm^{-1} to indirectly probe phase mixing in segmented PHUs. This approach has been used in many studies to determine the extent of phase mixing in segmented PUs as well as segmented PHUs (Leitsch 2016a, Kojio 2007, Park 2011, He 2014). Intersegmental hydrogen bonding to soft segment results in a decrease of hydrogen bonding between carbonyl groups and amide groups in the hard segments. Figures D17 and D18 in Appendix D show the relative levels of non-hydrogen-bonded carbonyl (at ~ 1720 cm^{-1}) and

hydrogen-bonded carbonyl (at ~1690-1700 cm^{-1}) in urethane groups present in the PHU hard segments of PTMO-based PHUs and PBN-based PHUs, respectively. As indicated in Figure D17 in Appendix D, PTMO-BPADC exhibits the highest level of non-hydrogen-bonded carbonyl to hydrogen-bonded carbonyl among PTMO-based PHUs. Figure D18 also shows that all PBN-based PHUs possess a higher proportion of hydrogen-bonded carbonyl than PTMO-based PHUs, which indicates that a higher level of interurethane hydrogen bonding is present in the hard segment in PBN-based PHUs.

Thus, the combined effects of hard-segment and soft-segment structures on the nanophase separation and associated properties of PHUs can be understood to arise from a competition between hydrogen bonding types. When this competition is absent because there is no viable route to achieve significant hard-segment to soft-segment hydrogen bonding, there is little or no cooperativity of effects, and a nanophase-separated system with relatively sharp interfaces will result. When this competition is present because the soft segment contains atoms that can undergo hydrogen bonding with hydroxyl groups, then the level of cooperativity can be significant. When sufficient levels of both inter-urethane group and intersegmental hydrogen bonding are present, a nanophase-separated structure with broad interphases will result. However, when the hard-segment molecular structure leads to a reduced probability of inter-urethane group hydrogen bond formation, as in the case of BPADC, then the hard-segment to soft-segment hydrogen bonding will be enhanced leading to the possibility of a phase-mixed system. Additionally, as shown in Chapter 3, when the density of atoms in the soft segment that are amenable to hydrogen bonding with a hydroxyl group is sufficiently high, as with poly(ethylene oxide)-based PHU relative to PTMO-based PHU, it is possible to obtain a phase-mixed system without nanophase separation even with the use of DVBDCC as hard segment.

Because PHU hydroxyl groups lead to steric issues which can reduce the effectiveness of inter-urethane group hydrogen bonding relative to PU and because PHU hydroxyl groups can

form hydrogen bonds with select atoms in many potential soft segments, special consideration should be given to the carbonate structure used to synthesize PHUs for particular applications, especially those for which nanophase separation is desired. Further studies of structure-property relationships in segmented PHUs are needed in order to optimize nanostructures and properties and to understand the limits relative to segmented PUs. An investigation of the role of chain extender structure on PHU nanophase separation and properties is underway in our laboratory.

6.4 Conclusion

We investigated the influence of hard-segment structures on the nanophase separation and physical properties of segmented PHUs with three carbonate molecules, namely DVBDCC, BPADC, and RBC. The hard segments were formulated in two soft-segment structures, namely PTMO-based and PBN-based soft-segments. The chain extender used was Dytek-A as and the hard-segment content was 40 wt% in all cases. The resulting PHUs were characterized using ^{1}H NMR, FTIR, SAXS, DMA, and tensile testing. Characterization results reveal that hard-segment and soft-segment structures may cooperatively influence the nanophase separation and physical properties of segmented PHUs. In PTMO-based soft segment, where there is significant potential for hydrogen bonding between hard-segment hydroxyl groups and ether oxygen atoms, BPADC results in a fully phase-mixed, single-phase PHU whereas DVBDCC and RBC produce nanophase-separated PHUs with relatively broad interphase regions. These results show that there is significant cooperativity by which hard- and soft-segment structures affect nanophase separation and properties of PTMO-based PHUs. In sharp contrast, by suppressing hydrogen bonding to the soft segment via the use of PBN-based soft segment, all three hard-segment structures produce well nanophase-separated PHUs with a much sharper domain interphase, indicating that there is little or no cooperativity between hard-segment and soft-segment structures on nanophase separation and associated properties. With highly effective nanophase

separation, reversible extension with some hysteresis characteristic of conventional TPU was also exhibited in all PBN-based PHUs.

APPENDIX D

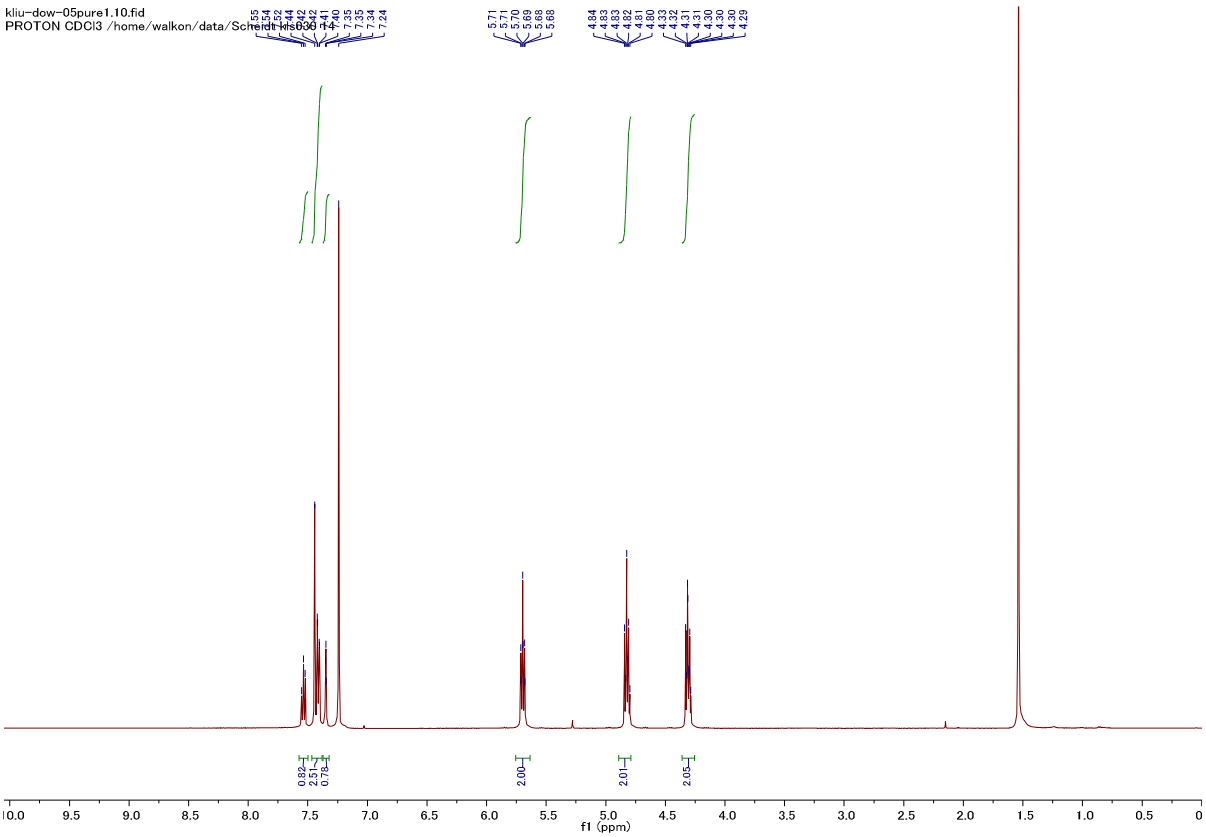

Figure D1: ^{1}H NMR spectrum of DVBDCC.

Divinyl Benzene Dicyclocarbonate (DVBDCC): ^{1}H NMR (500 MHz, CDCl3) δ 7.55 – 7.34 (m, 4H), 5.70 (td, J = 8.0, 2.0 Hz, 2H, CH), 4.82 (td, J = 8.4, 5.0 Hz, 2H, CH2), 4.31 (ddd, J = 8.6, 7.7, 4.9 Hz, 2H, CH2).

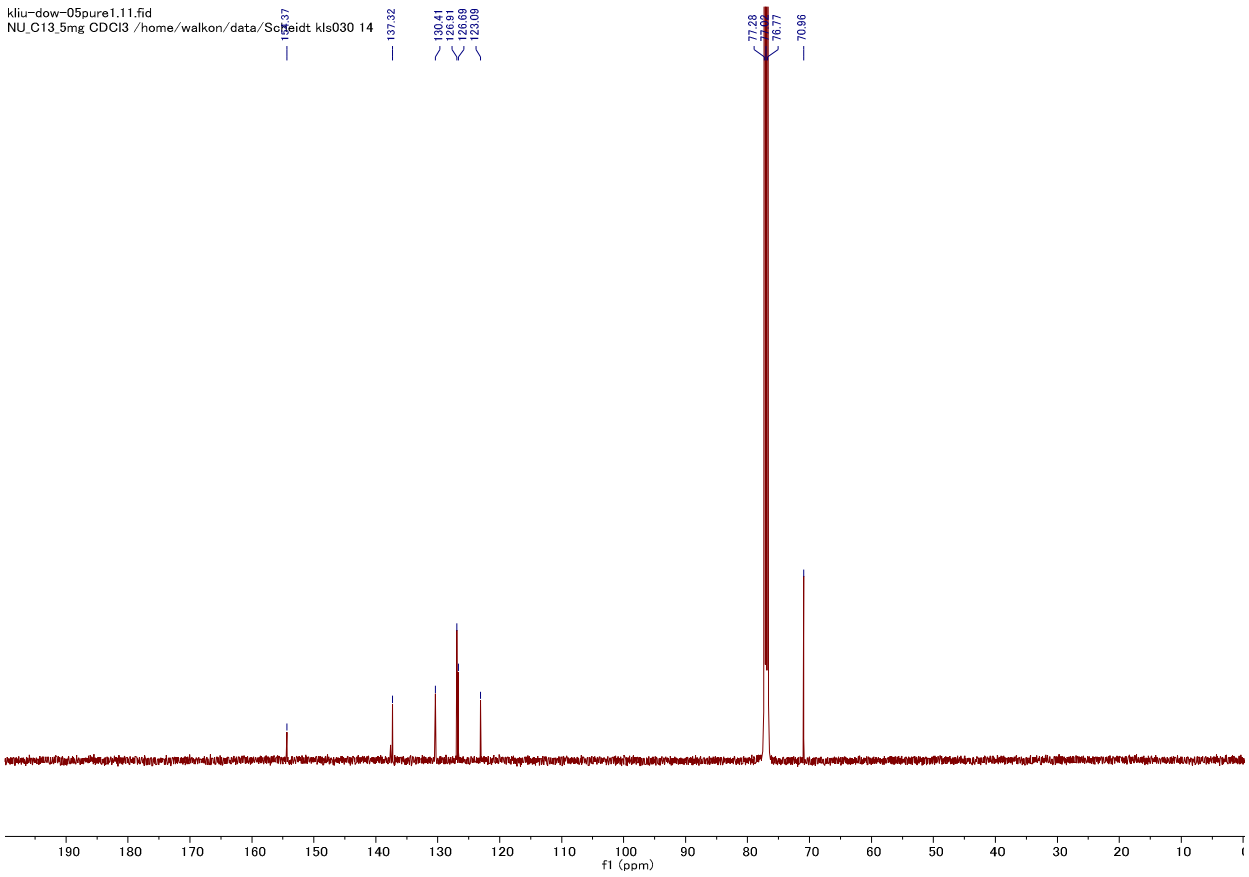

Figure D2: ^{13}C NMR spectrum of DVBDCC.

Divinyl Benzene Dicyclocarbonate (DVBDCC): ^{13}C NMR (CDCl3, 126 MHz) δ 154.3, 137.3, 130.4, 126.9, 126.6, 123.1, 70.9. LRMS (EI): Mass calcd for [M]+ C12H10O6: 250.0; found 250.1.

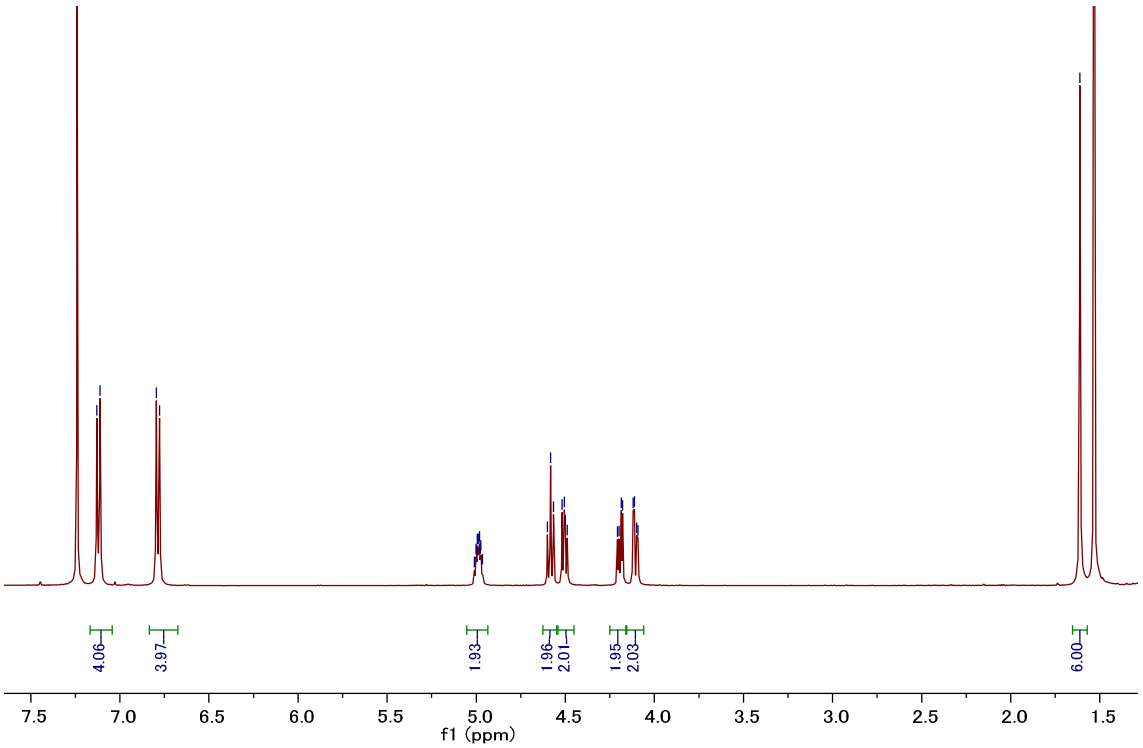

Figure D3: ^{1}H NMR spectrum of BPADC.

Bisphenol A Dicarbonate (BPADC): 1H NMR (500 MHz, CDCl3) δ, 7.12 (d, J = 8.8 Hz, 2H), 6.79 (d, J = 8.8 Hz, 2H), 5.01 – 4.97 (m, 2H, CH in cyclic carbonate moiety) 4.58 (t, J = 8.4 Hz, 2H, CH2 in cyclic carbonate moiety), 4.50 (dd, J = 8.5, 5.9 Hz, 2H, CH2 in cyclic carbonate moiety), 4.19 (dd, J = 10.6, 4.4 Hz, 2H, CHCH2OAr), 4.11 (dd, J = 10.5, 3.5 Hz, 2H, CHCH2OAr), 1.61 (s, 6H, CH3);

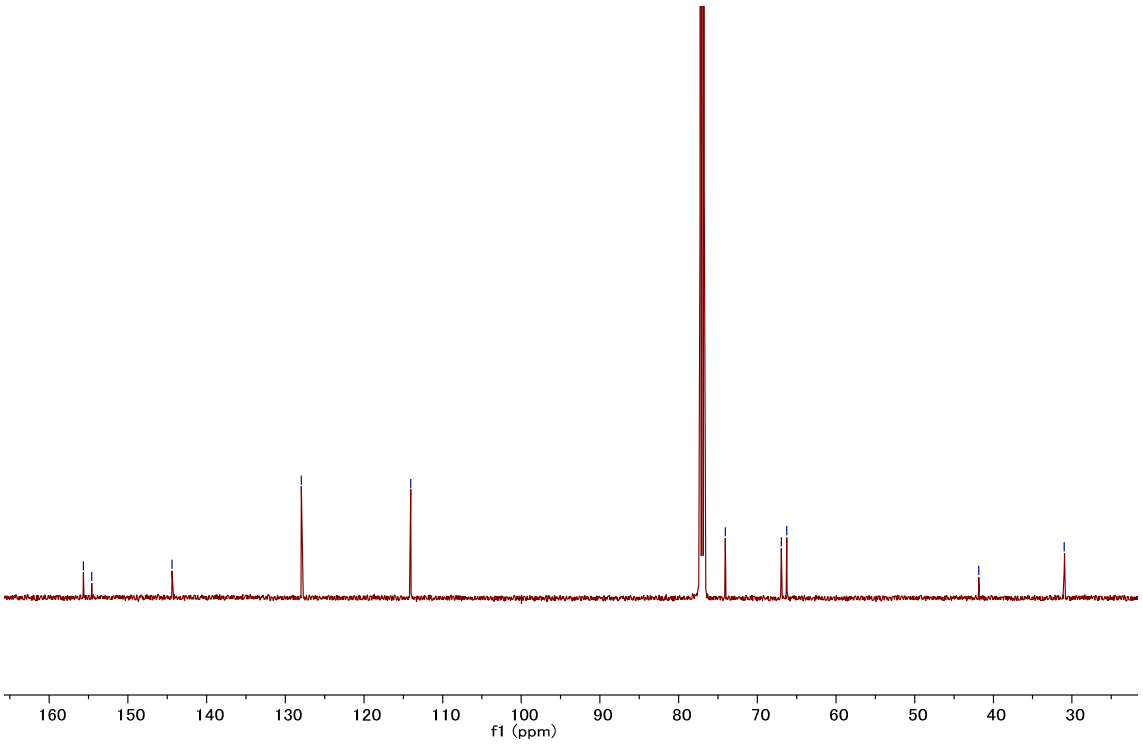

Figure D4: ^{13}C NMR spectrum of BPADC.

Bisphenol A Dicarbonate (BPADC): ^{13}C NMR (CDCl3, 126 MHz) δ 155.6, 154.6, 144.3, 127.9, 114.0, 74.0, 66.9, 66.2, 41.8, 30.9; LRMS (EI): Mass calculated for [M]+ C23H24O8: 428.0; found 428.0

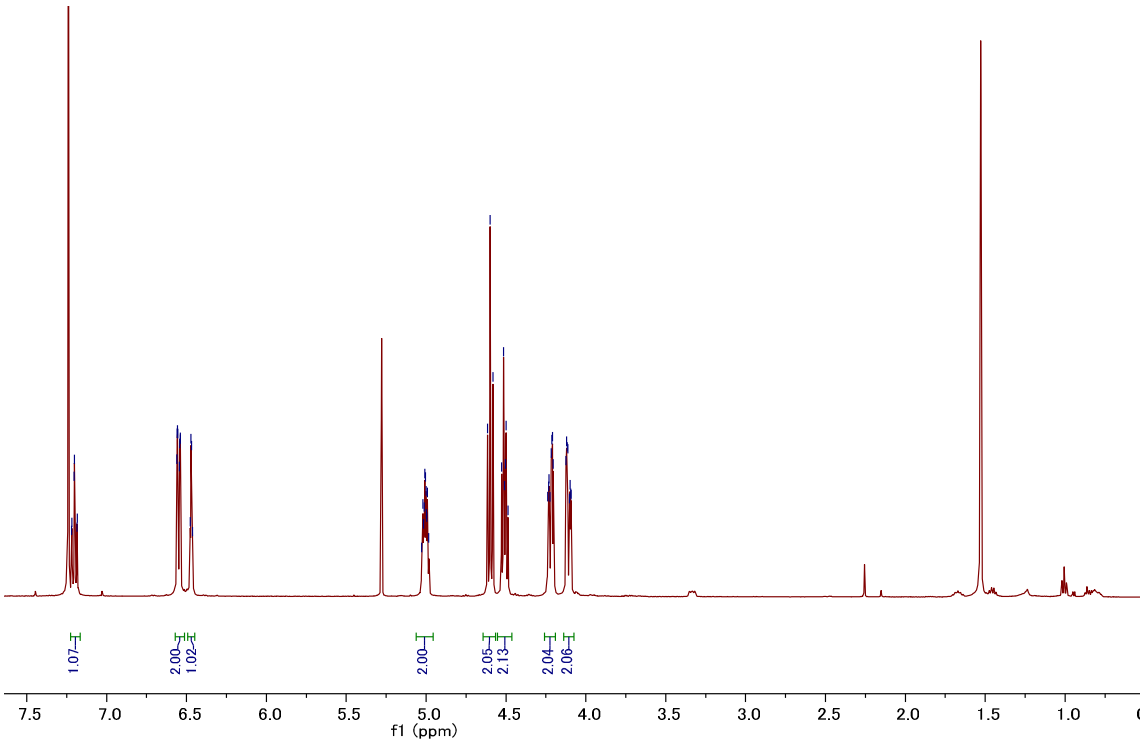

Figure D5: ^{1}H NMR spectrum of RBC.

Recorsinol Bis-carbonate (RBC): ^{1}H NMR (500 MHz, CDCl3) δ, 7.20 (td, J = 8.2, 0.9 Hz, 1H), 6.56 – 6.54 (m, 2H), 6.48 – 6.40 (m, 1H), 5.03 – 4.98 (m, 2H, CH in cyclic carbonate moiety) 4.60 (t, J = 8.5 Hz, 2H, CH2 in cyclic carbonate moiety), 4.51 (dt, J = 8.6, 5.8 Hz, 2H, CH2 in cyclic carbonate moiety), 4.22 (dd, J = 10.7, 3.9, 2.7 Hz, 2H, CHCH2OAr), 4.11 (ddd, J = 10.7, 3.5, 1.1 Hz, 2H, CHCH2OAr).

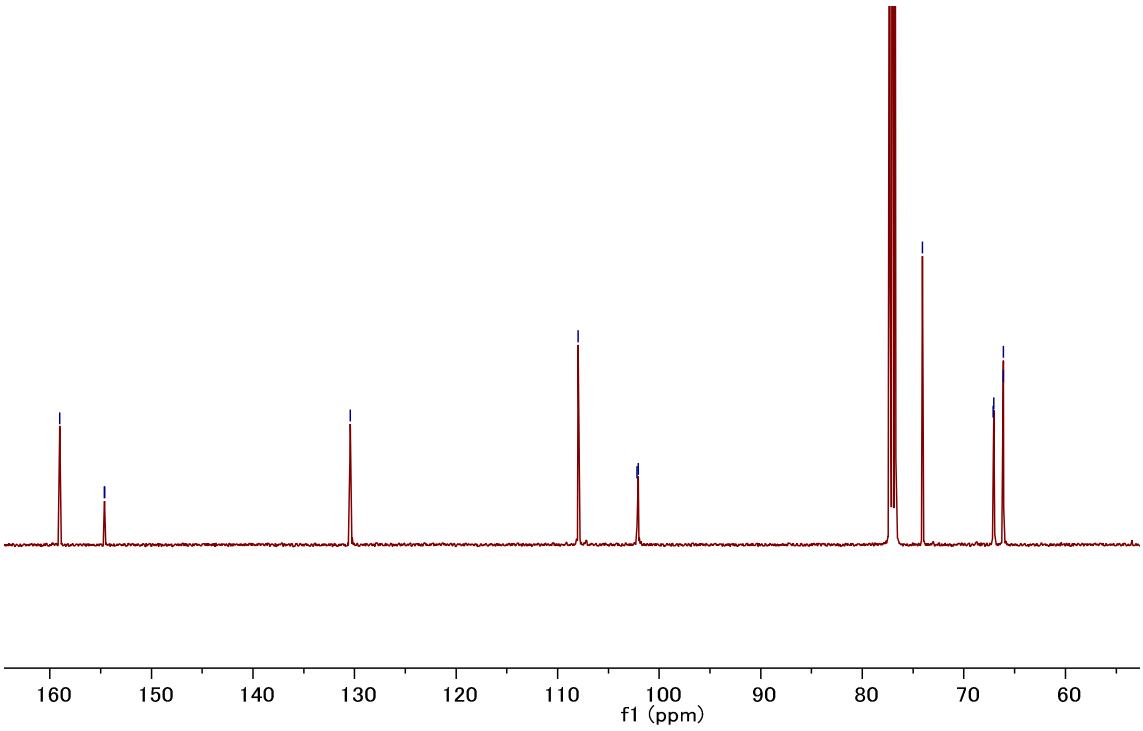

Figure D6:. ^{13}C NMR spectrum of RBC.

Recorsinol Bis-carbonate (RBC): ^{13}C NMR ($CDCl_3$, 126 MHz) δ 159.0, 154.6, 154.6, 130.4, 107.9, 102.1, 102.0, 74.0, 67.1, 67.0, 66.1, 66.0; LRMS (EI): Mass calculated for $[M]^+$ $C_{14}H_{14}O_8$: 310.1; found 310.1.

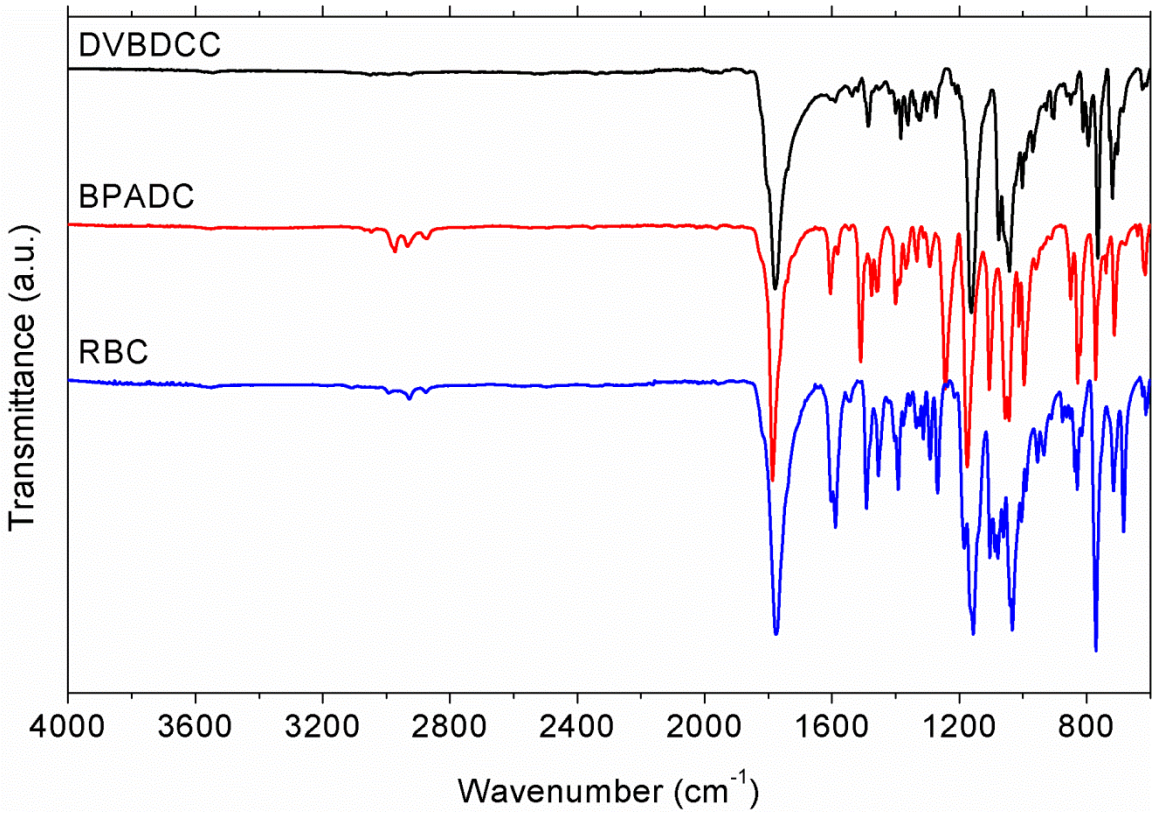

Figure D7: FTIR spectra of DVBDCC, BPADC, and RBC.

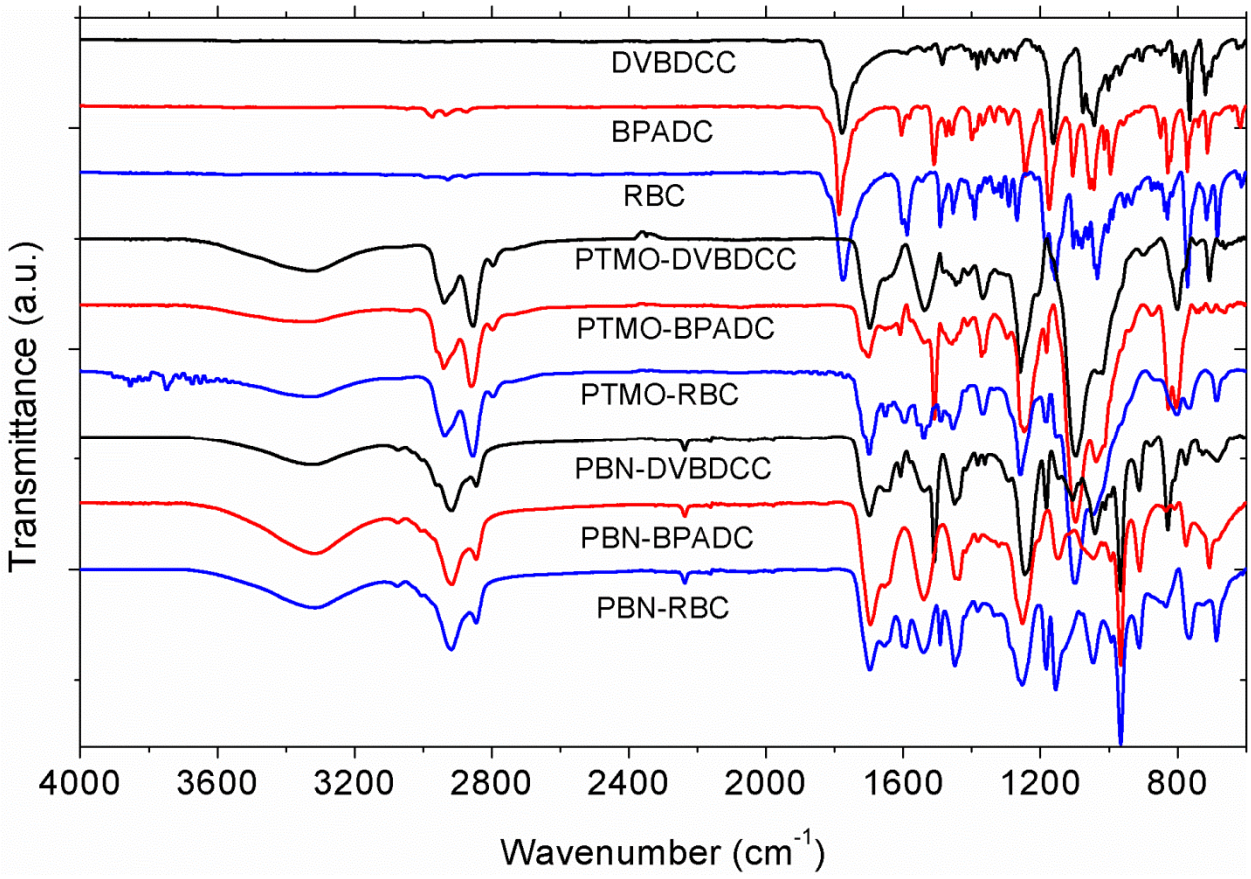

Figure D8: FTIR Spectra of all PHUs with their corresponding carbonate molecules.

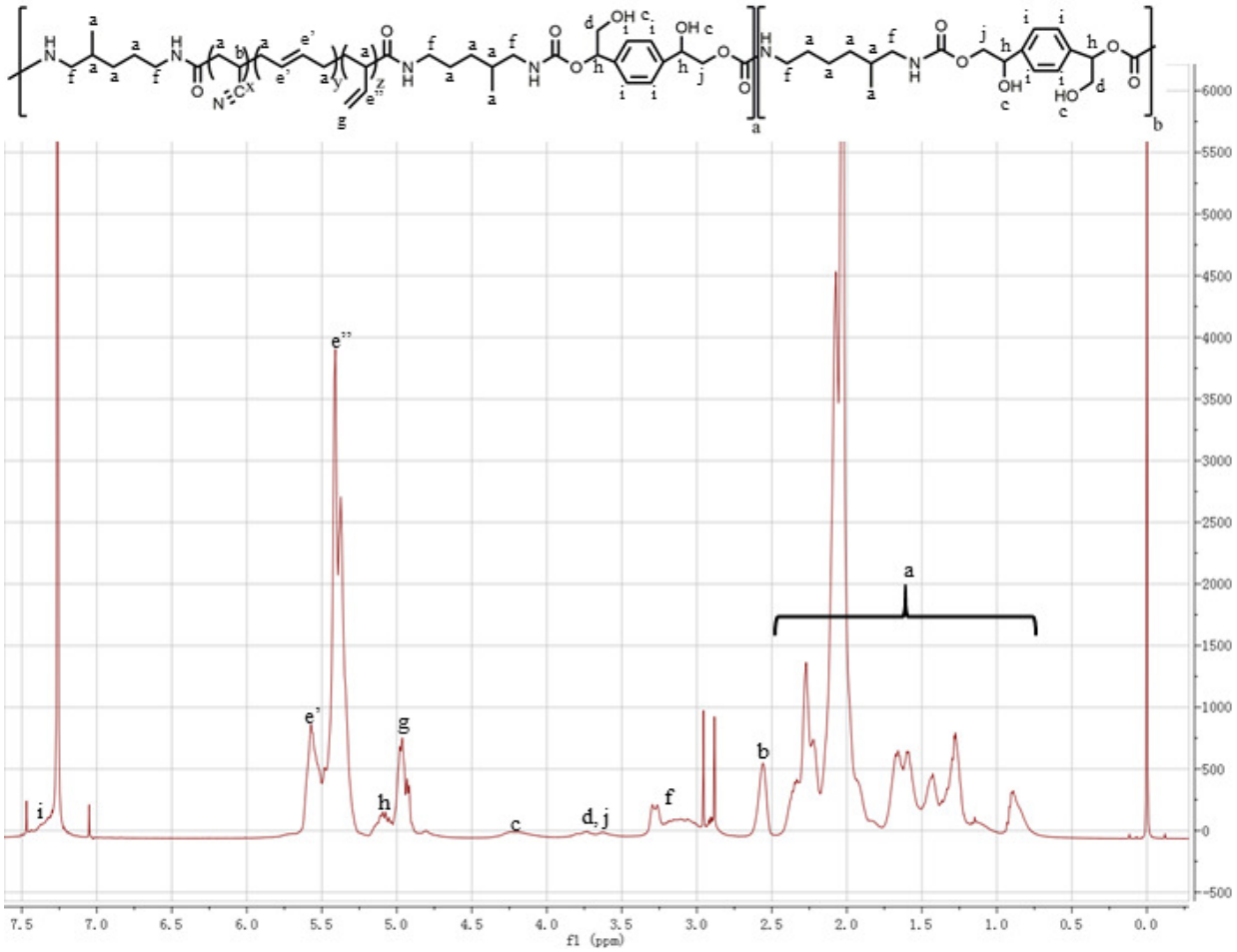

Figure D9: ^{1}H NMR spectrum of PBN-DVBDCC.

PBN-DVBDCC. ^{1}H NMR ($CDCl_3$, 500 MHz), δ (ppm): 0.6-2.4 (15H, -NHCH$_2$C***H***$_2$C***H***$_2$C***H***(C***H***$_3$)CH$_2$NH-, -C***H***$_2$C***H***(CH$_2$=CH$_2$)C***H***$_2$-, -C***H***$_2$CH(CN)-), 2.5-2.6 (1H, -CH$_2$C***H***(CN)-), 3.0-3.3 (2H, -C***H***$_2$NHC(=O)OCH$_2$-), 3.6-3.8 (4H, -C***H***$_2$OH, -C***H***$_2$OC(=O)NH)-), 4.1-4.3 (2H, -CH$_2$O***H*****,** PhCH(O***H***)CH$_2$-), 4.8-5.0 (2H, -CH(CH=C***H***$_2$)), 5.0-5.2 (1H, PhC***H***(OH)CH$_2$O-), 5.3-5.5 (1H, -CH(C***H***=CH$_2$)), 5.5-5.6 (2H, -CH$_2$C***H***=C***H***CH$_2$-), 7.0-7.5 (4H, Ph).

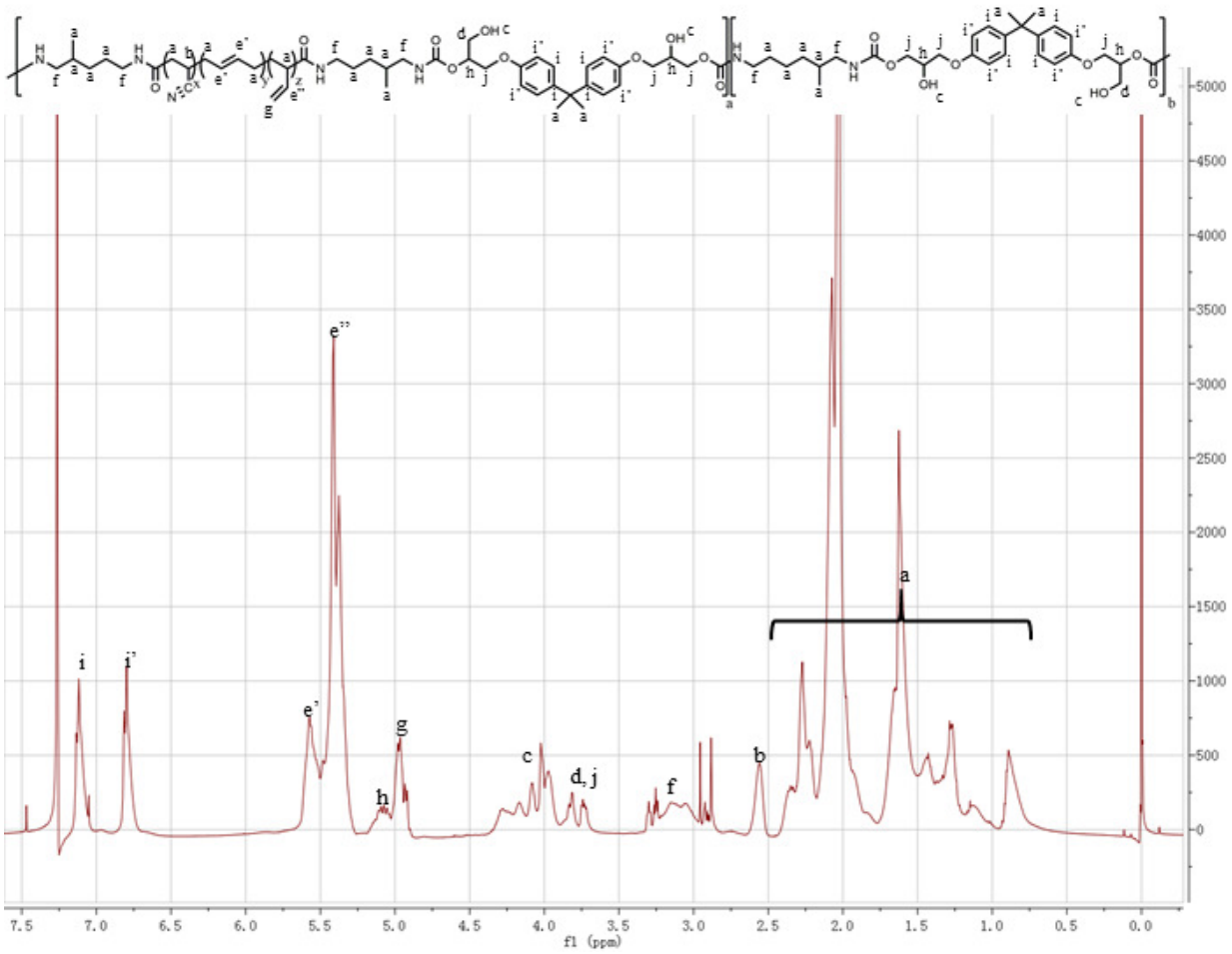

Figure D10: ^{1}H NMR spectrum of PBN-BPADC.

PBN-BPADC. ^{1}H NMR ($CDCl_3$, 500 MHz), δ (ppm):

0.6-2.4 (21H, -NHCH$_2$C***H***$_2$C***H***$_2$C***H***(C***H***$_3$)CH$_2$NH-, -C***H***$_2$C***H***(CH$_2$=CH$_2$)C***H***$_2$-, -C***H***$_2$CH(CN)-, PhC(C***H*****$_3$**)(C***H*****$_3$**)Ph), 2.5-2.6 (1H, -CH$_2$C***H***(CN)-), 3.0-3.3 (2H, -C***H***$_2$NHC(=O)OCH$_2$-), 3.6-3.8 (6H, -C***H***$_2$OH, -C***H***$_2$OC(=O)NH)-, -CH(CH$_2$OH)C***H*****$_2$**O-), 3.9-4.3 (2H, -CH$_2$O***H*****,** PhCH(O***H***)CH$_2$-), 4.8-5.0 (2H, -CH(CH=C***H***$_2$)), 5.0-5.2 (1H, PhC***H***(OH)CH$_2$O-), 5.3-5.5 (1H, -CH(C***H***=CH$_2$)), 5.5-5.6 (2H, -CH$_2$C***H***=C***H***CH$_2$-), 6.7-7.2 (8H, Ph).

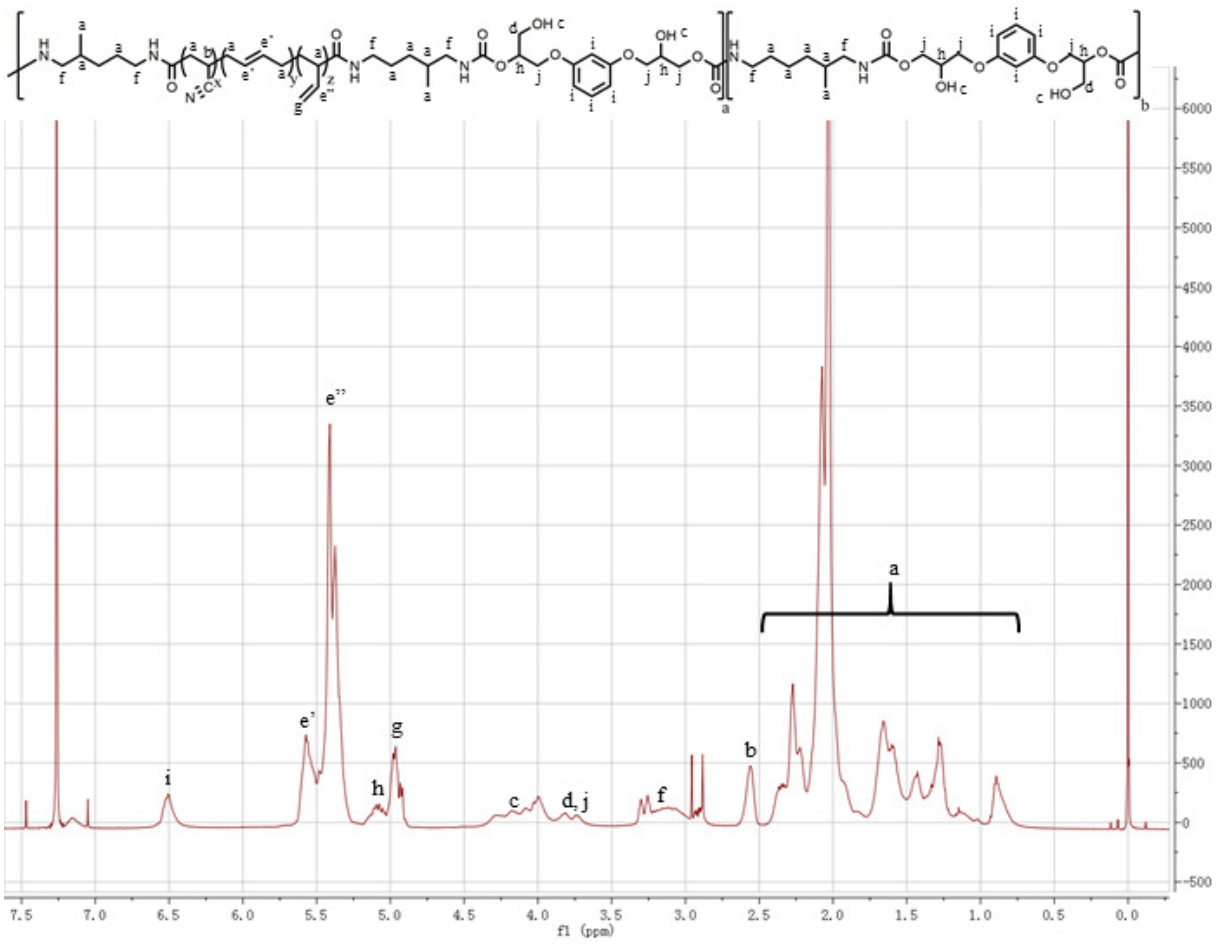

Figure D11: ^{1}H NMR spectrum of PBN-RBC.

PBN-RBC. ^{1}H NMR ($CDCl_3$, 500 MHz), δ (ppm): 0.6-2.4 (15H, -NHCH$_2$C***H***$_2$C***H***$_2$C***H***(C***H***$_3$)CH$_2$NH-, -C***H***$_2$C***H***(CH$_2$=CH$_2$)C***H***$_2$-, -C***H***$_2$CH(CN)-), 2.5-2.6 (1H, -CH$_2$C***H***(CN)-), 3.0-3.3 (2H, -C***H***$_2$NHC(=O)OCH$_2$-), 3.6-3.8 (6H, -C***H***$_2$OH, -C***H***$_2$OC(=O)NH)-, -CH(CH$_2$OH)C***H$_2$***O-), 3.9-4.4 (2H, -CH$_2$O***H*****,** PhCH(O***H***)CH$_2$-), 4.8-5.0 (2H, -CH(CH=C***H***$_2$)), 5.0-5.2 (1H, PhC***H***(OH)CH$_2$O-), 5.3-5.5 (1H, -CH(C***H***=CH$_2$)), 5.5-5.6 (2H, -CH$_2$C***H***=C***H***CH$_2$-), 6.4-6.6 (4H, Ph).

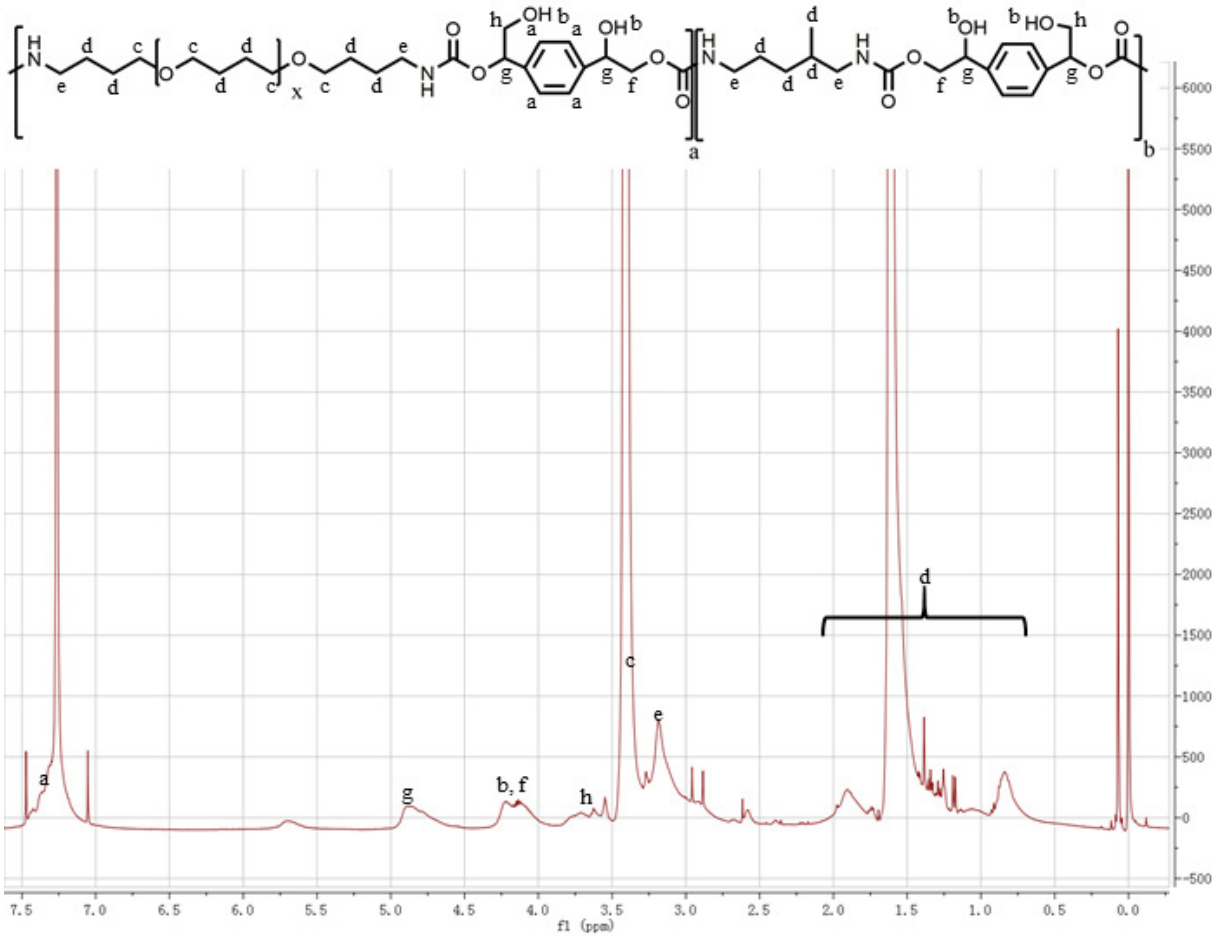

Figure D12: ^{1}H NMR spectrum of PTMO-DVBDCC.

PTMO-DVBDCC. ^{1}H NMR ($CDCl_3$, 500 MHz), δ (ppm): 0.5-2.0 (16H, -$OCH_2C\boldsymbol{H}_2C\boldsymbol{H}_2CH_2O$-, -$NHCH_2C\boldsymbol{H}_2C\boldsymbol{H}_2CH_2O$-, -$NHCH_2C\boldsymbol{H}_2C\boldsymbol{H}_2C\boldsymbol{H}(C\boldsymbol{H}_3)$CH2NH-), 2.8-3.2 (4H, -$NHC\boldsymbol{H}_2CH_2CH_2CH_2O$-, -$NHC\boldsymbol{H}_2$-), 3.3-3.5 (6H, -$C\boldsymbol{H}_2OC\boldsymbol{H}_2$-, -$NHC(=O)OC\boldsymbol{H}_2$-), 3.6-3.8 (1H, -$C\boldsymbol{H}_2OH$), 4.0-4.2 (2H, -$C\boldsymbol{H}_2OC(=O)NH$-), 4.2-4.3 (2H, -$CH_2O\boldsymbol{H}$, $PhCH(O\boldsymbol{H})CH_2$-), 4.8-5.0 (1H, $PhC\boldsymbol{H}(OH)CH_2$-), 7.0-7.5 (4H, Ph).

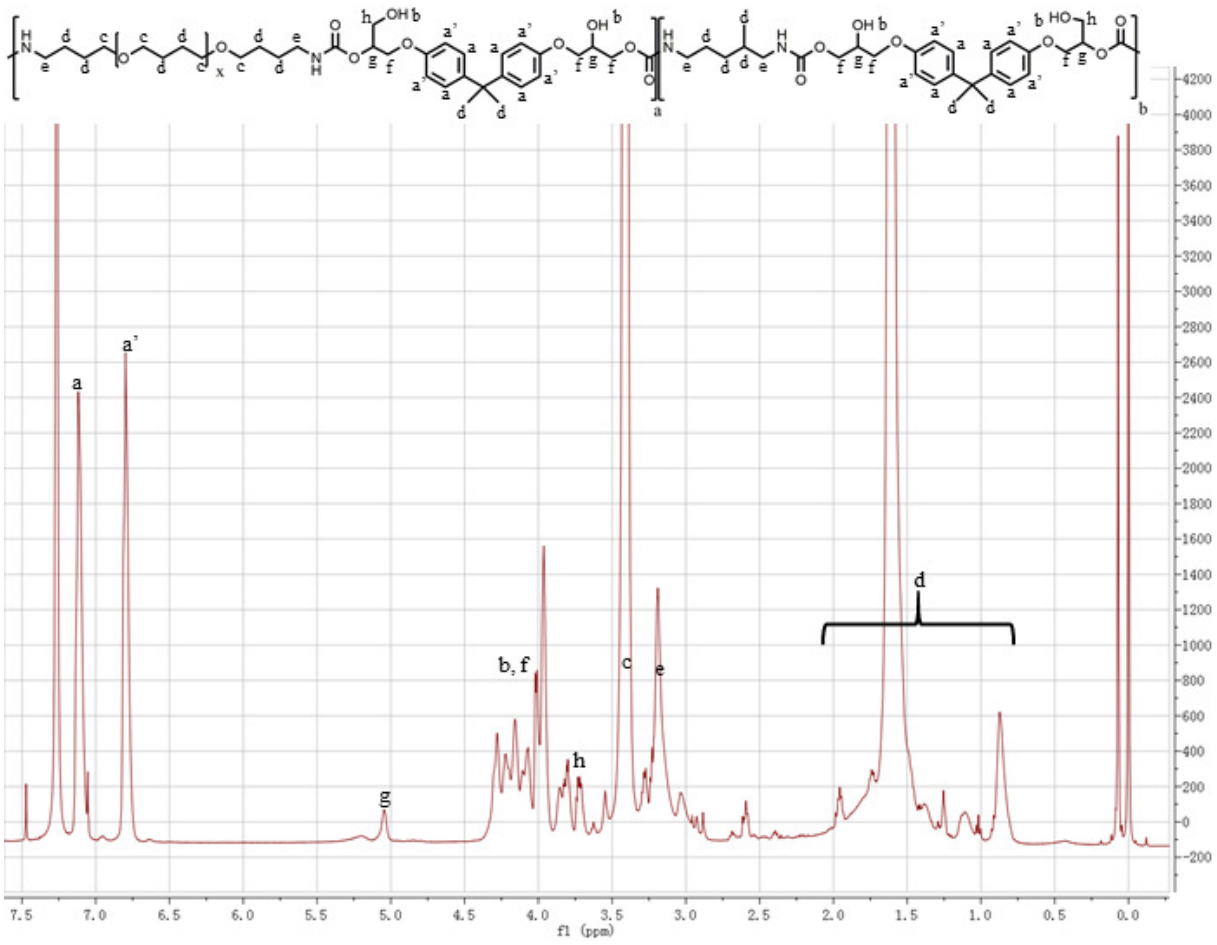

Figure D13: ^{1}H NMR spectrum of PTMO-BPADC.

PTMO-BPADC. ^{1}H NMR ($CDCl_3$, 500 MHz), δ (ppm): 0.5-2.0 (22H, -$OCH_2C\boldsymbol{H}_2C\boldsymbol{H}_2CH_2O$-, -$NHCH_2C\boldsymbol{H}_2C\boldsymbol{H}_2CH_2O$-, -$NHCH_2C\boldsymbol{H}_2C\boldsymbol{H}_2C\boldsymbol{H}(C\boldsymbol{H}_3)$CH2NH-, PhC($C\boldsymbol{H_3}$)($C\boldsymbol{H_3}$)Ph), 2.8-3.2 (4H, -$NHC\boldsymbol{H}_2CH_2CH_2CH_2O$-, -$NHC\boldsymbol{H}_2$-), 3.3-3.5 (6H, -$C\boldsymbol{H}_2OC\boldsymbol{H}_2$-, -NHC(=O)$OC\boldsymbol{H}_2$-), 3.6-3.8 (1H, -$C\boldsymbol{H}_2OH$), 4.0-4.2 (4H, -$C\boldsymbol{H}_2OC$(=O)NH-, -$CH(CH_2OH)C\boldsymbol{H_2}O$-), 4.2-4.3 (2H, -$CH_2O\boldsymbol{H}$, PhCH($O\boldsymbol{H}$)$CH_2$-), 4.8-5.0 (1H, PhC$\boldsymbol{H}(OH)CH_2$-), 6.7-7.2 (8H, Ph).

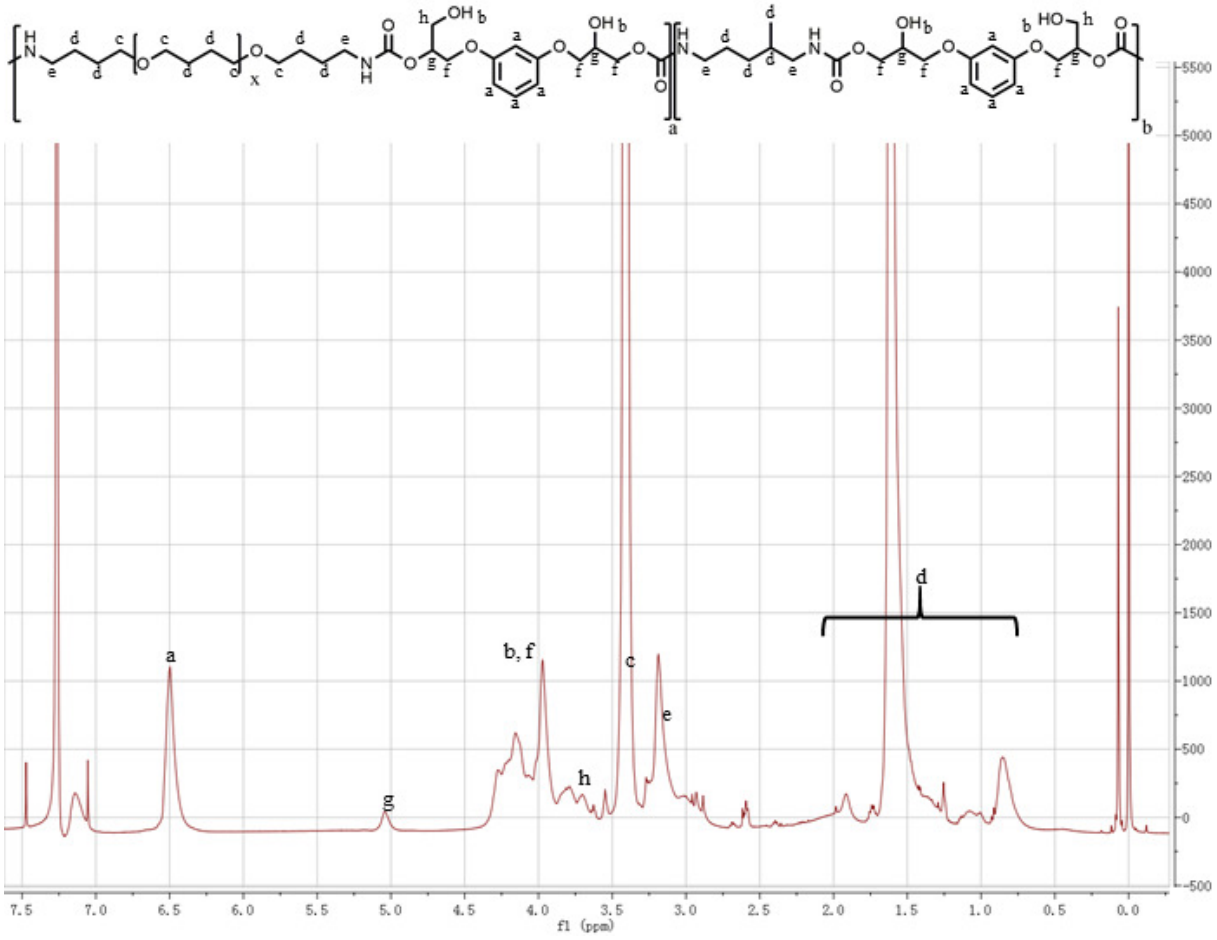

Figure D14: ^{1}H NMR spectrum of PTMO-RBC.

PTMO-RBC. ^{1}H NMR ($CDCl_3$, 500 MHz), δ (ppm): 0.5-2.0 (16H, -$OCH_2C\boldsymbol{H}_2C\boldsymbol{H}_2CH_2O$-, -$NHCH_2C\boldsymbol{H}_2C\boldsymbol{H}_2CH_2O$-,-$NHCH_2C\boldsymbol{H}_2C\boldsymbol{H}_2C\boldsymbol{H}(C\boldsymbol{H}_3)$CH2NH-), 2.8-3.2 (4H, -$NHC\boldsymbol{H}_2CH_2CH_2CH_2O$-, -$NHC\boldsymbol{H}_2$-), 3.3-3.5 (6H, -$C\boldsymbol{H}_2OC\boldsymbol{H}_2$-, -$NHC(=O)OC\boldsymbol{H}_2$-), 3.6-3.8 (1H, -$C\boldsymbol{H}_2OH$), 4.0-4.2 (4H, -$C\boldsymbol{H}_2OC(=O)NH$-, -$CH(CH_2OH)C\boldsymbol{H}_2O$-), 4.2-4.3 (2H, -$CH_2O\boldsymbol{H}$, $PhCH(O\boldsymbol{H})CH_2$-), 4.8-5.0 (1H, $PhC\boldsymbol{H}(OH)CH_2$-), 6.4-6.6 (4H, Ph).

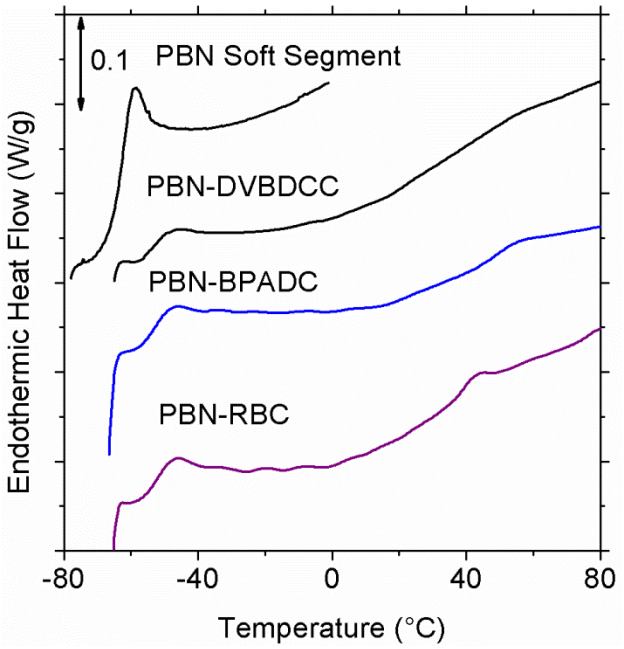

Figure D15: DSC heating scan of PBN-based PHUs.

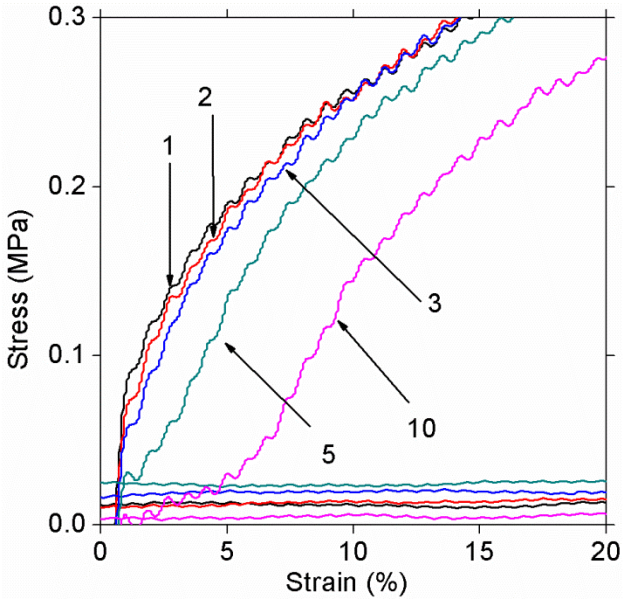

Figure D16: Zoomed version of PBN-RBC hysteresis.

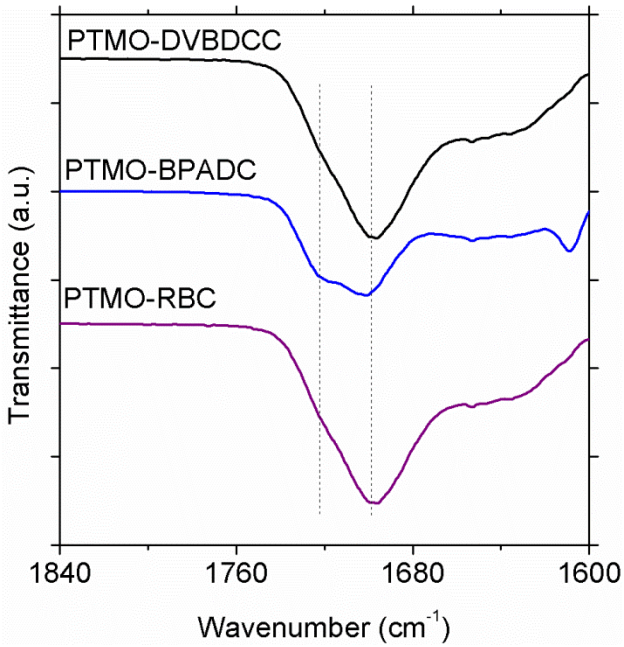

Figure D17: Comparison of FTIR spectra of PTMO-based PHUs in the carbonyl region. Free, non hydrogen-bonded carbonyl appears ~1720 cm^{-1} while hydrogen-bonded carbonyl appears ~1690 cm^{-1}.

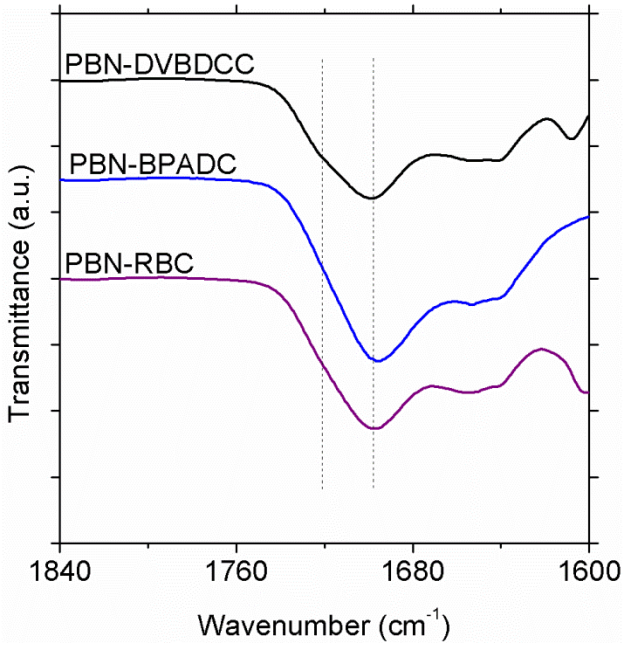

Figure D18: Comparison of FTIR spectra of PBN-based PHUs in the carbonyl region. Free, non hydrogen-bonded carbonyl appears ~1720 cm^{-1} while hydrogen-bonded carbonyl appears ~1690 cm^{-1}.

Table D1: Apparent Weight-Average Molecular Weights of PHUs.*

Sample	M_w (kg/mole)
PTMO-DVBDCC	30.8
PTMO-RBC	37.9
PTMO-BPADC	37.7
PBN-DVBDCC	37.0
PBN-RBC	22.4
PBN-BPADC	25.0

*The overall signal to noise in RI detector was not high enough to reveal the details of molecular weight moments. It is likely due to low dn/dc values of samples in DMF.

CHAPTER 7

Tuning the Properties of Segmented Polyhydroxyurethanes via Chain Extender Structure

7.1 Introduction

Polyhydroxyurethane (PHU) produced from cyclic carbonate aminolysis is a material with potential to replace isocyanate-based polyurethane (PU) (Guan 2011, Kathalewar 2013, Blattmann 2014, Maissoneuve 2015, Cornille 2016d). Isocyanate is facing increasing scrutiny from various regulatory bodies in recent years, thus necessitating the search for alternative chemistries to achieve non-isocyanate polyurethane (NIPU) material (Official Journal of European Union 2009, US EPA 2011, US EPA 2015). PHU is analogous to PU but possesses additional primary and/or secondary hydroxyl groups adjacent to the urethane linkages (Guan 2011, Kathalewar 2013, Blattmann 2014, Maissoneuve 2015, Cornille 2016d). Most previous PHU studies have focused on the synthesis of cyclic carbonate monomers and their subsequent polymerization into single-phase thermoplastics or crosslinked thermosets, or on catalysis of the cyclic carbonate aminolysis reaction (Kihara 1993, Steblyanko 2008, Ochiai 2005, Tomita 2001a, Tomita 2001b, Tomita 2001c, Tomita 2001d, Tomita 2001e, Ochiai 2005a, Ochiai 2005b, Tamami 2004, Javni 2008, Javni 2013, Bähr 2012, Fleischer 2013, Fortman 2015, Matsukizono 2015, Cornille 2015, Cornille 2016a, Schmidt 2016, Blattmann 2016a, Blattmann 2016b, Grignard 2016, Lambeth 2013, Lombardo 2015, Blain 2014). Few studies have investigated segmented, nanophase-separated PHU and established an understanding of their structure-property-relationships (Nanclares 2015, Leitsch 2016a, Beniah 2016, Zhang 2016). Torkelson and coworkers have successfully synthesized thermoplastic PHU elastomers with tunable mechanical properties and demonstrated that the hydroxyl group and soft-segment choice are

critical in controlling nanophase separation (Leitsch 2016a). They have also demonstrated that segmented PHUs with polytetramethylene oxide (PTMO)-based soft segment possess nanophase-separated structures with broad interphases having a wide range of local compositions, potentially useful in damping applications over broad range of use temperature (Beniah 2016). In Chapter 5, we have also demonstrated that nanophase separation in PHUs can be significantly tuned via judicious choice of soft segment. In Chapter 6, we also showed that both hard-segment and soft-segment structures cooperatively influence the nanophase separation and physical properties of segmented PHUs. Despite these advances, segmented PHUs exhibit generally inferior thermal and mechanical properties relative to isocyanate-based, segmented PU (Lee 2007, Lee 2000, Korley 2006, Sheth 2004, Klinedinst 2005, Martin 1996, Kojio 2007). Segmented PUs often possess tensile strength in excess of 20 MPa with upper softening temperature exceeding 100 °C in many cases (Lee 2007, Lee 2000, Korley 2006, Sheth 2004, Klinedinst 2005, Martin 1996, Kojio 2007). A potential approach to improve such properties is by changing chain extender structure.

The impact of the molecular structure of chain extender on the properties of segmented PU has been heavily investigated (Bae 1999, Adhikari 1999, Gisselfalt 2003, Priscariu 2001, Blackwell 1981, Chattopadhyay 2005, Hu 1982, Casey 1985, Seefried 1975d, Liaw 1997, Li 2002, Hergenrother 1992, Chen 2000, Oprea 2010, Ahn 1994, Tatai 2007, Korodi 1984, Nakamura 1990). For example, Bae et al. studied a PU system made from PTMO (with M_n=1000 g/mole) and 4,4'-diphenylmethane diisocyanate (MDI) with several aliphatic and cycloaliphatic chain extenders at a hard-segment content of 50 wt% (Bae 1999). From dynamic mechanical analysis (DMA), they found that cycloaliphatic chain extender increases the upper softening temperature or flow temperature (T_{flow}) of PU. Within the series of aliphatic chain extender studied, PU chain extended with 1,4-butanediol (BDO) shows the highest upper softening temperature and highest room temperature storage modulus (Bae 1999). This result is in

agreement with results obtained by Adhikari et al. who investigated PU systems made from hydrogenated MDI and a soft segment involving a mixture of polydimethylsiloxane and polyhexamethylene oxide (Adhikari 1999). PU chain extended with BDO also yields the highest value of tensile strength and Young's modulus. Blackwell et al. showed that that BDO affords the formation of crystalline hard domain due to its ability to adopt a low energy conformation resulting in better packing (Blackwell 1981). Chattopadhyay et al. investigated moisture-cured polyurethane-urea with a series of chain extenders and concluded that more bulky chain extenders promote better phase mixing than linear chain extender like BDO (Chattopadhyay 2005). Their studies also show that bulky and sulfone-containing chain extenders afford materials with superior tensile strength. In contrast to the many studies of chain extender structure in segmented PU, the role of chain extender structure in modulating the physical properties of segmented PHUs has not been investigated.

Here, we compare a series of chain extenders in segmented PHUs formulated with PTMO-based soft segment and divinyl benzene dicyclocarbonate (DVBDCC) as the hard-segment molecule. The diamine chain extenders are 1,4-diaminobutane (DAB), isophorone diamine (IPDA), methylene-bis(cyclohexyl amine) (MBC), and bis(aminomethyl) norbornane (NORB). DAB was selected as an analog to BDO, which results in PU with the best properties in various cases (Bae 1999, Adhikari 1999, Chattopadhyay 2005). Cycloaliphatic chain extenders with increasing ring rigidity from IPDA to MBC and NORB are intended to produce more rigid hard domains to achieve improved thermal and mechanical properties. Characterization via DMA and tensile testing reveals that norbornane-based chain extender results in PHU with the best tensile properties and the highest T_{flow}. Tensile strength of 22.4 MPa with elongation at break of 500% and T_{flow} of 105 °C are obtained. Further optimization through variation in hard-segment content from 30 to 50 wt% of norbornane-based PHUs allows tensile strength to be tuned from 0.5 to 22.4 MPa and elongation-at-break from 500% to greater than 2000%. DMA

characterization shows that all PHUs investigated in our study possess nanophase-separated structures with broad interphases. These PHUs exhibit tan $\delta \geq 0.30$ over very broad and tunable temperature ranges, demonstrating their capability to serve as damping materials over broad ranges of use temperature.

7.2 Experimental

7.2.1 Materials

Divinyl benzene dicyclocarbonate (DVBDCC) was synthesized according to the procedure outlined by Torkelson and coworkers (Leitsch 2016a). Diamine-terminated polytetramethylene oxide with M_n=1700 g/mole or Elastamine™ HT-1700 (also known as XTJ-548) was supplied by Huntsman Chemicals. 1,4-diaminobutane (DAB, 99 %), 5-amino-1,3,3-trimethylcyclohexanemethylamine, mixture of *cis* and *trans* or isophorone diamine (IPDA, ≥ 99%) were from SigmaAldrich. 4,4'-Methylene bis(cyclohexylamine) (mixture of isomers) (MBC, > 97%) and Bis(aminomethyl) norbornane (mixture of isomers) (NORB, > 98 %) were from TCI America. Dimethylformamide (DMF) was from Fisher Scientific.

7.2.2 Synthesis of PHUs

All PHUs were synthesized according to Scheme 7.1 with PTMO as soft segment and DVBDCC as cyclic carbonate. The nomenclature of the PHUs synthesized and characterized in this study is chain extender-content of hard segment where chain extender can be DAB, IPDA, MBC or NORB. For example, MBC-50 is PHU made with MBC chain extender at 50 wt% hard-segment content. The hard-segment content is defined as (weight of DVBDCC + weight of chain extender) / (weight of DVBDCC + weight of chain extender + weight of soft segment). In a typical synthesis of NORB-50, 2.5 g of PTMO (1.587 mmol), 0.802 g of NORB (5.199 mmol) and 1.698 g of DVBDCC (6.786 mmol) were combined in a 20-mL scintillation vial and 4 mL of

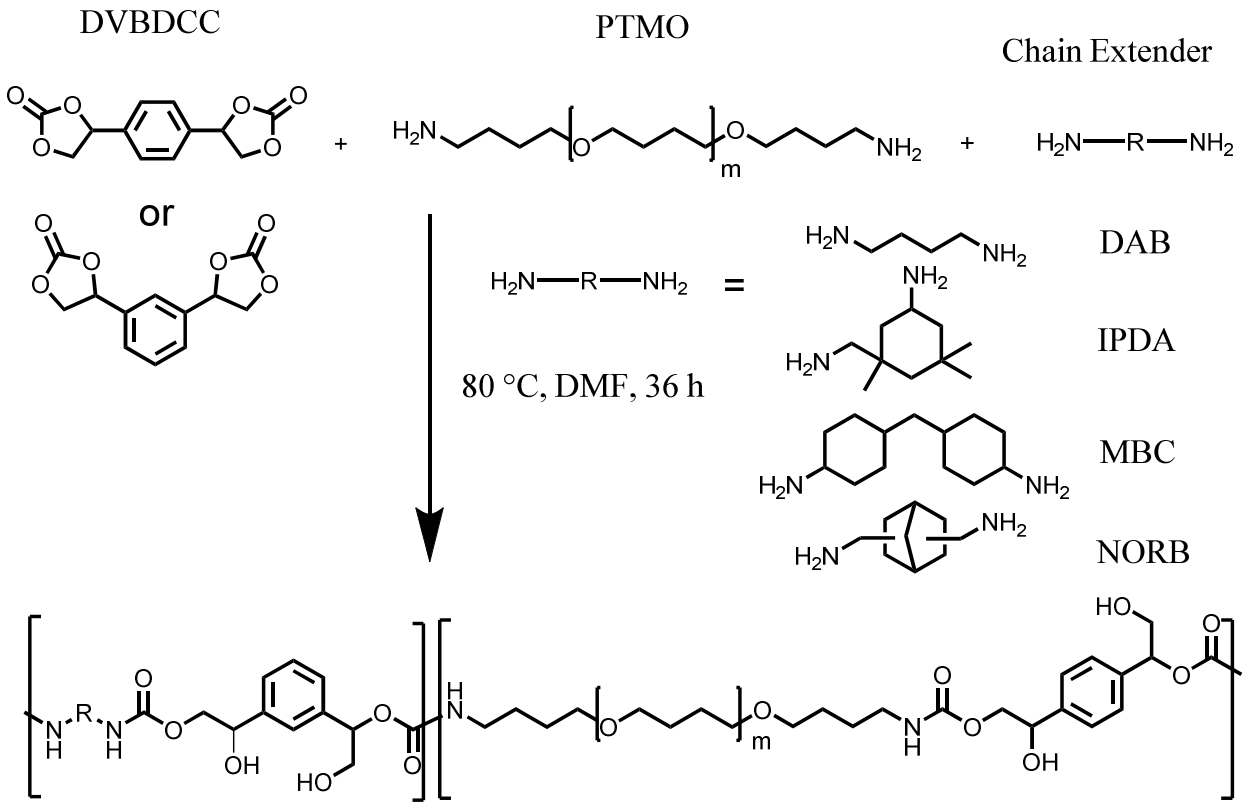

Scheme 7.1: Chemical structure of chain extenders used in this study.

DMF were added to adjust the concentration of reacting groups to ~0.70 M. The mixture was reacted at 80 °C for 36 h with stirring. The resulting polymer solution was poured into a mold and dried at 80 °C for 24 h under vacuum. (The total conversion achieved could be a combination of the polymerization step and the drying process as both occur at 80 °C.)

7.2.3 Characterization

^{1}H NMR spectra were recorded on a Bruker Avance III 500 MHz NMR spectrometer with a direct cryoprobe at room temperature in deuterated chloroform ($CDCl_3$). Spectra were reported in parts per million relative to tetramethylsilane. Attenuated total reflectance-Fourier transform infrared (ATR-FTIR) spectroscopy was performed with a Bruker Tensor 37 MiD IR FTIR spectrophotometer equipped with a diamond/ZnSe attachment. All PHUs were scanned at a resolution of 4 cm^{-1} and 32 scans were collected in the 4000-600 cm^{-1} range. The conversion of the starting materials was determined by analyzing carbonate carbonyl groups of DVBDCC at ~1800 cm^{-1}. Apparent molecular weight averages of PHUs were determined by gel permeation chromatography (GPC), using a Waters 2695 separation module and two Tosoh TSKgel Alpha-M columns (13 μm) in series. The eluent was DMF with 4 g/L of $LiNO_3$ at 40 °C; the elution rate was 0.5 mL/min. The detector was a Malvern OmniFACE analog-to-digital interface/Waters 2414 RI detector. Apparent molecular weight values are relative to polyethylene oxide standards (Agilent PEO/PEG EasiCal standards).

SAXS experiments were performed using a Rigaku S-MAX 3000 SAXS system emitting X-rays with a wavelength of 0.154 nm (Cu-Kα). The sample-to-detector distance was 1640 mm with silver behenate calibration. The 2D scattering patterns were azimuthally averaged to produce 1-D plots of intensity versus scattering vector q, where $q = 4\pi\sin\theta/\lambda$; θ is one-half of the scattering angle, and λ is the X-ray wavelength.

DMA experiments were performed with a TA Instruments Rheometrics Stress Analyzer-

GIII. Rectangular specimens measuring 8.0 mm in width and 0.9 mm in thickness were cooled with N_2 gas to -100 °C and subjected to a temperature sweep from -100 °C to 120 °C at a heating rate of 3 °C/min. The measurements were conducted in tensile mode at a frequency of 1 Hz and a strain of 0.03%. The storage modulus (E'), loss modulus (E") and loss tangent (tan δ) were recorded. The soft-segment glass transition temperature (T_g) was identified from the peak maximum in E"; the flow temperature was defined as the onset of inconsistent tan δ data, close to the temperature at which the sample was no longer mechanically robust. (Additionally, for comparison, we also provided T_{flow} values determined when E' = 0.5 MPa following the approach by De and Gaymans (De 2009).

Tensile properties were obtained according to ASTM D1708 standard with an MTS Sintech 20/G tensile tester. Dog bone-shaped samples (4.7 mm x 1.0 mm x 22 mm) were cut using a Dewes-Gumbs die from dried sheets and subjected to an extension rate of 130 mm/min. The Young's modulus, tensile strength and elongation at break were reported as average values of five specimens. Error represents one standard deviation.

7.3 Results and Discussion

All PHUs were synthesized according to Scheme 7.1 with four diamine chain extender molecules. Comparisons were first drawn from PHUs at 50 wt% hard-segment content. The successful synthesis of PHUs was confirmed via FTIR spectroscopy. Figure E1 and E2 in Appendix E report the FTIR spectra of all PHUs along with the spectrum of DVBDCC. The carbonate peak at ~1800 cm^{-1} present in the DVBDCC sample was very significantly reduced in all PHU samples, indicating close to complete conversion of carbonate functional groups into hydroxyurethane linkages. The urethane carbonyl stretch (1730-1700 cm^{-1}), amide stretch (3500-3300 cm^{-1}), and hydroxyl stretch (3500-3100 cm^{-1}) were present in the spectra of these PHUs. The successful formation of PHUs was also confirmed via ^1H NMR spectroscopy. Figures E3-E6

in Appendix E show NMR spectra of all PHUs. The positions of various protons within the polymer backbone were assigned accordingly. Our peak assignments concur with those of PTMO-based PHUs presented in our previous studies (Beniah 2016, Beniah 2017) and reports by other investigators (Zhang 2016, Carre 2016, Lamarzelle 2016). Apparent molecular weight (MW) averages of these PHUs were determined by GPC and are tabulated in Table E1 in Appendix E; all apparent MW averages are relatively low. Possible reasons for the low MW achieved include side reactions leading to urea formation and oxazolidinone as well as dehydration products as discussed by Besse et al. (Besse 2015) The achievement of relatively low MW during synthesis of PHUs was also reported in a recent study by Averous and coworkers (Carre 2016) who synthesized segmented PHUs using fatty-acid based diamine, terephthaloyl bis-carbonate and diamine-terminated polypropylene glycol (Jeffamine™ D2000); other studies have made related reports (Leitsch 2016a, Beniah 2016, Beniah 2016, Benyahya 2011, Benyahya 2012, Lamarzelle 2016, Besse 2015). All PHUs are synthesized via one-step synthesis. Segmented PUs can be synthesized via a one-step or two-step polymerization technique. The effect of polymerization technique on the attainable molecular weight and properties of segmented PHUs also deserves further study.

SAXS was used to demonstrate the presence of nanophase-separated morphology in these PHUs. Figure 7.1a shows the SAXS patterns of DAB-50, IPDA-50, MBC-50, and NORB-50. All PHUs show single interference peaks at specific scattering vector locations indicating that they are all nanophase-separated materials, in agreement with our previous study on PTMO-based PHUs (Beniah 2016). The interdomain spacings of these PHUs range from 12-16 nm.

The impact of chain-extender structure on thermomechanical properties of PHUs were evaluated with DMA. Figure 7.2a-d shows the temperature dependences of storage modulus (*E*'), loss modulus (*E*"), and tan δ of DAB-50, IPDA-50, MBC-50, and NORB-50, respectively. These profiles are consistent with the presence of nanophase-separated morphology as evidenced from

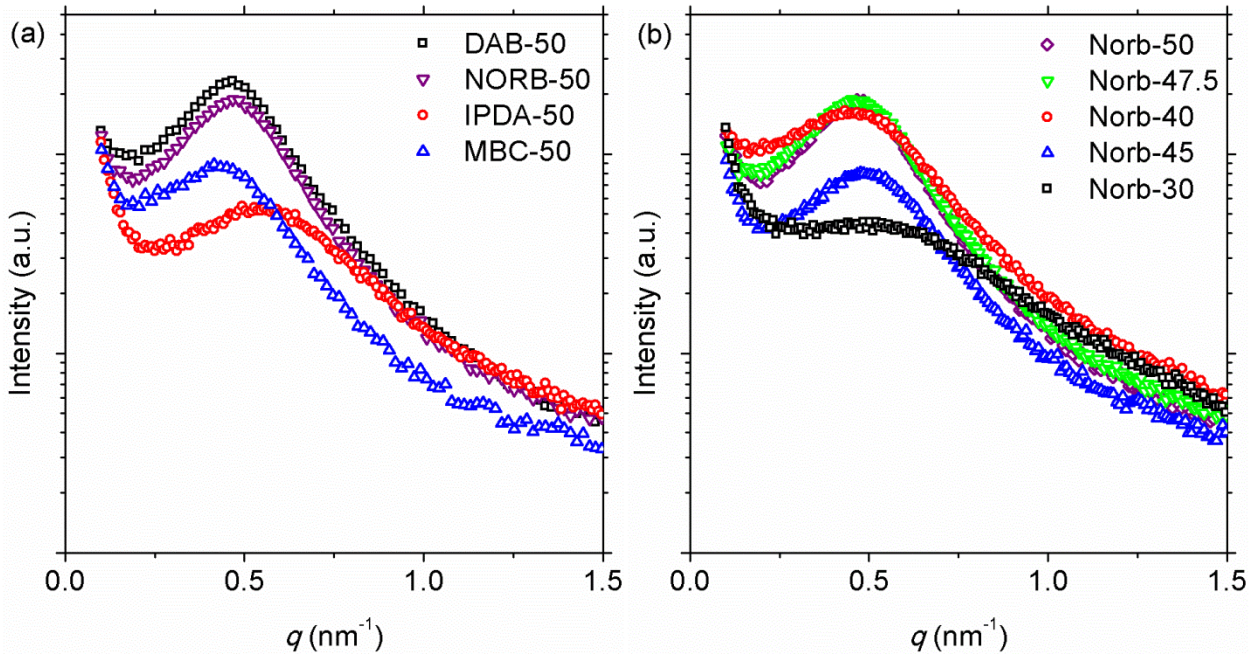

Figure 7.1: a) SAXS data of 50 wt% hard-segment content as a function of chain extender PHUs and b) SAXS data of NORB-based PHUs at several hard-segment contents.

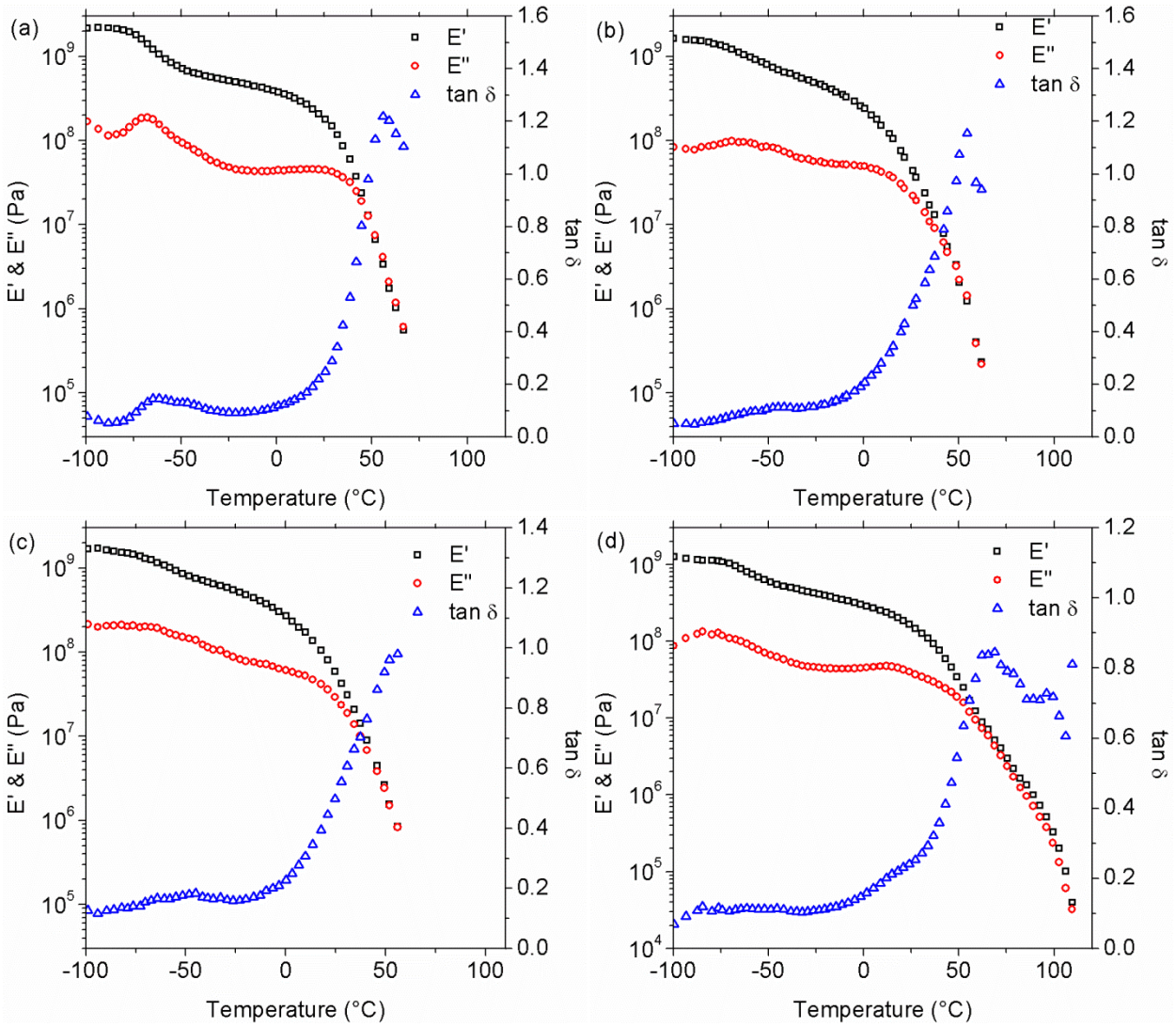

Figure 7.2: Temperature dependence of storage modulus (*E*'), loss modulus (*E*"), and tan δ of a) DAB-50, b) IPDA-50, c) MBC-50, and d) NORB-50.

the peak in *E*" indicative of a PTMO soft-segment T_g at -70 °C and T_{flow} above room temperature corresponding to dispersed hard-segment domain undergoing the glass transition.

The location of T_{flow} is significantly influenced by chain extender structure. DAB-50, with structure analogous to BDO, has a T_{flow} of 69 °C. This value is higher in comparison to the T_{flow} value of 57 °C in our previous study of segmented PHU chain extended with hexamethylene diamine (HMDA) at 50 wt% hard-segment content (Beniah 2016). A higher T_{flow} value is expected for DAB-50 because of a decrease in flexibility of the backbone caused by a decrease in the distance between urethane linkages. Incorporation of chain extenders with cycloaliphatic structure in the cases of IPDA-50 and MBC-50 results in somewhat lower T_{flow} values than DAB-50. IPDA-50 and MBC-50 reported T_{flow} values of 62 and 57 °C, respectively. These values are also lower than T_{flow} value of PHU chain extended with 1,3-cyclohexane bis(methylamine) (CYCDA) at 89 °C reported in our previous study (Beniah 2016). For IPDA-50, this might be caused by the more irregular (less symmetrical) structure of IPDA molecule compared to CYCDA molecule. The less symmetrical structure of IPDA might lead to less-ordered interurethane hydrogen bonding and consequently lower T_{flow}. For MBC-50, the lower T_{flow} value may be caused by the added flexibility of the methylene bridge between its two cycloaliphatic rings. Additionally, it could also be due to the decrease in urethane bond density caused by the less compact structure of MBC relative to CYCDA.

While cycloaliphatic chain extender may increase the rigidity of the hard segment, interactions between neighboring urethane linkages participating in hydrogen bonding are also important for hard-segment cohesion. Blackwell et al. investigated the hard segment of a series of PU elastomers made with aliphatic chain extenders using X-ray diffraction and conformational analysis (Blackwell 1981). The study considered the conformation of and bond angle between atoms of the chain extender species. An even-numbered diol chain extender like BDO can adopt the lowest energy fully extended conformations allowing for hydrogen bonding

in both directions perpendicular to the chain axis. Such a hydrogen bonding network is not possible with odd-numbered diol chain extender. BDO is analogous to 1,4-diaminobutane used in DAB-50. This could explain the higher T_{flow} in DAB-50. Interestingly, in the case of NORB-50, incorporation of a three-dimensional, norbornane ring structure affords the highest T_{flow} value (105 °C) of all PHUs in this study. The hard-segment chain rigidity is significantly increased due the bulky norbornane structure resulting in enhanced thermal properties. Nakamura et al. previously showed that PU chain extended with norbornane-containing diol resulted in a very high hard-segment T_g, up to 171 °C (Nakamura 1990). How the bulky, three-dimensional structure of the norbornane ring stacks in the hard segment is an interesting topic of study. Future study can investigate the three-dimensional conformation of hard segment made with NORB as well as with other cycloaliphatic chain extenders following the approach and analysis by Blackwell et al. (Blackwell 1981)

Figure 7.2 also shows that the nanophase-separated structures of these PHUs are accompanied by broad interphases having a wide range of local compositions. This response is similar to that exhibited by gradient copolymers (Mok 2008, Mok 2009). The *E*' value undergoes a very gradual decrease with temperature above the soft-segment T_g until the hard-segment T_{flow} is reached. The nanophase separation with broad interphases is a consequence of some level of phase mixing caused by the hydroxyl groups forming hydrogen bonds with ether oxygen atoms in the PTMO soft segment. FTIR was used to probe the aggregation structure of the hard segments in our PHUs. Figure E7 (see Appendix E) shows the FTIR spectra in the carbonyl regions of our PHUs. According to Figure E7, peaks associated with free, non-hydrogen bonded (~1730 cm^{-1}) and hydrogen-bonded carbonyls (~1700 cm^{-1}) are present. The free carbonyl group is an indication of some level of phase mixing present in PTMO-based PHUs contributed by the hydroxyl groups forming hydrogen bonds with ether oxygen atoms in the PTMO soft segment. The relative proportion of the free, non-hydrogen bonded and hydrogen-bonded carbonyl

generally agrees well with PTMO-based PHU systems in Chapters 3 to 5 (Leitsch 2016a, Beniah 2016, Beniah 2016).

These PHUs exhibit high tan δ values (≥ 0.30) over broad temperature ranges, indicating their potential as sound and vibration damping material over broad range of use temperature (Sophiea 1994, Huelck 1972a, Huelck 1972b, Hu 1997, Chern 1999, Qin 2004, Chen 1994, Yu 1999, Hourston 1996). The breadths of temperature range with high tan δ are also influenced by the chain extender structure. For DAB-50, this range spans 39 °C. This is narrower than the ranges reported by IPDA-50, MBC-50, and NORB-50 at 52, 47, and 74 °C, respectively, perhaps due to a higher degree of phase separation in DAB-50 relative to IPDA-50 and MBC-50. Cycloaliphatic structures may reduce the likelihood of interurethane hydrogen bonding in lieu of hydrogen bonding to the soft segment, thus resulting in more phase mixing and a broader glass transition region. With a bulky norbornane ring in its hard segment, NORB-50 exhibits tan δ ≥ 0.30 over a temperature range of 74 °C, the broadest temperature range in the series. The inclusion of the bulky norbornane structure significantly increases the higher upper softening temperature or T_{flow}. We note that attempt to characterize thermal transitions in our PHUs with differential scanning calorimetry (DSC) was met with limited success. DSC results of PTMO-based PHU systems often do not produce definitive thermal transitions likely due to the presence of broad interphases. This has also been discussed in Chapter 5 (Beniah 2017). The hard segment of our PHUs is also amorphous, in accord with results in previous chapters (Leitsch 2016a, Beniah 2016, Beniah 2017).

The impact of chain extender structure on the tensile properties of PHUs was evaluated with tensile testing. Figure 7.3 shows the representative stress-strain curves of all PHUs. Table 7.1 summarizes values associated with Young's modulus, tensile strength and elongation at break. Significant differences are observed in tensile properties with variation in chain extender structure. DAB-50 reports a Young's modulus value of 190 MPa and tensile strength of 9.7 MPa,

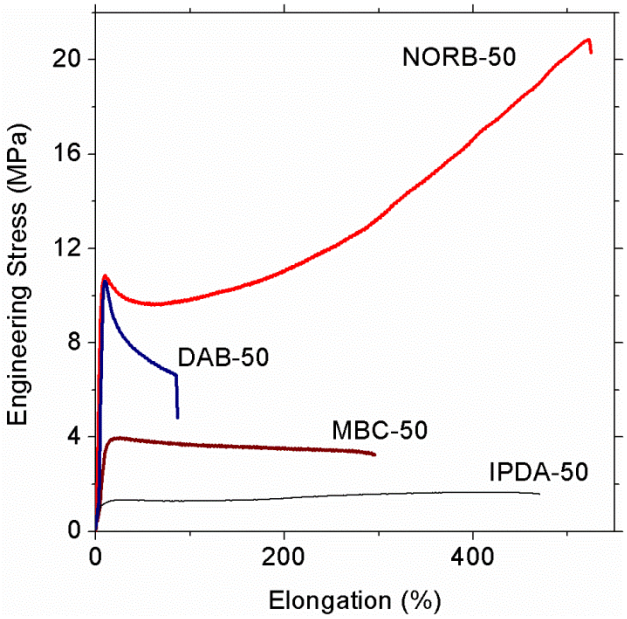

Figure 7.3: Representative stress-strain curves of 50 wt% hard-segment content PHUs as a function of chain extender.

Table 7.1: Summary of properties of 50 wt% hard-segment content PHUs as a function of chain extender structure.

Sample Name	*d*-spacing (nm)	SS T_g (°C)	T_{flow} (°C)	T_{flow}* (°C) E'=0.5 MPa	Young's Modulus (Mpa)	Tensile Strength (Mpa)	Yield Strength (Mpa)	Elongation at Break (%)	T (tan δ ≥ 0.3 – T_{flow})	ΔT (°C)
DAB-50	14.2	-68	69	67	190 ± 20	9.7 ± 0.9	9.7 ± 0.9	70 ± 10	30-69	39
IPDA-50	12.7	-69	62	57	61 ± 18	1.6 ± 0.6	NA	390 ± 200	10-62	52
MBC-50	15.5	-69	57	56	46 ± 12	3.7 ± 2.4	3.6 ± 2.4	350 ± 110	10-57	47
NORB-50	14.1	-76	105	97	152 ± 15	22.4 ± 5.0	10.7 ± 1.3	500 ± 60	31-105	74

*This approach of evaluating T_{flow} follows De and Gaymans (De 2009).

but it has the lowest elongation at break at 70 %. The Young's modulus and tensile strength of DAB-50 are significantly higher than previously reported values for segmented PHU with HMDA chain extender at 50 wt% hard-segment content, likely due the increased rigidity of DAB molecule and the increase in urethane bond density in the hard segment (Beniah 2016).

IPDA-50 and MBC-50 possess tensile strengths of 1.6 MPa and 3.7 MPa, respectively, with elongation at break of 390% and 350%, respectively. These tensile strength values are lower than that reported by DAB-50, possibly caused by the irregular cyclic structure of the IPDA molecule and dilution of urethane bond density with the MBC molecule. Those effects contribute to a lower density of hydrogen bonding in the hard segment. However, the more compact hard domain in DAB-50 also results in a much lower elongation at break of 70%.

NORB-50 possesses the highest tensile strength of 22.4 MPa, with elongation at break of 500 %, indicating that chain extender with a bulky norbornane ring structure can significantly improve the tensile properties of PHUs. The high tensile properties of NORB-50 could be caused by the norbornane ring acting as additional effective physical crosslinks. Perry et al. investigated a series of polycarbonate thermoplastic elastomers from phenolic-based monomers bearing a bulky, three-dimensional, norbornane ring (Perry 1965). They argued that the norbornane ring acts as an effective physical tie-down point since their elastomers contained no crystalline structure or hydrogen bonding. The ability of the bulky norbornane to act as physical crosslinks can help to restrict the chains from sliding past each other.

To the best of our knowledge, the values described for NORB-50 are the best tensile properties obtained by segmented, nanophase-separated PHUs to date. A study by Kojio et al. on segmented PU with norbornane diisocyanate and BDO chain extender with 50 wt% hard-segment content reported a tensile strength value of 28.4 MPa (with no report of experimental error) and elongation-at-break value of 380% (Kojio 2007). If we assume a 10% experimental error associated with the tensile properties reported by Kojio et al., then within error the tensile

strength of our NORB-50 PHU matches the value for the analogous PU and the elongation-at-break value exceeds that for the analogous PU.

Given the excellent properties of our NORB-50 segmented PHU, we further extended our study by examining the properties at other hard-segment contents ranging from 30 to 47.5 wt%. These PHUs were also characterized by SAXS, DMA, and tensile testing.

Figure 7.1b shows the SAXS data of NORB-30 to NORB-50. All norbornane-based PHUs possess nanophase-separated morphology with interdomain spacings ranging between 12.0 to 14.1 nm, increasing with an increase in hard-segment content. Figure 7.4 shows the temperature dependences of E', E'', and tan δ for NORB-30 through NORB-50, respectively. The soft-segment T_g values evaluated from the E'' peak are ~ - 65 °C whereas the hard-segment T_{flow} values increase with increasing hard-segment content. NORB-30 has the lowest T_{flow} value at 48 °C while NORB-50 has the highest T_{flow} of 105 °C. The increase in T_{flow} is due to a more perfected hard-segment domain and a better degree of nanophase separation at higher hard-segment content. Similar to other PTMO-based PHUs, all norbornane-based PHUs also exhibit potential as excellent damping materials over very broad and tunable temperature ranges. NORB-30 exhibits tan $\delta \geq 0.30$ from -37 to 48 °C, a temperature range of 85 °C. At higher hard-segment content, the range shifts to a higher temperature window; NORB-40 exhibits tan $\delta \geq 0.30$ from -2 to 80 °C, a range of 82 °C. Excellent tunability in the tan $\delta \geq 0.30$ temperature range from as low as -37 °C to as high as 105 °C is obtained with norbornane-based PHUs as a function of hard-segment content from 30 to 50 wt%.

Figure 7.5 shows representative tensile stress-strain curves of NORB-30 through NORB-50, and Table 7.2 summarizes values associated with Young's modulus, tensile strength and elongation-at-break. A broad range of tensile properties is obtained as a function of hard-segment content from 30 to 50 wt% in norbornane-based PHUs. Young's modulus values range from 39 to 152 MPa. Elongation at break decreases with increasing hard-segment content but remains

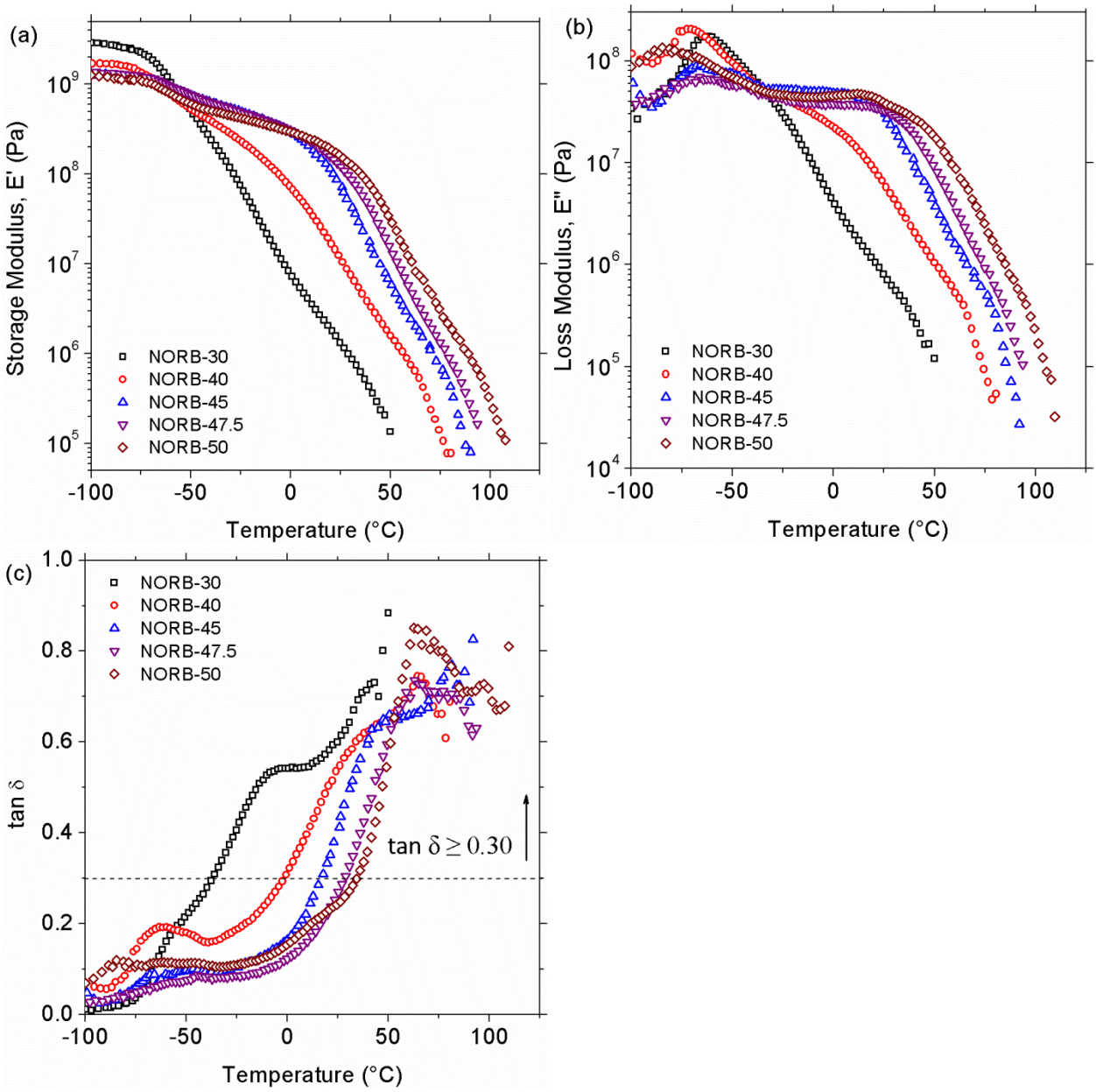

Figure 7.4: Temperature dependence of a) storage modulus (*E*'), b) loss modulus (*E*"), and c) tan δ of PHUs chain extended with norbornane diamine at several hard-segment contents.

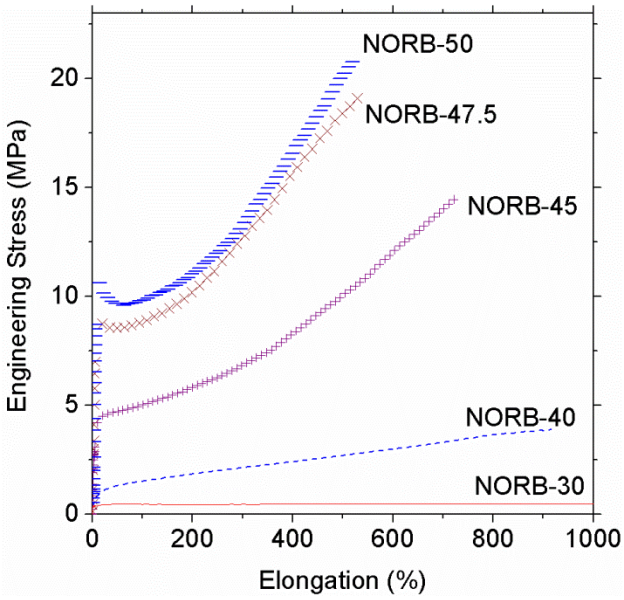

Figure 7.5: Representative stress-strain curves of PHUs chain extended with norbornane diamine at several hard-segment contents.

Table 7.2: Summary of properties of PHUs with norbornane diamine chain extender as a function of hard-segment content.

Sample Name	*d*-spacing (nm)	SS T_g (°C)	T_{flow} (°C)	T_{flow}* (°C) *E'*=0.5 MPa	Young's Modulus (MPa)	Tensile Strength (MPa)	Yield Strength (MPa)	Elongation at Break (%)	T (tan δ ≥ 0.3)-T_{flow} (°C)	ΔT (°C)
NORB-30	12.0	-66	48	38	39 ± 9	0.46 ± 0.05	NA	> 2000	-37-48	85
NORB-40	12.6	-72	80	70	34 ± 4	4.0 ± 0.4	NA	1100 ± 160	-2-80	82
NORB-45	13.2	-70	90	80	98 ± 14	14.4 ± 0.3	NA	720 ± 25	17-90	73
NORB-47.5	14.0	-69	96	86	124 ± 16	20.2 ± 2.4	8.7 ± 0.4	580 ± 30	29-96	67
NORB-50	14.1	-76	105	97	152 ± 15	22.4 ± 5.0	10.7 ± 1.3	500 ± 60	31-105	74

*This approach of evaluating T_{flow} follows De and Gaymans (De 2009).

high even at a 50 wt% hard-segment content. Interestingly, small increases in hard-segment content yield very large increases in tensile strength from 0.46 to 22.4 MPa, with a roughly linear relationship between tensile strength and hard-segment content in the range of 40 to 50 wt%. This result is consistent with the bulky norbornane ring having an important role as a physical tie-down point, in agreement with suggestion by Perry et al. (Perry 1965) In addition to hydrogen bonding among urethane groups, the bulky norbornane ring also prevents chains from sliding past each other. Table 7.2 also indicates that a yield point is present for both NORB-47.5 and NORB-50 but absent at lower norbornane hard-segment content. These results are consistent with the presence of well-percolated hard-segment domains in NORB-47.5 and NORB-50, which would also contribute to an increase in tensile strength (Sheth 2004, Klinedinst 2005).

Our study has demonstrated that chain extender structure and content very significantly affect the properties of segmented PHUs. Among the series of small-molecule diamines studied, the norbornane-based chain extender offers the most significant improvement in the thermal and mechanical properties of the resulting PHUs. In some cases, appropriate choice of chain extender structure and content can lead to PHUs exhibiting tensile properties that, within error, equal or exceed those of analogous PU. Further studies are warranted to explore the effect of norbornane-based chain extender with other soft-segment formulations as well as the effect of crystallizable chain extender in further improving nanophase separation and hard-domain cohesion in segmented PHUs.

7.4 Conclusions

The effects of chain extender structure on the properties of segmented PHUs were evaluated using 1,4-diaminobutane, isophorone diamine, methylene bis(cyclohexyl amine) and bis(aminomethyl) norbornane. The PHUs were synthesized with PTMO-based soft segment and characterized via ^{1}H NMR, FTIR, SAXS, DMA, and tensile testing. All synthesized PHUs

possess nanophase-separated morphology with interdomain spacings of 12-16 nm. DMA results indicate that the nanophase-separated PHUs have broad interphases with a wide range of local compositions, which makes these polymers potentially useful in vibration and acoustic damping applications over very broad ranges of use temperature. The chain extender structure significantly influences thermal and tensile properties of PHUs. For PHUs with 50 wt% hard-segment content, T_{flow} can range from 57 to 105 °C, tensile strength from 1.6 to 22.4 MPa, and elongation at break from 70 to 500% as a function of chain extender structure. Notably, use of a norbornane-based chain extender results in PHU with the best thermal and tensile properties with T_{flow} of 105 °C, tensile strength of 22.4 MPa, elongation-at-break of 500%, and tan $\delta \geq 0.30$ over 74 °C in breadth. Variation in hard-segment content (from 30 to 50 wt%) of norbornane-based PHUs affords extraordinary tunability in tensile strength from 0.5 to 22.4 MPa and in the temperature range associated with good damping properties from -37 to 105 °C.

APPENDIX E

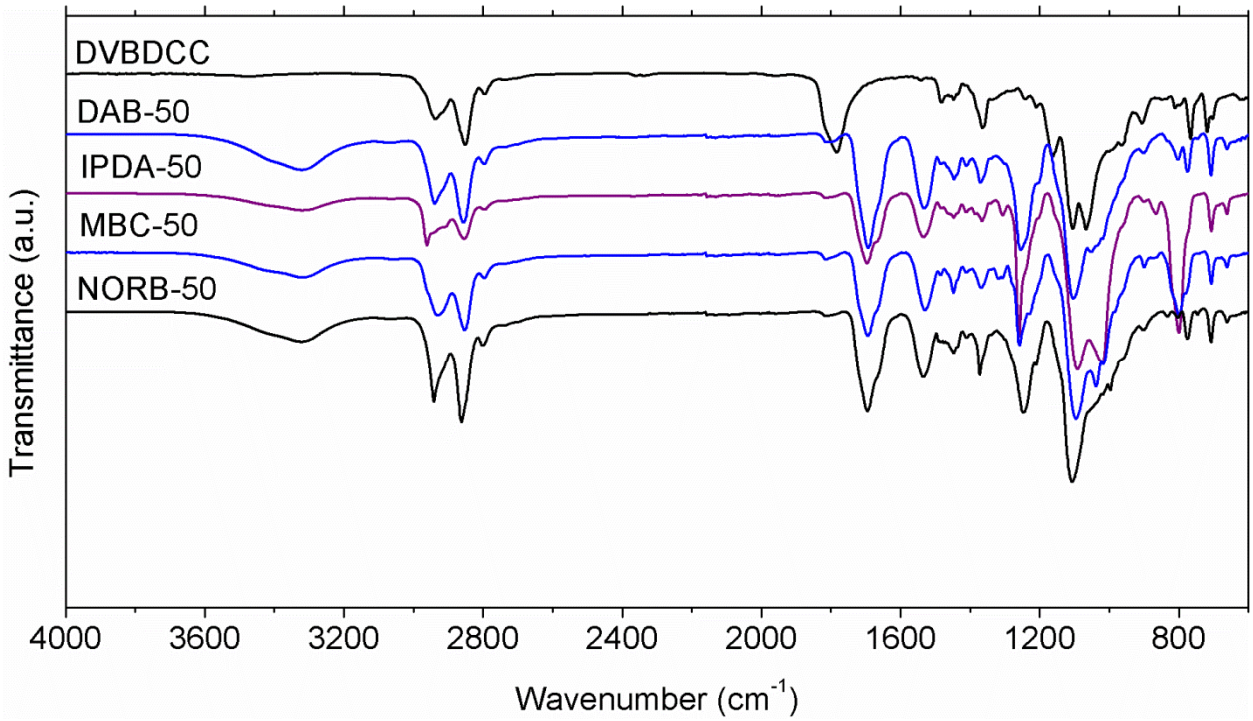

Figure E1: FTIR spectra of PHUs at 50 wt% hard-segment content.

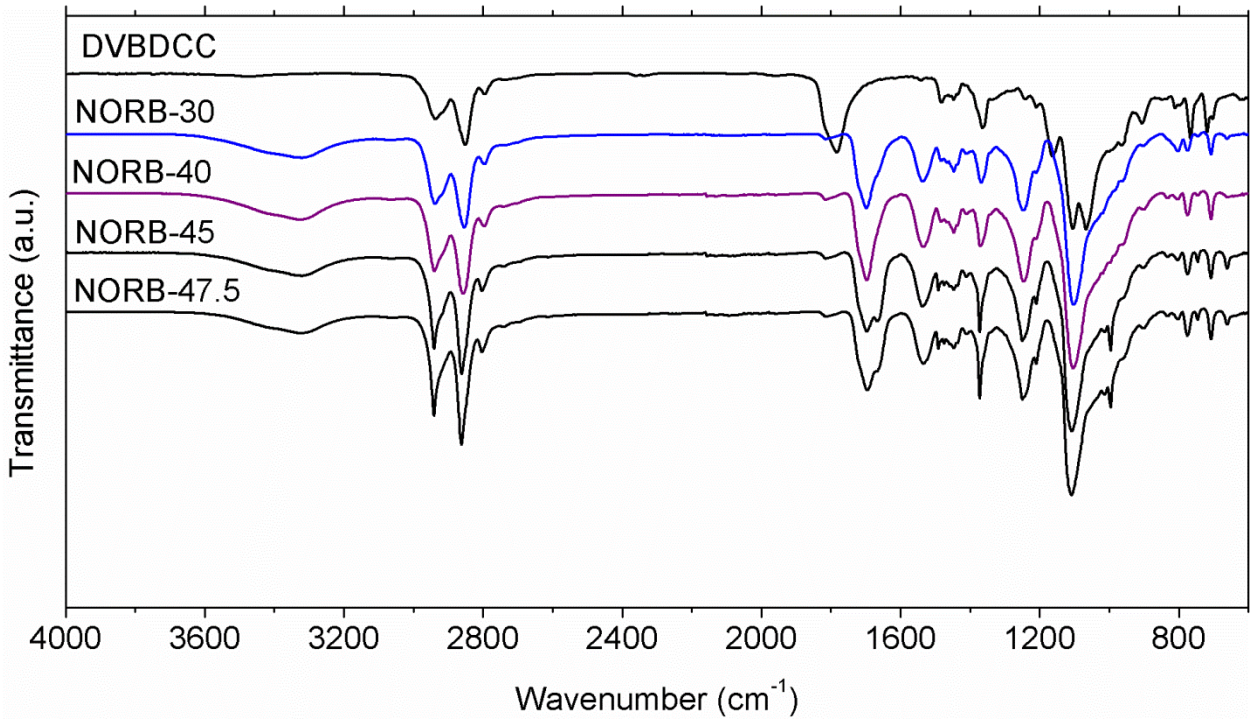

Figure E2: FTIR spectra of norbornane-based PHUs at various hard-segment contents.

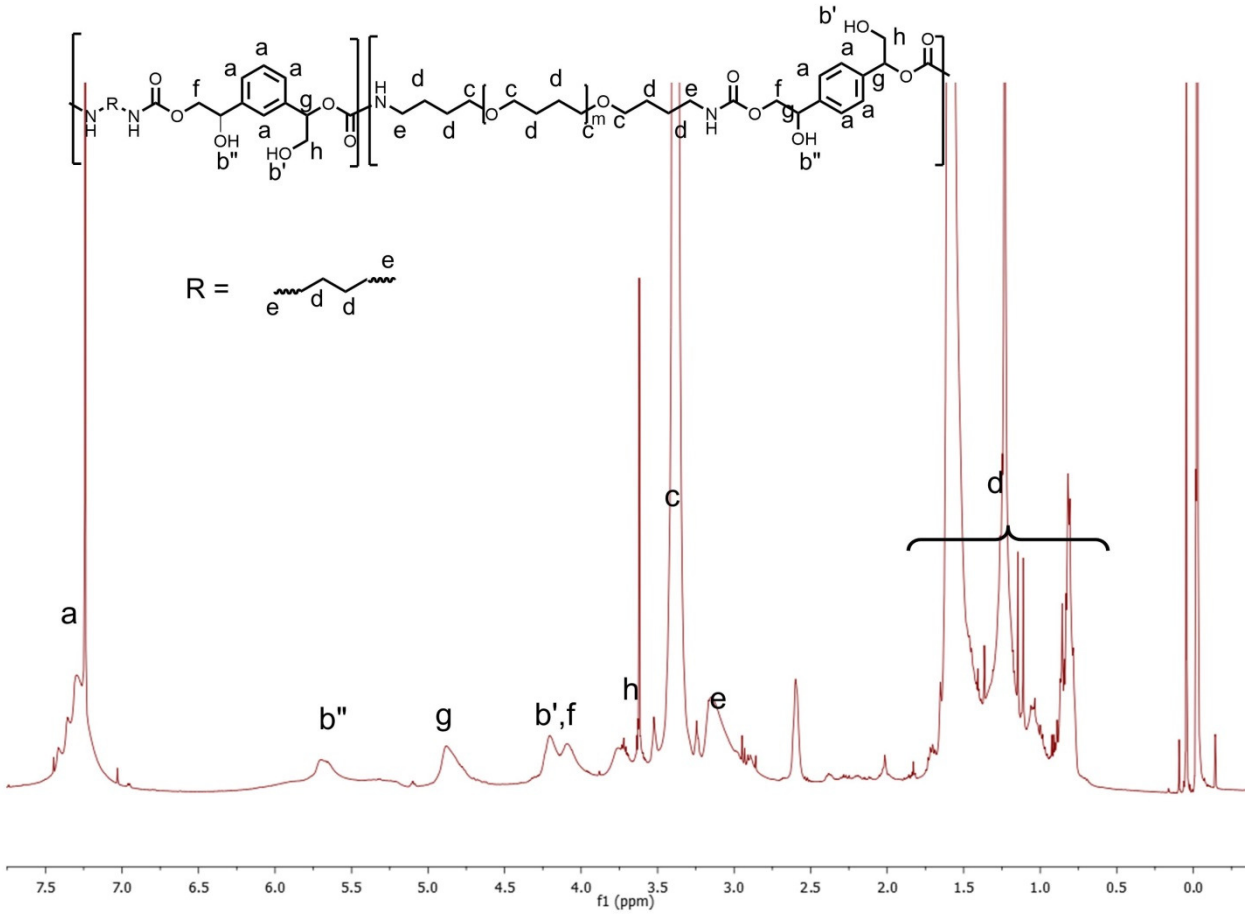

Figure E3: ^{1}H NMR Spectra of DAB-50

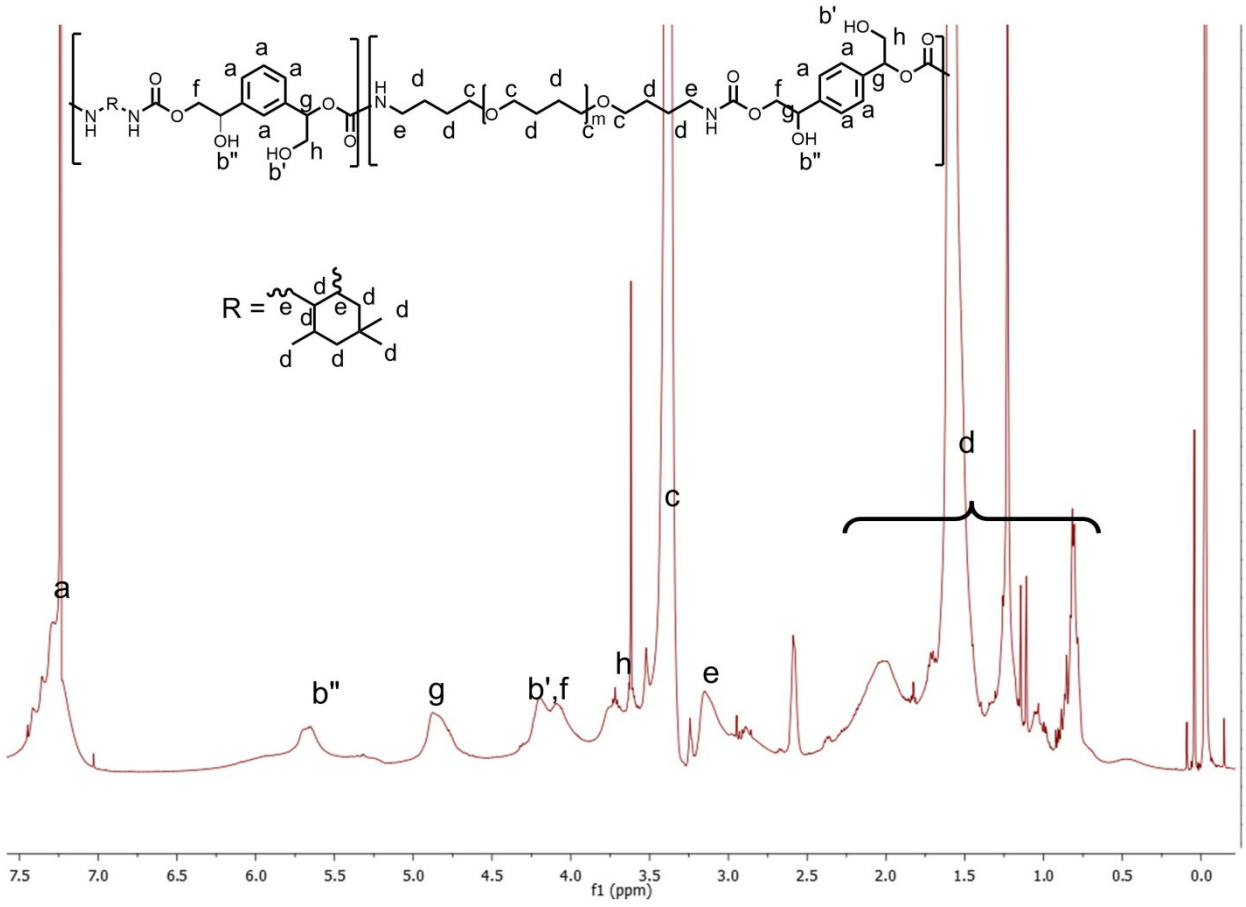

Figure E4: ^{1}H NMR Spectra of IPDA-50

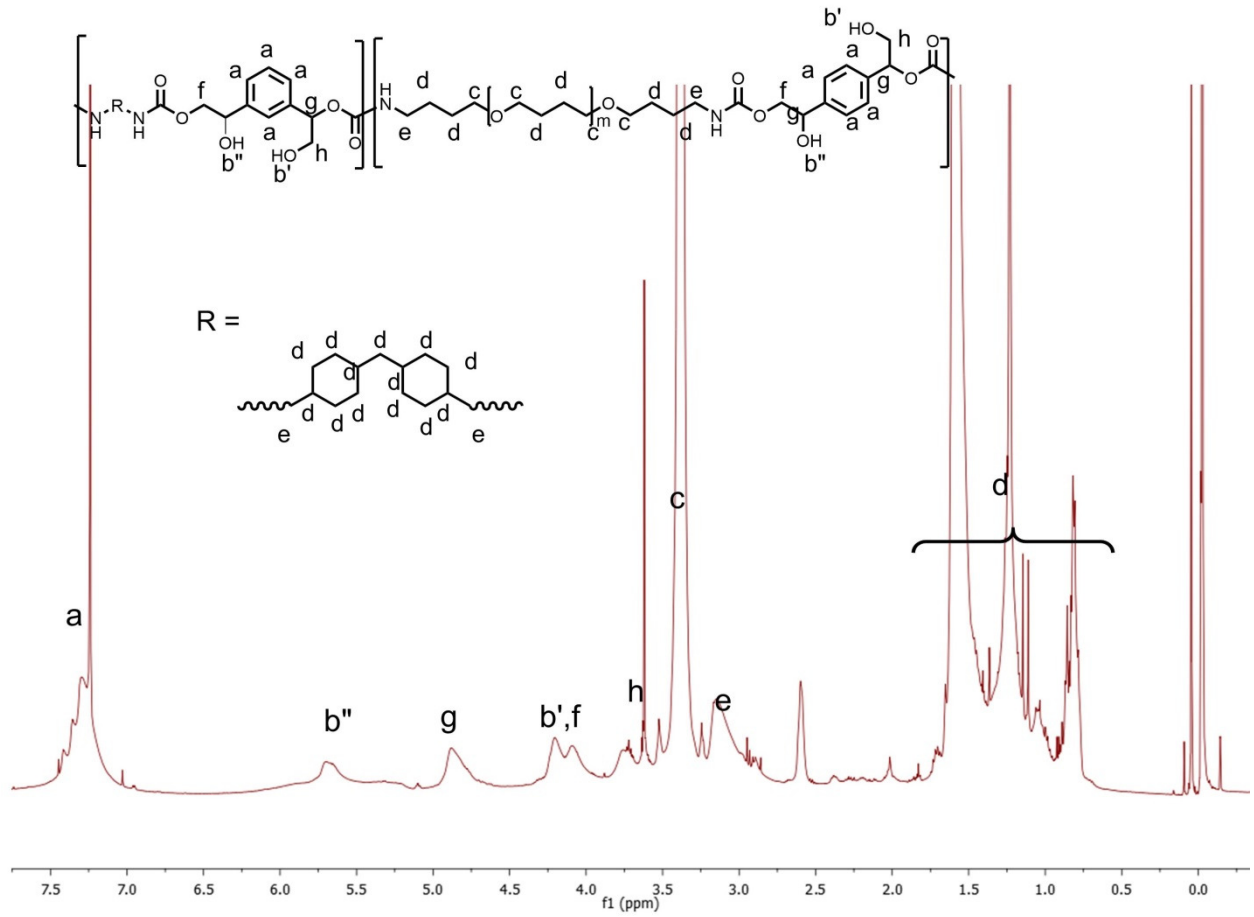

Figure E5: ^{1}H NMR Spectra of MBC-50.

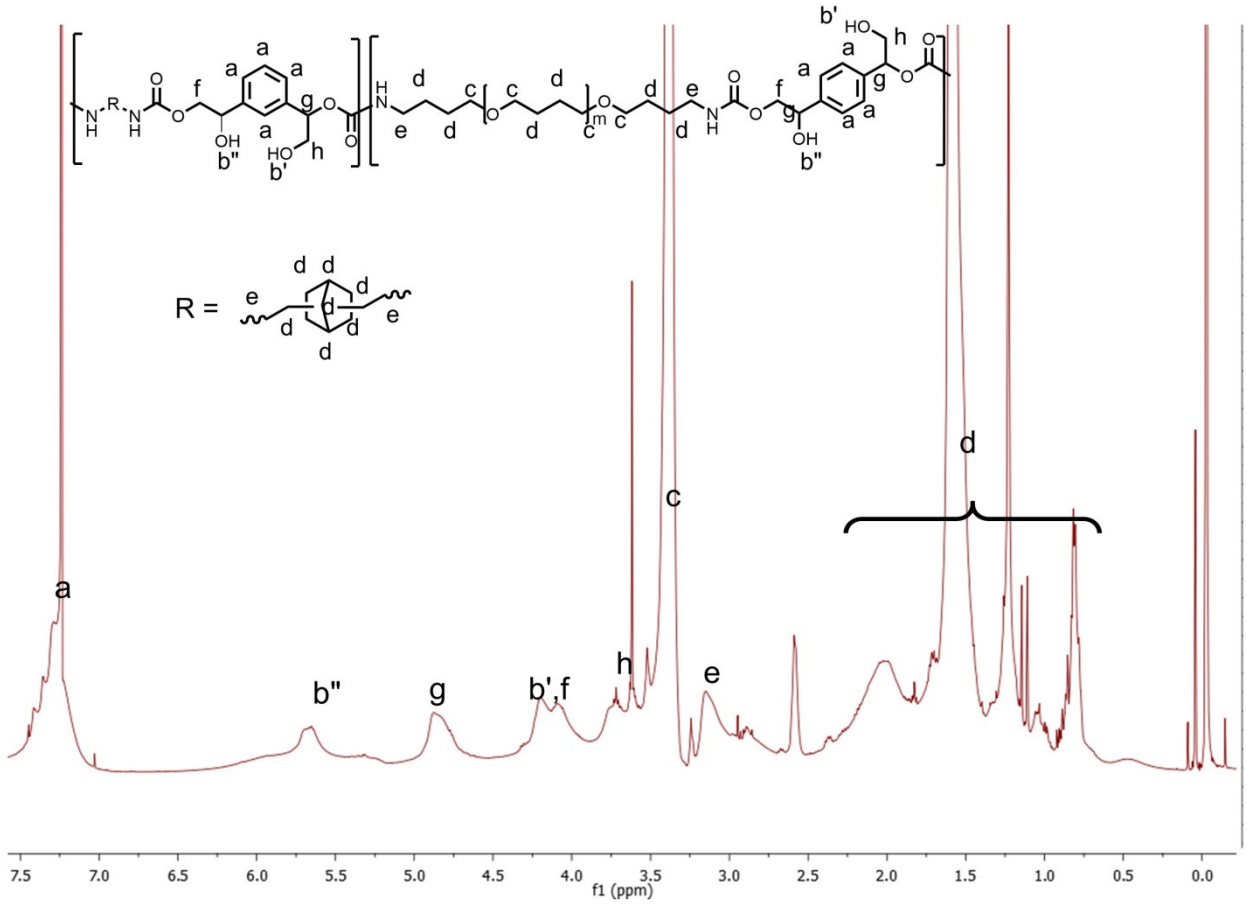

Figure E6: ^{1}H NMR Spectra of NORB-50.

Table E1. Apparent Molecular Weight Averages of PHUs

Sample	M_n (kg/mole)	M_w (kg/mole)	PDI
DAB-50	2.7	16.3	6.1
IPDA-50	2.9	15.2	5.1
MBC-50	3.7	19.0	5.2
NORB-50	3.8	19.9	5.3
NORB-30	3.4	20.9	6.0
NORB-40	3.6	26.8	7.5
NORB-45	3.6	19.7	5.5
NORB-47.5	3.8	21.1	5.6

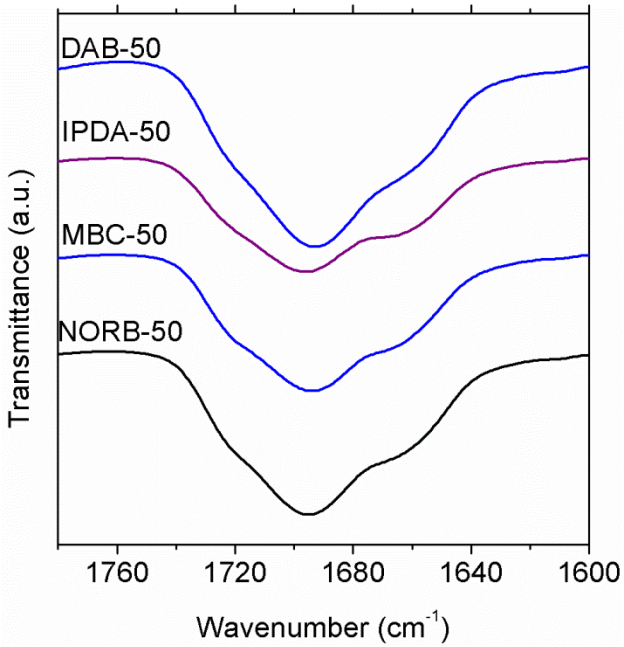

Figure E7. FTIR spectra of the carbonyl regions of PHUs.

CHAPTER 8

Non-Isocyanate Polyurethane Thermoplastic Elastomer: Amide-based Chain Extender Yields Enhanced Nanophase Separation and Properties in Polyhydroxyurethane

8.1 Introduction

Polyurethane (PU), synthesized from a step-growth reaction between isocyanates and alcohols, is one of the most important commodity polymers having a broad range of uses such as foams, elastomers, coatings, films and adhesives (Oertel 1994, Delebecq 2013, Engels 2013, Nohra 2013). With total global production reaching an estimated 18 million tons in 2016, PU ranks sixth in total global polymer production (Delebecq 2013). However, isocyanates are facing increasing regulatory scrutiny across the world, e.g., the United States Environmental Protection Agency and the European Union REACH regulation (Official Journal of European Union 2009, US EPA 2015). Consequently, research and development efforts on non-isocyanate polyurethane (NIPU) materials have intensified in recent years with cyclic carbonate aminolysis leading to polyhydroxyurethane (PHU) as one of the most promising chemistries available (Guan 2011, Kathalewar 2013, Blattmann 2014, Maisonnneuve 2015, Cornille 2016e).

Investigations on PHU synthesis are mostly concerned with cyclic carbonate monomer synthesis, and its subsequent polymerization into single-phase thermoplastics or crosslinked thermosets and reaction catalysis (Kihara 1993, Steblyanko 2000, Tomita 2001a, Tomita 2001b, Tomita 2001c, Tomita 2001d, Tomita 2001e, Yuen 2016, Carré 2016, Mazurek-Budzyńska 2016, Cornille 2016c, Matsukizono 2015, Fortman 2015, Blattmann 2016a, Blattmann 2016b, Blattmann 2016c, Cornille 2016b, Van Velthoven 2015, Rix 2016, Duval 2016, Cornille 2016a, Poussard 2016, Schmidt 2016, Lombardo 2015, Lambeth 2013, Blain 2014, Cornille 2016d). There have been very limited studies on the synthesis of segmented, nanophase-separated PHUs

and on understanding of their structure-property relationships (Nanclares 2015, Leitsch 2016a, Beniah 2016, Zhang 2016, Beniah 2017). Torkelson and coworkers recently reported the synthesis of segmented, nanophase-separated PHUs for thermoplastic elastomer applications (Leitsch 2016a). They found that the hydroxyl groups and the choice of soft segment play a critical role in the development of nanophase separation in polyether-based PHUs. Use of a polyethylene oxide (PEO)-based soft segment resulted in single-phase PHUs due to significant phase mixing caused by hydrogen bonding from hydroxyl groups in the hard segment to ether oxygen in the soft segment. The intersegmental hydrogen bonding can be tuned by providing steric hindrance in the case of polypropylene oxide (PPO)-based soft segment or via dilution of oxygen atom density in the case of polytetramethylene oxide (PTMO)-based soft segment, resulting in nanophase-separated PHUs. Such PHUs with soft segment as the matrix and hard segment as dispersed domains exhibit reversible elastomeric response similar to that of conventional thermoplastic polyurethane (TPU) elastomer (Leitsch 2016a). However, in PTMO-based PHUs, the nanophase separation is accompanied by broad interphases having a wide range of local compositions due to some level of intersegmental hydrogen bonding from the hydroxyl groups to the PTMO soft segments. Dynamic mechanical analysis reveals that these PTMO-based PHUs exhibit tan $\delta \geq 0.30$ over very broad temperature ranges, thus making PTMO-based PHUs potentially useful as effective damping materials over broad temperature ranges (Beniah 2016). Torkelson and coworkers also showed that polybutadiene-co-acrylonitrile (PBN)-based soft segment can produce nanophase-separated PHUs with a much sharper interphase, similar to nanophase separation characteristics of conventional TPUs (Beniah 2017). However, PBN-based soft segment is not a commonly used soft segment in comparison with polyether- or polyester-based soft segments in segmented PU synthesis (Oertel 1994, Delebecq 2013, Engels 2013). Additionally, the thermal and mechanical properties of polybutadiene-based PHUs and segmented PHUs in general are still inferior to conventional TPUs (Yilgor 2009, Yilgor 2006,

Kojio 2007, Klinedinst 2012, Petrovic 1991, Sheth 2005).

Gaymans and coworkers have previously shown that monodisperse, crystallizable, diamine-diamide (DDA) chain extender can be used to drive nanophase separation in segmented PUs and polyamides via hard-segment crystallization (Van der Schuur 2006b, De 2009, Biemond 2008, Biemond 2012, Biemond 2007, Biemond 2010, Biemond 2009, Van der Schuur 2006a, Van der Schuur 2005, Huskens 2009, Huskens 2007, Huskens 2008, Krijgsman 2003, Fukushima 2013). For example, Van der Schuur et al. (Van der Schuur 2006b) synthesized a series of segmented polyurethane-urea-amide (PUUA) copolymers using PPO-based soft segment with 2,4-toluene diisocyanate (TDI) as the hard segment and DDA chain extender (Van der Schuur 2006b). This DDA chain extender was synthesized using dimethyl terephthalate (T) and hexamethylene diamine (6) resulting in a diamine molecule with two amide bonds (6T6) in the center (see Scheme 8.1 for the structure of 6T6 DDA chain extender). Segmented PUs made using 2,4-TDI typically possess amorphous hard segments (Sung 1978, Sung 1977), and thus are not expected to possess crystalline hard domains. However, the reported PUUA copolymers had crystalline hard domains (Van der Schuur 2006b). The PUUA copolymers also exhibited relatively temperature-independent rubbery plateau regions and high flow temperature (T_{flow}) ranging from 103 °C to 264 °C. De and Gaymans (De 2009) also investigated the 6T6-DDA chain extender in segmented PUUAs made from PTMO-based soft segments of several molecular weights and 2,4-TDI. Similar to the study by Van der Schuur et al. (Van der Schuur 2006b), these PUUAs also exhibited crystalline hard domains, wide and relatively temperature-independent rubbery plateau region, as well as high T_{flow} up to 183 °C. Biemond et al. employed a variant of 6T6-DDA chain extender based on adipic acid in the synthesis of segmented PUUA using PTMO-based soft segment and three different diisocyanates (Biemond 2008). All copolymers exhibited crystalline hard domain with T_{flow} values varying across different diisocyanate structures. Given the effect of amide-based chain extender on the physical

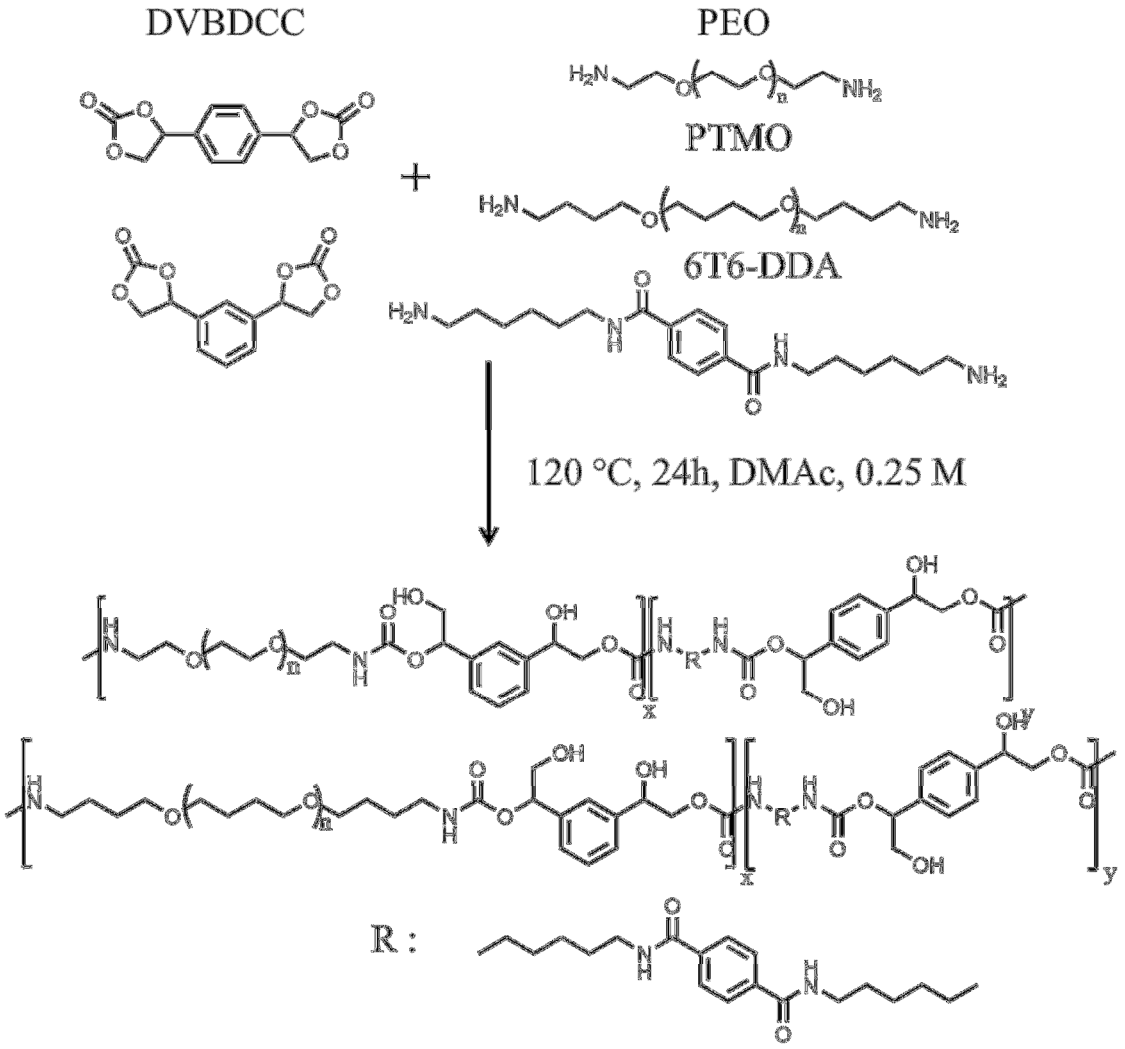

Scheme 8.1: Reaction scheme for the syntheses of PEO- and PTMO-based PHUs with diamine diamide (DDA) chain extender.

properties of segmented PUs, we hypothesized that incorporation of amide-based chain extender into segmented PHU structures can improve nanophase separation characteristics as well as thermal and mechanical properties of segmented PHUs.

Here, we describe our investigation of NIPU thermoplastic elastomers made via cyclic carbonate aminolysis. These segmented PHUs were synthesized using divinylbenzene dicyclocarbonate (DVBDCC) as hard segment, PEO and PTMO as soft segments, and DDA chain extender. Use of DDA chain extender achieves dramatic improvement in nanophase separation and properties of the resulting segmented PHUs relative to segmented PHUs made without DDA chain extender. DDA chain extender yields nanophase-separated PHUs above a certain hard-segment content in PEO-based soft-segment PHUs, previously known to only produce phase-mixed, segmented PHUs (Leitsch 2016a). In PTMO-based soft-segment PHUs, DDA chain extender results in excellent nanophase separation with sharp domain interphase. The PTMO-based PHUs exhibit wide, relatively temperature-independent, rubbery plateau regions characteristic of conventional TPU elastomer, with thermal and mechanical properties that are significantly enhanced relative to PTMO-based PHUs synthesized without DDA chain extender. These PHUs possess T_{flow} values ranging from 115 to as high as 200 °C, tunable mechanical properties with tensile strength ranging from 2.4 to 6.7 MPa, and elastomeric recovery similar to that of conventional TPUs.

8.2 Experimental

8.2.1 Materials

Hexamethylene diamine (98%), dimethyl terephthalate (purum, ≥ 99%), N,N-dimethylacetamide (DMAc, ≥ 99%), dimethyl sulfoxide-d6 (DMSO, 99.9 atom %D), deuterium oxide (D_2O, 99.9 atom %D) were purchased from Sigma-Aldrich. Diamine-terminated polytetramethylene oxide M_n = 1700 g/mole (Elastamine™ HT-1700), diamine-terminated

polyethylene oxide M_n = 1700 g/mole (Elastamine™ HE-1700) were supplied by Huntsman Chemical. Divinylbenzene dicyclocarbonate (DVBDCC) was synthesized according to the procedure outlined in Chapter 3 (Leitsch 2016a).

8.2.2 Synthesis of Diamine Diamide Chain Extender

DDA chain extender was synthesized using a slightly modified procedure by Krijgsman et al. (Krijgsman 2003) Hexamethylenediamine (19.72 g, 170 mmol) was added to a round-bottom flask under nitrogen. The flask was heated to 80 °C to melt the hexamethylenediamine. Solid dimethyl terephthalate (4.063 g, 20.9 mmol) was subsequently added. The mixture initially became homogeneous and was allowed to stir at 80 °C for 6 h, as a white precipitate slowly formed. The resulting mixture was poured into tetrahydrofuran (600 ml) and allowed to stir for 30 min. The resulting precipitate was filtered and recrystallized from dioxane (800 ml) to give the product as a white solid (3.56 g, 47%).

8.2.3 Synthesis of PHUs

All PHUs were synthesized according to Scheme 8.1. Table 8.1 and Table 8.2 list all PHUs and the ratio of hard segment, soft segment, and chain extender used in the formulations. The hard-segment content is defined as (weight of DVBDCC + weight of DDA chain extender)/(total weight of material). In a typical synthesis of PTMO3, 1 g of DVBDCC (3.99 mmole), 482.9 mg of DDA (1.33 mmole), and 4.2 g of Elastamine™ HT-1700 (2.66 mmole) were combined in a 20-mL scintillation vial. Then, 10.3 mL of DMAc was added to dissolve the reactants and adjust the carbonate concentration to 0.25 M. The mixture was reacted at 120 °C for 24 h. After 24 h, the polymer solution was poured into a cup and dried at 80 °C for 24 h.

8.2.4 Characterizations

Table 8.1: Summary of properties of PEO-based PHUs.

Sample Name	Molar Ratio HS/CE/SS	% HS	SS T_g (°C)	T_{flow} (°C)	*d*-spacing (nm)
PEO1	1.5/0.5/1	24.7	-28[a]	31	-
PEO2	2/1/1	33.7	-49	115	14.8
PEO3	2.5/1.5/1	40.8	-46	147	16.2

[a]This value reflects the T_g of the single-phase system.

Table 8.2: Summary of properties of PTMO-based PHUs.

Sample Name	Molar Ratio HS/CE/SS	% HS	SS T_g (°C)	T_{flow} (°C)	*d*-spacing (nm)	Young's Modulus (MPa)	Tensile Strength (MPa)	Elongation at break (%)
PTMO1	1.25/0.25/1	19.2	-65	126	19.3	6.6 ± 0.7	2.4 ± 0.6	330 ± 130
PTMO2	1.33/0.33/1	21.0	-65	158	20.6	13.7 ± 3.5	3.0 ± 0.4	330 ± 80
PTMO3	1.5/0.5/1	24.7	-64	167	20.6	21.4 ± 1.9	3.9 ± 0.6	300 ± 100
PTMO4	2/1/1	33.7	-64	200	19.9	43.2 ± 13.5	6.7 ± 1.4	320 ± 90

^{1}H NMR spectra were obtained using a Bruker Avance III 500 MHz NMR spectrometer with a direct cryoprobe at room temperature and deuterated DMSO as solvent. Spectra were reported in parts per million relative to tetramethylsilane. Proton-decoupled ^{13}C-NMR spectra were obtained using a Bruker Avance 500 MHz w/ direct cryoprobe (126 MHz).

Attenuated total reflectance-Fourier transform infrared (ATR-FTIR) spectroscopy was performed with a Bruker Tensor 37 MiD IR FTIR spectrophotometer equipped with a diamond/ZnSe attachment. All PHUs were scanned at a resolution of 4 cm^{-1}; 32 scans were collected in the 4000-600 cm^{-1} range. The conversion of the starting materials was determined by analyzing carbonate group conversion at ~1780 cm^{-1}.

SAXS experiments were performed using a Rigaku S-MAX 3000 SAXS system emitting X-rays with a wavelength of 0.154 nm (Cu-Kα). The SAXS system was calibrated with silver behenate. The sample-to-detector distance was 1640 mm. The 2D scattering patterns were collected and azimuthally averaged using Fit2D software (from the European Synchrotron Radiation Facility website) to produce 1-D plots of intensity versus scattering vector q, where $q = 4\pi(\sin\theta)/\lambda$; θ is one-half of the scattering angle, and λ is the X-ray wavelength.

The DMA results were obtained using a TA Instruments Rheometrics Stress Analyzer-GIII. Rectangular specimens measuring 8.0 mm in width and 0.9 mm in thickness were cooled with N_2 gas to -100 °C for PTMO-based PHU and to -80 °C for PEO-based PHU. Temperature sweep experiments were conducted until 200 °C at a heating rate of 3 °C/min or until the sample flowed out of the grips. Measurements were conducted in tensile mode at a frequency of 1 Hz and a strain of 0.03%, resulting in characterization of storage modulus (E'), loss modulus (E") and loss tangent (tan δ). The soft-segment T_g was identified from the peak maximum in E"; the flow temperature was defined as the onset of inconsistent tan δ data, close to the temperature at which the sample was no longer mechanically robust. Differential scanning calorimetry was performed using a Mettler Toledo DSC 822e. Samples were cooled to -50 °C and heated at 10

°C/min to 200 °C.

Tensile testing was performed according to ASTM D1708 using an MTS Sintech 20/G tensile tester. Dog bone-shaped samples (4.7 mm x 1.0 mm x 22 mm) were cut using a Dewes-Gumbs die from dried sheets and an extension rate of 130 mm/min. The Young's modulus, tensile strength and elongation at break were reported as average values of five specimens. Error represents one standard deviation. Hysteresis testing was performed on PTMO-based PHUs. Dog bone-shaped samples were stretched to 100 % strain at a cross-head speed of 130 mm/min and returned to 0 % strain. Ten cycles were performed with a 5-min interval between cycles.

8.3 Results and Discussion

Here, we describe the effects of amide-based chain extender on the nanophase separation and properties of segmented PHUs made using PEO- and PTMO-based soft segments. Significant phase mixing resulting in single-phase materials was previously observed in PEO-based PHUs due to hydrogen bonding from the hydroxyl groups to highly-densed ether oxygen in PEO-based soft segment (Leitsch 2016a). This intersegmental hydrogen bonding was shown to be tunable diluting the oxygen atom density with PTMO-based soft segment, resulting in nanophase-separated PHUs with broad interphases having a wide range of local composition (Beniah 2016).

The synthesis of DDA chain extender follows a procedure reported by Krijgsman et al. (Krijgsman 2003) Its successful synthesis was confirmed via ^{1}H NMR and ^{13}C NMR spectroscopy. Figures F1-F2 in Appendix F show the ^{1}H NMR spectra, and Figures F3-F4 in Appendix F show the ^{13}C NMR spectra of the DDA chain extender. The ^{1}H and ^{13}C NMR data are consistent with those reported in literature (Fukushima 2013).

The successful synthesis of PHUs was confirmed via FTIR and NMR spectroscopies. The FTIR spectra of PEO-based and PTMO-based PHUs, plotted with the spectrum of DVBDCC, are

shown in Figure F5 and Figure F6, respectively. (See Appendix F.) The disappearance of the carbonate carbonyl stretching peak at ~1780 cm^{-1} indicates the complete conversion within experimental error of carbonate functional groups into urethane linkages. Peaks associated with the stretching of free and hydrogen-bonded urethane carbonyls (1730-1700 cm^{-1}) are present. Amide carbonyl stretching peaks, associated with the DDA chain extender, appear as a shoulder at 1665 cm^{-1} for free, non-hydrogen bonded carbonyl and as a sharp peak at 1625 cm^{-1} for hydrogen-bonded carbonyl, indicating successful incorporation of DDA chain extender into the polymer chains. Amide N-H stretching appears as a sharp peak at ~3290 cm^{-1}, and the hydroxyl group (O-H) stretch appears as a broad shoulder near 3400 cm^{-1}. This shoulder is more apparent in PEO-based PHUs than in PTMO-based PHUs as there is a higher concentration of hydroxyl groups due to the higher hard-segment contents investigated in PEO-based PHUs. Representative ^{1}H NMR spectra of PEO- and PTMO-based PHUs are also provided in Figures F7 and F8, respectively, along with the assignments of various protons within the polymer chain. (See Appendix F.)

We used SAXS to probe the presence of nanophase-separated morphology in all PHUs. Figure 8.1 shows room-temperature SAXS results of PEO-based PHUs. The PEO1 sample, with 24.7 wt% hard segment, exhibits no scattering peak, consistent with the absence of significant nanophase separation. This is similar to our previous observation for PEO-based PHUs synthesized at 30 wt% hard-segment content without amide chain extender (Leitsch 2016a). However, with increasing hard-segment content, PEO2 with 33.7 wt% hard segment and PEO3 with 40.8 wt% hard segment show single SAXS peaks consistent with the presence of nanophase separation. Although it is difficult to assign exact SAXS peak locations for PEO2 and PEO3, the results are consistent with interdomain spacings of ~15 nm. These results indicate that DDA chain extender is capable of driving nanophase separation in PEO-based segmented PHUs, which otherwise have been found to be single-phase materials due to major intersegmental

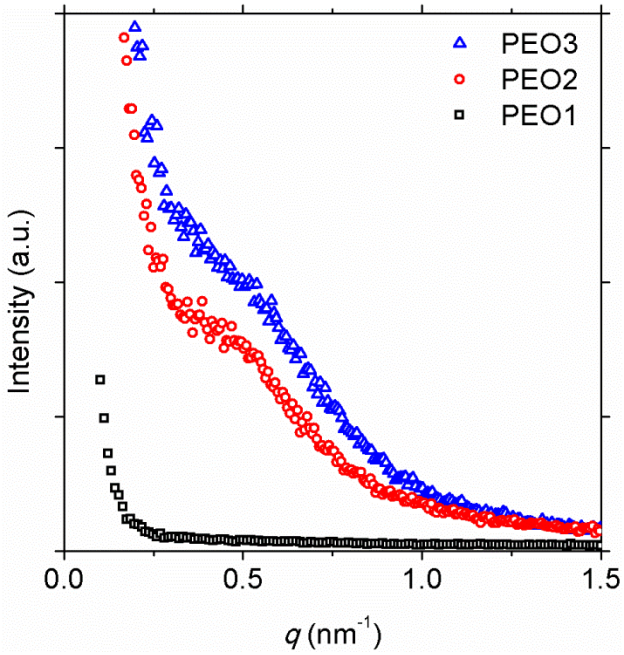

Figure 8.1: SAXS patterns of PEO-based PHUs.

hydrogen bonding between hard-segment hydroxyl groups and ether oxygen in PEO-based atoms (Leitsch 2016a).

The thermomechanical properties of PEO-based PHUs were characterized with DMA. Figure 8.2 shows the temperature dependences of storage modulus (*E*'), loss modulus (*E*") and tan δ of PEO1, PEO2, and PEO3. The DMA results are in agreement with SAXS measurements. The DMA profile of PEO1 (Figure 8.2a) indicates that PEO1 lacks significant nanophase separation, exhibiting a single T_g (via the peak in *E*") at -28 °C, far above the T_g of the pure PEO soft segment (~ -57 °C) (Hood 2010). With increasing temperature and following the initial drop in *E*', PEO1 maintains its mechanical integrity because the PEO soft segment is crystalline. However, as the crystalline PEO melts, *E*' experiences a major drop off, and PEO1 loses its mechanical robustness at 31 °C.

In sharp contrast, as shown in Figures 8.2b and 8.2c, PEO2 and PEO3 maintain their mechanical integrity at high temperature far above the melting temperature of soft segment. This behavior indicates that there are hard-segment domains within the soft-segment matrix that have high thermal transitions, consistent with the existence of nanophase-separated structures. Upon passing the PEO melt transition with increasing temperature, PEO2 exhibits a relatively temperature-independent, rubbery plateau region of roughly 40 °C in breadth, starting from about 38 °C. This is followed by a further drop in *E*' until T_{flow} is reached at 115 °C due to the thermal transition of the hard segment. In PEO3, following the initial decrease due to soft-segment T_g, *E*' experiences an upturn, likely due to cold crystallization of the PEO soft segment. Soft-segment cold crystallization has been observed in phase-separated, PEO-based segmented PUs for PEO with molecular weight above 1000 g/mole (Huskens 2007). Thus, it is reasonable to expect cold crystallization in our PHU systems, which are made with PEO with M_n = 1700 g/mole. Similar to PEO2, PEO3 also exhibits a wide and relatively temperature-independent rubbery plateau region starting from about 38 °C, extending over a slightly broader temperature range than PEO2. This

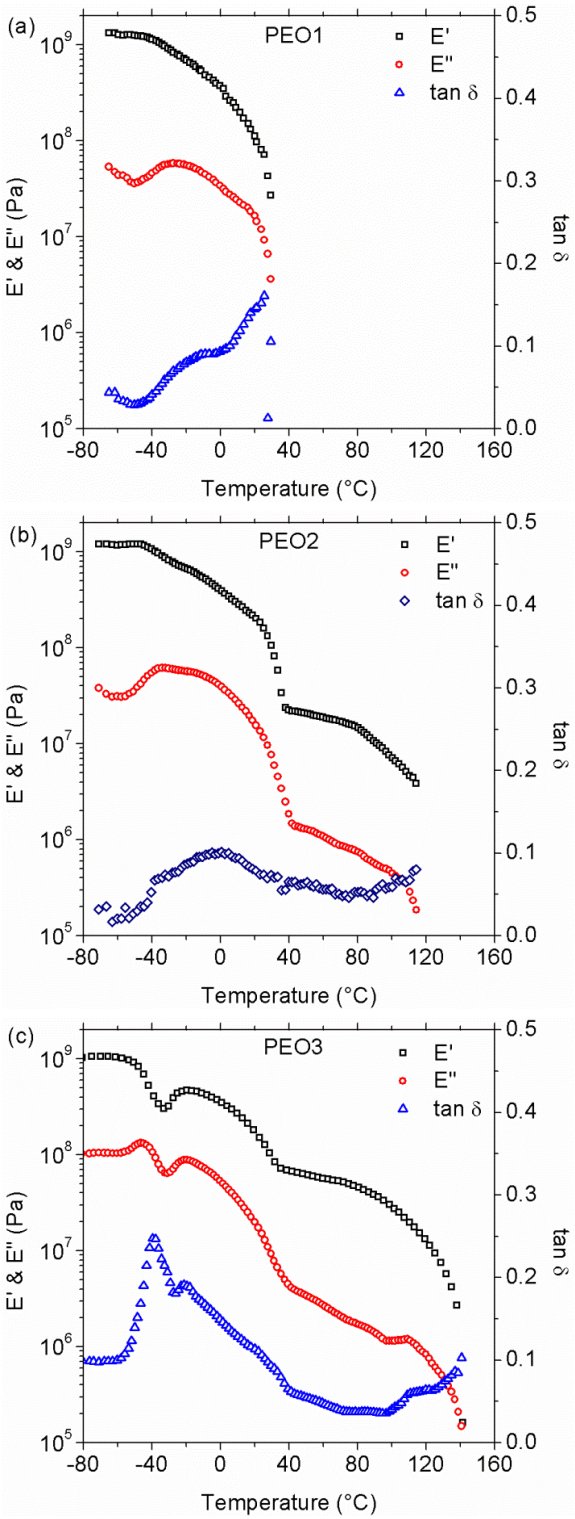

Figure 8.2: Temperature dependences of tensile storage modulus (*E*'), loss modulus (*E*''), and tan δ of a) PEO1, b) PEO2, and c) PEO3.

is followed by a gradual decrease in E' until T_{flow} is reached at 147 °C. As expected with increasing hard-segment content, PEO3 exhibits a higher rubbery plateau modulus and a higher T_{flow} value than PEO2.

The presence of relatively temperature-independent rubbery plateau regions in PEO2 and PEO3 means that DDA chain extender can produce nanophase-separated, PEO-based PHUs with sharp domain interphase. This is in sharp contrast with earlier results by Torkelson and coworkers who showed that nanophase separation is not obtained in segmented, PEO-based PHUs that were synthesized without DDA chain extender (Leitsch 2016a). These results indicate that the presence of DDA chain extender in the hard segment affords significant improvement in nanophase separation and thermal properties of PEO-based PHUs. The amide linkages in DDA chain extender lead to stronger hydrogen bonding in the hard segment, thereby overcoming the competing effect of intersegmental hydrogen bonding from the hydroxyl groups. Thus, PEO2 and PEO3 represent the first segmented, nanophase-separated PHUs made with PEO-based soft segment to exhibit nanophase-separation characteristics comparable to those of conventional thermoplastic PU elastomers.

FTIR has been widely employed to investigate the nature of hydrogen bonding and the extent of nanophase separation in segmented PUs (Huskens 2008, Krijgsman 2003, Fukushima 2013, Sung 1978). A peak associated with free, non-hydrogen bonded carbonyl typically appears at ~1730 cm^{-1} whereas that associated with hydrogen bonded carbonyl appears at ~1700 cm^{-1} (Huskens 2008, Krijgsman 2003, Fukushima 2013, Sung 1978, Sung 1977, Hood 2010). Figure 8.3 shows the FTIR spectra of PEO-based PHUs in the carbonyl regions. In our PHUs, the free carbonyl appears at ~1720 cm^{-1} whereas the hydrogen-bonded carbonyl appears at ~1695 cm^{-1}. In PEO1, the proportion of free carbonyl is higher than that of hydrogen-bonded carbonyl, consistent with major phase mixing. However, the proportion of hydrogen-bonded carbonyl relative to the free carbonyl increases with increasing hard-segment content in PEO2 and PEO3,

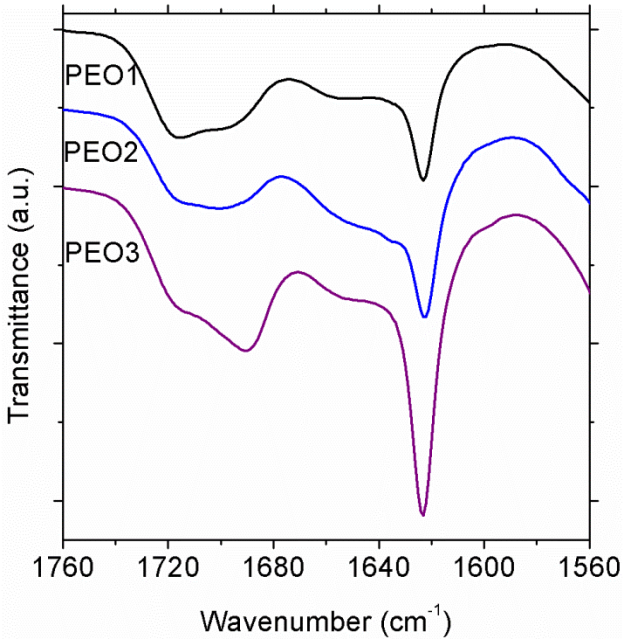

Figure 8.3: FTIR spectra of PEO-based PHUs in the carbonyl regions.

providing the molecular basis for the improvement in phase separation. The amide carbonyl stretching bands also appear as shoulders at ~1660 cm^{-1} for free amide and as sharp peaks at ~1625 cm^{-1} for hydrogen bonded amide. The intensity of hydrogen-bonded amide also increases as the hard-segment content is increased from PEO1 to PEO3.

We further investigated the effect of DDA chain extender in PTMO-based PHUs. We synthesized four PTMO-based PHUs with hard-segment contents ranging from 19.2 wt% to 33.7 wt%. (See Table 8.2 for exact compositions.)

Figure 8.4 shows the SAXS patterns of PTMO1 to PTMO4. All PTMO-based PHUs exhibit single scattering peaks indicating that all are nanophase-separated PHUs. The interdomain spacings of these PHUs are roughly 20 nm. Stronger nanophase separation can be expected from the reduced density of oxygen atom content in PTMO-based soft segment relative to PEO-based soft segment. Additionally, the presence of DDA chain extender, which yielded significant improvement in nanophase separation in PEO-based PHUs, will further improve the nanophase separation in PTMO-based PHUs.

Figure 8.5 shows the DMA results of the four PTMO-based PHUs. The soft-segment T_gs (as made evident by *E*" peaks) appear at ~-65 °C. Following the initial decrease due to the soft-segment glass transitions, *E*' exhibits another upturn, caused by cold crystallization of the PTMO soft segment, and then decreases further at slightly below room temperature due to the melting of PTMO soft segment. All PTMO-based PHUs exhibit relatively wide and temperature-independent rubbery plateau regions of at least 75 °C in breadth. The rubbery plateau modulus and the values of T_{flow} increase with increasing hard-segment content, with T_{flow} values ranging from 126 to 200 °C.

It is worth noting that the presence of rubbery plateau regions in PTMO1 to PTMO4 means that they possess nanophase separation characteristic of systems with sharp domain interphases, qualitatively similar to that of conventional, isocyanate-based TPUs (Yilgor 2006,

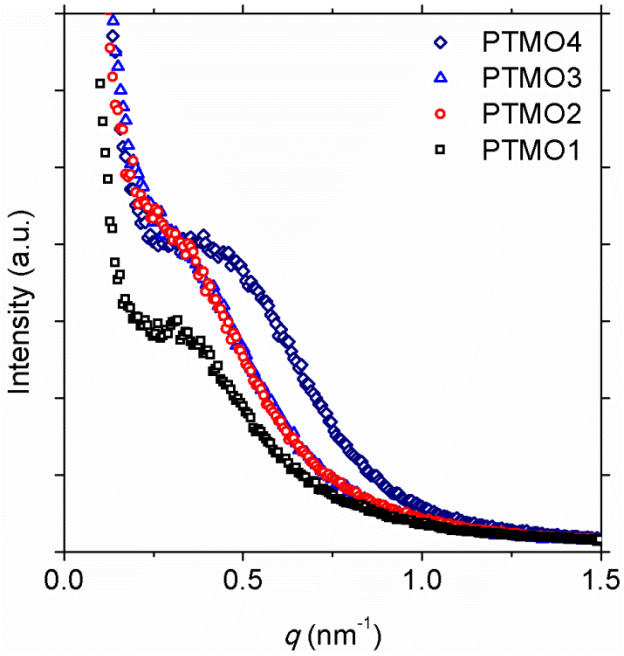

Figure 8.4: SAXS patterns of PTMO-based PHUs.

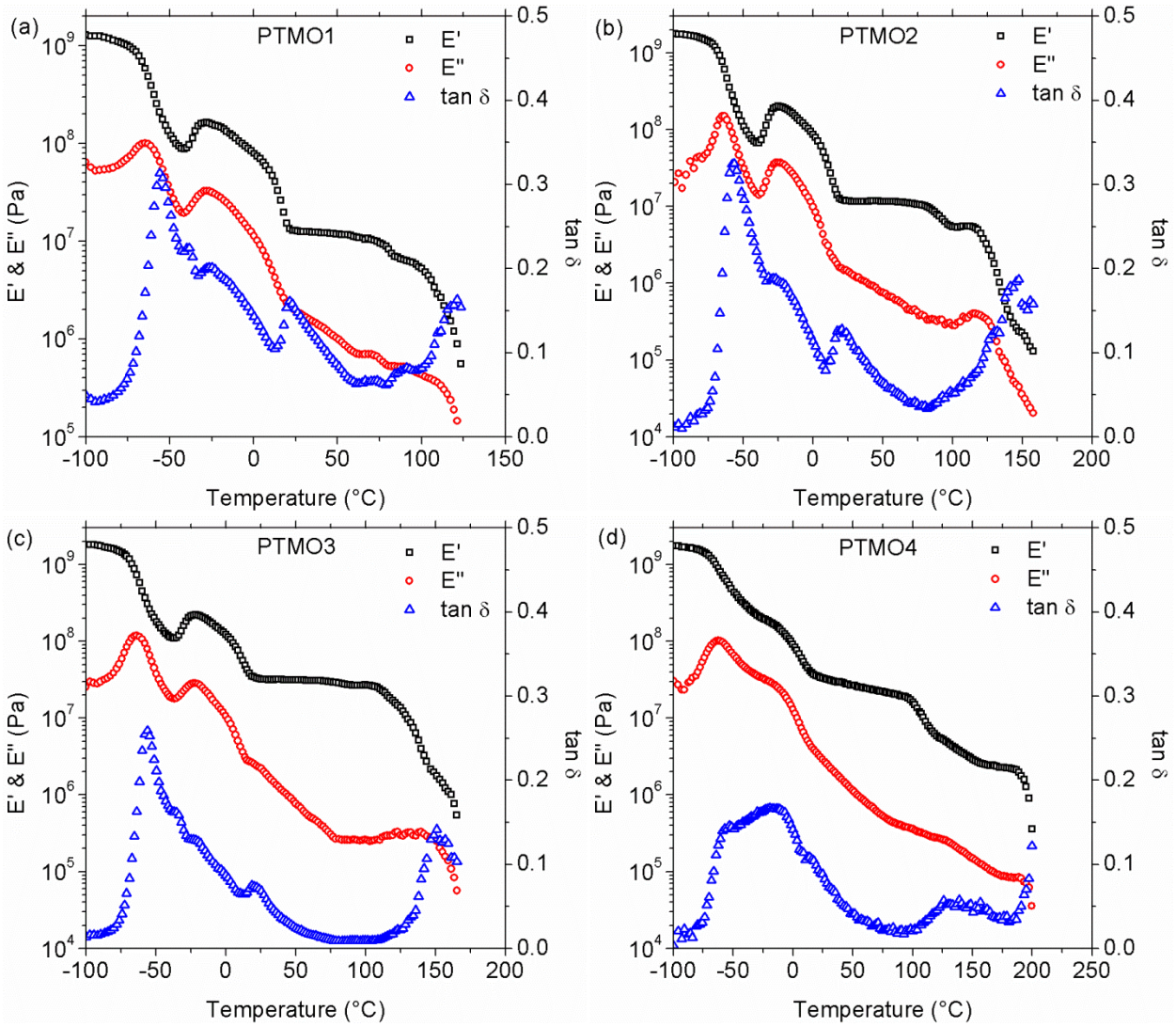

Figure 8.5: Temperature dependences of tensile storage modulus (*E*'), loss modulus (*E*''), and tan δ of a) PTMO1, b) PTMO2, c) PTMO3, and d) PTMO4.

Yilgor 2009, Kojio 2007, Klinedinst 2012, Petrovic 1991, Sheth 2005). This behavior is significantly different from response seen in PTMO-based PHUs synthesized without DDA chain extender (Beniah 2016). Torkelson and coworkers recently reported the synthesis and characterization of a PTMO-based PHU series using DVBDCC as hard segment and several diamine molecules as chain extenders (Beniah 2016). As a comparison, the DMA profile of a PHU sample made with hexamethylene diamine at 30 wt% hard-segment content (with very similar composition to PTMO4) is provided in Figure F10 in Appendix F. Figure F10 in Appendix F shows that nanophase separation of this PHU is accompanied with broad interphases having a wide range of local composition, resulting from some level of phase mixing from the hard-segment hydroxyl groups forming hydrogen bonds to ether oxygen in the soft segment. Figure F10 shows that *E*' exhibits a very gradual decrease with increasing temperature starting from the soft-segment T_g until the hard-segment T_{flow} without any rubbery plateau region, consistent with behavior of a nanophase-separated system with broad interphases (Mok 2008). In contrast, all PTMO-based PHUs synthesized with DDA chain extender exhibit sharp thermal transitions and relatively temperature-independent rubbery plateau regions. Thus, by incorporating amide linkages interspersed among hydroxyurethane linkages in the hard segment via the use of DDA chain extender, nanophase separation can be significantly improved. In the case of the PTMO1 PHU, as little as one amide linkage per every five hydroxyurethane linkages is sufficient to achieve this effect. It is likely that an even smaller proportion of amide linkage may be sufficient. Further study is warranted to investigate this limit.

Another important point to note is that the thermal properties achieved by PTMO1 to PTMO4 are far superior in comparison with other PTMO-based PHUs and PBN-based PHUs reported to date made without DDA chain extenders (Nanclares 2015, Leitsch 2016a, Beniah 2016, Beniah 2017, Zhang 2016). The highest T_{flow} value attained for PTMO-based PHUs is 105 °C as reported in Chapter 7. In PBN-based PHUs with nanophase separation characteristic

similar to that of conventional TPU elastomer, the highest T_{flow} value reported is 73 °C (Beniah 2017). Nanclares et al. (Nanclares 2015) reported a hard-segment T_g of 47 °C for a segmented PHU system made with PTMO, Bisphenol A dicarbonate, and m-xylylene diamine at 70 wt% hard segment. In contrast, all PTMO-based PHUs with DDA chain extender exhibit significantly higher T_{flow} values ranging from 126 to 200 °C and the T_{flow} values of nanophase-separated, PEO-based PHUs range from 115 to 147 °C. Thus, the use of DDA chain extender dramatically improves the thermal properties of segmented PHUs. Equally important is the fact that the T_{flow} values obtained by segmented NIPUs in this study are comparable to those of conventional TPUs (Kojio 2007, Klinedinst 2012, Sung 1978, Sung 1977, Hood 2010). These results indicate that incorporating DDA chain extender is a good strategy in designing NIPU materials with both nanophase separation and thermal properties comparable to TPU elastomers.

The significantly enhanced thermal properties of segmented PHUs made with DDA chain extenders, as evidenced by their high T_{flow} values, can be ascribed to the high melting points of their semi-crystalline hard segments. Gaymans and coworkers have studied several amide-based chain extenders in segmented PU synthesis. Use of DDA chain extender in their system yields crystalline hard domains in PUs made with 2,4-TDI, which usually possess amorphous hard segments (Sung 1978, Sung 1977). Figure F11 (see Appendix F) shows the DSC thermograms of our PTMO-based PHUs from the first heating cycle, which clearly indicate the presence of crystalline hard domains. Since the entalphy of purely crystalline hard-segment homopolymer is unknown, our explanation of the DSC results will be relatively qualitative. Several melting exotherms centered around 108, 131, and 172 °C are observed. These exotherms are likely due to the melting of different crystal structures. The exotherms are less obvious for low hard-segment content materials but become more pronounced as the hard-segment content increases especially in the case of PTMO4. These temperatures correspond well to the onset of flow seen with DMA in Figure 8.5. The DSC thermograms also show cold crystallization and melting events from -41

to 21 °C, associated with the PTMO soft segment. These results explain the upturn in *E*' at temperatures above the soft-segment T_g and the subsequent drop in *E*' seen with DMA results in Figure 8.5. Figure F12 (see Appendix F) shows the DSC thermograms of PEO-based PHUs. Similar to PTMO-based PHUs, PEO-based PHUs also exhibit signatures of melting transition at elevated temperatures, which correspond well with the onset of flow as judged from the DMA results in Figure 8.2. The DSC results together with other characterization results indicate that the regular structure of amide-based segments in the DDA chain extender helps to drive hard-segment crystallization, thereby resulting in significantly enhanced nanophase separation and thermal properties over PHUs made without DDA chain extender.

The mechanical properties of PTMO-based PHUs were evaluated with uniaxial tensile testing. Figure 8.6 shows the representative tensile stress-strain curves of PTMO-based PHUs, reflecting their elastomeric-like tensile response. Table 8.2 summarizes the values associated with Young's modulus, tensile strength and elongation at break. These PHUs possess highly tunable mechanical properties, with Young's modulus ranging from 6.6 to 43.2 MPa and tensile strength ranging from 2.4 to 6.7 MPa as the hard-segment content is increased from 19.2 to 33.7 wt%. These tensile strength values are significantly higher than those of analogous PHUs made without DDA chain extender (Beniah 2016). Previously, we reported a tensile strength value of 0.5 MPa for PHU made with DVBDCC, PTMO, and hexamethylene diamine at 30 wt% hard segment (Beniah 2016). The tensile strength achieved by PTMO4 (with similar hard-segment content) is 13 times higher. These results clearly indicate that DDA chain extender also enables major improvement in mechanical properties of segmented PHUs.

To evaluate the utility of PTMO-based PHUs as thermoplastic elastomer, we performed cyclic tensile testing on PTMO3 and PTMO4. It is well known that TPU elastomers exhibit reversibility of extension with hysteresis as well as permanent set and softening with increasing number of cycles (Qi 2005, Buckley 2010). Figure 8.7 shows the cyclic tensile testing results of

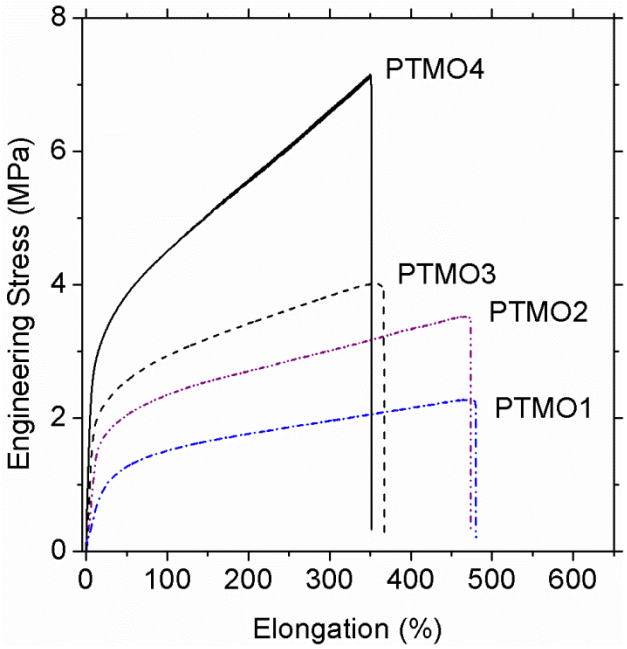

Figure 8.6: Representative stress-strain curves of PTMO-based PHUs.

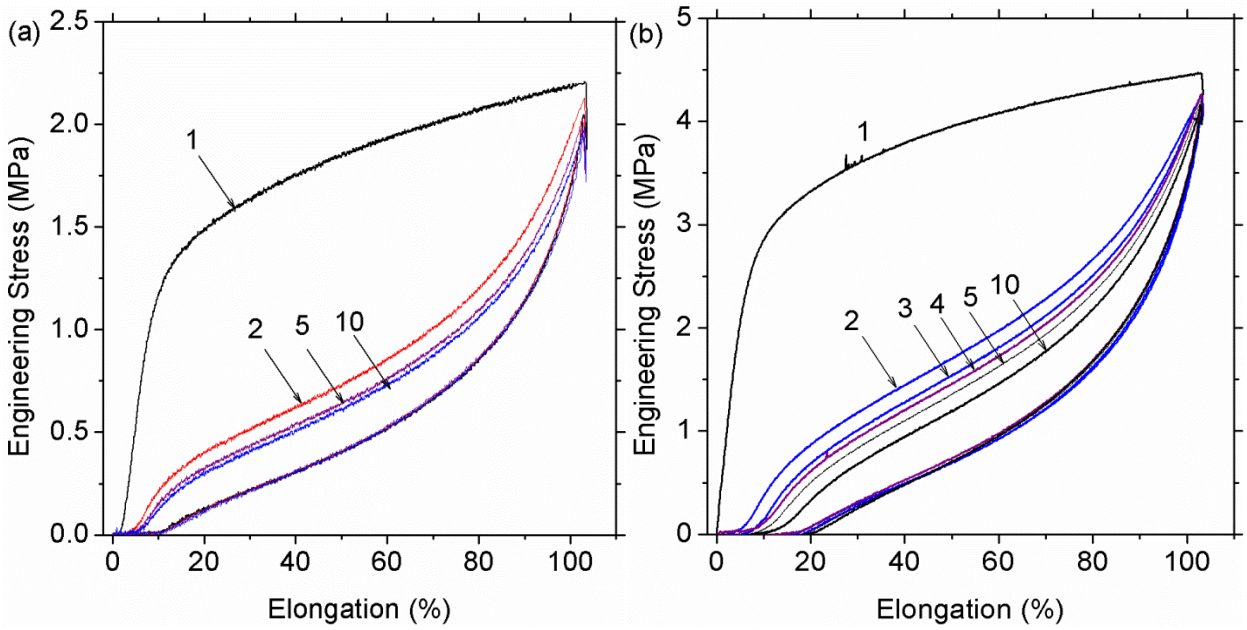

Figure 8.7: Hysteresis profile of a) PTMO3, and b) PTMO4.

PTMO3 and PTMO4. These PHUs exhibits good elastomeric recovery with some hysteresis, permanent set, and softening. In the first cycle, these materials exhibit higher stiffness and hysteresis. In subsequent cycles, these materials exhibit lower modulus and hysteresis. The loading-unloading paths after the first cycle follow similar trajectory. Such response, known as the Mullins effect, is typically seen in TPU elastomers (Qi 2005, Buckley 2010). The results shown in Figure 8.7 demonstrate that these PHUs possess attributes similar to conventional, isocyanate-based TPU elastomers, testifying to their utility as NIPU thermoplastic elastomer.

8.4 Conclusions

NIPU thermoplastic elastomers were synthesized via cyclic carbonate aminolysis from DVBDCC hard segment, PEO- and PTMO-based soft segments, and DDA chain extender. Use of amide-based DDA chain extender leads to unprecedented improvement in nanophase separation and thermal and mechanical properties over segmented PHUs made without DDA chain extender. DDA chain extender affords nanophase-separated PHUs above certain hard-segment content with PEO-based soft segment; PHUs made with PEO-based soft segment were previously known to yield only single-phase materials. DMA measurements of PEO-based PHUs reveal high T_{flow} values of up to 147 °C and, via rubbery plateau regions, the presence of nanophase separation with sharp interphase. Use of DDA chain extender with PTMO-based soft segment also produces nanophase-separated systems with sharp interphase; PHUs with PTMO-based soft segment were previously known to yield nanophase-separated systems with broad interphase. These PTMO-based PHUs possess wide, relatively temperature-independent rubbery plateau regions with high T_{flow} values ranging from 127 to 200 °C for the hard-segment contents under study. The thermal properties of PHUs synthesized with DDA chain extender are comparable to those of conventional, isocyanate-based TPU elastomers. DSC measurements reveal the presence of crystalline hard domain with high melting temperature, in agreement with

the onset of flow in DMA results. The PTMO-based PHUs exhibited tunable mechanical properties with Young's modulus ranging from 6.6 to 43.2 MPa and tensile strengths from 2.4 to 6.7 MPa with elongation at break of ~300 %. Cyclic tensile testing reveals that these PHUs exhibit elastomeric recovery with attributes very similar to conventional, isocyanate-based TPU elastomers.

APPENDIX F

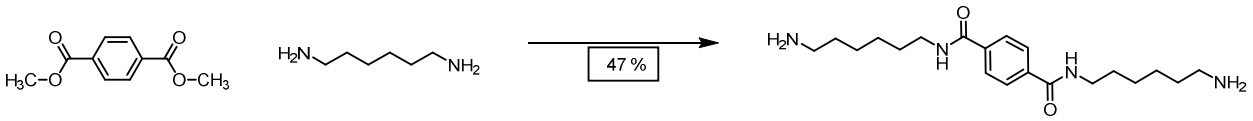

Scheme F1: Synthesis of diamine diamide chain extender.

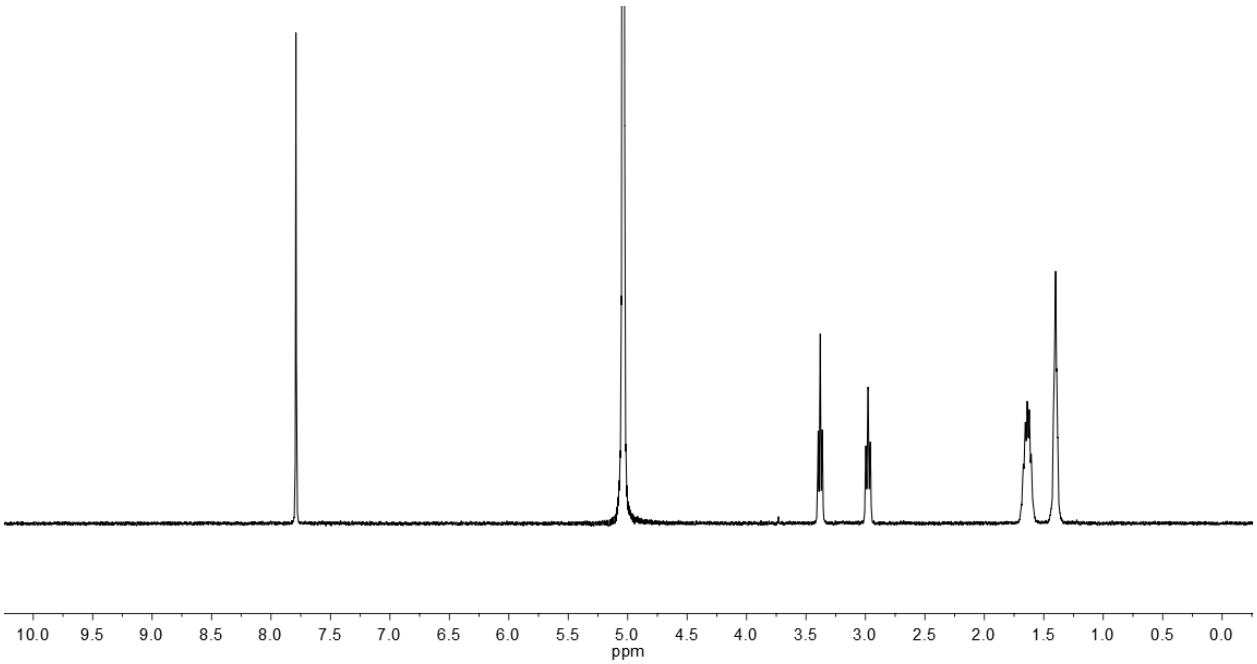

Figure F1: ^{1}H NMR Spectrum (400 MHz, D_2O with H_2SO_4)

^{1}H NMR (400 MHz, D_2O containing a drop of H_2SO_4, dioxane as internal standard) δ 7.79 (s, 4H), 3.38 (t, J = 6.6 Hz, 4H), 3.00 (t, J = 8.0 Hz, 4H), 1.72-1.59 (m, 8H), 1.41 (quintet, J = 3.8 Hz, 8H). ^{13}C NMR (100 MHz, D_2O containing a drop of H_2SO_4, dioxane as internal standard) δ 170.2, 137.3, 128.0, 40.5, 40.1, 28.8, 27.3, 26.2, 25.9. LRMS (APCI) calculated for $[C_{24}H_{34}N_4O_2+H]^+$ 363.3, found 363.3.

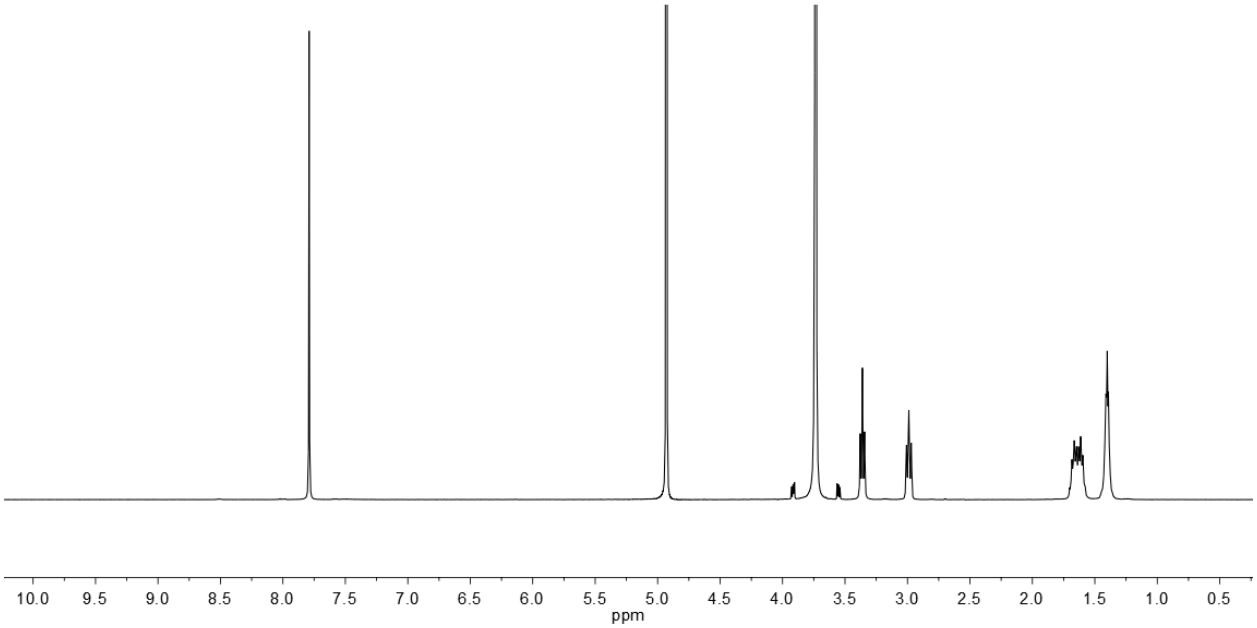

Figure F2: ^{1}H NMR Spectrum (400 MHz, D_2O with H_2SO_4, dioxane)

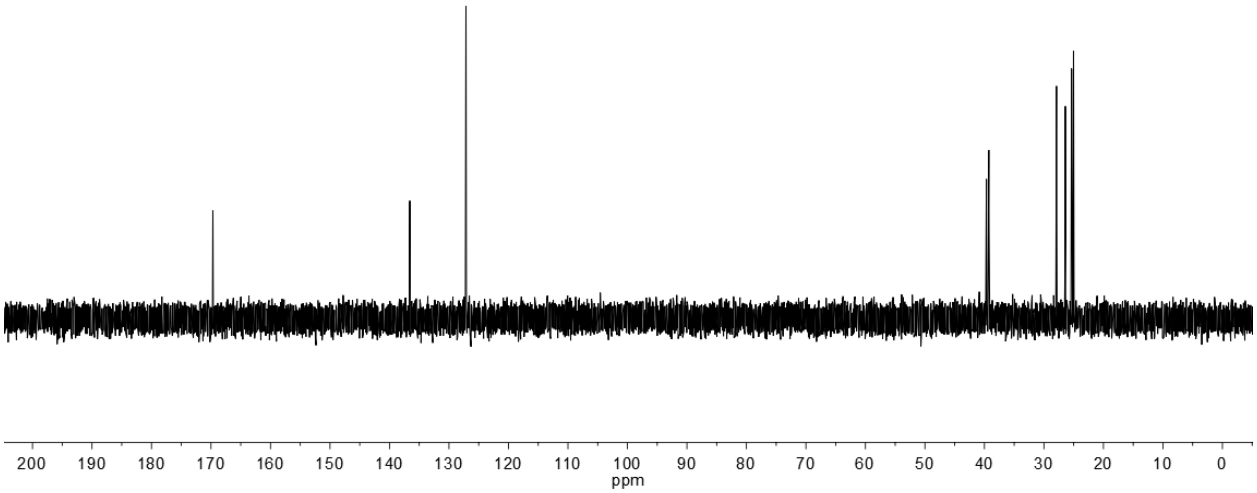

Figure F3: ^{13}C NMR Spectrum (100 MHz, D_2O with H_2SO_4)

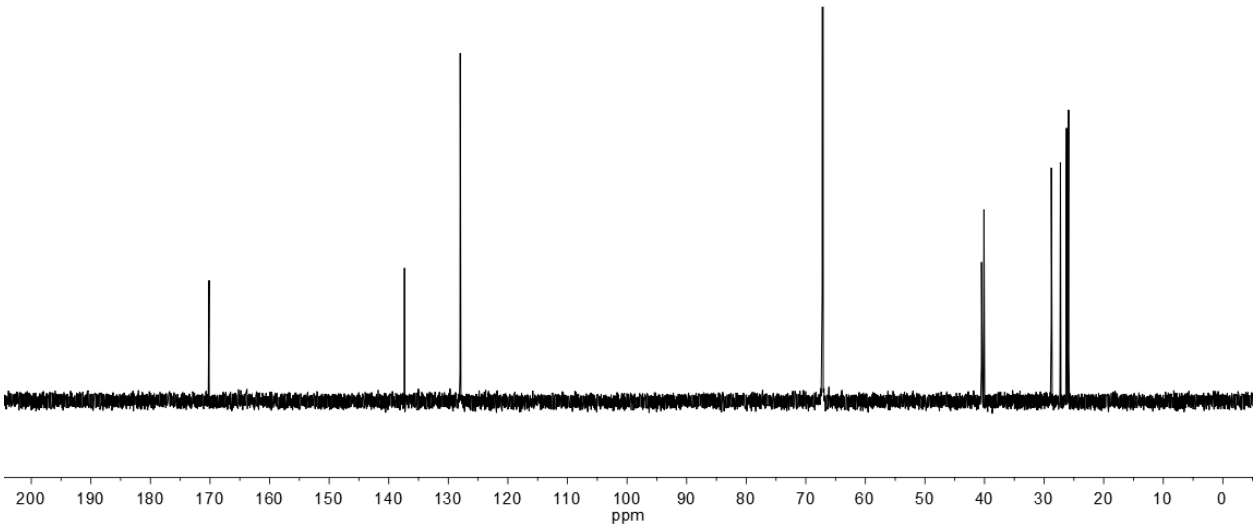

Figure F4: ^{13}C NMR Spectrum (100 MHz, D_2O with H_2SO_4, with dioxane as internal standard).

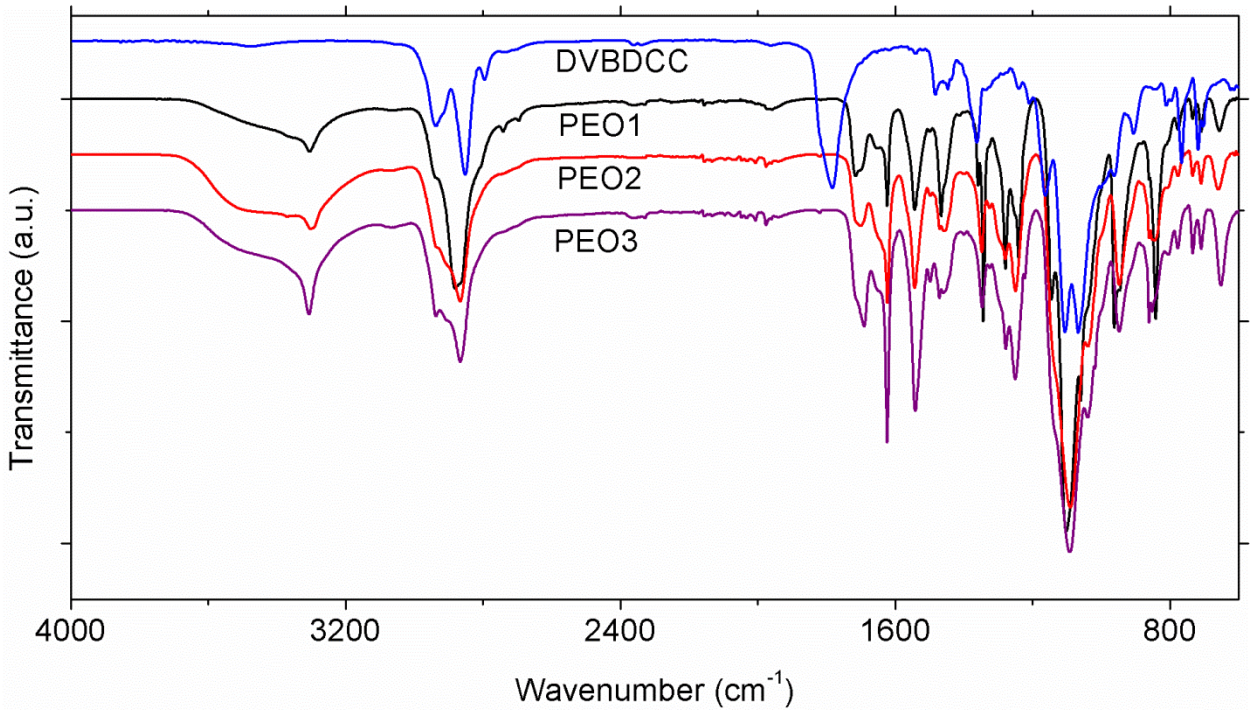

Figure F5: FTIR spectra of PEO-based PHUs.

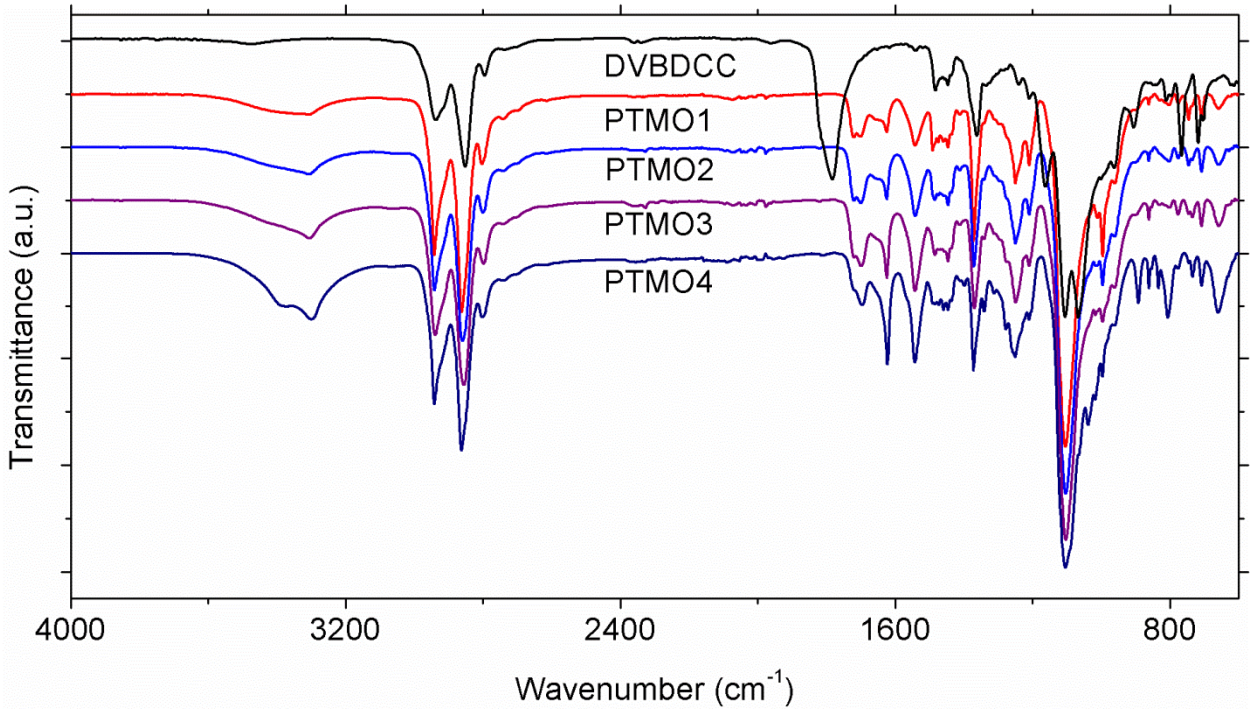

Figure F6: FTIR spectra of PTMO-based PHUs.

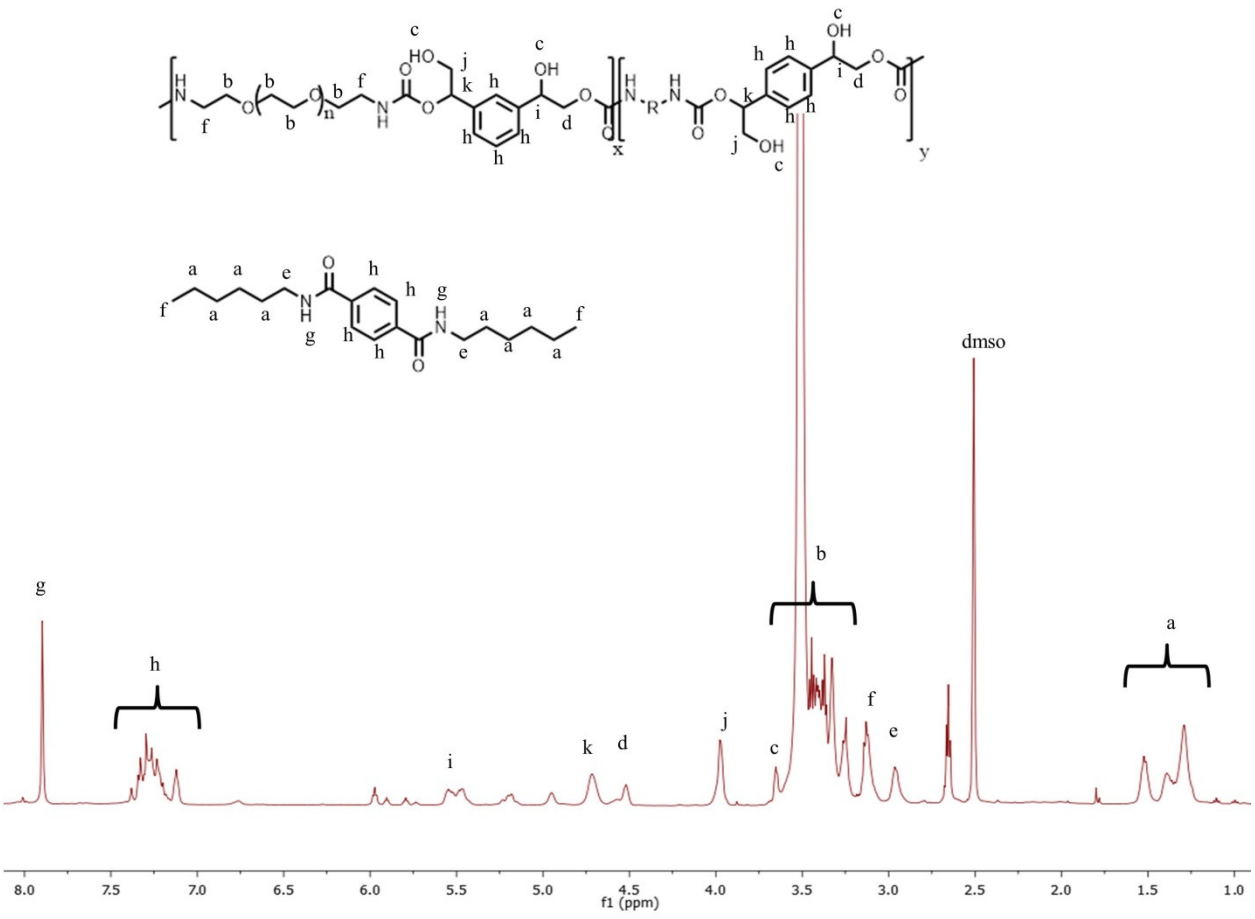

Figure F7: ^{1}H NMR Spectra of PEO1

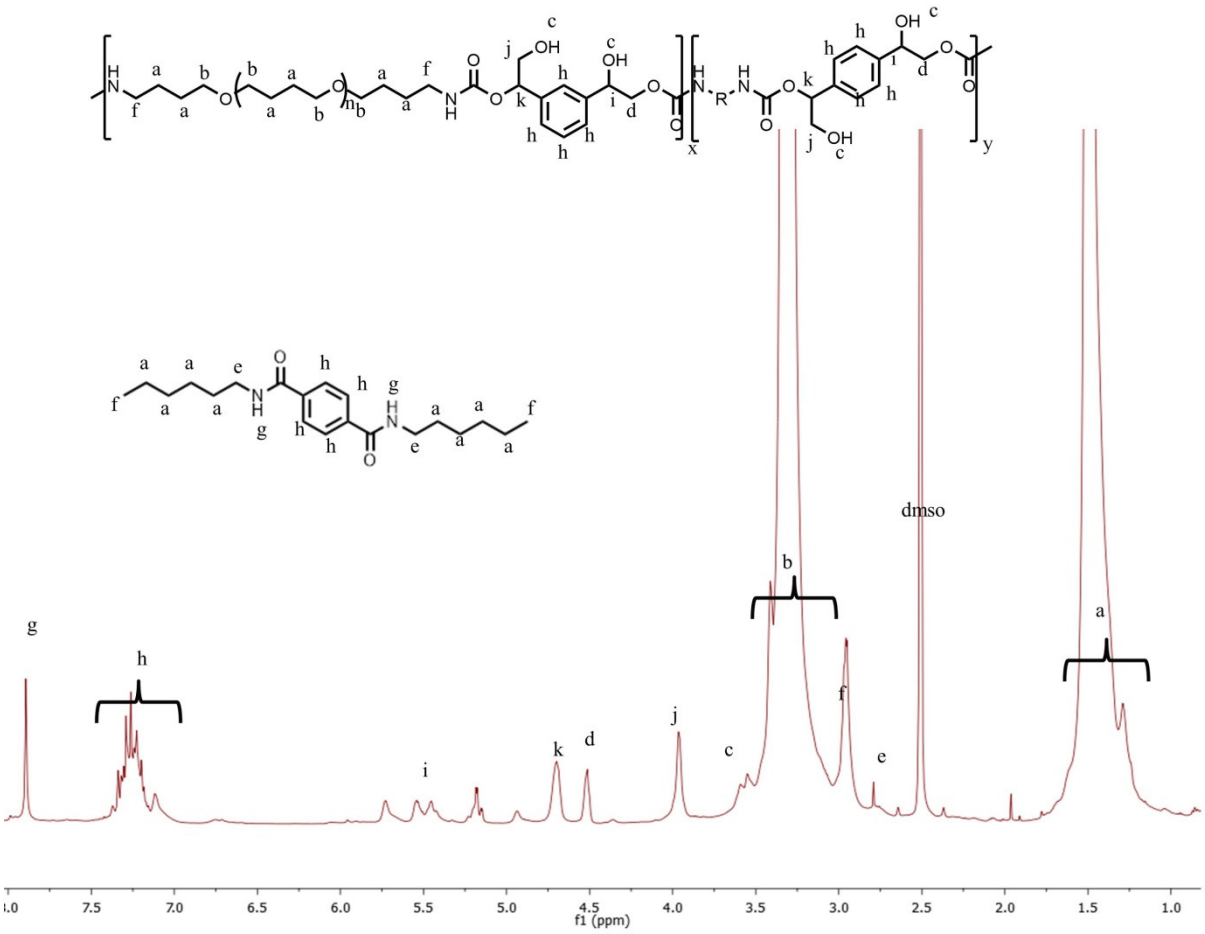

Figure F8: ^{1}H NMR Spectra of PTMO1

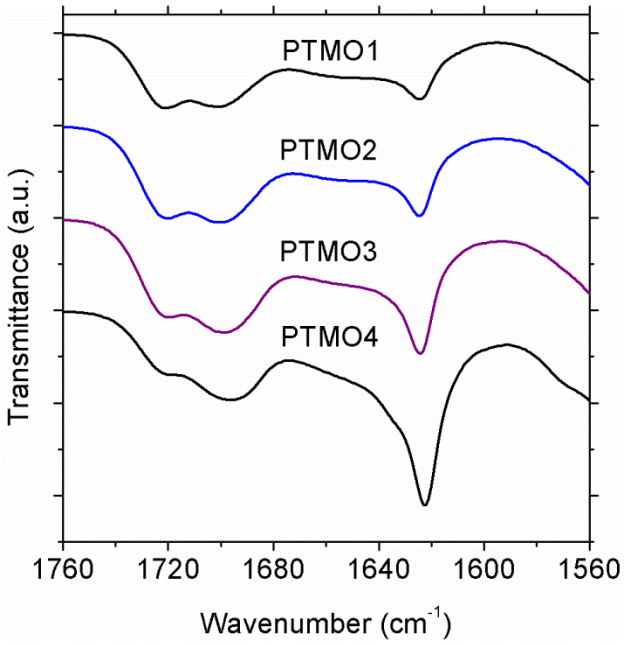

Figure F9: FTIR spectra of PTMO-based PHUs.

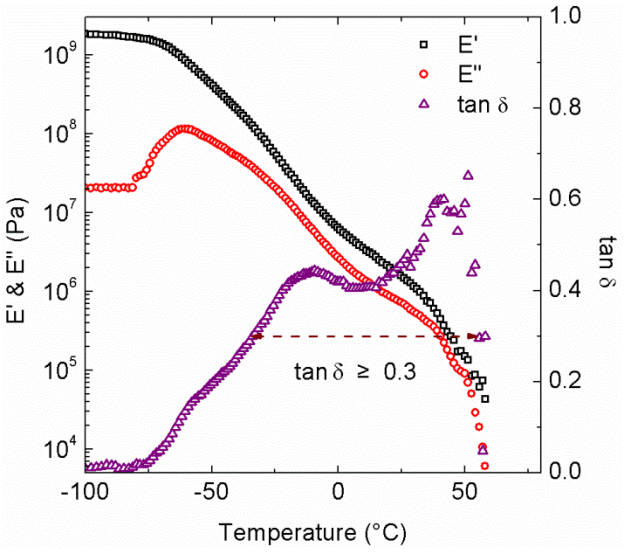

Figure F10. DMA profile of PTMO-based PHU synthesized with PTMO, DVBDCC, and hexamethylene diamine with 30 wt% hard segment

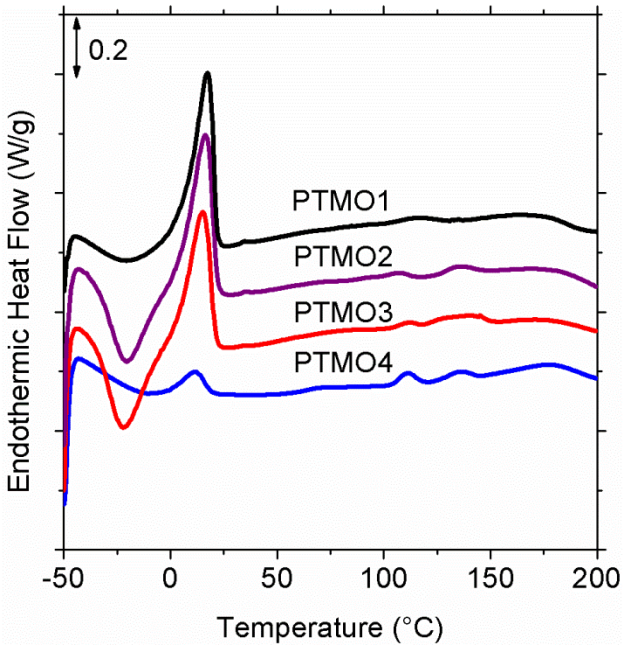

Figure F11: DSC thermograms of PTMO-based PHUs.

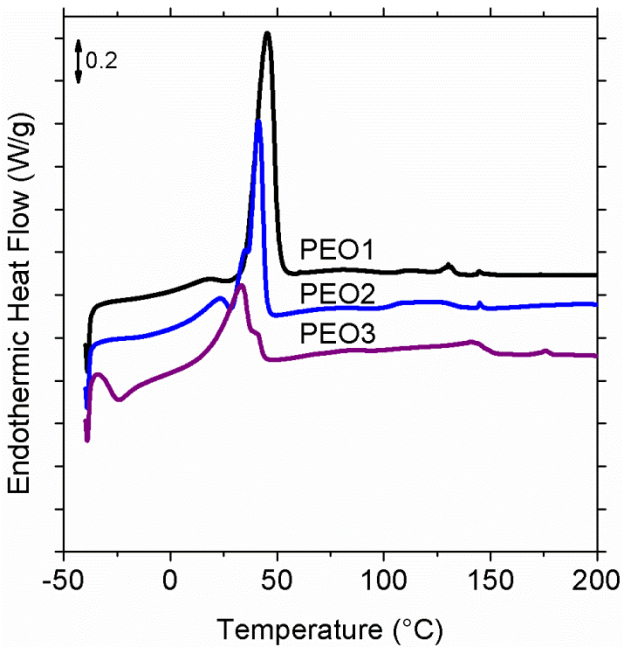

Figure F12: DSC thermograms of PEO-based PHUs.

CHAPTER 9

Functionalization of Hydroxyl Groups in Segmented Polyhydroxyurethane Eliminates Nanophase Separation

9.1 Introduction

Polyurethane (PU) is one of the most important commodity polymers with a broad range of uses such as foams, elastomers, adhesives, and coatings (Nohra 2013, Maisonneuve 2014a, Engels 2013, Guan 2011). Its annual global production was estimated to be about 18 million tons in 2016 (Nohra 2013). Increasing regulations on isocyanates have prompted intensive research into alternative chemistries for non-isocyanate polyurethane (NIPU) with aminolysis of cyclic carbonate producing polyhydroxyurethane (PHU) being one of the most promising chemistries available. PHU is analogous to PU but possesses an additional hydroxyl group adjacent to every urethane linkage (Nohra 2013, Maisonneuve 2014a, Engels 2013, Guan 2011, US EPA 2011, Official Journal of European Union 2009). Although there have been numerous studies on PHU synthesis in recent years (Tomita 2001a, Tomita 2001b, Tomita 2001c, Tomita 2001d, Tomita 2001e, Ochiai 2005a, Ochiai 2005b, Matsukizono 2016a, Matsukizono 2016b, Matsukizono 2015, Schmidt 2016, Poussard 2016, Maisonneuve 2014b, Lamarzelle 2016), very limited studies have been focused on segmented, nanophase-separated PHUs (Nanclares 2015, Leitsch 2016a, Beniah 2016, Beniah 2017, Zhang 2016). A significant fraction of conventional PU is segmented types of copolymer (Engels 2013).

Torkelson and coworkers have previously shown that the hydroxyl groups and the choice of soft segment are critical to the development of nanophase separation in PHU (Leitsch 2016a). Because of extensive phase mixing from the hard-segment hydroxyl groups to soft-segment ether oxygen, only phase-mixed, single-phase PHUs result when polyethylene oxide (PEO)-based soft

segment is used. Providing steric hindrance to the oxygen atom via polypropylene (PPO)-based soft segment and dilution of oxygen atom content via polytetramethylene oxide (PTMO)-based soft segment yield nanophase-separated PHUs with elastomeric-like properties at appropriate hard-segment content. The nanophase separation in PTMO-based PHU is accompanied with broad interphase, which is due to a significant level of intersegmental hydrogen bonding between the hydroxyl groups to the soft segment (Beniah 2016). When a soft segment with no potential for intersegmental hydrogen bonding is used, such as polybutadiene-based soft segment, nanophase-separated PHUs with a much sharper domain interphase like that exhibited by conventional thermoplastic PU elastomer are obtained (Beniah 2017). If another method of eliminating intersegmental hydrogen bonding in PHUs is employed, in particular, via functionalization of the hard-segment hydroxyl group, will well nanophase-separated PHUs with sharp domain interphases result? Ochiai et al. synthesized PHUs and performed subsequent functionalization of the pendant hydroxyl groups with acetyl chloride, benzoyl chloride, and t-butyldimethylsilyl chloride (Ochiai 2005b), but their study was performed on single-phase PHU. Here, we report the first study of the effect of hydroxyl group functionalization on the properties of segmented, nanophase-separated PHUs.

9.2 Experimental

Materials

Benzoyl chloride (> 98 %) and *p*-xylylene diamine (>99 %) were purchased from TCI America. 4-(Dimethylamino)pyridine (DMAP) was purchased from Sigma-Aldrich. Diamine-terminated polytetramethylene oxide M_n = 1700 g/mole (Elastamine™ HT-1700) was supplied by Huntsman Chemical. Divinylbenzene dicyclocarbonate (DVBDCC) was synthesized according to the procedure outlined in Chapter 3 (Leitsch 2016a).

Synthesis and Functionalization of PHU

PHU-O was synthesized according to the procedure outlined in Chapter 4 (Beniah 2016). PHU-F was synthesized under nitrogen atmosphere. In a typical synthesis of PHU-F, 4.080 g of PHU-O (2.338 theoretical mole of hydroxyl group) was dissolved in 50 mL of anhydrous THF in a three-necked round bottom flask. Subsequently, 1.64 g (1.43 mmole) of DMAP was added to the solution. The flask is cooled in an ice bath and 1.34 g of benzoyl chloride (9.54 mmole) was slowly injected into the flask. The solution was stirred for 24 hours as the DMAP.Cl salt precipitates. The solution was decanted and precipitated in excess water. Following another round of dissolution in THF and precipitation in water, the polymer was dried under vacuum at 80 °C for 6 h.

Characterization

^{1}H NMR spectra were obtained using a Bruker Avance III 500 MHz NMR spectrometer with a direct cryoprobe at room temperature and deuterated chloroform as solvent. Spectra were reported in parts per million relative to tetramethylsilane. Proton-decoupled ^{13}C-NMR spectra were obtained using a Bruker Avance 500 MHz w/ direct cryoprobe (126 MHz).

SAXS experiments were performed using a Rigaku S-MAX 3000 SAXS system emitting X-rays with a wavelength of 0.154 nm (Cu-Kα). The SAXS system was calibrated with silver behenate. The sample-to-detector distance was 1640 mm. The 2D scattering patterns were collected and azimuthally averaged using Fit2D software (from the European Synchrotron Radiation Facility website) to produce 1-D plots of intensity versus scattering vector q, where $q = 4\pi\sin\theta/\lambda$; θ is one-half of the scattering angle, and λ is the X-ray wavelength.

The DMA results were obtained using a TA Instruments Rheometrics Stress Analyzer-GIII. Rectangular specimens measuring 8.0 mm in width and 0.9 mm in thickness were cooled with N_2 gas to -100 °C for PTMO-based PHU and to -80 °C for PEO-based PHU. Temperature

sweep experiments were conducted until 100 °C at a heating rate of 3 °C/min or until the sample flowed out of the grips. Measurements were conducted in tensile mode at a frequency of 1 Hz and a strain of 0.03%, resulting in characterization of storage modulus (*E*'), loss modulus (*E*") and loss tangent (tan δ). The soft-segment T_g was identified from the peak maximum in *E*"; the flow temperature was defined as the onset of inconsistent tan δ data, close to the temperature at which the sample was no longer mechanically robust.

9.3 Results and Discussion

We investigated the properties of segmented, nanophase-separated PHUs before and after hydroxyl group functionalization. Segmented PHU was synthesized using PTMO-based soft segment, divinylbenzene dicyclocarbonate (DVBDCC) as hard segment, and *p*-xylylene diamine as chain extender at 40 wt% hard-segment content. The pendant hydroxyl groups were subsequently functionalized with benzoyl chloride, and the properties of PHUs before and after functionalization were characterized with ^{1}H NMR spectroscopy, small-angle X-ray scattering (SAXS), and dynamic mechanical analysis (DMA).

The original (unfunctionalized) segmented PHU (PHU-O) was synthesized according to Figure 9.1. PHU-O was further reacted with benzoyl chloride. The resulting PHU functionalized with benzyl chloride will be referred to as PHU-F. The functionalization follows a procedure by Ochiai et al. (Ochiai 2005b) The successful formation of PHU-O was verified by ^{1}H and ^{13}C NMR spectroscopies. Figures G1 and G2 in Appendix G show the ^{1}H and ^{13}C NMR spectra of PHU-O. The successful conjugation of hydroxyl groups with benzoyl chloride in PHU-F was verified by ^{1}H and ^{13}C NMR as shown in Figures G3 and G4 in Appendix G.

The thermomechanical properties of PHUs before and after hydroxyl group functionalization were characterized by DMA. Figure 9.2 shows the temperature dependences of storage modulus (*E*'), loss modulus (*E*"), and tan δ of PHU-O and PHU-F. Figure 9.2a shows

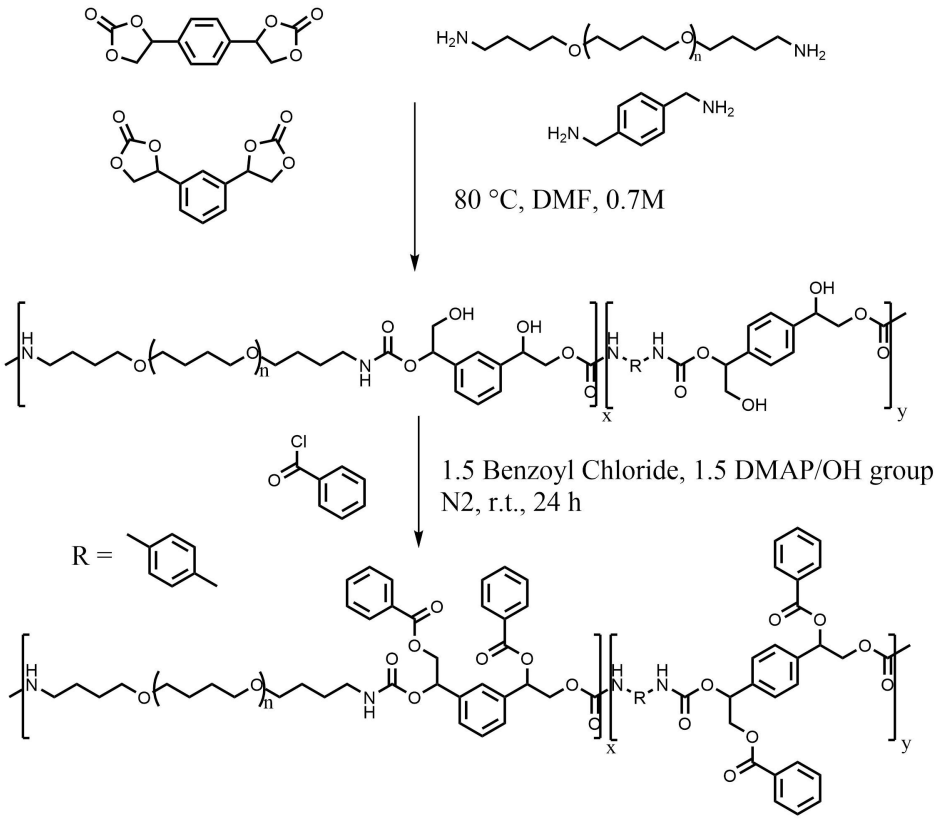

Figure 9.1: Reaction scheme for the synthesis of segmented polyhydroxyurethane and subsequent functionalization of hydroxyl groups with benzoyl chloride.

that PHU-O is a nanophase-separated system as evidenced from the presence of soft-segment glass transition temperature (T_g) identified from the peak in E" well below room temperature at -65 °C and the hard-segment flow temperature (T_{flow}) well above room temperature at 80 °C. The E' of PHU-O exhibits a very gradual decrease with temperature beginning at temperatures just above the soft segment T_g until the hard-segment T_{flow} is reached. This behavior is consistent with a nanophase-separated system with broad interphase having a wide range of local compositions and is consistent with our previous reports of PTMO-based PHU (Beniah 2016, Beniah 2017). In addition, these results are consistent with those exhibited by gradient copolymer with nanophase separation exhibiting a sinusoidal composition profile (Mok 2012, Mok 2009). The response shown in Figure 9.2a is due to some level of phase mixing caused by intersegmental hydrogen bonding from hard-segment hydroxyl group to the PTMO-based soft-segment ether oxygen.

The thermomechanical properties of PHU-O after functionalization (PHU-F) were assessed with DMA. Figure 9.2b shows that PHU-F exhibits only a single T_g at -20 °C. Upon heating past its T_g, PHU-F ultimately flows at ~30 °C, indicating that PHU-F is a phase-mixed, single-phase material. These results show that hydroxyl group functionalization with benzoyl chloride results in loss of nanophase separation despite the absence of hydroxyl groups which participate significantly in intersegmental hydrogen bonding in PTMO-based PHU (Beniah 2016). Thus, although elimination of intersegmental hydrogen bonding in PHU by using polybutadiene-based soft segment leads to excellent nanophase separation with narrow interphase (Beniah 2017), the elimination of hydroxyl groups necessary for such intersegmental hydrogen bonding in PTMO-based PHU by functionalization with benzoyl chloride results in the loss of nanophase separation itself.

The impact of hydroxyl group functionalization on PHU nanophase separation was further studied with SAXS. Figure 9.3 shows room-temperature SAXS patterns of both PHU-O

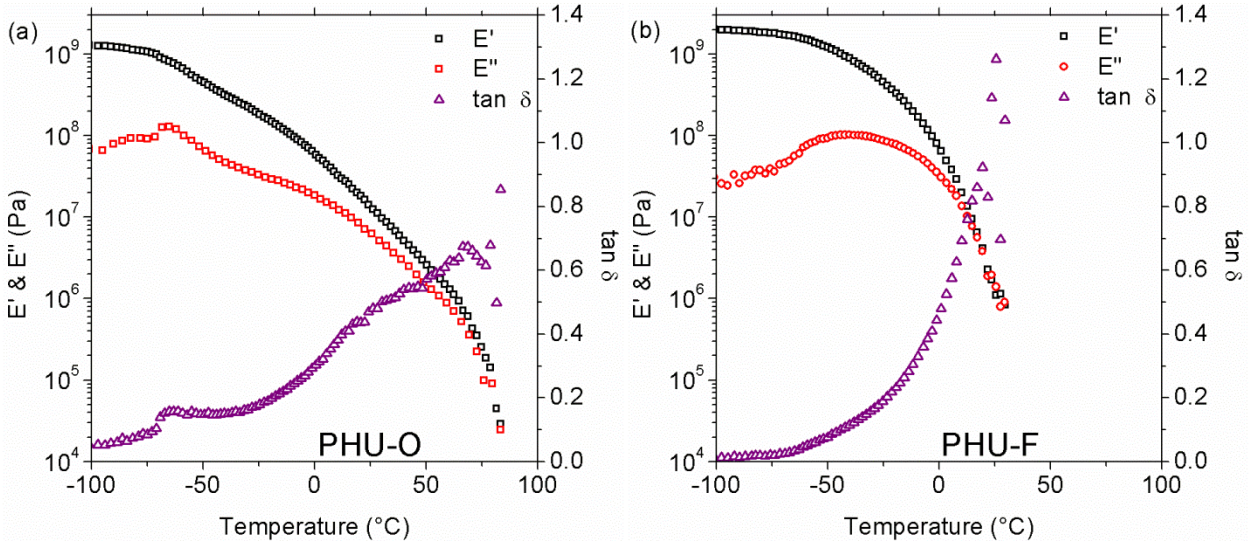

Figure 9.2. Temperature dependences of storage modulus (*E*'), loss modulus (*E*") and loss tangent (tan δ) for a) segmented PHU before functionalization (PHU-O), and b) after functionalization (PHU-F).

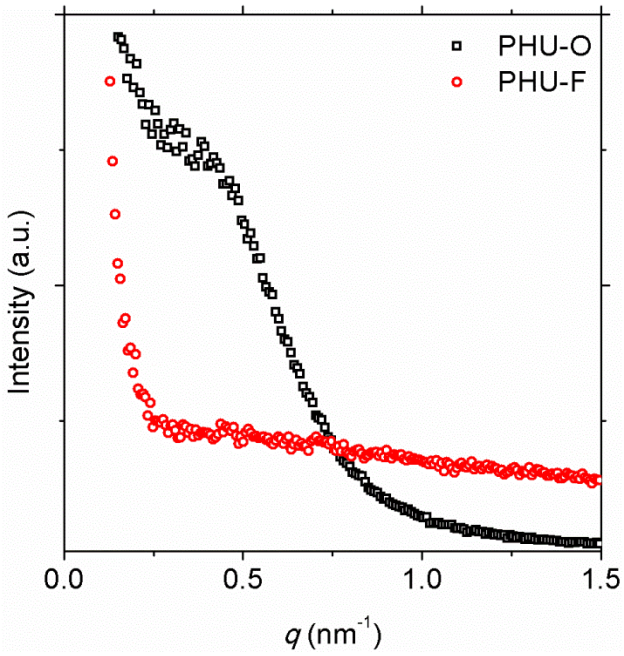

Figure 9.3: SAXS results of segmented PHU before functionalization (PHU-O) and after functionalization (PHU-F).

and PHU-F. PHU-O shows a single peak in its scattering pattern, indicating that it is nanophase separated. Its interdomain spacing, identified from the location of maximum scattering intensity (q_{max}), is ~13 nm. By contrast, the SAXS pattern of PHU-F shows no scattering peak, indicating the absence of nanophase separation. This result is in agreement with the DMA results for PHU-F shown in Figure 9.2b.

Fourier Transform Infrared (FTIR) spectroscopy was used to probe the extent of hydrogen bonding in the hard segment of PHU-O and PHU-F. Figure G5 in Appendix G shows the FTIR spectra of both PHUs in the carbonyl region. PHU-O exhibits absorbance associated with free, non-hydrogen bonded carbonyl at ~1720 cm^{-1} and hydrogen bonded carbonyl at ~1700 cm^{-1}, with a higher proportion of hydrogen bonded carbonyl indicative of interurethane hydrogen bonding in the hard segment with some phase mixing. In contrast, the carbonyl region of PHU-F shows a higher proportion of free carbonyl, consistent with significant phase mixing after hydroxyl group functionalization. However, although a higher proportion of free carbonyl absorbance indicates significant phase mixing, we also note that the high proportion or absorbance at ~1720 cm^{-1} could also be contributed by that of ester carbonyl resulting from the functionalization.

As evidenced from DMA and SAXS results, functionalization of the hydroxyl groups in PTMO-based PHU does not eliminate phase mixing and thereby yield excellent nanophase separation in PTMO-based PHU but instead leads to a total loss of nanophase separation. These results can be explained by the loss of interurethane hydrogen bonding in the hard segment due to the presence of bulky groups adjacent to the urethane bonds. The bulky phenyl ring in PHU-F presents substantial steric hindrance to interurethane hydrogen bonding, leading to phase mixing. Additionally, the urethane amide could undergo hydrogen bonding with the ester carbonyl side group instead of the urethane carbonyl. This competition could disrupt interurethane hydrogen bonding and lead to loss of hard-segment cohesion, resulting in phase mixing.

It has long been understood that nanophase separation in segmented PUs results from the thermodynamic incompatibility between the hard and soft segments as well as the interurethane hydrogen bonding in the hard domain (Engels 2013). However, studies by Harrell and coworkers on segmented PUs chain extended with piperazine (which resulted in PU without N-H groups as H-bond donors) indicated that interurethane hydrogen bonding is unnecessary for nanophase separation to occur (Harrell 1969, Ng 1973). This conclusion might be misconstrued as the hard segment in the PU system studied by Harrell and coworkers can crystallize. Simultaneous FTIR, SAXS, and rheological studies by Ryan and coworkers indicate that nanophase separation during synthesis of segmented PU occurs after a critical conversion and hydrogen bonding as well as vitrification of the hard domain set the structure in place (Elwell 1996a). By a simple analogy, nanophase separation is considered to be the "closing of the door" and hydrogen bonding is the "turning of the door handle" (Elwell 1996a). The results shown here clearly indicate that interurethane hydrogen bonding is a necessary prerequisite for the formation of nanophase-separated morphology in PHU with ether-based soft segments. The functionalization of PHU hydroxyl groups via reaction with benzoyl chloride introduces a bulky phenyl ring next to the urethane linkage. This functionalization adds additional steric hindrance for hydrogen bonding between the urethane carbonyl and amide hydrogen, likely preventing any significant interurethane hydrogen bonding in functionalized PHU and leading to phase mixing. Moreover, intramolecular hydrogen bonding of the amide hydrogen to the adjacent ester carbonyl is likely in competition with interurethane hydrogen bonding to the urethane carbonyl and would also lead to phase mixing.

9.4 Conclusions

In summary, we studied the effect of hydroxyl group functionalization on PTMO-based segmented PHU. Hydroxyl group functionalization leads to a loss of nanophase-separated

morphology in PHU as confirmed via SAXS and DMA. This is likely caused by steric hindrance introduced by the bulky side groups and hydrogen bonding competition from the ester carbonyl, both of which hinder interurethane hydrogen bonding and lead to phase mixing. This study shows that effective interurethane hydrogen bonding is a necessary prerequisite for nanophase separation in segmented PHU synthesized with common ether-based soft segments. Future study is warranted to determine whether interurethane hydrogen bonding is necessary for nanophase separation in segmented PHU even when uncommon soft segments are employed that are considered to be extremely incompatible with the hard segments, e.g., poly(dimethyl siloxane)- or polybutadiene-based soft segments.

APPENDIX G

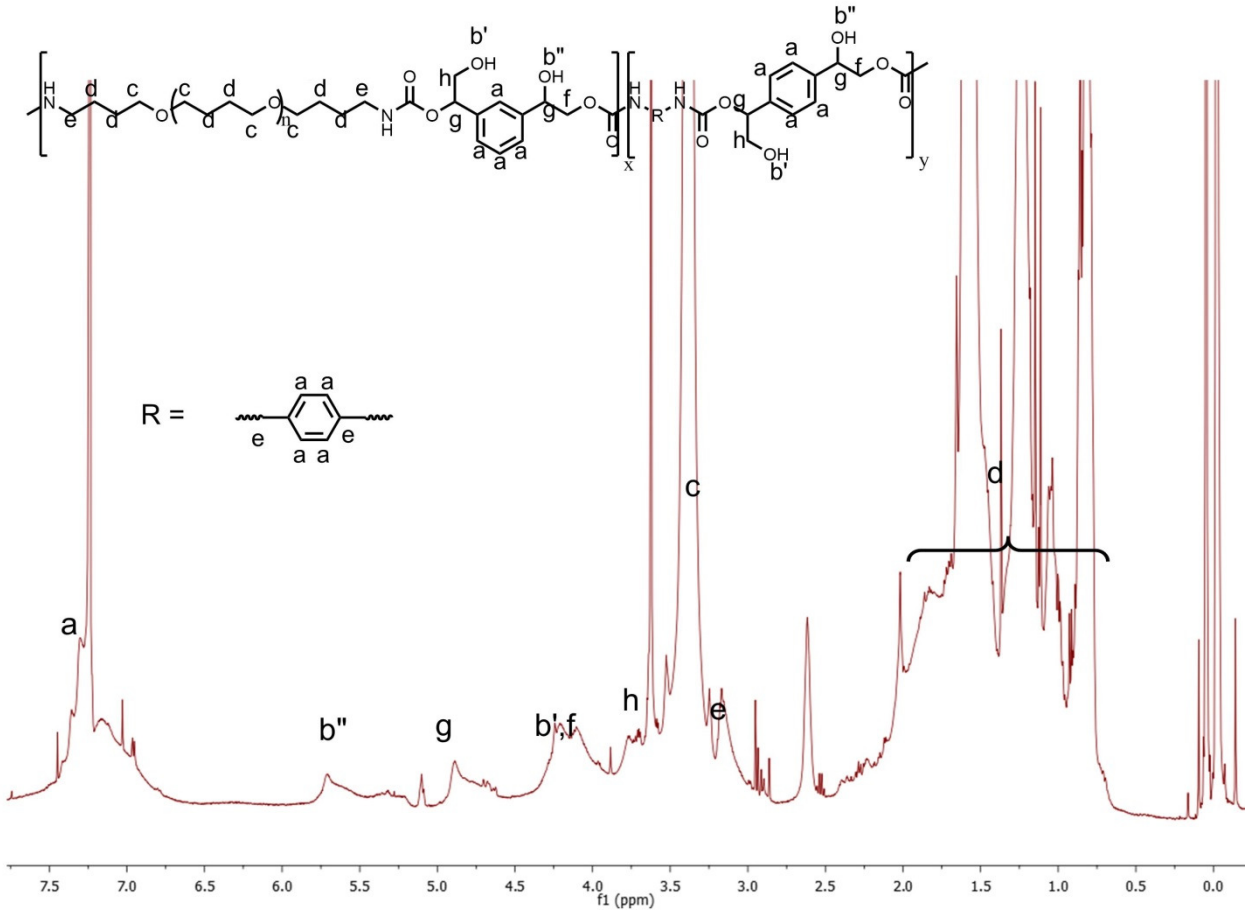

Figure G1. ^{1}H NMR spectrum of PHU-O.

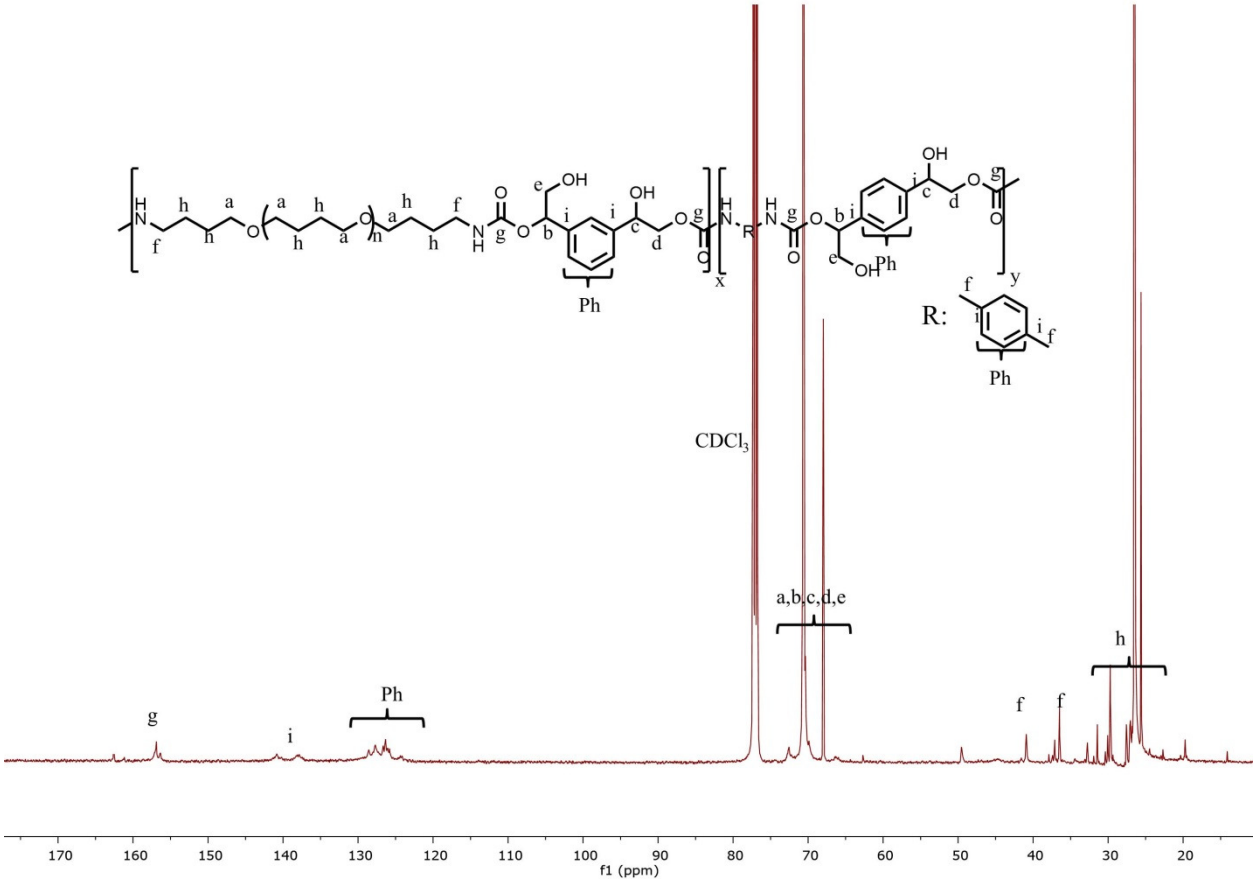

Figure G2. ^{13}C NMR spectrum of PHU-O.

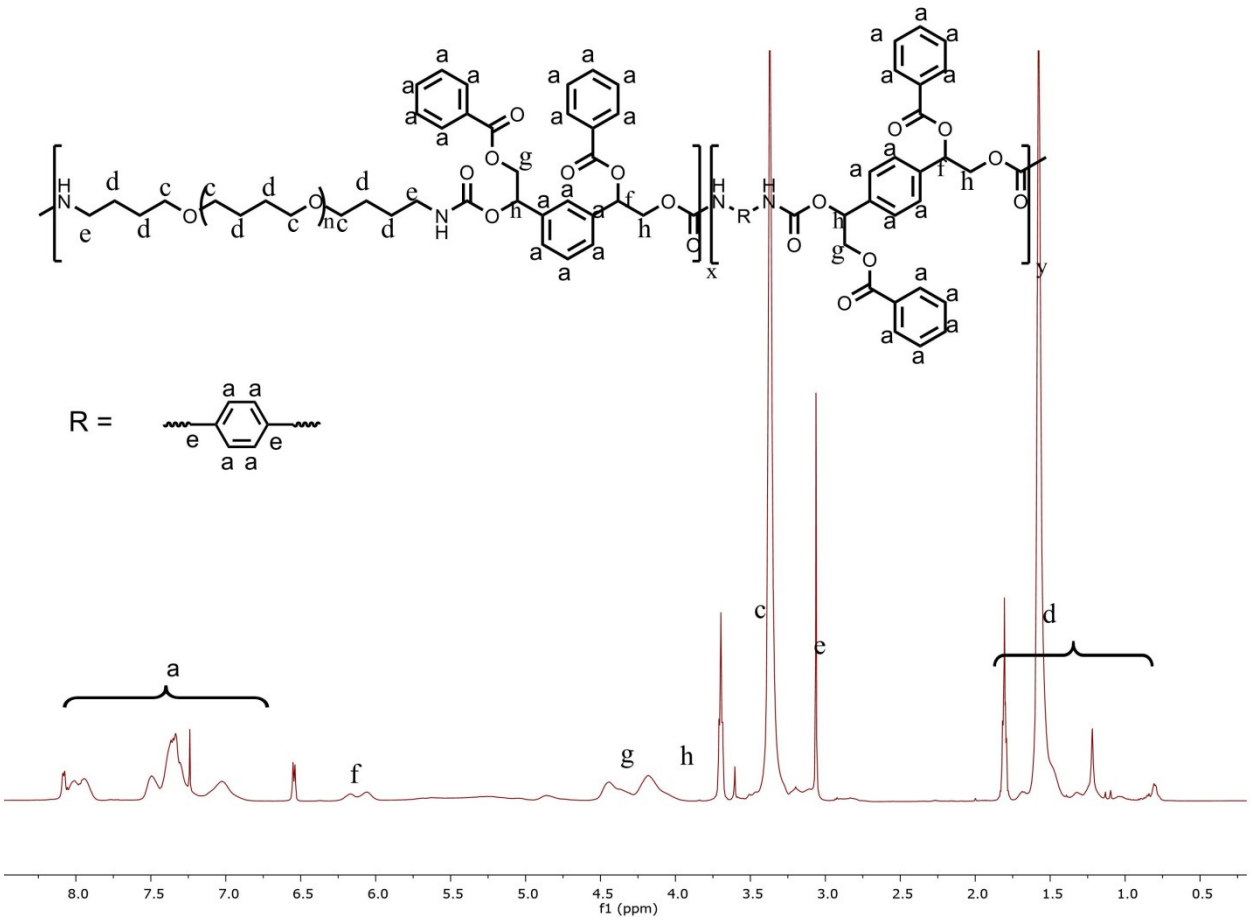

Figure G3. ^{1}H NMR spectrum of PHU-F.

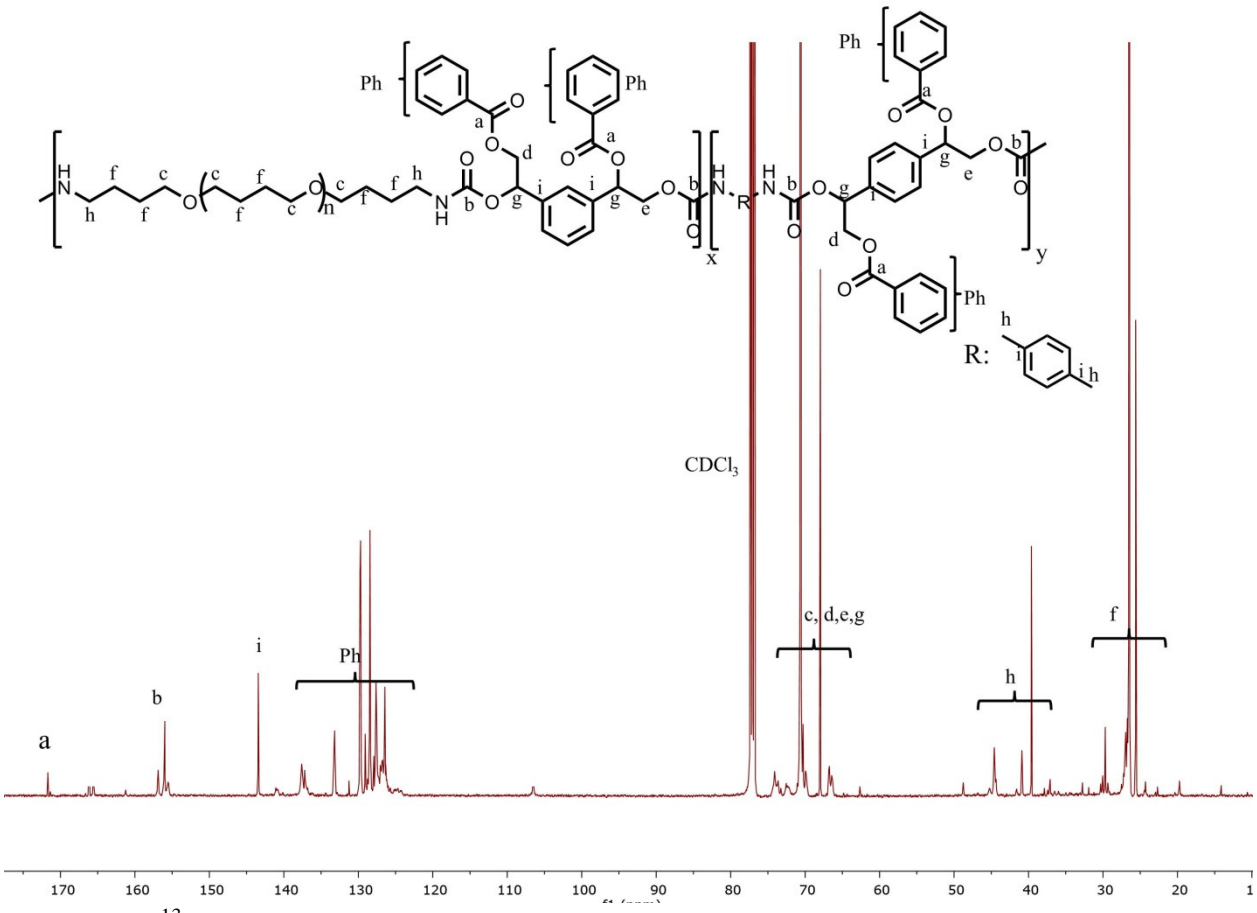

Figure G4. ^{13}C NMR spectrum of PHU-F.

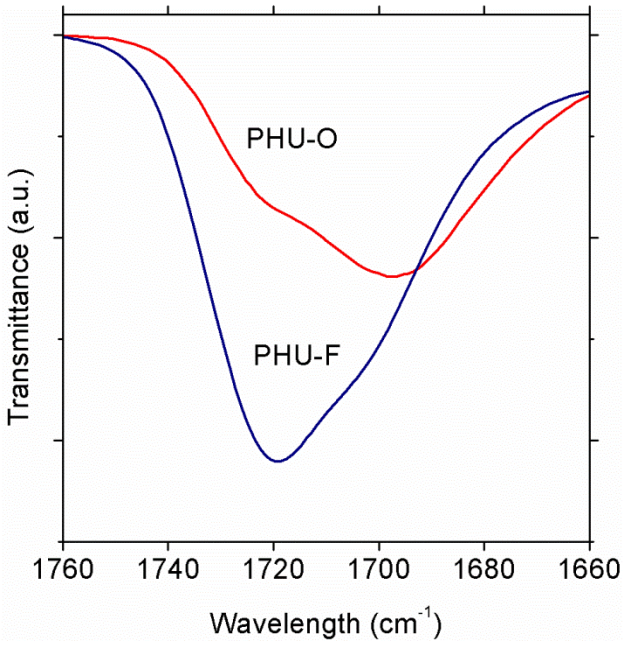

Figure G5. FTIR spectra of PHU-O and PHU-F in the carbonyl region.

CHAPTER 10

Conclusions and Recommendations

10.1 Conclusions

This dissertation focuses on the synthesis and characterization of segmented polyhydroxyurethanes (PHUs) as non-isocyanate polyurethane (NIPU) materials via cyclic carbonate aminolysis of five-membered-ring carbonates. These efforts are motivated by increasing regulations on isocyanates from various regulatory bodies as well as concerns over the effect of isocyanate on human health. Although there are a large number of past investigations on PHU synthesis, these studies focused on cyclic carbonate monomer synthesis and their subsequent polymerizations into single-phase linear PHUs, crosslinked PHUs, and reaction catalysis, with almost no attention being paid to segmented PHUs.

This dissertation describes the first fundamental investigation on the synthesis and properties of segmented PHUs. Because of the presence of a hydroxyl group adjacent to every urethane linkage, the nanophase separation behavior of segmented PHU is generally very different than that in conventional, isocyanate-based segmented polyurethane (PU). This dissertation fundamentally examined the role of hydroxyl groups in modifying nanophase separation and investigated various ways to control and tune nanophase separation behavior and properties of PHUs. By taking advantage of the extensive knowledge that has been established and practiced by past studies of segmented PUs, we have performed structure-property-relationships studies to understand the impact of structural compositions on PHU properties. Through these investigations, we discover ways to obtain PHUs with properties that are competitive to those of PUs and at least equally interesting from both scientific and technological standpoints, how segmented PHUs may yield properties that are not obtained with conventional,

segmented PUs.

In Chapter 3, the synthesis and characterization of segmented, nanophase-separated PHUs for thermoplastic elastomer application were described. Segmented PHUs were synthesized via cyclic carbonate aminolysis employing divinylbenzene dicyclocarbonate (DVBDCC) hard segment, polyether-based soft segments and several chain extenders at various hard-segment contents. It was demonstrated that the hydroxyl groups play a critical role in influencing nanophase separation in PHUs and the choice of soft segment is very important to obtain nanophase-separated PHUs. Use of a polyethylene oxide (PEO)-based soft segment yields fully phase-mixed PHUs with a single glass transition temperature (T_g) and without significant mechanical integrity, whereas conventional isocyanate-based PUs are nanophase-separated materials. This is attributed to extensive phase mixing due to hydrogen bonding from the hard-segment hydroxyl groups to soft-segment ether oxygens in PEO-based soft segment. The hydrogen bonding can be tuned by providing steric hindrance to oxygen atoms in the case of polypropylene oxide (PPO)-based soft segment and dilution of oxygen atom content in the case of polytetramethylene oxide (PTMO)-based soft segment, which resulted in nanophase-separated PHUs with tunable mechanical properties. PTMO-based PHUs also show reversible elastomeric extension with some hysteresis like that demonstrated by conventional, isocyanate-based thermoplastic PU elastomers. Furthermore, PTMO-based PHUs are nanophase-separated system with broad interphases, having a wide range of local compositions, potentially useful as sound and vibration damping applications over broad temperature ranges (Leitsch 2016).

In Chapter 4, the synthesis and characterization of PTMO-based PHUs and their utility as effective damping materials were further investigated in greater details. PTMO-based PHUs were synthesized with DVBDCC hard segment and three different chain extenders at hard-segment contents ranging from 30 to 60 wt%. These PTMO-based PHUs possess very different nanophase separation behavior than that exhibited by isocyanate-based TPUs; this difference is a

result of some level of phase mixing caused by hydrogen bonding between hard-segment hydroxyl groups and oxygen atoms in the PTMO soft segment. Notable features include a gradual decrease in *E*' with temperature and high tan δ values (≥ 0.30) over broad temperature ranges, indicative of a system with a wide range of local composition. Using a common criterion for excellent damping materials, tan δ ≥ 0.30, these PHUs were demonstrated to possess potential as excellent damping materials over broad temperature ranges, as large as 80 °C. This function is not observed in conventional, neat TPU. The temperature ranges for good damping were shown to be easily tunable via simple variation of hard-segment content and chain extender structure (Beniah 2016).

In Chapter 3 and Chapter 4, the synthesis and characterization of segmented PHUs using polyether-based soft segment were successfully described. However, the nanophase separation behavior of segmented PHUs made with polyether-based soft segments is accompanied with varying levels of phase mixing. In PEO-based PHUs, there is a significant phase mixing leading to totally phase-mixed, single-phase materials. In PTMO-based PHUs, the nanophase separation is accompanied with broad interphases having a wide range of local compositions due to some level of phase mixing. Segmented PUs are typically nanophase-separated materials with a much sharper domain interphase. That level of nanophase separation was not achieved for PHUs described in Chapter 3 and Chapter 4. In Chapter 5, we demonstrated that we can significantly tune nanophase separation behavior to a level commonly achieved in segmented PUs via a judicious choice of soft segment. By using polybutadiene-co-acrylonitirle (PBN)-based soft segments with varying levels of low acrylonitrile content, we obtained nanophase-separated PHUs with a much sharper domain interphase. This outcome is characterized by two, stepwise decreases in *E*', sharp tan δ maxima at two distinct locations associated with the glass transitions of the soft and hard segments, and quasi-rubbery plateau regions, all of which are associated with characteristic thermomechanical responses of conventional, isocyanate-based TPUs. The low

amounts of acrylonitrile does not significantly affect the levels of nanophase separation in PBN-based PHUs. The lack of hydrogen bonding acceptor in polybutadiene-based soft segment and acrylonitrile unit self-association are contributing factors to the much improved nanophase separation in PBN-based PHUs. The hypothesis of acrylonitrile unit self-association is supported by FTIR measurements (Beniah 2017).

As hard-segment structure is one of the many factors controlling the properties of segmented PUs, it can be expected that carbonate hard-segment structure will also influence PHU properties. In Chapter 6, the impact of carbonate hard-segment molecular architecture on nanophase separation and properties of segmented PHUs were investigated with three different carbonates: divinylbenzene dicyclocarbonate (DVBDCC), Bisphenol A dicarbonate (BPADC), and resorcinol bis-carbonate (RBC). These carbonates were formulated into two different soft segments: PTMO-based and PBN-based soft-segments. Characterization results reveal that there is significant cooperativity between hard-segment and soft-segment structures on the resulting properties of PHUs. In PTMO-based formulation, where intersegmental hydrogen bonding can occur, PTMO-BPADC is phase-mixed single-phase PHUs whereas PTMO-DVBDCC and PTMO-RBC are nanophase-separated PHUs with broad interphase, revealing that there is significant cooperativity between both hard- and soft-segment structures on the resulting PHU properties. The BPADC molecule is significantly larger than the other two bis-carbonates, thereby reducing the density of urethane groups formed in hypothetical hard-segment domains of BPADC-based PHUs relative to hard-segment domain of PHUs made with DVBDCC and RBC. Additionally, based on its molecular structure BPADC is likely to exhibit more steric hindrance for effective packing than DVBDCC and RBC. Both factors should lead to a reduced likelihood for inter-urethane group hydrogen bonding in BPADC-based PHUs. In PBN-based PHUs, where intersegmental hydrogen bonding is not permitted, all carbonates produce nanophase-separated PHUs with a much sharper domain interphase. With PBN-based PHUs, there is little or no

potential for hydrogen bonding between a hard-segment hydroxyl group and atoms present in soft segments. Hence, there is little or no cooperative effect of carbonate and soft-segment structures on nanophase separation and associated properties.

In Chapter 7, the impact of chain extender structure on the properties of segmented PHUs was investigated in PTMO-based PHUs with a series of diamine molecules. The diamine molecules investigated were 1,4-diaminobutane, isophorone diamine, methylene bis(cyclohexyl) amine, and bis(aminomethyl) norbornane. The flow temperature (T_{flow}), the temperature range with tan $\delta \geq 0.30$, and the tensile properties of these PHUs are strongly affected by the molecular structure of the chain extender used in synthesis. At 50 wt% hard-segment content, values of T_{flow}, tensile strength, and elongation at break can be tuned via chain extender from 57 to 105 °C, 1.6 to 22.4 MPa, and 70 to 500 %, respectively. Notably, PHU at 50 wt% hard-segment content, synthesized with norbornane-based chain extender exhibits the best thermal and mechanical properties with T_{flow} of 105 °C, tensile strength of 22.4 MPa, elongation-at-break of 500%, and tan $\delta \geq 0.30$ over 74 °C in breadth. This significant enhancement is attributed to bulky norbornane ring structure which may act as additional physical crosslinking site, enabling improvement in tensile properties. Due to the superior properties of norbornane-based PHUs, further investigations or norbornane-based PHUs were carried out at varying hard-segment content. By varying hard-segment content between 30 and 50 wt%, norbornane-based PHUs afford broad tunability in tensile strength from 0.5 to 22.4 MPa with tan $\delta \geq 0.30$ spanning temperature range as large as 85 °C.

Amide-based diamine diamide (DDA) chain extenders, when employed in the synthesis of segmented PUs, can result in crystallizable hard-segment domain and much improved thermal properties for PUs synthesized with diisocyanates usually not expected to produce crystalline hard domain (Biemond 2007, Biemond 2008, Biemond 2009, Biemond 2010, Biemond 2012, De 2009, Huskens 2007, Huskens 2008, Huskens 2009). Inspired by these results, we hypothesized

that using crystallizable DDA chain extender can yield improvements in nanophase separation and properties of segmented PHUs by virtue of its regular structure. In Chapter 8, this hypothesis was tested on PEO- and PTMO-based PHUs, where varying levels of phase mixing have been previously observed (Leitsch 2016, Beniah 2016). Use of DDA chain extender affords nanophase-separated PHUs above certain hard-segment content in PEO-based soft segment, previously known to yield only single-phase PHUs. DMA measurements of PEO-based PHUs reveal the presence of nanophase separation characteristics with sharp interphase with rubbery plateau regions and high T_{flow} of up to 147 °C. Use of DDA chain extender also produced nanophase-separated system with sharp interphase in PTMO-based soft segment, previously known to yield nanophase-separated system with broad interphase. These PTMO-based PHUs possess wide, relatively temperature-independent rubbery plateau regions with high T_{flow} values ranging from 127 to 200 °C. The thermal properties achieved by PHUs synthesized with DDA chain extender are comparable to those of conventional, isocyanate-based TPU elastomers. DSC measurements reveal the presence of crystalline hard domain with high melting temperature, in agreement with the onset of flow in DMA results. The PTMO-based PHUs made with DDA chain extender exhibited tunable mechanical properties with Young's modulus from 6.6 to 43.2 MPa, tensile strengths from 2.4 to 6.7 MPa, and elongation at break of ~300 %. Cyclic tensile testing reveals that these PHUs exhibit elastomeric recovery with very similar attributes to conventional, isocyanate-based TPU elastomers.

In Chapter 9, the impact of hydroxyl group functionalization on the properties of segmented PHUs was investigated. Segmented PHU was synthesized using PTMO-based soft segment and the resulting hydroxyl groups were functionalized via an esterification reaction with benzoyl chloride. Hydroxyl group functionalization led a loss of nanophase-separated morphology as verified by SAXS and DMA. The loss of nanophase separation was attributed to steric hindrance to interurethane hydrogen bonding and competition with ester carbonyl. This

study gives a strong indication that interurethane hydrogen bonding is necessary to produce nanophase separation in PHUs.

10.2 Recommendations for Future Study

The research in this dissertation has provided extensive investigation on the synthesis and properties of segmented PHUs. However, many opportunities are worth investigating further. In Chapter 5, it was demonstrated that nanophase separation can be significantly tuned to match that seen in conventional, isocyanate-based TPU by using PBN-based soft segments. In the future, it is worthwhile to examine the effect of mixed soft segments. For example, a combination of PBN- and PTMO-based soft segments. Other nonpolar soft segments such as polydimethylsiloxane, polyisobutylene, or pure polybutadiene can also be investigated.

The characterization of the extent of nanophase separation behavior in all segmented PHUs synthesized in this research is mostly qualitative in nature. Future studies may consider quantitative treatment of SAXS data to determine the degree of nanophase separation by following procedure originally developed by Bonart and Muller and extensively used by others (Bonart 1974, Castagna 2012, Choi 2009, Fragiadakis 2013, He 2014, Li 1992a, Li 1992b, Li 1993, Li 1994, Abouzahr 1982).

In Chapter 7, we demonstrated that chain extender has a significant influence on the properties of PHUs. In particular, use of a norbornane-based chain extender in PTMO-based PHUs affords broad tunability in achievable thermal and mechanical properties. In the future, it is worthwhile to examine the effect of norbornane-based chain extender in other soft-segment formulation such as PBN-based soft segments to obtain better thermal and mechanical properties.

The impact of diamine diamide chain extender on properties of segmented PHUs was investigated in Chapter 8, but only one chain extender structure was used. Previous study by

Gayman and coworkers (Biemond 2007, Biemond 2008, Biemond 2009, Biemond 2010, Biemond 2012, Huskens 2007, Huskens 2008, Huskens 2009) have investigated a series of DDA chain extender including hexamethylene diadipamide (based on hexamethylene diamine and adipic acid) as well as that containing an aramid segment. An aramid structure is a structural constituent of Kevlar™, an important and very successful commercial material used for various applications requiring high tensile strength. If an aramid-like structure is incorporated in the hard-segment domain of PHUs, stronger nanophase separation and hard-segment cohesion can be obtained. We envisioned that further enhancement in thermal and mechanical properties of PHUs can be achieved.

In Chapter 9, we demonstrated that hydroxyl group functionalization in segmented PHU led to a loss of nanophase-separated morphology. This study was performed with benzoyl chloride, which resulted in a bulky phenyl ring placed adjacent to the urethane linkage. It can be argued that the bulky phenyl ring sterically hinders interurethane hydrogen bonding. Thus, it is worthwhile to investigate the effect of hydroxyl group functionalization with smaller molecule, like for example, acetyl chloride. It is also worthwhile to investigate the impact of hydroxyl group functionalization on PBN-based PHUs since PBN-based soft segment affords strong nanophase separation in segmented PHU.

Although many PHUs have been synthesized and investigated in literature and in this dissertation, the kinetics of cyclic carbonate aminolysis of five-membered-ring carbonate is still too slow for this polymerization to be practical. Furthermore, the attainment of high molecular weight in PHU still remains an outstanding challenge. In several studies, organic catalyst like triazabicyclodecene has been reported to be an excellent catalyst for cyclic carbonate aminolysis (Lambeth 2015, Lombardo 2015). Future studies need to examine the synthesis of segmented PHUs in the presence of TBD. Although TBD was found to accelerate PHU polymerization, it is a very expensive chemical. Future efforts need to be dedicated toward finding more candidate as

effective catalyst for PHU polymerization.

Very recently, several studies have reported the synthesis of cyclic thiocarbonate molecules and their subsequent polymerization into polythiourethane bearing pendant thiol group or polymercaptothiourethane. Endo and coworkers reported that the polymerization of cyclic thiocarbonate occurs at a faster rate under mild condition (30 °C) (Tomita 2001f). The resulting polymers possess thiourethane linkages instead of urethane linkages. Guillaume and coworkers reported the synthesis of difunctional cyclic thiocarbonate-terminated long chain polyolefins via ring opening metathesis polymerization (Vanbiervliet 2016). These polymers were further reacted with diamine to yield polymercaptothiourethane with molecular weights that are greater than 50 kDa. Future studies can also investigate the synthesis, nanophase separation behavior, as well as thermal and mechanical properties of segmented polymercaptothiourethane. Shin et al. have previously studied segmented polythiourethane elastomer produced from reaction of thiol and isocyanate (Shin 2009). Their segmented polythiourethane are nanophase separated and possess excellent tensile properties. Since thiol groups are weaker hydrogen bond donor compared to hydroxyl groups, it is perhaps easier to achieve nanophase-separated polymercaptothiourethane with lesser complication from intersegmental hydrogen bonding like certain PHUs experience. Consequently, segmented polymercaptothiourethane might be a promising PU-mimic material with competitive properties.

As a final note, the exploration in the field of non-isocyanate polyurethane and the study of their properties are still nascent. There are huge opportunities ahead for research in this field.

REFERENCES

Abouzahr, S.; Wilkes, G. L.; Ophir, Z. *Polymer* **1982**, 23, 1077-1086.

Adhikari, R.; Gunatillake, P. A.; McCarthy, S. J.; Meijs, G. F. *J. Appl. Polym. Sci*. **1999**, 74, 2979-2989.

Ahn, T. O.; Jung, S.-U.; Jeong, H. M.; Lee, S. W. *J. Appl. Polym. Sci*. **1994**, 51, 43-49.

Alia, J. M.; Edwards, H. G. M.; Fawcett, W. R.; Smagala, T. G. *J. Phys. Chem. A* **2007**, 111, 793-804.

Arunan, E.; Desiraju, G. R.; Klein, R. A.; Sadlej, J.; Scheiner, S.; Alkorta, I.; Clary, D. C.; Crabtree, R. H.; Dannenberg, J. J.; Hobza, P.; Kjaergaard, H. G.; Legon, A. C.; Mennucci, B.; Nesbitt, D. J. *Pure Appl. Chem*. **2011**, 83, 1637-1641.

Bae, J. Y.; Chung, D. J.; An, H.; Shin, D. H. *J. Mater. Sci*. **1999**, 34, 2523-2527.

Bähr, M.; Mülhaupt, R. *Green Chem*. **2012a**, 14, 483-489.

Bähr, M.; Bitto, A.; Mülhaupt, R. *Green Chem*. **2012b**, 14, 1447-1454.

Bayer, O. *Angew. Chem*. **1947**, 59, 257-272.

Bengston, B.; Feger, C.; MacKnight, W. J.; Schneider, N. S. *Polymer* **1985**, 26, 895-900.

Beniah, G.; Liu, K.; Heath, W. H.; Scheidt, K. A.; Miller, M. D.; Torkelson, J. M. *Eur. Polym. J*. **2016**, 84, 770-783.

Beniah, G.; Uno, B. E.; Lan, T.; Jeon, J.; Heath, W. H.; Scheidt, K. A.; Torkelson, J. M. *Polymer* **2017**, 110, 218-227.

Benyahya, S.; Desroches, M.; Auvergne, R.; Carlotti, S.; Caillol, S. *Polym. Int*. **2011**, 2, 2661-2667.

Benyahya, S.; Habas, J.-P.; Auvergne, R.; Lapinte, V.; Caillol, S. *Polym. Int*. **2012**, 61, 1666-1674.

Besse, V.; Auvergne, R.; Carlotti, S.; Boutevin, G.; Otazaghine, B.; Caillol, S.; Pascault, J.-P.; Boutevin, B. *React. Funct. Polym*. **2013a**, 73, 588-594.

Besse, V.; Camara, F.; Voirin, C.; Auvergne, R.; Caillol, S.; Boutevin, B. *Polym. Chem*. **2013b**, 4, 4545-4561.

Besse, V.; Camara, F.; Mechin, F.; Fleury, E.; Caillol, S.; Pascault, J.-P.; Boutevin, B. *Eur. Polym. J*. **2015**, 71, 1-11.

Biemond, G. J. E.; Feijen, J.; Gaymans R. J. *J. Appl. Polym. Sci*. **2007**, 105, 951-963.

Biemond, G. J. E.; Braspenning, K.; Gaymans R. J. *J. Appl. Polym. Sci*. **2008**, 107, 2180-2189.

Biemond, G. J. E.; Feijen, J.; Gaymans, R. J. *Macromol. Mater. Eng*. **2009**, 294, 492-501.

Biemond, G. J. E.; Gaymans, R. J. *J. Mater. Sci*. **2010**, 45, 157-167.

Biemond, G. J. E.; Brasspenning, K.; Gaymans, R. J. *J. Appl. Polym. Sci*. **2012**, 124, 1302-1305.

Birukov, O.; Figovsky, O.; Leykin, A.; Potashnikov, R.; Shapovalov, L. Method of producing hybrid polyhydroxyurethane network on a base of carbonated-epoxidized unsaturated fatty acid triglycerides. US Patent 20120208967, Aug 16, 2012.

Blackwell, J.; Nagarajan, M. R.; Hoitink, T. B. *Polymer* **1981**, 7, 950-956.

Blain, M.; Jean-Gérard, L.; Auvergne, R.; Benazet, D.; Caillol, S.; Andrioletti, B. *Green Chem*. **2014**, 16, 4286-4291.

Blattmann, H.; Fleischer, M.; Bähr, M.; Mülhaupt, R. *Macromol. Rapid Commun*. **2014**, 35, 1238-1254.

Blattmann, H.; Lauth, M.; Mülhaupt, R. *Macromol. Mater. Eng*. **2016a**, 8, 944-952.

Blattmann, H.; Mülhaupt, R. *Green Chem*. **2016b**, 18, 2406-2415.

Blattmann, H.; Mülhaupt, R. *Macromolecules* **2016c**, 49, 742-751.

Bonart, R.; Muller, E. H. *J. Macromol. Sci. Phys*. **1974**, 10, 345-357.

Brunette, C. M.; Hsu, S. L.; Macknight, W. J.; Schneider, N. S. *Polym. Eng. Sci*. **1981**, 21, 668-674.

Buckley, C. P.; Prisacariu, C.; Martin, C. *Polymer* **2010**, 51, 3213-3224.

Carré, C.; Zoccheddu, H.; Delalande, S.; Pichon, P.; Avérous, L. *Eur. Polym. J*. **2016**, 84, 759-

769.

Casey, J. P.; Milligan, B.; Fasolka, M. J. *J. Elastom. Plast*. **1985**, 17, 218-233.

Castagna, A. M.; Pangon, A.; Choi, T.; Dillon, G. P.; Runt, J. *Macromolecules* **2012**, 45, 8438-8444.

Chattopadhyay, D. K.; Sreedhar, B.; Raju, K. V. S. N. *Ind. Eng. Chem. Res*. **2005**, 44, 1772-1779.

Chen, K.-Y.; Kuo, J.-F. *Macromol. Chem. Phys*. **2000**, 18, 1676-2686.

Chen, Q.; Ge, H.; Chen, D.; He, X.; Yu, X. *J. Appl. Polym. Sci*. **1994**, 54, 1191-1197.

Chen-Tsai, C. H.Y.; Thomas, E. L.; MacKnight, W. J.; Schneider, N. S. *Polymer* **1986**, 27, 659-666.

Chern, Y. C.; Tseng, S. M.; Hsieh, K. H. *J. Appl. Polym. Sci*. **1999**, 74, 328-335.

Choi, T.; Weksler, J.; Padsalgikar, A.; Runt, J. *Polymer* **2009**, 50, 2320-2327.

Chu, B.; Gao, T.; Li, Y.; Wang, J.; Desper, C. R.; Byrne, C. A. *Macromolecules* **1992**, 25, 5724-5729.

Comerford, J. W.; Ingram, I. D. V.; North, M.; Wu, X. *Green Chem*. **2015**, 17, 1966-1987.

Cornille, A.; Dworakowska, S.; Bogdal, D.; Boutevin, B.; Caillol, S. *Eur. Polym. J*. **2015**, 66, 129-138.

Cornille, A.; Serres, J.; Michaud, G.; Simon, F.; Fouquay, S.; Boutevin, B.; Caillol, S. *Eur. Polym. J*. **2016a**, 75, 175-189.

Cornille, A.; Michaud, G.; Simon, F.; Fouquay, S.; Auvergne, R.; Boutevin, B.; Caillol, S. *Eur. Polym. J*. **2016b**, 84, 404-420.

Cornille, A.; Guillet, C.; Benyahya, S.; Negrell, C.; Boutevin, B.; Caillol, S. *Eur. Polym. J*. **2016c**, 84, 873-888.

Cornille, A.; Blain, M.; Auvergne, R.; Andrioletti, B.; Boutevin, B.; Caillol, S. *Green. Chem*. **2016d** DOI: 10.1039/c6py01854h

Cuvé, L.; Pascault, J.-P.; Boiteux, G.; Seytre, G. *Polymer* **1991**, 32, 343-352.

Cuvé, L.; Pascault, J.-P.; Boiteux, G. *Polymer* **1992**, 32, 3957-3967.

Damle, S. B. *Chem. Eng. News* **1993**, 71, 4.

Das, S.; Cox, D. F.; Wilkes, G. L.; Klinedinst, D. B.; Yilgor, I.; Yilgor, E.; Beyer, F. L. *J. Macromol. Sci., Part B: Phys*. **2007**, 46, 853-875.

De, D.; Gaymans, R. J. *Macromol. Mater. Eng*. **2009**, 294, 405-413.

Delebecq, E.; Pascault, J. -P.; Boutevin, B.; Ganachaud, F. *Chem. Rev*. **2013**, 113, 80-118.

Deng, Y.; Li, S.; Zhao, J.; Zhang, Z.; Zhang, J.; Yang, W. *RSC Adv*. **2014**, 4, 43406-43415.

Duval, C.; Kébir, N.; Jauseau, R.; Burel, F. *J. Polym. Sci., Part A: Polym. Chem*. **2015**, 54,758-764.

Eceiza, A.; Martin, M. D.; de la Caba, K.; Kortaberria, G.; Gabilondo, N.; Corcuera, M. A.; Mondragon, I. *Polym. Eng. Sci*. **2008**, 297-306.

Elwell, M. J.; Ryan, A. J.; Grünbauer, H. J. M.; Van Lieshout, H. C. *Macromolecules* **1996a**, 29, 2960-2968.

Elwell, M. J.; Ryan, A. J. *Polymer* **1996b**, 8, 1353-1361.

Engels, H.-W.; Pirkl, H.-G.; Albers, R.; Albach, R. W.; Krause, J.; Hoffman, A.; Casselmann, H.; Dormish, J. *Angew. Chem. Int. Ed*. **2013**, 52, 9422-9441.

Ertem, S. P.; Yilgor, E.; Kosak, Wilkes, G. L.; Zhang, M.; Yilgor, I. *Polymer* **2012**, 53, 4614-4622.

Figovsky, O. L.; Shapovalov, L. D. *Macromol. Symp*. **2002**, 187, 325-332.

Firdaus, M.; Meier, M. A. R. *Green Chem*. **2013**, 15, 370-380.

Fleischer, M.; Blattmmann, H.; Mülhaupt, R. *Green Chem*. **2013**, 15, 934-942.

Fortman, D. J.; Brutman, J. P.; Cramer, C. J.; Hillmyer, M. A.; Dichtel, W. R. *J. Am. Chem. Soc*. **2015**, 137, 14019-14022.

Fragiadakis, D.; Runt, J. *Macromolecules* **2013**, 46, 4184-4190.

Fu, B.; MacKnight, W. J.; Schneider, N. S. *Rubber Chem. Tech*. **1986**, 59, 896-911.

Fukushima, K.; Lecuyer, J.; Wei, D.; Horn, H.; Jones, G.; Al-Megren, H.; Alabdlrahman, A.; Elsewilem, F.; McNeil, M.; Rice, J.; Hedrick, J. *Polym. Chem*. **2013**, 4, 1610-1616.

Furukawa, M.; Mitsui, Y.; Fukumaru, T.; Kojio, K. *Polymer* **2005**, 46, 10817-10822.

Garrett, J. T.; Xu, R.; Cho, J.; Runt, J. *Polymer* **2003**, 44, 2711-2719.

Gisselfalt, K.; Helgee, B. *Macromol. Mater. Eng*. **2003**, 288, 265-271.

Grignard, B.; Thomassin, J.-M.; Gennen, S.; Poussard, L.; Bonnaud, L.; Raquez, J.-M.; Dubois, P.; Tran, M.-P.; Park, C. B.; Jerome, C.; Detrembleur, C. *Green Chem*. **2016**, 18, 2206-2215.

Guan, J.; Song, Y.; Lin, Y.; Yin, X.; Zuo, M.; Zhao, Y.; Tao, X.; Zheng, Q. *Ind. Eng. Chem. Res*. **2011**, 50, 6517-6527.

Hashimoto, T.; Tsukahara, Y.; Tachi, K.; Kawai, H. *Macromolecules* **1983**, 16, 648-657.

He, Y.; Zhang, X.; Runt, J. *Polymer* **2014**, 55, 906-913.

Healy, M. H.; Wieserman, L. F.; Arnett, E. M.; Wefers, K. *Langmuir* **1989**, 5, 114-123.

Hepburn, C.; Polyurethane Elastomers, Chapter 3, Structure Property Relationship.

Hergenrother, R. W.; Wabers, H. D.; Cooper, S. L. *J. Appl. Polym. Sci*. **1992**, 3, 17-22.

Hood, M. A.; Wang, B.; Sands, J. M.; La Scala, J. J.; Beyer, F. L.; Li, C. Y. *Polymer* **2010**, 51, 2191-2198.

Hourston, D. J.; Schäfer, F.-U. *Polym. Adv. Tech*. **1996**, 62, 273-280.

Hsu, J. M.; Yang, D.-L.; Huang, S. K. J. *Polym. Res*. **1999**, 6, 67-78.

Hu, C. B.; Ward, R. S.; Schneider, N. S. *J. Appl. Polym. Sci*. **1982**, 27, 2167-2177.

Hu, R.; Dimonie, V. L.; El-Aasser, M. S.; Pearson, R. A.; Hiltner, A.; Mylonakis, S. G.; Sperling, L. H. *J. Polym. Sci., Part B: Polym. Phys*. **1997**, 35, 1501-1514.

Huang, S.-L.; Lai, J.-Y. *Eur. Polym. J*. **1997**, 33, 1563-1567.

Huelck, V.; Thomas, D. A.; Sperling, L. H. *Macromolecules* **1972**, 5, 340-347.

Huelck, V.; Thomas, D. A.; Sperling, L. H. *Macromolecules* **1972**, 5, 348-353.

Huskens, D.; Feijen, J.; Gaymans, R. J. *J. Polym. Sci., Part A: Polym. Chem*. **2007**, 45, 4522-4535.

Huskens, D.; Feijen, J.; Gaymans, R. J. *Macromol. Chem. Phys*. **2008**, 209, 525-534.

Huskens, D.; Gaymans, R. J. *J. Mater. Sci*. **2009**, 44, 2656-2664.

Hwang, K. K. S.; Lin, S. B.; Tsay, S. Y.; Cooper, S. L. *Polymer* **1984**, 25, 947-955.

Javni, I.; Hong, D. P.; Petrovic, Z. S. *J. Appl. Polym. Sci*. **2008**, 108, 3867-3875.

Javni, I.; Hong, D. P.; Petrovic, Z. S. *J. Appl. Polym. Sci*. **2013**, 128, 566-571.

Karaky, K.; Péré, E.; Pouchan, C.; Desbrières, J.; Dérail, C.; Billon, L. *Soft Matter* **2006**, 2, 770-778.

Karaky, K.; Billon, L.; Pouchan, C.; Desbrières, J. *Macromolecules* **2007**, 40, 458-464.

Karaky, K.; Derail, C.; Reiter, G.; Billon, L. *Macromol. Symp*. **2008**, 267, 31-40.

Kathalewar, M. S.; Joshi, P. B.; Sabnis, A. S.; Malshe, V. C. *RSC Adv*. **2013**, 3, 4110-4129.

Kathalewar, M.; Sabnis, A.; D'Mello, D. *Eur. Polym. J*. **2014**, 57, 99-108.

Kihara, N.; Endo, T. *J. Polym. Sci., Part A: Polym. Chem*. **1993a**, 31, 2765-2773.

Kihara, N.; Hara, N.; Endo, T. *J. Org. Chem*. **1993b**, 58, 6198-6202.

Kim, M.-R.; Kim, H.-S.; Ha, C.-S.; Park, D.-W.; Lee, J.-K. *J. Appl. Polym. Sci*. **2001**, 81, 2735-2743.

Kim, J.; Mok, M. M.; Sandoval, R. W.; Woo, D. J.; Torkelson, J. M. *Macromolecules* **2006**, 39, 6152-6160.

Klinedinst, D. B.; Yilgor, E.; Yilgor, I.; Beyer, F. L.; Wilkes, G. L. *Polymer* **2005**, 46, 10191-10201.

Klinedinst, D. B.; Yilgor, I., Yilgor, E.; Zhang, M.; Wilkes, G. L. *Polymer* **2012**, 53, 5358-5366.

Knoezinger, H.; Krietenbrink, H. *J. Chem. Soc., Faraday Trans*. **1975**, 71, 2421-2430.

Kojio, K.; Furukawa, M.; Motokucho, S.; Shimada, M.; Sakai, M. *Macromolecules* **2009**, 42,

8322-8327.

Kojio, K.; Nakashima, S.; Furukawa, M. *Polymer* **2007**, 48, 997-1004.

Korley, L. T. J.; Pate, B. D.; Thomas, E. L.; Hammond, P. T. *Polymer* **2006**, 47, 3073-3082.

Korodi, T.; Marcu, N.; Tirnaveanu, A. *Polymer* **1984**, 25, 1211-1213.

Krakovský, I.; Bubeníková, Z.; Urakawa, H.; Kajiwara, K. *Polymer* **1997a**, 38, 3637-3643.

Krakovský, I.; Urakawa, H.; Kajiwara, K. *Polymer* **1997b**, 38, 3645-3653.

Krijgsman, J.; Husken, D.; Gaymans, R. J. *Polymer* **2003**, 44, 7043-7053.

Lachat, V.; Varshney, V.; Dhinojwala, A.; Yeganeh, M. S. *Macromolecules* **2009**, 42, 7103-7107.

Lamarzelle, O.; Durand, P.-L.; Wirotius, A.-L.; Chollet, G.; Grau, E.; Cramail, H. *Polym. Chem*. **2016**, 7, 1439-1451.

Lambeth, R.; Henderson, T. J. *Polymer* **2013**, 54, 5568-5573.

Lebarbé, T.; More, A. S.; Sane, P. S.; Grau, E.; Alfos, C.; Cramail, H. *Macromol. Rapid Commun*. **2014**, 35, 479-483.

Lee, A.; Deng, Y. *Eur. Polym. J*. **2015**, 63, 67-73.

Lee, D.-K.; Tsai, H.-B. *J. Appl. Polym. Sci*. **2000**, 75, 167-174.

Lee, D.-K.; Tsai, H.-B.; Tsai, R.-S.; Chen, P.-H. *Polym. Eng. Sci*. **2007**, 47, 695-701.

Lee, H. S.; Wang, Y. K.; Hsu, S. L. *Macromolecules* **1987**, 20, 2089-2095.

Lee, H. S.; Wang, Y. K.; MacKnight, W. J.; Hsu, S. L. *Macromolecules* **1988**, 21, 270-273.

Leitsch, E. K.; Beniah, G.; Liu, K.; Lan, T.; Heath, W. H.; Scheidt, K. A.; Torkelson, J. M. *ACS Macro Lett*. **2016a**, 5,424-429.

Leitsch, E. K.; Heath, W. H.; Torkelson, J. M. *Int. J. Adhes. Adhes*. **2016b**, 64, 1-8.

Li, C.; Goodman, S. L.; Albrecht, R. M.; Cooper, S. L. *Macromolecules* **1988**, 21, 2367-2375.

Li, S.; Zhao, J.; Zhang, Z.; Zhang, J.; Yang, W. *Polymer* **2015**, 57, 1664-1672.

Li, W.; Ryan, A. J.; Meier, K. I. *Macromolecules* **2002**, 35, 6306-6312.

Li, Y.; Gao, T.; Chu, B. *Macromolecules* **1992a**, 25, 1737-1742.

Li, Y.; Gao, T.; Liu, J.; Liu, K. L.; Desper, C. R.; Chu, B. *Macromolecules* **1992b**, 7365-7372.

Li, Y.; Ren, Z.; Zhao, M.; Yang, H.; Chu, B. *Macromolecules* **1993**, 26, 612-622.

Li, Y.; Kang, W.; Stoffer, J. O.; Chu, B. *Macromolecules* **1994**, 27, 612-614.

Liaw, D. J. *J. Appl. Polym. Sci*. **1997**, 66, 1251-1265.

Lombardo, V. M.; Dhulst, E. A.; Leitsch, E. K.; Wilmot, N.; Heath, W. H.; Gies, A. P.; Miller, M. D.; Torkelson, J. M.; Scheidt, K. A. *Eur. J. Org. Chem*. **2015**, 13, 2791-2795.

Maglio, G.; Palumbo, R.; Sepede, F. C. *Polym. Bull*. **1994**, 32, 565-571.

Maisonneuve, L.; More, A. S.; Foltran, S.; Alfos, C.; Rober, F.; Landais, Y.; Tassaing, T.; Grau, E.; Cramail, H. *RSC Adv*. **2014a**, 4, 25795-25803.

Maisonneuve, L.; Wirotius, A.-L.; Alfos, C.; Grau, E.; Cramail, H. *Polym. Chem*. **2014b**, 5, 6142-6147.

Maissoneuve, L.; Lamarzelle, O.; Rix, E.; Grau, E.; Cramail, H. *Chem. Rev*. **2015**, 115, 12407-12439.

Martin, D. J.; Meijs, G. F.; Gunatillake, P. A.; McCarthy, S. J.; Renwick, G. M. *J. Appl. Polym. Sci*. **1996**, 60, 557-571.

Martin, D. J.; Meijs, G. F.; Gunatillake, P. A.; McCarthy, S. J.; Renwick, G. M. *J. Appl. Polym. Sci*. **1996**, 60, 557-571.

Matsukizono, H.; Endo, T. *J. Mater. Res*. **2016a**, 5, 11-28.

Matsukizono, H.; Endo, T. *Polym. Chem*. **2016b**, 7, 958-969.

Matsukizono, H.; Endo, T. *RSC Adv*. **2015**, 5, 71360-71369.

Mazurek-Budzyńska, M. M.; Rokicki, G.; Drzewicz, M.; Guńka, P. A.; Zachara, J. *Eur. Polym. J*. **2016**, 84, 799-811.

Meckel, W.; Goyert, W.; Wieder, W.; Wussow, H.-G.; Thermoplastic Elastomers, 3rd Edition, Editors: G. Holden, H. R. Kricheldorf, E. P. Quirk, Hanser, Munich, 2004, 15-43.

Miller, J. A.; Lin, S. B.; Hwang, K. K. S.; Wu, K. S.; Gibson, P. E.; Cooper, S. L. *Macromolecules* **1985**, 18, 32-44.

Mok, M. M.; Kim, J.; Marrou, S. R.; Torkelson, J. M. *Eur. Phys. J. E*. **2010**, 31, 239-252.

Mok, M. M.; Kim, J.; Torkelson, J. M. *J. Polym. Sci., Part B: Polym. Phys*. **2008**, 46, 48-58.

Mok, M. M.; Torkelson, J. M. *J. Polym. Sci., Part B: Polym. Phys*. **2012**, 50, 189-197.

Mok, M. M.; Wong, C. L. H.; Marrou, S. R.; Woo, D.; Dettmer, C. M.; Nguyen, S. T.; Ellison, C. J.; Shull, K. R.; Torkelson, J. M. *Macromolecules* **2009**, 42, 7863-7876.

Nakamura, H.; Takata, T.; Endo, T. *Macromolecules* **1990**, 23, 3032-3035.

Nanclares, J.; Petrovic, Z. S.; Javni, I.; Ionescu, M.; Jaramillo, F. *J. Appl. Polym. Sci*. **2015**, 42492.

Nohra, B.; Candy, L.; Blanco, J.-F.; Guerin, C.; Raoul, Y.; Mouloungui, Z. *Macromolecules* **2013**, 46, 3771-3792.

Ochiai, B.; Inoue, S.; Endo, T. *J. Polym. Sci., Part A: Polym. Chem*. **2005a**, 43, 6282-6286.

Ochiai, B.; Inoue, S.; Endo, T. *J. Polym. Sci., Part A: Polym. Chem*. **2005b**, 43, 6613-6618.

Ochiai, B.; Satoh, Y.; Endo, T. *Green Chem*. **2005c**, 7, 765-767.

Ochiai, B.; Utsuno, T. *J. Polym. Sci., Part A: Polym. Chem*. **2013**, 51, 525-533.

Oertel, G. Polyurethane Handbook. 2nd ed; Hanser Gardner, 1994.

Official Journal of European Union; Commision Regulation (EC) No 552, 2009.

Oprea, S.; *Polym. Bull*. **2010**, 65, 753-766.

O'Sickey, M. J.; Lawrey, B. D.; Wilkes, G. L. *Polymer* **2002a**, 43, 7399-7408.

O'Sickey, M. J.; Lawrey, B. D.; Wilkes, G. L. *J. Appl. Polym. Sci*. **2002b**, 84, 229-243.

O'Sickey, M. J.; Lawrey, B. D.; Wilkes, G. L. *J. Appl. Polym. Sci*. **2003**, 89, 3520-3529.

Padhye, M. R.; Karandikar, A. V. *J. Appl. Polym. Sci*. **1985**, 30, 667-673.

Park, K.; Lim, W. H.; Ko, E.-A.; Lee, H. S. *J. Polym. Sci. Part B: Polym. Phys*. **2011**, 49, 890-897.

Perry, K. P.; Jackson Jr, W. J.; Caldwell, J. R. *J. Appl. Polym. Sci*. **1965**, 9, 3451-3463.

Petrovic, Z. S.; Ferguson, J. *Prog. Polym. Sci*. **1991**, 16, 695-836

Phadke, M. A.; Musale, D. A.; Kulkarni, S. S.; Karode, S. K. *J. Polym. Sci., Part B: Polym. Phys*. **2005**, 43, 2061-2073.

Poussard, L.; Mariage, J.; Grignard, B.; Detrembleur, C.; Jerome, C.; Calberg, C.; Heinrichs, B.; De Winter, J.; Gerbaux, P.; Raquez, J.-M.; Bonnaud, L.; Dubois, Ph. *Macromolecules* **2016**, 49, 2162-2171.

Priscariu, C.; Scortanu, E. *High Perform. Polym.* **2001**, 308-311.

Pyo, S.-H. ; Persson, P.; Mollaahmad, M. A.; Sörensen, K.; Lundmark, S.; Hatti-Kaul, R. *Pure Appl. Chem*. **2012**, 84, 637-661.

Qi, H. J.; Boyce, M. C. *Mech. Mater*. **2005**, 37, 817-839.

Qin, C.-L.; Cai, W.-M.; Cai, J.; Tang, D.-Y.; Zhang, J.-S.; Qin, M. *Mater. Chem. Phys*. **2004**, 85, 402-409.

Rix, E.; Grau, E.; Chollet, G.; Cramail, H. *Eur. Polym. J*. **2016**, 84, 863-872.

Roland, C. M.; Twigg, J. N.; Vu, Y.; Mott, P. H. *Polymer* **2007**, 48, 574-578.

Ryan, A. J.; Macosko, C. W.; Bras, W. *Macromolecules* **1992**, 25, 6277-6283.

Ryan, A. J.; Willkomm, W. R.; Bergstrom, T. B.; Koberstein, J. T.; Yu, C. C.; Russell, T. P. *Macromolecules* **1991**, 24, 2883-2889.

Sarva, S. S.; Deschanel, S.; Boyce, M. C.; Chen, W. *Polymer* **2007**, 48, 2208-2213.

Schmidt, S.; Ritter, B. S.; Kratzert, D.; Bruchmann, B.; Mülhaupt, R. *Macromolecules* **2016**, 49, 7268-7276.

Schneider, N. S.; Sung, C. S. P.; Matton, R. W.; Illinger, J. L. *Macromolecules* **1975**, 8, 62-67.

Schneider, N. S.; Matton, R. W. *Polym. Eng. Sci*. **1979**, 19, 1122-1128.

Seefried, C. G.; Koleske, J. V.; Critchfield, F. E. *J. Appl. Polym. Sci*. **1975a**, 19, 2493-2502.

Seefried, C. G.; Koleske, J. V.; Critchfield, F. E. *J. Appl. Polym. Sci*. **1975b**, 19, 2503-2513.

Seefried, C. G.; Koleske, J. V.; Critchfield, F. E. *J. Appl. Polym. Sci*. **1975c**, 19, 3185-3191.

Seefried, C. G.; Koleske, J. V.; Critchfield, F. E. *Polym. Eng. Sci*. **1975d**, 15, 646-650.

Seymour, R. W.; Estes, G. M.; Cooper, S. L. *Macromolecules* **1970**, 3, 579-583.

Sheng, X.; Ren, G.; Qin, Y.; Chen, X.; Wang, X.; Wang, F. *Green Chem*. **2015**, 17, 373-379.

Sheth, J. P.; Aneja, A.; Wilkes, G. L.; Yilgor, E.; Atilla, G. E.; Yilgor, I.; Beyer, F. L. *Polymer* **2004**, 45, 6919-6932.

Sheth, J. P.; Klinedinst, D. B.; Wilkes, G. L.; Yilgor, I.; Yilgor, E. *Polymer* **2005**, 46, 7317-7322.

Sheth, J. P.; Klinedinst, D. B.; Pechar, T. W.; Wilkes, G. L.; Yilgor, E.; Yilgor, I. *Macromolecules* **2005**, 38, 10074-10079.

Shin, J.; Matsushima, H.; Chan, J. W.; Hoyle, C. E. *Macromolecules* **2009**, 42, 3294-3301.

Siegmann, A.; Cohen, D.; Narkis, M. *Polym. Eng. Sci*. **1987**, 27, 1187-1194.

Sophiea, D.; Klempner, D.; Sendijarevic, V.; Suthar, B.; Frisch, K. C.; "Interpenetrating Polymer Networks as Energy-Absorbing Materials" in Interpenetrating Polymer Networks, Advances in Chemistry Series 239, ACS Washington, DC 1994. Edited by Klempner, D.; Sperling, L. H.; Utracki, L. A.

Speckhard, T. A.; Ver Strate, G.; Gibson, P. E.; Cooper, S. L. *Polym. Eng. Sci*. **1983**, 23, 337-349.

Speckhard, T. A.; Gibson, P. E.; Cooper, S. L.; Chang, V. S. C.; Kennedy, J. P. *Polymer* **1985a**, 26, 55-69.

Speckhard, T. A.; Hwang, K. K. S.; Cooper, S. L.; Chang, V. S. C.; Kennedy, J. P. *Polymer* **1985b**, 26, 70-78.

Speckhard, T. A.; Cooper, S. L. *Rubber Chem. Tech*. **1986**, 59, 405-431.

Steblyanko, A.; Choi, W.; Sanda, F.; Endo, T. *J. Polym. Sci., Part A: Polym. Chem*. **2008**, 38, 2375-2380.

Sung, C. S. P.; Schneider, N. S. *Macromolecules* **1975**, 8, 68-73.

Sung, C. S. P.; Schneider, N. S. *Macromolecules* **1977**, 10, 452-458.

Sung, C. S. P.; Schneider, N. S. *J. Mater. Sci*. **1978**, 13, 1689-1699.

Tamami, B.; Sohn, S.; Wilkes, G. L. *J. Appl. Polym. Sci*. **2004**, 92, 883-891.

Tang, C. N.; Nulwala, H. B.; Damodaran, K.; Kaur, P.; Luebke, D. R. *J. Polym. Sci., Part A: Polym. Sci*. **2011**, 49, 2024-2032.

Tang, D.; Macosko, C. W.; Hillmyer, M. A. *Polym. Chem*. **2014**, 5, 3231-3237.

Tatai, L.; Moore, T. G.; Adhikari, R.; Malherbe, F.; Jayasekara, R.; Griffiths, I.; Gunatillake, P. A. *Biomaterials* **2007**, 28, 5407-5417.

Tomita, H.; Sanda, F.; Endo, T. *J. Polym. Sci., Part A: Polym. Chem*. **2001a**, 39, 162-168.

Tomita, H.; Sanda, F.; Endo, T. *J. Polym. Sci., Part A: Polym. Chem*. **2001b**, 39, 851-859.

Tomita, H.; Sanda, F.; Endo, T. *J. Polym. Sci., Part A: Polym. Chem*. **2001c**, 39, 860-867.

Tomita, H.; Sanda, F.; Endo, T. *J. Polym. Sci., Part A: Polym. Chem*. **2001d**, 39, 3678-3685.

Tomita, H.; Sanda, F.; Endo, T. *J. Polym. Sci., Part A: Polym. Chem*. **2001e**, 39, 4091-4100.

Tomita, H.; Sanda, F.; Endo, T. *Macromolecules* **2001f**, 34, 727-733.

Tryznowski, M.;Zolek-Trzynowska, Z.; Swiderska, A.; Parzuchowski, P. G. *Green Chem*. **2016**, 18, 802-807.

US Environmental Protection Agency; EPA Proposes Rule to Protect Customers from Harmful Chemicals Found in Homes and Schools. 2015. EPA news release, www.epa.gov accessed on December 04, 2012.

US Environmental Protection Agency; Methylene Diphenyl Isocyanate (MDI) and Related Compounds Action Plan, Toluene Diisocyanate (TDI) Action Plan. 2011a, accessed on November 21, 2015.

US Environmental Protection Agency; EPA Proposed Significant New Use Rules (SNURs). 2016. https://www.regulations.gov/document?D=EPA-HQ-OPPT-2015-0810-0238 accessed on December 17, 2016

Vanbiervliet, E.; Fouquay, S.; Michaud, G.; Simon, F.; Carpentier, J.-F.; Guillaume, S. M. Macromolecules **2016**, **DOI:** 10.1021/acs.macromol.6b02137

Van der Schuur, M.; De Boer, J.; Gaymans, R. J. *Polymer* **2005**, 46, 9243-9256.

Van der Schuur, M.; Gaymans, R. J. *J. Polym. Sci., Part A: Polym. Chem*. **2006a**, 44, 4769-4781.

Van der Schuur, M.; Noordover, B.; Gaymans, R. J. *Polymer* **2006b**, 47, 1091-1100.

Van Ekeren, P. J.; Carton, E. P. *J. Thermal. Anal. Calorim*. **2011**, 105, 591-598.

Van Velthoven, J. L. J.; Gootjes, L.; van Es, D. S.; Noordover, B. A. J. Meuldijk, *Eur. Polym. J*. **2015**, 70, 125-135.

Waletzko, R. S.; Korley, L. T. J.; Pate, B. D.; Thomas, E. L.; Hammond, P. T. *Macromolecules* **2009**, 42, 2041-2053.

Wang, Z.; Zhang, X.; Zhang, L.; Tan, T.; Wong, W. *ACS Sustainable Chem. Eng*. **2016**, 4, 2762-2770.

Wilkes, G. L.; Abouzahr, S. *Macromolecules* **1981**, 14, 456-458.

Wingborg, N. *Polym. Test*. **2002**, 21, 283-287.

Wong, C. L. H.; Kim, J.; Torkelson, J. M. *J. Polym. Sci., Part B: Polym. Phys*. **2007**, 45, 2842-2849.

Xu, J.; Shi, W.; Pang, W. *Polymer* **2006**, 47, 457-465.

Yi, J.; Boyce, M. C.; Lee, G. F.; Balizer, E. *Polymer* **2006**, 47, 319-329.

Yilgör, E.; Burgaz, E.; Yurtsever, E.; Yilgör, I. *Polymer* **2000**, 41, 849-857.

Yilgor, I.; Yilgor, E.; Guclu Guler, I.; Ward, T. C.; Wilkes, G. L. *Polymer* **2006**, 47, 4105-4114.

Yilgor, I.; Yilgor, E.; Das, S.; Wilkes, G. L. *J. Polym.Sci., Part B: Polym. Phys*. **2009**, 47, 471-483.

Yilgor, I.; Yilgor, E.; Wilkes, G. L. *Polymer* **2015**, 58, A1-A36.

Yu, X.; Gao, G.; Wang, J.; Li, F.; Tang, X. *Polym. Int*. **1999**, 48, 805-810.

Yuen, A.; Bossion, A.; Goméz-Bengoa, E.; Ruipérez, F.; Isik, M.; Hedrick, J. L.; Mecerreyes,

D.; Yang, Y. Y.; Sardon, H. *Polym. Chem*. **2016**, 7, 2105-2111.

Zhang, K.; Nelson, A. M.; Talley, S. J.; Chen, M.; Margaretta, E.; Hudson, A. G.; Moore, R. B.; Long, T. E. *Green Chem*. **2016**, 18, 4667-4681.

Zou, R.; Tan, J.; Liu, K.; Liang, L.; Cheng, X.; Zhang, X.; Zhang, L.; Yue, D. *RSC Adv*. **2016**, 6, 20198-20201.